Molecular mechanisms of *GBA*-linked PD

By

Merfat Mohammed Halawani

A thesis submitted for the degree of Doctor of Philosophy

Department of Clinical Neuroscience, Institute of Neurology
University College London

September 2020

Declaration

I, Merfat Halawani confirm that the work presented in this thesis is my own. Where information has been derived from other sources, I confirm that this has been indicated in the thesis.

Dedication

To my parents…

To whom I promised to dedicate this work before they lift this world

Acknowledgments

The work presented in this thesis would not have been possible without my close association with many people. I take this opportunity to extend my sincere gratitude and appreciation to all those who made this PhD thesis possible.

First and foremost, praises and thanks to the **God**, the Almighty, for his showers of blessings throughout my research to complete the research successfully.

I would like also to express my deep and sincere gratitude to my primary supervisor, **Prof Anthony Schapira** for giving me the opportunity to do this research and providing me an invaluable guidance throughout this journey.

A special thank you to my secondary supervisor, **Dr Matthew Gegg** for his continuous support of my PhD study, for his motivation and immense knowledge. His dynamism, vision and sincerity had deeply inspired me. He has thought me the methodology to carry out this research and present this work as clearly as possible. I would like also to appreciate his acceptance and patience during all discussions and meetings I had with him about this research work and writing my thesis. He has shown me, by his example, what a great scientist (and person) should be. I feel privileged to be supervised by him and I could not have imagined having a better mentor for my PhD study.

Nobody has been more important to me in my life than my family and my brothers with a special thanks to**, Tareef, Hussain, Osama, Hasan, Samia & Sami.** Their infallible love and support have always been my strength and they and **untie Fawzia** deserve my wholehearted thanks as well. Most importantly, I would like to express my heartfelt thanks to my younger sister **Wisam** for her unconditional support, love and care not only throughout writing this thesis but in my life in general.

As always it is impossible to mention everybody who had an impact to this work however there are those whose spiritual support is even more important. I cannot forget to thank my loving friends especially **Amel, Nojoud, Hend, Arwa and Reema,** for always standing by my side and sharing a great relationship as compassionate friends. I will always cherish the warmth shown by them.

Thanks to **Ola, Ezzat, Aaron, Michele** and many more for their constant spiritual support and cooperation during my stay. Their friendship shall always be remembered.

Last but not the least, a very special gratitude goes out to all members of **Saudi Arabian Cultural bureau** for helping me and providing the funding for the work.

Thank you all for your encouragement!

Abstract

Objective: To investigate the effect of *GBA* heterozygote L444P (wt/L444P) mutation in human dermal fibroblasts and mouse cortical neurons models (MCN) and find if glucocerebrosidase (GCase) deficiency in these cells impair the lysosomal function and induce unfolded protein response (UPR). In addition, to investigate the consequent impairment of alpha synuclein (A-SYN) metabolism in the form of increased intracellular accumulation and extracellular release of fibrillar A-SYN following seeding MCN and differentiated SH-SY5Y neuronal cultures with preformed A-SYN fibrils (PFFs).

Background: *GBA* heterozygous mutations are numerically the most important predisposing factor for developing PD. They contribute to the earlier age of onset and increased cognitive decline in *GBA*-PD. L444P mutation is proposed to induce unfolded protein response (UPR) and perturbed autophagy pathways. This consequently can lead to impairment of (A-SYN) turnover and eventually result in the loss of substantia nigra dopaminergic cells, the most vulnerable type of cells affected in PD. It is hypothesized that A-SYN pathology can spread through brain regions to reach SNpc thereby supporting the prion-like theory. Fibrillar forms of A-SYN are thought to contribute to this spread as they can induce the endogenous A-SYN to recruit, misfold, and become insoluble aggregates like that observed in Lewy bodies.

Methods:

Functions of ALP and UPS, protein degradation pathways, were assessed in L444P heterozygous fibroblasts and MCN models. ER stress and UPR investigated in all disease models including fibroblasts, wt/L444P MCN and

differentiated SH-SY5Y neurons overexpressing (O/E) L444P *GBA*. Both differentiated SH-SY5Y treated with the GCase inhibitor (CBE) and wt/L444P mutant MCN were incubated with PFFs to initiate A-SYN pathology. Misfolded and aggregated A-SYN was assessed by western blotting and dot blot.

Results: wt/L444P fibroblasts and MCN cellular models showed no impairment of protein quality control systems. There was ER retention of mutant enzyme in wt/ L444P fibroblast but this was not enough to induce UPR in cells. There was also subtle or no alteration in endogenous A-SYN level in wt/L444P MCN and differentiated SH-SY5Y neurons treated with CBE until the addition of another stress such as PFFs seeding. Treating cells with PFFs for 10 days enhanced the recruitment and aggregation of endogenous A-SYN that were phosphorylated at Ser129 with evidence of HMW species. Differentiated SH-SY5Y neurons O/E wildtype *SNCA* and preloaded with PFFs showed enhanced extracellular release of fibrillar A-SYN. In addition, differentiated cells O/E L444P *GBA*, but not MCN or fibroblasts, showed evidence of ER stress and UPR.

Conclusions: Wt/L444P MCN and differentiated SH-SY5Y dopaminergic neurons treated with CBE showed augmented A-SYN pathology. The increased release of pathogenic A-SYN fibrils was more evident in cells with higher endogenous A-SYN levels and only differentiated SHSY5Y cells O/E L444P *GBA* showed evidence of UPR.

Impact Statement

In modelling *GBA*-PD, GCase deficient wt/L444P MCN and differentiated SH-SY5Y dopaminergic neurons treated with CBE showed subtle or no alteration in endogenous A-SYN level until the addition of PFFs to initiate endogenous A-SYN to misfold. Ten days PFFs treatment enhanced formation of insoluble A-SYN, part of which exhibited Ser129 hyperphosphorylation. Lewy bodies are known to contain high amounts of Ser129 phosphorylation. This was also associated with appearance of higher molecular weight A-SYN species.

Also, cell models with increased intracellular A-SYN levels such as differentiated SH-SY5 over-expressing wildtype A-SYN displayed an increased extracellular release of pathological A-SYN fibrils following PFFs treatment. This observation was suggestive that the pathology spread is greatest from neuronal populations with higher endogenous levels of A-SYN.

We only observed noticeable induction of UPR in differentiated SH-SY5Y dopaminergic neurons overexpressing L444P *GBA* whereas other cellular models, such as MCN and fibroblasts showed no ER stress or enhancement of UPR. This might suggest that the L444P *GBA* mutation might have a toxic gain of function in particular cellular environments such as the presence of dopamine, that could increase these cells susceptibility to neurodegeneration.

Table of Contents

List of Figures

List of Tables

List of Abbreviations

ALP–Autophagy Lysosomal Pathway

AP –Autophagosome

Atg –Autophagy-related protein

A-SYN – Alpha Synuclein

Baf–Bafilomycin

BCA –Bicinchoninic acid

BDNF – Brain Derived Neurotrophic Factor

BiP–Immunoglobulin Binding Protein

CathD–Cathepsin D

CMA–Chaperon Mediated Autophagy

CNS Central Nervous System

cPD–clinical Parkinson's Disease

DMEM –Dulbecco's Modified Eagle Medium

DIV – Days In Vitro

Endo-H –Endoglycosidase-H

ER– Endoplasmic Reticulum

ERAD–ER-associated degradation

FBS –Fetal Bovine Serum,

GluCer– Glucosylceramide

GluSph – Glycosphingolipid

GBA – Glucocerebrosidase Gene

GCase – Glucocerebrosidase Enzyme

GD – Gaucher Disease

HMW – High Molecular Weight

Hsc70 – Heat Shock Protein of 70 kDa

iPCs – Induced Pluripotent Stem Cells

ILV– Intraluminal Vesicles

KO MEF–Knockout Mouse Embryonic Fibroblasts

LIMP2–Lysosomal Integral membrane protein 2

LAMP1–Lysosomal Associated Membrane Protein 1

LAMP2A– Lysosome-Associated Membrane Protein 2A

LBs–Lewy bodies

LC3–Microtubule-Associated Protein 1 Light Chain 3,

LN–Lewy Neurites

LP– Lewy Pathology

MA– Macroautophagy

MCN – Mouse Cortical Neurons

MPTP –1-methyl-4-phenyl-1,2,3,6-tetrahydropyridine

NB – Neuroblastoma

N-SMase – Neutral Sphingomyelinase

NMC– Non-Manifesting Carriers

RA– Retinoic Acid

ROS –Reactive Oxygen Species

SN– Substantia Nigra

SNpc. – Substantia Nigra Pars Compacta

SDS – Sodium Dodecyl Sulphate

Ser129–Serine 129

SNCA – Alpha Synuclein Gene

TH – Tyrosine Hydroxylase

PD – Parkinson's Disease

PBS – phosphate buffered saline

PCR – Polymerase Chain Reaction

PFFs – Preformed Alpha-Synuclein Fibrils

PSAP – Prosaposin Precursor Protein

Ub – Ubiquitin

UPR – Unfolded protein response

UPS– Ubiquitin proteasomal System

WB – Western Blot

WT–Wild Type

Wt/△– Heterozygous Mutation

1.Introduction

1.1 Gaucher Disease

Gaucher disease (GD) is the most common lysosomal storage disease with an autosomal recessive mode of inheritance. It is caused by mutation in the glucocerebrosidase gene (*GBA*) that leads to deficiency of lysosomal β glucocerebrosidase (GCase), the enzyme which breaks down the glycolipid glucosylceramide (GluCer) into glucose and ceramide. GD is a rare and pan-ethnic disorder with an estimated incidence of 1 in 40,000-50,000 to 1 in 100,000 birth in general population. GD was traditionally classified into three clinical subtypes on the basis of central nervous system involvement, its severity and deterioration, age of onset and disease prognosis (Grabowski, 2008, Alaei et al., 2019, Gan-Or et al., 2009, Westbroek et al., 2011, Roshan Lal and Sidransky, 2017). Type I GD, also known as adult or chronic GD, is characterized by vesical presentation with absence of CNS involvement. This is the most prevalent type of the disease in western countries and among Ashkenazi Jews in which the incidence can reach up to 1/ 800 live birth (Alaei et al., 2019, Grabowski, 2008). Both type II (1% of all GD) and III GD (5%) are classified as neuropathic forms but they differ in the onset and the rate of disease progression (Alaei et al., 2019, Sestito et al., 2017), (

Figure 0.1). However, due to previous evidences of phenotypic variation and genotypic homogeneity, the introduction of new variant of GD and the recognition of patients with type I disease who develop neurological manifestation (Biegstraaten et al., 2008) and Parkinsonism (Gan-Or et al., 2009), the customary classification of neuropathic GD was expanded to include a continuum of clinical phenotypes (Linari and Castaman, 2015, Alaei et al., 2019). In addition the

spectrum of phenotypic variation of neuropathic GD was previously determined and an intermediate phenotype between type II and III GD was reported (Goker-Alpan et al., 2003). Saposins are important cofactors that participate in glycosphingolipids (GluSphs) degradation. There are four homologous forms of Saposin, A-D resulting from the sequential post-translational cleavage of a precursor protein, prosaposin (PSAP). Sap C is required for the activation of GCase enzyme (Tatti et al., 2012) and a rare variant of the GD, presented clinically as that of type I GD (Tylki-Szymańska et al., 2007), is caused by mutations in Sap C coding region of the Prosaposin precursor protein (PSAP) and associated with an invitro normal GCase activity (Tamargo et al., 2012, Tylki-Szymańska et al., 2007).

The classic pathological hallmark in Gaucher disease is substrate laden macrophages due to accumulation of GlcCer substrate in the cell of reticulo-endothelial system. These macrophages accumulating in the spleen and liver result in organomegaly, as well as inflammation (Westbroek et al., 2011). However, the exact mechanism of neurotoxicity in GD is not clearly understood and was previously reported to be different than that of other involved systems (Chen and Wang, 2008, Conradi et al., 1984, Alaei et al., 2019, Wong et al., 2004). Because GSLs are essential components of cell membrane and they are vital for cell life (Ferreira and Gahl, 2017), Gaucher cells and neuronal cell loss can be found in brain parenchyma especially in cortex, hippocampus and in the brainstem of neuronopathic GD patients (Wong et al., 2004, Orvisky et al., 2002). The new expanded non-conventional classification of GD is illustrated in Figure 0.2).

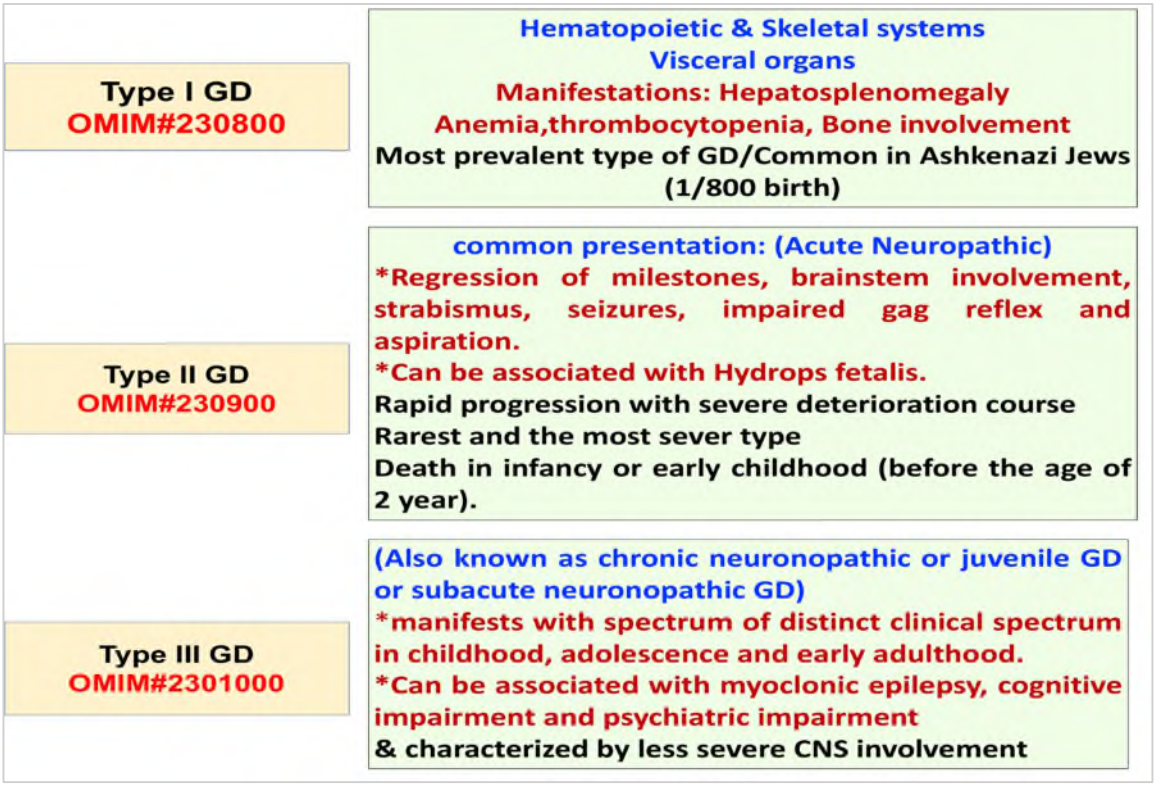

Figure 0.1 The three types of Gaucher disease.

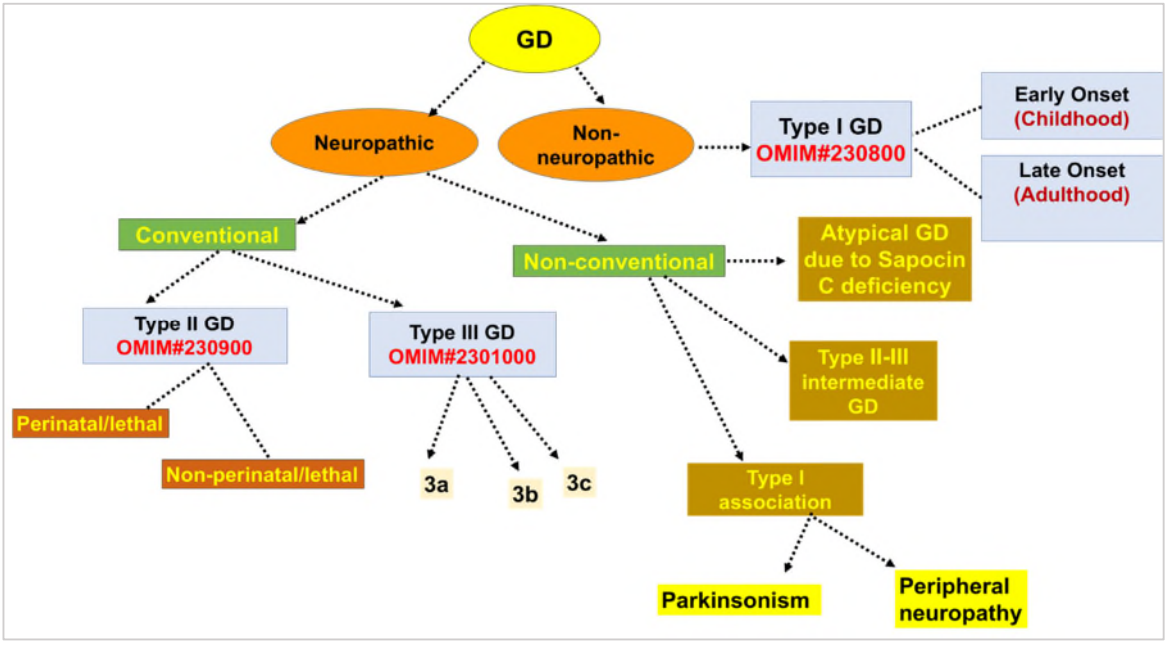

Figure 0.2 New expanded classification of GD (Alaei et al., 2019, Westbroek et al., 2011).

1.2 Parkinson disease

Parkinson disease (PD), by James Parkinson in 1817, is a progressive neurodegenerative disorder affecting between 10 to 50/100,000 person per year. Although it is the second most common neurodegenerative disease after Alzheimer's, PD is relatively uncommon with a worldwide estimated prevalence of 1087/100,000 individuals between the age of 70 and 79 and 1,903/100,000 individuals over 80 (Pringsheim et al., 2014). However, being an age-related disorder and due to the general aging of the population, the number of PD patients over age 50 was between 4.1 and 4.6 million in 2005 and is expected to double by 2030 (Dorsey et al., 2007). PD is diagnosed by Queen Square brain bank diagnostic criteria; Bradykinesia (slowness of initiation of voluntary movement with progressive reduction in speed and amplitude of repetitive actions) and at least one of the following: (I) muscular rigidity, (II) 4–6 Hz rest tremor and (III) postural instability not caused by primary visual, vestibular, cerebellar or proprioceptive dysfunction (Davie, 2008). However, these clinical features may not all be present all together and the symptomatology of Parkinson's disease is now recognized as heterogeneous with a spectrum of clinically significant non-motor features like sleep disorders, cognitive decline, psychiatric problems, dementia, various sensory and autonomic dysfunctions (Kalia and Lang, 2015, Langston, 2006). The most important pathological hallmark in PD is the selective dopaminergic neuronal loss in the ventral components of Substantia Nigra Pars compacta (SNpc) with the cardinal motor manifestations caused by this loss (Surmeier et al., 2017). By the time of death, 50 to 70% of neurons in SNPc is lost (Davie, 2008). In addition to cell death, histological examination of PD brains showed fibrillary aggregates referred to as

Lewy bodies (LBs) and Lewy neurites (Surmeier et al., 2017). LBs as a marker of neurodegeneration, are usually present in the sites of neuronal loss residing in the surviving neurons. Alpha-Synuclein (A-SYN) is the major component of Lewy pathology (LP), usually presents with a mixture of molecules including PD-linked gene products (DJ-1, LRRK2, parkin, and PINK-1), mitochondrial proteins, and molecules involved in protein degradation systems (Wakabayashi et al., 2013). PD is also characterized by neuroinflammation partly due to the activation of the microglia (Dauer and Przedborski, 2003, Hirsch and Hunot, 2009). It is considered as a fundamental event to protect against neurodegeneration. However its toxic effect could, on the other hand, exacerbate the neuronal damage in PD (Lee et al., 2019). Braak et al. group staged PD according to the evolutional distribution and spread of LP over time from a well-defined starting point (Braak et al., 2003). PD patients are usually pre-symptomatic in the earliest documented pathology (Braak stages 1 and 2). However, as the disease progresses (Braak stages 3 and 4), areas of midbrain and forebrain become involved to initiate the loss of neurons and symptoms onset. Finally, LP starts to appear in the neocortex and is associated with sever motor clinical features (Braak stages 5 and 6), (Table 0.1).

While dopaminergic cell loss is believed to be responsible for the motor alteration in PD, other neurons including glutamatergic, cholinergic, GABAergic, adrenergic and noradrenergic are also affected. This heterogenous involvement may explain the diverse symptomatology of PD, which includes the common PD-associated non-motor symptomatology (Paredes-Rodriguez et al., 2020, Schapira et al., 2017). In fact, PD is more likely to be a multisystem rather than pure motor disease.

Table 0.1 Braak Staging of PD-related Pathology (Braak et al., 2003)

Stage	Evolution of PD-related pathology
Stage 1 (Medulla Oblongata)	Lesions in the of IX/X motor nucleus and/or intermediate reticular zone
Stage 2 (Medulla Oblongata and pontine tegmentum)	Pathology of stage 1 plus lesion in caudal raphe nuclei, gigantocellular reticular nucleus and coeruleus- subcoeruleus complex
Stage 3 (Midbrain)	Pathology of stage 2 plus midbrain lesions, in particular in pars compacta of Substantia Nigra
Stage 4 (Basal prosencephalon and Mesocortex)	Pathology of stage 3 plus prosencephalic lesions. Cortical involvement is confined to the temporal mesocortex (trans-entorhinal region) and allocortex (CA2-plexus). The neocortex is unaffected
Stage 5 (Neocortex)	Pathology of stage 4 plus lesions in high order sensory association areas of the neocortex and prefrontal neocortex
Stage 6 (Neocortex)	Pathology of stage 5 plus lesions in first order sensory association areas of the neocortex and premotor areas, occasionally mild changes in primary sensory areas and the primary motor field

Most clinicians standardize a combination of clinical presentation with pathological syndrome to diagnose clinical PD (cPD), (Berg et al., 2014). Nevertheless, despite that LP is commonly present in brain regions of PD patients especially in the brainstem, they also occur in other age related synucleinopathies even in the absence of PD (Surmeier et al., 2017).

Tyrosine Hydroxylase (TH), the rate limiting enzyme in dopamine synthesis, and dopamine transporters were shown to be severely reduced in the SN of PD patients (Kastner et al., 1993). It has become increasingly clear that PD starts many years before the motor symptoms become evident and PD is diagnosed (Savica et al., 2010). In fact, some features, appearing early in the course of the disease, might give a useful diagnostic clue such as early postural instability backwards with a history of falls, although it is more suggestive of progressive supranuclear palsy (PSP).

In addition, idiopathic rapid eye movement (REM) behavioural disorders (iRBD) is known to precede PD by as much as 50 years with 50–75% of patients who

present with iRBD will go on to develop PD within 10 years of iRBD diagnosis (Tekriwal et al., 2017). Change in hand writing, micrographia and loss of arm swinging are usual early features same as reduced facial expression and saliva drooling. Loss of smell sensation and constipation frequently predate, sometimes by decade, the onset of PD and are therefore worth asking about (Davie, 2008, Langston, 2006).

1.3 Genetic overview

Although it has a relatively narrow clinical phenotype, PD is a complex disease with wide multifactorial etiology including environmental and genetic factors. It is assumed that the PD is caused, in most cases, by an interplay of the genetic suitability factors and the environment acting on the background of an aging brain. In fact, aging is probably the single most important “environmental” risk factor that eventually tip the balance toward neurodegeneration and PD in a genetically susceptible individual (Gasser, 2009). The complexity of Parkinson disease is underlined by the notion that 28 distinct chromosomal regions are related to PD. The majority of PD is sporadic and about 10% of patients have a positive family history and a series of genes such as SNCA (PARK1, 4), LRRK2 (PARK8), PINK1(PARK6), DJ-1(PARK7) and ATP13A2 cause familial PD (Klein and Westenberger, 2012), (Table 0.2).

Table 0.2 PARK designated PD-Loci

Symbol	Gene locus	disease	Inheritance mode	Gene
PARK1	**4q21-22**	**EOPD**	**AD**	**SNCA**
PARK2	**6q25.2–q27**	**EOPD**	**AR**	***Parkin***
PARK6	**1p35–p36**	**EOPD**	**AR**	***PINK1***
PARK7	**1p36**	**EOPD**	**AR**	***DJ-1***
PARK8	**12q12**	**Classical PD**	**AD**	***LRRK2***

1.4 Link between *GBA* mutations and PD

One of the most significant current notions in PD is the high association between *GBA* mutation and PD. Both homozygous and heterozygous *GBA* gene mutations constitute numerically the most important predisposing factor for developing PD. Compared to the general population, patients with type 1 GD have increased risk of developing PD (Sidransky et al., 2009). The proportion of PD patients carrying *GBA* mutation is estimated to be 5 to 10% depending whether the entire exome has been sequenced or not (Kumar et al., 2013, Lesage et al., 2011, McNeill et al., 2012a, Sidransky et al., 2009, Neumann et al., 2009). The interest in *GBA* as a risk factor for PD followed the clinical observation that GD patients had Parkinsonian symptoms (McKeran et al., 1985, Turpin et al., 1988, Tayebi et al., 2001). This was further supported by the incidence of PD among relatives of patients with GD indicating high association of both homozygous and heterozygous *GBA* mutations with PD (Goker-Alpan et al., 2004, Halperin et al., 2006). Despite the discrepancies of the populations studied, subsequent *GBA* related studies and multicenter meta-analysis showed that both homozygous and heterozygous mutations confer up to a 20-to 30-fold increased risk for the development of PD depending on age ethnicity, and type of *GBA* mutation (Sidransky et al., 2009, McNeill et al., 2012a, McNeill et al., 2012b).

N370S and L444P are among the most common *GBA* mutations associated with PD and in vitro studies showed that prevalent allele mutants with L444P and N370S produce enzyme with activity ranging from 6% to 14% of the wild type (Horowitz et al., 2011, Montfort et al., 2004). More “severe” mutations like L444P are associated with higher risk for PD than “milder” mutations (e.g., N370S) and with earlier PD onset (Gan-Or et al., 2015). However, *GBA* polymorphic variants like E326K and T369M did not lead to GD in homozygous state have been associated with increased risk of PD (Duran et al., 2013, Han et al., 2016). Although the molecular mechanism by which gene mutation results in the disease are not clear, previous theories have proposed that as in idiopathic PD, *GBA* mutation could result in mutant protein misfolding leading to activation of the UPR, ER stress, (see section1.8 for more details), autophagy-lysosomal dysfunction (section 1.6.11.6.1), mitochondrial dysfunction, inflammation, and oxidative stress (Alcalay et al., 2015, Schapira and Tolosa, 2010). Interestingly, GCase activity was found reduced in post mortem brain samples from patients with no *GBA* mutations signifying that the reduced enzymatic activity per se may contribute to the pathogenesis of the disease (Gegg et al., 2012, Murphy et al., 2014, Rocha et al., 2015a). In contrast to the autosomal recessive and dominant familial PD, *GBA*-PD supports both modes of inheritance due to proposed hypotheses of loss and gain of function in mutant gene respectively. Nevertheless, neither one of these hypotheses can explain why the majority of mutation carriers do not develop PD (Migdalska-Richards and Schapira, 2016). Whether *GBA*- linked or idiopathic PD, both appear to have similar LB pathology (Westbroek et al., 2011, Swan and Saunders-Pullman, 2013), but earlier age of onset (4-5 years earlier), more cognitive impairment and neuropsychiatric deficits

are more associated with *GBA*-PD (Tan et al., 2007, Neumann et al., 2009, Sidransky et al., 2009, Brockmann et al., 2011, McNeill et al., 2012b, Winder-Rhodes et al., 2013).

The point mutations c.1226A4G (N370S) and c.1448T4C (L444P) are the most commonly associated with GD accounting for 70% of mutant alleles and were the first two *GBA* mutations described in the late 1980s (Tsuji et al., 1987, Tsuji et al., 1988, Hruska et al., 2008). Although different *GBA* mutations are encountered in GD, it is of importance to identify the causative mutation for genotype-phenotype correlation and assessing disease prognosis. Additional *GBA* mutations such as complex alleles where the *GBA* gene recombines with the pseudogene (*GBAP*) are implicated in serious clinical consequences (Hruska et al., 2006). Similarly, *GBA* null alleles which do not result in protein expression like IVS2+1G and 84GG confer over 13 times increased risk of PD (Gan-Or et al., 2009). By comparison, patients with homozygous or compound heterozygous N370S mutation tend to develop non-neuropathic type 1 GD, and those with homozygous L444P mutation will be strongly but not exclusively associated with neuropathic type 3 GD, while patients identified with a complex allele and a heterozygous L444P mutation are most likely to develop type 2 GD (Grabowski, 2008). It was first reported by Tsuji et al. that the occurrence of single base substitution in exon X of GBA gene resulting in ^{444}leucine to proline mutation is frequently found in the neurologic phenotypes of Gaucher's disease (Tsuji et al., 1987). Perhaps L444P mutation, situated at the hydrophobic core of domain II, conformationally changes the folding state of domain II. Also, the substitution site is situated closed to the proposed catalytic site of GCase and thus results in the generation of defective enzyme (Tsuji et al., 1987). N370S mutation, on the other

hand, is located further away from this catalytic site of domain III and might have less of an effect on the catalytic activity. Furthermore, glycosylation of human GCase at four asparagine residues (N19, N59, N146, and N270) is essential for its normal catalytic activity. It has been shown that site-directed mutagenesis of asparagine residues N19 results in destruction of the potential glycosylation site in GCase and subsequent enzymatic inactivity (Berg-Fussman et al., 1993).

1.5 GCase activity in PD

As mutant gene results in a production of no protein or misfolded protein with significantly reduced activity, GD patients typically have 10-20% GCase activity as compared to normal individuals whereas heterozygous mutation carriers have about 50% of the activity. Since *GBA* mutations are numerically the greatest known genetic risk factor for developing PD, measuring enzyme level and GCase activity is considered as the important entry point in several studied disease models. Therefore, several groups have studied GCase activity and protein level and found it to be defective in different disease models harboring L444P or N370S *GBA* mutations; this included GD fibroblasts (McNeill et al., 2014, de la Mata et al., 2015, Sanchez-Martinez et al., 2016, Collins et al., 2017), inducible pluripotent stem cell-derived dopaminergic neurons (Schondorf et al., 2014, Fernandes et al., 2016, Woodard et al., 2014, Yang et al., 2020) and in mouse cortical neurons (Fishbein et al., 2014, Li et al., 2019). GCase activity and protein levels were also found reduced by ~33% in different brain regions of sporadic PD (Gegg et al., 2012, Rocha et al., 2015a, Chiasserini et al., 2015, Murphy et al., 2014), signifying the potential importance of GCase in the development of idiopathic Parkinson's disease. Also, reduced GCase activity was reported in different brain regions of L444P transgenic mice (Migdalska-Richards et al.,

2017). Despite the reduction in GCase activity in these studies, screened beta-hexosaminidase and beta-galactosidase activities were not significantly altered indicating that the effect on GCase was due *GBA* mutation and not due to change in lysosomal mass.

1.6 Protein Degradation Systems

The autophagy lysosome pathways (ALP) and ubiquitin proteasome (UPS) are the two main cornerstone pathways of protein and organelle catabolism. They are also implicated in a wide spectrum of pathological states, among which is neurodegeneration and aging (Rubinsztein, 2006).

1.6.1 Autophagy–lysosome pathways (ALP)

ALP is the process of cellular self-cannibalism which involves breakdown of endogenous cellular components and foreign substances by the cell and is accomplished by the lysosome. It is an orchestrated mechanism which is considered cytoprotective rather than a self-destructive (Levine and Kroemer, 2008). During autophagy, cytoplasmic macromolecules can be degraded to provide a source of energy for metabolism or building blocks for the synthesis of macromolecules when the cell has dwindling external or internal resources (Rubinsztein, 2006, Rubinsztein et al., 2011, Chun and Kim, 2018). Autophagy can be induced within short periods of nutrient deprivation, and opposite to the UPS, it is likely the primary mechanism for the degradation of dysfunctional long-lived entire organelles such as mitochondria (Chun and Kim, 2018). Because of small barrel shape proteasome, large proteins and complexes (including oligomers and aggregates) cannot pass through and therefore are not degraded by UPS (Levine and Klionsky, 2004, Thibaudeau et al., 2018, Hideshima et al., 2005). Autophagy substrates also include aggregate-prone proteins such as

mutant alpha-synuclein (ASYN) which is associated with Parkinson's diseases (Rubinsztein et al., 2011). Depending on the different routes of delivering cytoplasmic substrates to lysosomes, autophagy is classified in to three types which are macroautophagy (MA), chaperone-mediated autophagy (CMA), and microautophagy which has been reported in yeast where cargoes are directly engulfed by a yeast lysosomal compartment (Levine and Klionsky, 2004, Chun and Kim, 2018).

Macroautophagy is a multistep process involving initially the formation of a phagophore, (also called isolation membrane), engulfment of cytoplasmic material by the phagophore, elongation of the phagophore membrane, then fusion of its edges to close the autophagosome (AP), (Bento et al., 2016, Ktistakis and Tooze, 2016). AP then fuses with lysosomes to form autolysosomes, a step that is governed by a number of factors including dynein activity (Pu et al., 2016). Autophagic clearance of aggregation prone protein has shown to be impaired even with mutation of dynein machinery (Ravikumar et al., 2005). Inside the autolysosomes, the luminal contents are degraded by hydrolytic enzymes and the resulting products are then recycled back to the cytoplasm (Yim and Mizushima, 2020, Rubinsztein, 2006, Chun and Kim, 2018). In fact, the formation of AP requires a set of autophagy-related proteins (Atg) and protein complexes which are sequentially involved in the pathway. Atg proteins can be categorized functionally according to their role in the AP nucleation and expansion steps. They are Atg1 complex which includes ULK1, Atg13 and Atg17 responsible for the induction of autophagosome, the PI3K complex III (including phosphatidyl inositol 3-phosphate kinase, vps34, Beclin1 and UV radiation resistance associated gene (UVRAG) which regulates vesicle nucleation, and the two-

interconnected ubiquitin-like conjugation systems which promote vesicle expansion and sealing, (Figure 0.3). The first of these conjugation molecules are E1-like enzyme (Atg7) and the E2-like enzyme (Atg10) which facilitate the formation of Atg5-12 conjugate. The second is (Atg7), along with (Atg3) as the E2-like enzyme which regulate the conjugation of Atg8 (known as microtubule-associated protein 1 light chain 3, LC3 in mammalian cells) to the lipid phosphatidylethanolamine, a process known as LC3 lipidation (Wesselborg and Stork, 2015, Suzuki and Ohsumi, 2007, Nishimura and Tooze, 2020).

Following the formation of autophagosome, Atg5-12 conjugate will be eventually removed leaving LC3 attached to the vesicle. Thus, LC3 serves as an autophagosomal marker to estimate both the rates of autophagosome formation and degradation (Klionsky et al., 2008, Yim and Mizushima, 2020, Rubinsztein et al., 2011), (Figure 0.3). One characteristic feature of autophagy is its dynamic regulation; autophagy is usually low under basal conditions, but can be markedly upregulated by several physiological and pathological conditions; starvation and pharmacological agents such as rapamycin positively regulate autophagy (Mizushima et al., 2010).

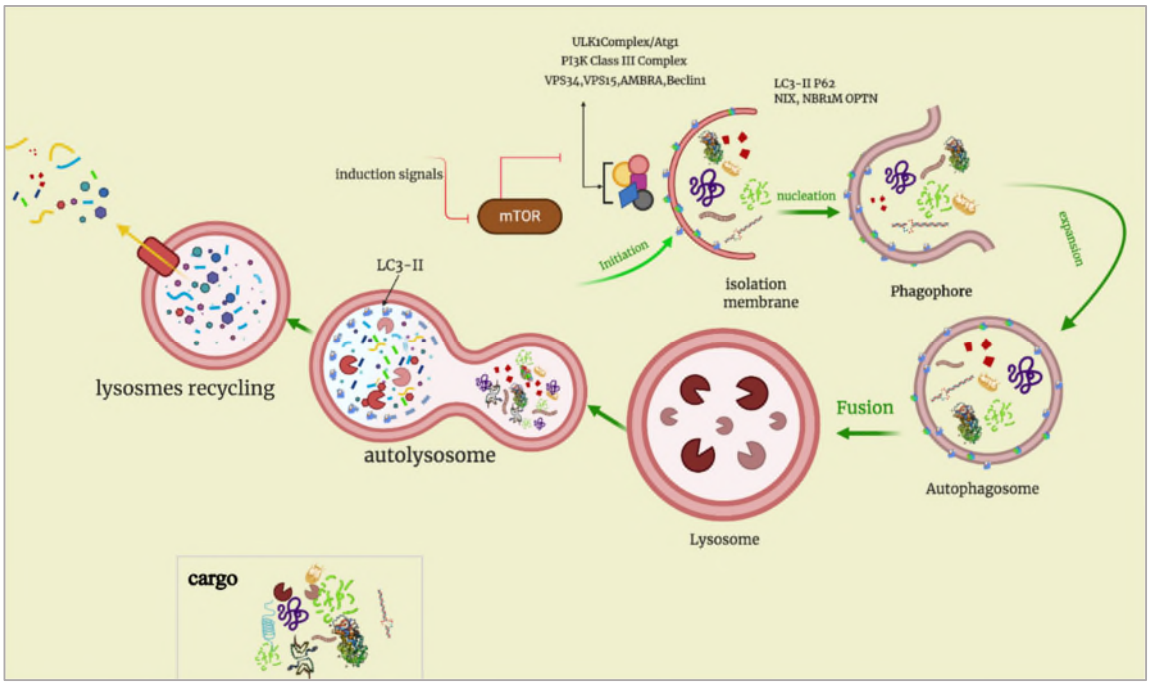

Figure 0.3 Schematic Representation of Macroautophagy Pathway.

Another pathway for cytosolic protein clearance through lysosomes is chaperone-mediated autophagy (CMA), (Figure 0.4). All CMA substrate proteins are characterized by the presence of a targeting pentapeptide motif biochemically related to KFERQ Lys-Phe-Glu-Arg-Gln in its amino acid sequence (Massey et al., 2004, Alfaro et al., 2019, Juste and Cuervo, 2019, Park and Cuervo, 2013, Dice, 1990). This motif, which is present in ~30% of cytosolic proteins is recognized by a cytosolic chaperone, the heat shock protein of 70 kDa (Hsc70). The substrate protein is unfolded when bound to hsc70 (Salvador et al., 2000, Alfaro et al., 2019), a step not required in the other types of autophagy (Figure 0.4). The chaperon-substrate complex then docks at the lysosomal membrane by binding to the cytosolic tail of a single transmembrane protein receptor called lysosome-associated membrane protein 2A (LAMP2A) delivering the target into the lysosomal lumen for degradation by hydrolases and proteases (Cuervo et al., 1999, Cuervo and Wong, 2014, Xilouri and Stefanis, 2016). Lysosomes can also directly engulf cytoplasm by invagination or protrusion of the lysosomal

membrane, a process known as microautophagy. However, this process is poorly understood in mammalian cells (Rubinsztein, 2006), (Figure 0.5).

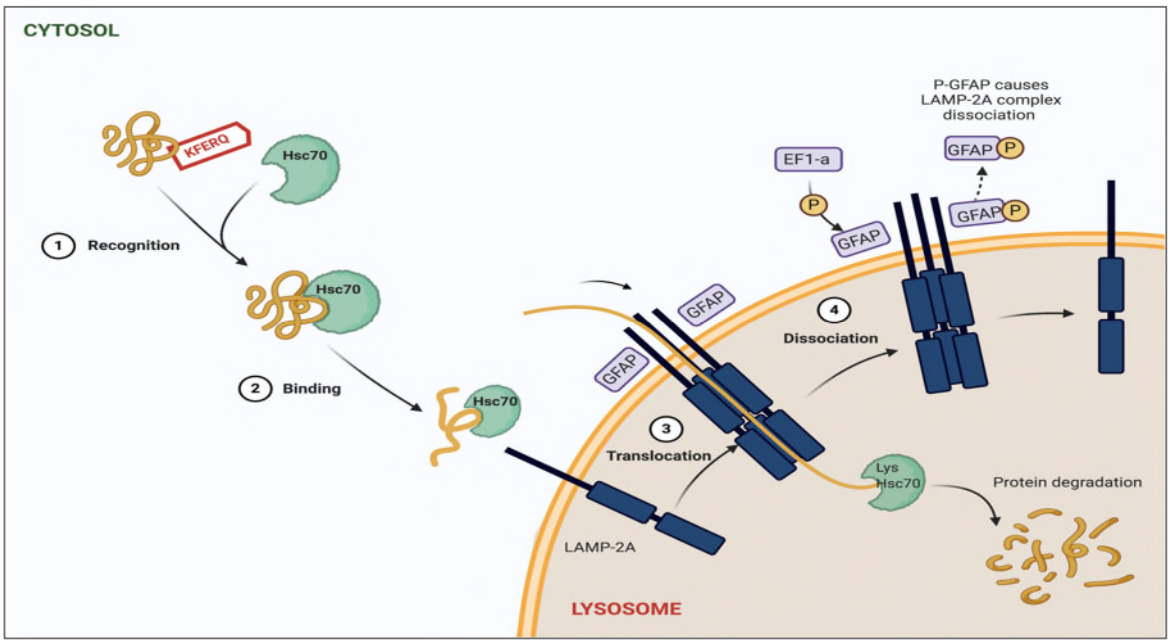

Figure 0.4 Steps of Chaperon Mediated Autophagy Pathway.

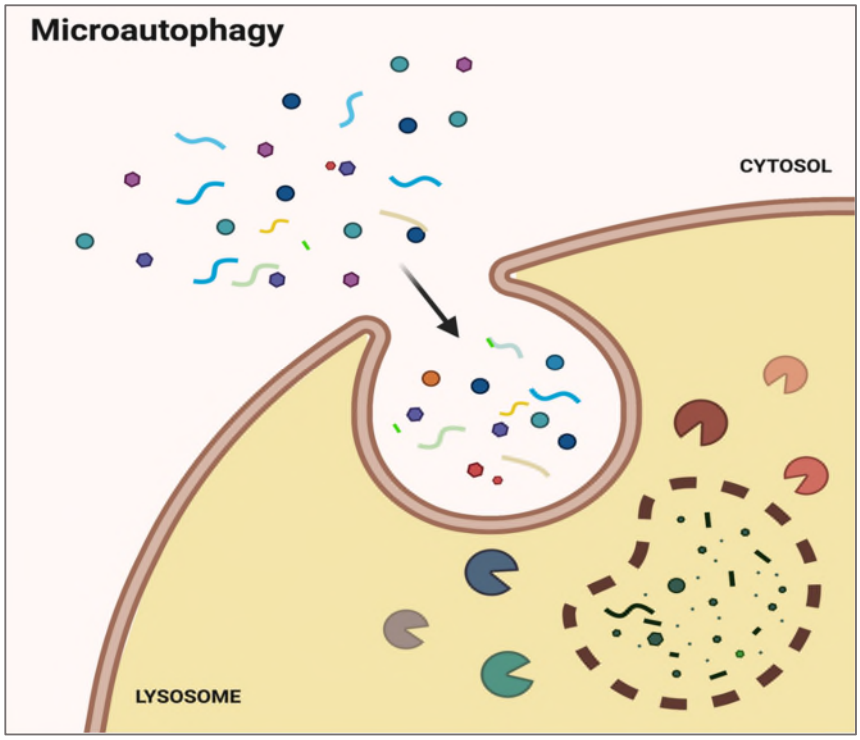

Figure 0.5 schematic representation of Microautophagy process.

Several mouse models have shown the essential role of autophagy for neuronal survival. For instance, knockout of specific autophagy genes (*Atg5* and *Atg7*) in mice led to early neonatal lethality (Komatsu et al., 2005, Kuma et al., 2004, Yoshii et al., 2016). Furthermore, loss of dynein function in mice showed impaired fusion of AP with lysosome and defective clearance of toxic aggregate prone proteins, a process thought to occur in PD with accumulation of aggregated Alpha-synuclein (A-SYN), (Ravikumar et al., 2005, Li et al., 2013). The impairment of lysosomal pathways, although it is not fully understood, has been increasingly viewed as a major event in PD pathogenesis (Dehay et al., 2013).

Robak et al recent study using whole exome sequencing (WES) has identified that, not only *GBA,* but other putative damaging variants of lysosomal storage disease (LSDs) such as Cathepsin D gene (*CTSD)* in Neuronal ceroid lipofuscinosis*, SMPDI* in Niemann-pick disease (type A, B) and *ASAH1* in Farber Lipogranulomatosis are implicated as PD susceptibility genes. This suggests that the impairment of lysosomal function by combination of multiple genetic hits predispose to PD (Robak et al., 2017, Blumenreich et al., 2020). Defective autophagy has been shown both in brain tissue samples from idiopathic, familial PD patients and toxic mouse models of PD (Chu et al., 2009, Alvarez-Erviti et al., 2010, Vila et al., 2011, Sanchez-Danes et al., 2012, Dehay et al., 2010). In terms of PD, it is also well established that wild-type A-SYN is selectively targeted by both the CMA pathway and proteasome for degradation (Vogiatzi et al., 2008, Cuervo et al., 2004, Webb et al., 2003). Meanwhile, mutant A-SYN is mainly degraded by macroautophagy pathway and the proteasome (Yan et al., 2018, Park and Cuervo, 2013, Stefanis et al., 2001, Webb et al., 2003) pointing out to the availability of different pathways for single substrate. There is evidence of

impaired CMA clearance of pathogenic A53T and A30P A-SYN which was compensated by induction of autophagy both in the PC12 cells and neuronally differentiated SH-SY5Y cells (Xilouri et al., 2009). It was previously reported that the selectivity of protein degradation systems is cell type specific. Nevertheless, if a protein cannot be degraded by its “usual” degradation pathway, another system can ship in and take care of its disposal which suggests a cross-talk between different proteolytic pathways. This pattern is therefore considered beneficial to guarantee the elimination of unwanted aggregation prone protein in cell even if it’s selectively degrading pathway is compromised (Park and Cuervo, 2013). Also, mutant A-SYN has been reported to block binding to the CMA receptor (LAPM2A) on the lysosomal membrane thus and inhibiting their own degradation (Cuervo et al., 2004). LAMP2A was found to be neuroprotective by promoting autophagy flux and preventing A-SYN-induced Parkinson like symptoms in Drosophila brain (Issa et al., 2018). Furthermore, decreased levels of hsc70 and LAMP2A have been reported in the substantia nigra pars compacta and amygdala of PD brains (Alvarez-Erviti et al., 2010) and in early stages of sporadic PD brains (Murphy et al., 2015). In these studies, the defect in CMA pathway was associated with increased level of A-SYN which suggests that dysfunction in this pathway may precede pathogenic A-SYN accumulation in PD. Additionally, induction of CMA both in vitro in SHSY5Y and mouse cortical neurons and in vivo in dopaminergic striatal neurons alleviated A-SYN induced neurodegeneration and provided a potential therapeutic strategy in PD and related synucleinopathies (Xilouri et al., 2013). *GBA* mutations and subsequent loss of GCase activity alter A-SYN metabolism. Therefore, and to further implicate the role of autophagy in *GBA* linked PD, Magalhaes et al. work has

previously showed that macroautophagy flux was inhibited and autophagy lysosomal reformation (ALR), a cellular process controlled by mTOR, was compromised in both mouse cortical neurons (MCN) treated with CBE and in fibroblasts with L444P *GBA* mutations (Magalhaes et al., 2016). In this study, Inhibiting GCase was associated with accumulation, Ser129 phosphorylation and induced extracellular release of A-SYN from cells. Similarly, perturbed autophagy pathway was reported previously in *GBA*-N370S- and L444P-mutant induced pluripotent stem cells (iPCs) derived dopaminergic neurons (Fernandes et al., 2016, Schondorf et al., 2014). Recent study by Li et al. reported impaired induction of autophagy and accumulated A-SYN triggered by heterozygous L444P mutation in hippocampal neurons derived from transgenic mice (Li et al., 2019). (Li et al., 2019). However, the effect of *GBA* mutation on autophagy is variable in fibroblast; de la mata *et al*. (2015) found the that ratio of LC3-II to LC3-I and ATG12-ATG5 conjugates were significantly increased in L444P Gaucher fibroblasts, signifying enhanced autophagosome formation in these cells (de la Mata et al., 2015). However, studies by other groups showed no evidence of impaired macroautophagy, with no significant differences in p62 or LC3 levels under basal condition (Tatti et al., 2012, Ambrosi et al., 2015, McNeill et al., 2014).

1.6.2 Ubiquitin Proteasomal System (UPS)

Proteasomes are barrel-shaped complexes that degrade mainly short-lived nuclear and cytosolic proteins (Ciechanover, 2006). It is also involved in the process known as endoplasmic reticulum-associated degradation (ERAD) in which misfolded proteins in ER are translocated back into the cytoplasm for

degradation (Stolz and Wolf, 2010, Olzmann et al., 2013). Before degradation by the proteasome, target proteins are covalently conjugated to ubiquitin (Ub). The process principally involves three types of enzymes: E1 (ubiquitin-activating enzyme) hydrolyses ATP and forms a thioester link with ubiquitin; E2 (ubiquitin-conjugating enzyme) receives ubiquitin from E1 and forms a similar thioester intermediate with it; and E3 (ubiquitin ligase) binds both E2 and the substrate, and transfers the ubiquitin to the substrate (Rubinsztein, 2006, Pohl and Dikic, 2019), (Figure 0.6).

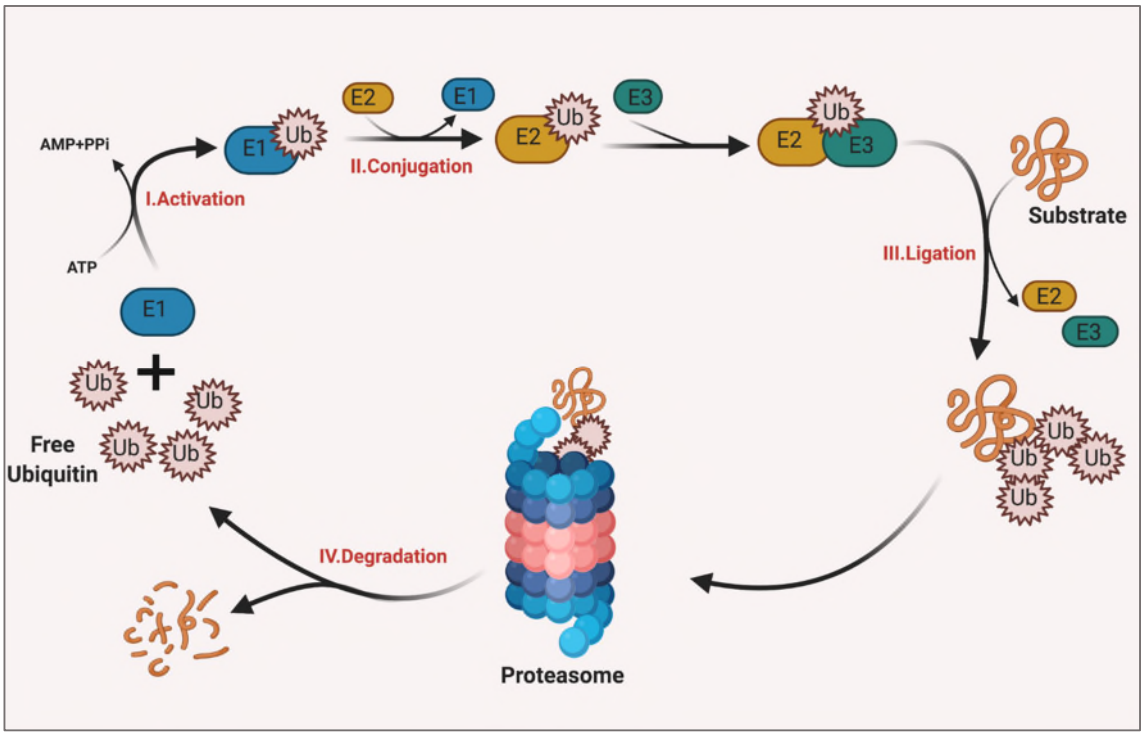

Figure 0.6 Schematic representation of the Ub-proteasome pathway.

A polyubiquitin chain of up to 8 molecules is frequently formed in order for the substrate to be recognized and shuttled to proteasome for degradation. Ubiquitin molecules in the chain are linked together between the terminal G76 residue of each ubiquitin unit and a specific lysine (K) residue (most commonly K48) of the previous ubiquitin (Ikeda and Dikic, 2008). The G76–K48 polyubiquitylated substrate is then targeted for degradation by the 26S proteasome, a large protease complex consisting of a barrel-shaped 20S proteolytic core in association with two 19S regulatory caps, one on each side of the barrel's openings (Saeki, 2017, Chau et al., 1989). The UPS has been considered as the central protease in the ATP- and Ub-dependent degradation of proteins with its 26S catalytic subunit responsible for the degradation of abnormal and damaged proteins (Coux et al., 1996, Hochstrasser, 1996, Hershko and Ciechanover, 1998, Lupas et al., 1995, Collins and Goldberg, 2017). Importantly, wild-type proteins are more efficiently cleared by proteasomes under basal conditions than

by macroautophagy (see section 1.6.1). This might be related to the selectivity of UPS in tagging and targeting proteins before degradation (Rubinsztein, 2006, Wong and Cuervo, 2010). However, when proteins become aggregate prone, they become poor proteasomal substrate and cleared more effectively by macroautophagy (Ciechanover and Kwon, 2015, Rubinsztein, 2006)

Altered UPS leads to protein accumulation and cell death (Voges et al., 1999, Bence et al., 2001, McNaught et al., 2003, Korolchuk et al., 2009, Stefanis et al., 2001, Chau et al., 2009). In fact, inhibiting proteasomal activity was reported to initiate an apoptotic cascade in SH-SY5Y and T98G cellular models (Pilchova et al., 2017). In addition, accumulated Ser129 phosphorylated A-SYN and 40% cell loss were reported in nigral neurons following Lactacystin-induced proteasomal inhibition in mice (Bentea et al., 2015). The genetic analysis of inactive mutant components of UPS has suggested their potential involvement in neurodegeneration and evidence of direct role for the UPS in PD was established from the association of genetic mutations in the *parkin* (*PARK2*) gene with familial parkinsonism (Kitada et al., 1998, Klein and Westenberger, 2012, Gegg et al., 2010, Shimura et al., 2000, Selvaraj and Piramanayagam, 2019, Ferreira and Massano, 2017). This finding was supported by subsequent studies demonstrating that parkin functions as a ubiquitin E3 ligase in UPS (Imai *et al.,* 2000; Zhang *et al.,* 2000). It plays a role in the cell's quality control system with the help of UPS and maintains the healthy mitochondrial network (Selvaraj and Piramanayagam, 2019). Parkin was found involved in the interaction with and degradation of N370S mutant GCase which further support the occurrence of GD and PD (Ron et al., 2010). It also rescues catecholaminergic neurons from toxicity associated with mutant A-SYN including proteasome dysfunction (Petrucelli et al.,

2002). UPS dysfunction was reported as a center of neurodegenerative disease etiology by the knockout of 20S proteasomal unit in mouse model (Bedford et al., 2008). This study showed Lewy body inclusions as a sign of neurodegeneration and provided the evidence that ubiquitin-positive inclusions act as a consistent feature of neurodegenerative diseases. Furthermore, Parkin itself is found as a component of Lewy bodies (Fahn and Sulzer, 2004) and it was previously reported that in HEK 293 and the human neuroblastoma cell line (BE-M17), both aggregated and monomeric A-SYN exerts it's toxic effect by selectively binding to S6 proteasomal protein, a subunit of the 19S cap (Snyder et al., 2003). Furthermore, following proteasomal inhibition in dopaminergic SH-SY5Y cells, the accumulated Ser129 phosphorylated A-SYN was found toxic to cells (Chau et al., 2009). Recent work by (Pantazopoulou et al., 2020) showed that epoxomicin-induced proteasomal inhibition in a PFFs seeded and neuronally differentiated SH-SY5Y cells led to accumulation of Ser129 phosphorylated A-SYN. This observation suggests the proteasome is responsible for selective clearance of PFFs-induced phosphorylated A-SYN aggregates. Similar observation was reported by (Arawaka et al., 2017); In SH-SY5Y cells overexpressing wild-type A-SYN, in which proteasomal clearance of accumulated Ser 129 phosphorylated A-SYN was more enhanced under lysosome inhibition. Overexpression of wild-type or mutant A-SYN in different cell and animal models perturbed proteasomal function and increased susceptibility to cell death (Vekrellis et al., 2009, Stefanis et al., 2001, Chen et al., 2006). This raises the possibility that in addition to the toxic effect of A-SYN on proteasome activity (Ghee et al., 2000), the presence of large amounts of misfolded or unfolded protein might also overwhelm UPS (Bence et al., 2001). Consistent with an

implicated role of UPS in familial parkinsonism, the impairment of 20S activity with selective decrease of proteasomal subunit has been observed in SNpc of sporadic PD patients (McNaught et al., 2003). UPS was also found defective in mixed cortical neuronal culture of (*GBA*-/-) mouse model (Osellame et al., 2013) and in GD fibroblasts (Ambrosi et al., 2014). Although pharmacological inhibition of proteasome in animal models has supported the genetic data and either partially or fully recapitulated the clinicopathological features of PD (Schapira et al., 2006, McNaught et al., 2004), other groups when using the proteasomal inhibitors in rat and primates, failed to observe any clinicopathological features (Beal and Lang, 2006).

1.7 Alpha Synuclein protein metabolism in PD

1.7.1 Accumulated intracellular A-SYN in *GBA*-Linked PD

Alpha-synuclein (A-SYN) is a natively unfolded protein abundantly present in neurons with a small amount also released from cells (Zhang et al., 2018, Lee et al., 2005, Stefanis, 2012). Despite its uncertain function, this protein has been suggested to play a role in synaptic vesicle biogenesis, modulation of synaptic transmission, and brain lipid metabolism (Desplats et al., 2009). In human, A-SYN is present in body fluids like plasma, CSF and interstitial fluid (Mollenhauer et al., 2012, Atik et al., 2016, El-Agnaf et al., 2003, Mollenhauer et al., 2017, Borghi et al., 2000). Clearance of A-SYN can occur via both CMA and macroautophagy, both processes were viewed to be impaired in PD (Alvarez-Erviti et al., 2010, Xilouri and Stefanis, 2016, Cuervo et al., 2004); see section 1.6 for details). Neurons secrete A-SYN normally in culture (Lee et al., 2005), but its secretion increases under stress conditions such proteasomal and lysosomal

dysfunction, as well as oxidative stress (Huse et al., 2005). In fact, A-SYN has a central role in the pathogenesis of PD and other synucleinopathies (Spillantini and Goedert, 2000) and the first link between PD and A-SYN was described in 1997 with the identification of point mutations -A53T- in the *SNCA* gene in autosomal-dominant forms of PD (Polymeropoulos et al., 1997, Athanassiadou et al., 1999, Spira et al., 2001, C-S et al., 2007, Choi et al., 2008, Puschmann et al., 2009). Given that the lysosomal dysfunction is a well-established major pathological event in PD (Dehay et al., 2013), the relationship between GCase mutation and A-SYN accumulation must be studied. In fact, A-SYN levels have been shown to be altered in response to pharmacological inhibition of autophagy pathway (Klucken et al., 2012) and ER stress (Hoepken et al., 2008). Also, accumulated phosphorylated A-SYN species were found in the brains of PD patients and in mouse model of synucleinopathies (Oueslati, 2016). A number of suggested hypotheses have been proposed to link GCase and A-SYN to the pathogenesis of PD (Velayati et al., 2010, Goldin, 2010). The first of these theories is that in the gain of function model of PD, mutant misfolded GCase results in aggregation of A-SYN through direct interaction between the two proteins (Sidransky and Lopez, 2012). Direct molecular and biochemical interaction between GCase and A-SYN mediated at membrane sites was proposed by Yap *et al.,* (2011). This hypothesis requires a co-localization of GCase in the aggregate with A-SYN; significant co-localization between GCase and A-SYN was detected in up to 90% of Lewy neurites and positive A-SYN inclusions in PD patients with *GBA* mutations (Goker-Alpan et al., 2012, Yap et al., 2011). Another study in cell models overexpressing different *GBA* mutations (L444P, N370S, D409V, E235A or E340A) in MES23 neuronal cells and

pheochromocytoma cells (PC12) showed significant increase in endogenous A-SYN aggregation by 121% to 248% (Cullen et al., 2011). Evidence supporting the gain of function theory was also provided by work on murine model with D409V *GBA* mutation; this study showed age-related deposition of A-SYN aggerates in the hippocampal region of mutant mice when compared to control and these deposits were ubiquitin positive and proteinase K insensitive (Sardi et al., 2011). Hippocampal localization of LB and LN has been reported in N370S mutation carriers and in GD patients with Parkinsonism symptoms (Tayebi et al., 2003) and in PD patients carrying various *GBA* mutations (Neumann et al., 2009). The second hypothesis explaining the pathology of A-SYN is that the loss of GCase function leads to accumulation of the substrate glucosylceramide (GluCer) and subsequent perturbation of lipid metabolism promoting an increase in intracellular A-SYN (Pelled et al., 2005). Subsequently, the elevated A-SYN inhibits the intracellular trafficking and the lysosomal function of the normal GCase which will lead eventually to a self-propagating positive feedback loop and ultimately causing neurodegeneration. Intra-lysosomal accumulation of GlcCer in mouse model was proposed as the most likely pathogenic mechanism linked to *GBA* loss-of-function homozygous mutations (Xu et al., 2011). Previous Studies by Mazzulli *et al*., 2011 and Aflaki *et al*., 2016 using iPCs derived dopaminergic neurons from GD patients with N370S and L444P mutations as well as *GBA* KD primary neuronal culture cells showed significant increase in the A-SYN level due to accumulated substrate stabilizing soluble oligomeric intermediates Importantly, defective proteolysis of the long-lived protein was proved in the studied models which indicates that GCase depletion compromises the lysosomal degradation pathway. Chaperoning GCase to the lysosome

significantly restored its activity and reduced A-SYN accumulation, an approach that can be used as a potential therapeutic strategy in PD (Aflaki et al., 2016, Mazzulli et al., 2011). The immunofluorescence for both A-SYN and tyrosine hydroxylase (TH) has previously suggested accumulated of A-SYN in neuronal models with N370S *GBA* mutations (Woodard et al., 2014). Other studies using iPCs derived neurons with N370S, L444P or recombinant alleles (RecNciI), (Schondorf et al., 2014) or using dried blood spots (DBS) from GD patients carrying the same mutations (Pchelina et al., 2017) have also reported increased intracellular A-SYN levels. However, neither the gene dosage, nor type of mutation, appeared to noticeably affect the degree of A-SYN accumulation in Schondorf study. Enhanced accumulation of A-SYN was observed following conduritol b-epoxide (CBE) exposure in SH-SY5Y cell model and substantia nigra of CBE injected mice (Manning-Bog et al., 2009, Cleeter et al., 2013, Magalhaes et al., 2016, Rocha et al., 2015b). CBE is an inhibitor of GCase and studies in which A-SYN accumulates suggested that the loss of GCase activity alone (e.g. no presence of ER stress) can affect A-SYN metabolism. Indeed A-SYN accumulation has been reported in *GBA* knock out mouse (*GBA*-/-), (Osellame et al., 2013). The exact mechanism controlling A-SYN aggregation and toxicity remain in part non-elucidated in which impairment of lysosomal function and recycling has been suggested (Magalhaes et al., 2016); see 1.6.1 for lysosomal function and A-SYN metabolism in PD.

1.7.2 A-SYN extracellular release

Interestingly, A-SYN can be released from cells and when aggregated in to fibrils and may have a prion like features that enable cell to cell transmission. This might explain the progression of Lewy pathology (LP) through the brain that was initially proposed by Braak (Lee et al., 2014, Braak et al., 2003). Different pathways have been suggested to explain how A-SYN is released and spread to other cells. When exogenous fibrillar A-SYN is taken up be 'naïve' cells, it becomes accessible to the soluble A-SYN for a period of time until it recruits the endogenous A-SYN and enhances the formation of insoluble Ser129 phosphorylated A-SYN and LB inclusions (Lee et al., 2014, Oueslati et al., 2014). There is an increasing evidence that phosphorylation of A-SYN is considered critical for aggerates formation and A-SYN mediated neurotoxicity (Oueslati, 2016) and as phosphorylated A-SYN makes 90% of the total A-SYN that is present in LB, posttranslational modifications is believed to be implicated in LB pathology (Migdalska-Richards and Schapira, 2016, Oueslati, 2016, Oueslati et al., 2010). Many studies reported accumulation of phosphorylated S129 A-SYN in the brain of PD patients as well as transgenic animal models of synucleinopathies (Fujiwara et al., 2002, Anderson et al., 2006, Neumann et al., 2002, Migdalska-Richards et al., 2017, Walker et al., 2013, Zhou et al., 2011).

In addition, converging lines of evidence indicate the A-SYN can be self-templated and aggregated in to fibrils that spread from cell to cell (Braak et al., 2003, Oueslati et al., 2014, Oueslati, 2016, Ugalde et al., 2016, Lee et al., 2014).

Post-mortem studies showed that PD patients who received fetal dopaminergic neuronal grafts revealed inclusion bodies similar to the Lewy bodies in these grafts several years after receiving the implants (Li et al., 2008, Kordower et al., 1995). PFFs seeding of neuronal cultures and wild type non-transgenic mice leads to recruitment of endogenous A-SYN which undergo conformational modification and convert in to fibrillar, Ser 129 phosphorylated protein and LB inclusions resembling those involved in PD pathology (Masuda-Suzukake et al., 2013, Grassi et al., 2018, Tapias et al., 2017, Luk et al., 2012, Emmanouilidou et al., 2010, Volpicelli-Daley et al., 2011, Zhang et al., 2019, Gegg et al., 2020). Furthermore, the extracellular fibrillary A-SYN species can induce chronic inflammatory response when taken up by microglia or astrocytes, the major scavengers of extracellular A-SYN which will further affect protein aggregation and neuronal viability when establishing a positive feedback loop between the neurons and the glial cells (Lee et al., 2014). The extracellular release of A-SYN fibrils from cells is strongly dependent of efficiency of protein degradation systems and neurons are releasing synuclein, perhaps in a free form or via exosomes, as a protective way to remove PFFs-induced accumulated intracellular A-SYN (Fussi et al., 2018). Evidence of exosomal dependent release of A-SYN has been proposed when lysosomal pathway was blocked in H4 cell culture and SHSY5Y cell lines overexpressing A-SYN (Danzer et al., 2012, Alvarez-Erviti et al., 2011, Emmanouilidou et al., 2010). Also, Desplats et al. study demonstrated that neuron-derived A-SYN can be transmitted from A-SYN overexpressing cells into transplanted embryonic stem cells in tissue culture and in to hippocampus of transgenic animals (Desplats et al., 2009). These findings further support the hypothesis by in which exosomes are described as "Trojan

horses" of neurodegeneration shipping toxic materials from prion infected cells to recipient cell and thus acting as initiators of cell death propagation (Ghidoni et al., 2008). In a recent work in our lab, it was shown that seeding MCN or differentiated SH-SY5Y dopaminergic cell cultures with PFFs has significantly induced the secretion and spread of A-SYN fibrils from neurones with GCase deficiency and could therefore account for increased spread of LP through the brain (Gegg et al., 2020).

1.8 Endoplasmic Reticulum (ER) Stress and Unfolded Protein Response (UPR)

Under physiological conditions, the newly synthesized proteins are subjected to ER quality control (ERQC) and only misfolded ones are retained in the ER (Bendikov-Bar et al., 2011). Proteins require chaperones to acquire a proper folding state and enter the secretory pathway (Malhotra and Kaufman, 2007, Dubnikov and Cohen, 2017) Accumulation of misfolded proteins in the ER leads to activation of the unfolded protein response (UPR), with persistent activation of the UPR inducing ER stress (Amen et al., 2019, Lindholm et al., 2017, Colla, 2019). The most immediate response to ER stress is upregulation of binding immunoglobulin protein (BiP)/GRP78, an ER HSP70 family protein, due to its release from the three ER sensors and subsequently turning them to the active state. In response to this, the three ER localized transducers IRE1, PERK and ATF6 dissociated from (Bip/GRP78) become activated to initiate an adaptive unfolded protein response (UPR), (Amen et al., 2019, Colla, 2019, Remondelli and Renna, 2017, Lehtonen et al., 2019), (Figure 0.7).

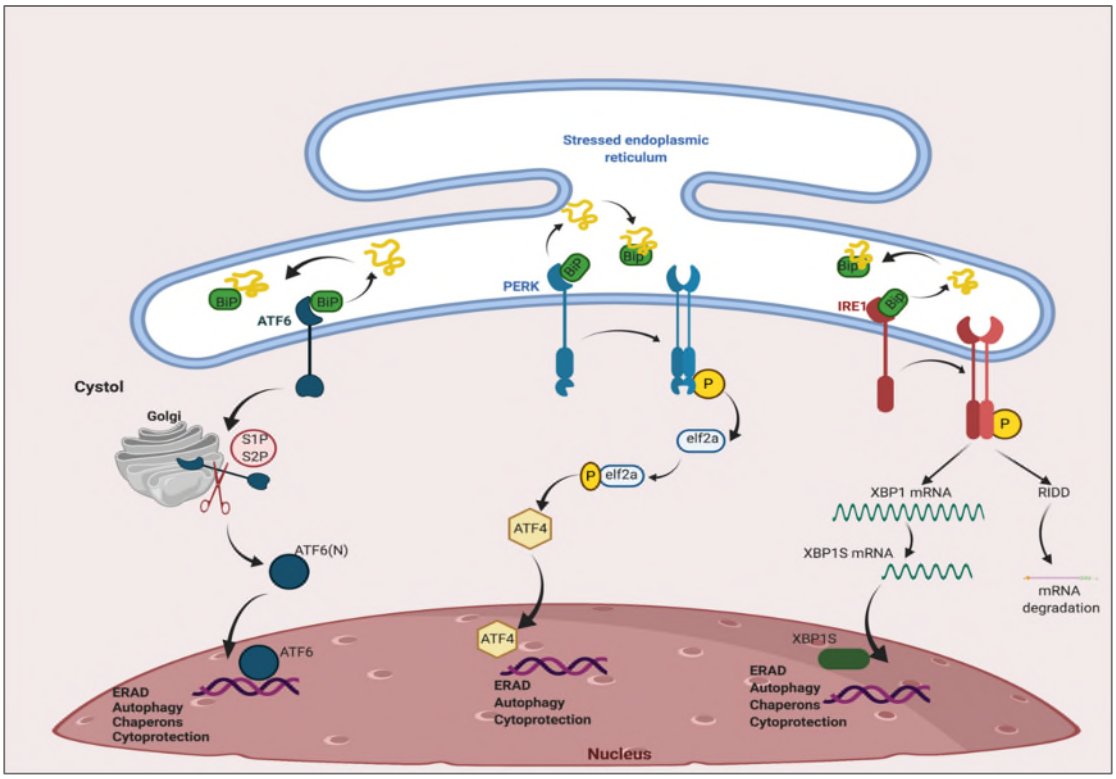

Figure 0.7 ER stress and Unfolded Protein Response (UPR): In the absence of stress, the, PERK, ATF6 and IRE1 sensors remain in the inactive state due to their association with the chaperone BiP/GRP78. Once detached from BiP, IRE1 and PERK self-phosphorylate and become activated for downstream signaling; the first branch of the UPR is PERK signalling cascade which is capable of phosphorylating eukaryotic translational initiation factor 2 (elf2α). This phosphorylation inactivates elf2α to reduces general protein synthesis. and alleviates the folding machinery. Blockage of elf2α also leads to activation of the transcription factor ATF4, which is directed to the nucleus to bind to several genes involved in the control of antioxidant response, ERAD, Lipid synthesis, and ER translocation. After it dissociates from BiP, the transmembrane protein ATF6 translocates into Golgi apparatus where it is cleaved by S1P and S2P proteases to produce a cytosolic fragment. This fragment interacts with different nuclear partners, allowing it to upregulate the transcription of ER chaperones involved in ERAD process and activation of macroautophagy. The third of UPR players is IRE1 which is constitutively inactive when associated to BiP. Accumulated misfolded proteins in ER, however, lead to dissociation of IRE1 from BiP with subsequent dimerization and autophosphorylation to completely activate its endoribonuclease function. IRE1 activity results in atypical splicing of XBP1 mRNA in the cytoplasm to generate a stable and active XBP1 protein known as XBP1-S (XBP1-spliced). This is a transcription factor composed of a nuclear compartment targeting signal sequence which control the expression of factors modulating amino acids synthesis and transport, ERAD, autophagy, CHOP and apoptosis.

Under ER stress, the activated PERK arm phosphorylates elf2 α to become inactivate and thus eventually attenuates mRNA translation. This helps to prevent synthesis of new proteins that might augment the already present stress. Collectively, this indicates that UPR is a tightly orchestrated collection of signaling pathways which acts as sensitive surveillance for unfolded proteins to restore homeostasis and ensure a proper folding state of protein before directing them to the secretory pathway (Malhotra and Kaufman, 2007, Díaz-Villanueva et al., 2015, Colla, 2019, Hetz et al., 2020).

UPR delivers information about protein folding to nucleus and cytosol and adjusts the protein folding capacity of the cell by removing misfolded proteins from the ER towards the proteasome via protein chaperones for degradation in a process called ER-associated degradation (ERAD), (Stolz and Wolf, 2010, Hetz et al., 2020, Colla, 2019, Remondelli and Renna, 2017). However, and despite being protective response of the cell, persistent stress and UPR will render the cell sensitive to apoptotic stimuli and may predispose to death (Malhotra and Kaufman, 2007, Sano and Reed, 2013, Iurlaro and Muñoz-Pinedo, 2016).

UPR is also an energy dependent mechanism that need ATP for maintaining high Ca^{2+} pool required for chaperon function and ERAD (Malhotra and Kaufman, 2007). Thapsigargin is known to block the ER Ca^{2+}-ATPase through non-competitive inhibition leading to perturbed Ca^{2+} homeostasis and activation of UPR (Sehgal et al., 2017b, Dubois et al., 2020, Quynh Doan and Christensen, 2015). It has been previously observed that the use of even low concentration (0.1uM) of Thapsigargin targeted prostate and breast cancer cells induced ER stress via extensive drainage Ca^{2+} storage leading ultimately to cellular death and

apoptosis. In this study, the induced apoptotic pathway was mainly mediated through CHOP/GADD153 (Sehgal et al., 2017a).

ER stress and UPR also play fundamental role in the pathogenesis of neurodegenerative disease like PD (Remondelli and Renna, 2017). Phosphorylated PERK and eIF2α were found co-localized with A-SYN, in dopaminergic neurons of PD patients (Sugeno et al., 2008). Furthermore, null mutation in CHOP reduced the 6-hydroxydoamine-induced apoptosis in substantia nigra of PD animal model (Silva et al., 2005). Aggregated oligomeric A-SYN in the ER of A53T *SNCA* transgenic mouse model induced ER stress and UPR that eventually resulted in inflammation and neurodegeneration (Colla et al., 2012).

ER stress and UPR are also pathologically relevant to *GBA*-PD. Analysis of the two ER-resident chaperones involved in UPR, Bip/GRP78 and calreticulin, revealed significant upregulation of these chaperons as well as activation of the IRE component of the UPR in *GBA*-N370S dopaminergic neurons from PD patients (Fernandes et al., 2016) and in GD fibroblast (McNeill et al., 2014) Furthermore, GCase mutant protein undergoes ERAD in skin fibroblasts originated from GD patients homozygous for L444P mutation (Bendikov-Bar et al., 2011). Dysregulation of calcium homeostasis and increased vulnerability to stress responses and neurodegeneration has been observed in iPCs-derived neurons and patients derived fibroblast with *GBA* mutation (Schondorf et al., 2014, Kilpatrick et al., 2016). PFF s seeding of differentiated SH-SY5Y cells and MCN treated with CBE has recently showed to inhibit lysosomal GCase activity and induce upregulation of BiP marker of UPR reflecting impaired trafficking of GCase in to the lysosomes (Gegg, 2020).

Under normal physiological conditions, GCase is transported by LIMP2 and not by mannose phosphate receptor (MPR). In MPR double KO MEF, GCase sorting and activity was not affected confirming that the enzyme is trafficked to the lysosome by binding to LIMP2 in the ER and not via MPR dependent manner (Reczek et al., 2007). The tow common *GBA* mutations associated with GD and PD such as N370S and L444P activate the UPR and undergo ERAD when unable to be refolded. One of the key regulators of this process is the E3 ubiquitin ligase ITCH (also known as atrophin-1-interacting protein 4). ITCH chaperone was seen to interact with mutant GCase variants and mediate their polyubiquitination and subsequent proteasomal degradation in GD fibroblasts (Maor et al., 2013). Likewise, in the case of N370S and L444P mutations, GCase was found to bind firstly to Hsp70 for proper folding, and upon failure of this, to Hsp90 which directed the protein to the UPS (Lu et al., 2011). Ambroxol and Isofagomine are identified as a pharmacological chaperone for mutant GCase, they enhanced the proper folding and increase activity of the mutant enzyme in GD fibroblast and animal model. Therefore, they should be considered as a potential therapeutic agent for Parkinson disease in terms of both increasing trafficking of GCase to the lysosome and reducing ER stress (Ambrosi et al., 2015, Sanchez-Martinez et al., 2016, Bendikov-Bar et al., 2011, McNeill et al., 2014).

1.9 Mitochondrial Dysfunction in *GBA*-Linked PD

Loss of GCase activity in *GBA*-PD can also result in mitochondrial dysfunction (Gegg and Schapira, 2016). Lysosomes are essential for autophagic clearance of dysfunctional mitochondria and represent an important element of mitochondrial quality control (de la Mata et al., 2016). Defective NADH-ubiquinone reductase (Complex I) activity was first observed in the substantia nigra of sporadic PD patients (Schapira et al., 1989, Schapira et al., 1990). Accordingly, many laboratories have developed PD models by utilization of compound such as MPTP (1-methyl-4-phenyl-1,2,3,6-tetrahydropyridine) and pesticide like rotenone which act as a well-known mitochondrial complex I inhibitors (Langston et al., 1999, Martinez and Greenamyre, 2012, Cassarino et al., 1999). Degeneration of substantia nigra neurons through inhibition of complex I activity was reported in PD patients years after exposure to MPTP (Langston et al., 1999) In addition, Rotenone has been reported to selectively damage nigral dopaminergic neurons in vitro (Marey-Semper et al., 1995, Wang et al., 2020, Cheng et al., 2020, Testa et al., 2005) and in vivo (Betarbet et al., 2000, Feng et al., 2006, Guo et al., 2018, Wen et al., 2011, Sanders and Timothy Greenamyre, 2013, Wang et al., 2020, Miyazaki et al., 2020) which further supports the involvement of mitochondrial complex inhibition in PD pathogenesis.

Mutations in PARK2, PINK1, and DJ-1 redox sensing genes are associated with defective mitochondria and cause familial PD (Schapira, 2008, Cookson, 2012, Pickrell and Youle, 2015, Grünewald et al., 2019). In *GBA* linked PD, perturbation of mitophagy, accumulation of A-SYN, defective calcium homeostasis and build-up of oxygen free radical species are all implicated in the pathogenesis and increase vulnerability to neuronal cell death (Gegg and Schapira, 2018).

The presence of mitochondrial dysfunction with significant reduction in mitochondrial membrane potential (ΔΨm) and diminished ATP production has been reported in GD fibroblasts harboring the L444P mutation (de la Mata et al., 2015). Also, pharmacological inhibition of GCase by CBE in SH-SY5Y cells also reduced mitochondrial membrane potential (ΔΨm) and increase production of reactive oxygen species (ROS), together with accumulation of A-SYN. These observations were indicative that GCase loss-of-function can trigger oxidative stress and mitochondrial dysfunction in human dopaminergic cell lines (Cleeter et al., 2013). Additionally, defective mitochondrial quality control has been proposed to contribute to the mitochondrial dysfunction observed in the brains of a mouse *GBA* knockout model (Osellame et al., 2013). Recently, Li et al. (2019) investigated the link between heterozygous L444P mutation and mitochondrial dysfunction and showed that *GBA* mutation triggers mitochondrial dysfunction by blocking induction of mitophagy. Moreover, Schöndorf et al. (2018) demonstrated that iPCs neurons derived from GD patients showed alterations in morphology, energy metabolism, and mitochondrial dysfunction (Schondorf et al., 2018, Li et al., 2019). Importantly, mitochondrial defects were more exacerbated in *GBA* wt/L444P mice and in primary neuronal cultures derived from the same mice. The defective mitochondrial dysfunction detected in wt/L444P mice was more exacerbated after being exposed to MPTP treatment (Yan et al., 2018). This observation was suggestive that L444P *GBA* heterozygous mutation can lead to mitochondria defects both in vitro and in vivo.

1.10 Hypothesis and Aim of work

GBA gene mutations are numerically the most important predisposing factor for developing PD. We hypothesized that heterozygous L444P mutation is implicated in the pathophysiology of PD through a gain-of-toxic function as a result of trapped mutant misfolded GCase in ER with subsequent induction of ER stress and unfolded protein response (UPR). Failure to properly refold GCase may ultimately lead to ER associated degradation (ERAD) with a concomitant impaired trafficking of enzyme to lysosomes. This secondary loss-of-function effect may therefore perturb the lysosomal function and consequently result in defective protein quality control leading to A-SYN dysmetabolism and mitochondrial impairment observed in PD pathogenesis.

In addition, it is well established that homozygous L444P mutations cause type 2 and 3 GD which are severe clinical subtypes associated with death in infancy or early adolescence Also, patients with homozygous L444P mutations will not reach an age to develop PD. We therefore sought to investigate the effects of heterozygous L444P mutation.

The aim of this work will be to investigate the effect of heterozygote L444P mutation in human dermal fibroblasts and mouse cortical neurons. We will be studying specifically the pathological process involved in PD progression including defects in A-SYN dysmetabolism caused by ALP and UPS dysfunction, ER stress and UPR, mitochondrial dysfunction and cell death. Since dopaminergic neurons in the substantia nigra are the most vulnerable type of cells affected in PD, the above mechanisms will also be investigated in differentiated dopaminergic SH-SY5Y cells treated with the GCase inhibitor CBE or over expressing L444P *GBA*.

2.Material and methods

2.1 Cell lines and Cultures

2.1.1 Chemical and Reagents used in Cell Cultures

Unless otherwise stated, chemicals and reagents used in culturing MCN, fibroblasts and different differentiating SHSY5Y cell lines were obtained from Sigma (Gillingham, Dorset, UK) and ThermoFisher Scientific (Paisley, UK).

2.1.2 Human Dermal Fibroblast Culture

Establishment of fibroblast cultures was done previously by members of our laboratory following experimental approach and guidelines described in (section 3.3). Dermal fibroblasts were generated following local ethical approval from the Hampstead Research Ethics Committee; reference number 10/H0720/21. All individuals provided a written informed consent. Briefly, human dermal fibroblasts lines used in the experiments were obtained from 5 wild type and 5 L444P heterozygous mutants with and without PD (Table 0.3).

Table 0.3 Demographic data of human dermal fibroblast lines used in this project.

Patient	Age at time of Biopsy (years)	Gender	Genotype	+/- PD
Ctl9	52	F	wt/wt	—
EOR	50	F	wt/wt	—
JEC	82	F	wt/wt	—
JER	52	F	wt/wt	—
MCL	59	M	wt/wt	—
CHM	72	M	wt/△	+PD
TCH	45	F	wt/△	—
MBA	67	M	wt/△	—
BSL	85	M	wt/△	+PD
PJR	62	M	wt/△	—

The culture media was comprised of Dulbecco's Modified Eagle Medium (DMEM) with 1X Glutamax and Glucose (4.5 g/L) supplemented with 10% (v/v) Fetal bovine serum, Sodium Pyruvate (1mM final concentration), 50U/ml Penicillin, 50 μg/ml streptomycin antibiotics, and 0.1 mM of NEAA: (glycine, L-alanine, L-asparagine, L-aspartic acid, L-glutamic acid, L-proline and L-serine). For routine cell culture, each cell line was passaged in 10cm plate when reaching 80% confluent by trypsinization for enzymatic detachment. Cells were washed once with 1X Sterile phosphate buffered saline (PBS) and incubated in 1ml of trypsin (0.25% (w/v) trypsin in Versene) for 5 minutes at 37°C. Plates were then tapped to encourage mechanical detachment and after neutralizing trypsin with growth media, cells were centrifuged at 200 xg for 5 minutes at room temperature (RT) to produce cell pellet.

Following this, supernatant was discarded and pellets were resuspended in either fresh media and re-plated accordingly (usual dilution1:3) or in freezing medium (1/3 of 80% confluent plate in 90% (v/v) FBS, 10% (v/v) DMSO) and cryopreserved in a stepwise manner starting first with -80 °C then transferred to Liquid Nitrogen for maintaining cell line stock.

2.1.3 Primary Neuronal Culture (Mouse Cortical Neurons (MCN))

Mice were treated in accordance with local ethical committee guidelines and the UK Animals (Scientific Procedures) Act 1986. The colony was maintained under project license 70/7685 issued by the UK Home Office. B6;129S4-Gbatm1Rlp/Mmnc (000117-UNC) mice expressing heterozygous knock-in L444P mutation in the murine *GBA* gene (L444P/+ mice) were purchased from the

Mutant Mouse Regional Resource Centre (MMRRC; Davis, CA, USA), (Liu et al., 1998).

For setting up mouse cortical neuronal (MCN) cultures, primary neuronal cultures were prepared from embryonic day 15-17 mouse brain following the standard procedures. Briefly 6 wells plates were first coated with1ml of 0.1 mg/ml poly-ornithine solution for an hour. After removing poly-ornithine, each well washed with 1 ml 1xPBS and left to dry in hood for 60 minutes prior to experiment. Dissected head and body of each embryo was placed separately in ice cold PBS-G (1.6% (w/v) glucose in PBS). A shallow cut of skin along midline to snout was made and peeled back to scoop out the cortex. Cerebellar tissue was taken from each embryo and stored at -20°C for genotyping. The 2 cortices were then placed in a small petri dish with 1mL of PBS-G (1dish/brain) after removing meninges under the microscope. Homogenization of the dissected cortex was done several times with a syringe (23G) until 100% homogeneous. Homogenate was then transferred to a 15mL Falcon tube (with 1mL of PBS-G) and incubated for 10 minutes at RT to allow debris to settle. After discarding debris, homogenate was centrifuged for 10 minutes at 500 x g with supernatant aspirated from the resulting cell pellet. Neurons were resuspended in serum free neurobasal medium supplemented with 1X B27 supplement, 1x Glutamax and 5 ml antimycotic/antibiotic solution. Typically, 2 cortices were seeded in to 6-wells at a cell density of $1X10^6$ cells/ 2 wells. Cultures were maintained in a humidified 37°C incubator with 5% CO_2 for no longer than 14 days with media replaced every 3 days. At end of experiment, conditioned media was collected and the detached cells and debris were removed by centrifugation at 200 xg after which the media were frozen at -80°C. Neurons were harvested with 100µl trypsin/well

and following neutralization with media, easily detached cell monolayer was collected using 1ml pipette and centrifuged at 200 xg for 5 minutes. Cell pellet was resuspended in 1X PBS and recentrifuged for another 5 minutes after which supernatant was discarded and pellets were frozen at -80°C for downstream experiments.

For cell viability assay, neurons were cultured in 96 well plate precoated with poly-ornithine solution, seeded with PFFs (5 µg/ml) on 4 or 5 DIV and assay was conducted on 14 DIV.

2.1.4 Generation of Overexpressing (O/E) WT *GBA* and (O/E) wt/L444P *GBA* SH-SY5Y Cell Lines

The human neuroblastoma SH-SY5Y cell lines were obtained from the European Collection of Cell Cultures and cultured in DMEM/F-12 Nutrient Mix (1:1) with GlutaMAX^{TM}-I supplemented with 10 % (v/v) fetal calf serum (FCS, BioSera), penicillin (50 U/ml final), streptomycin (50 ng/ml), sodium pyruvate (1 mM) and non-essential amino acids.

Human wild-type *GBA* or mutant L444P *GBA* in mammalian expression vector pCDNA3.1 (generated by David Chau, Department of Clinical and Movement Neurosciences, UCL) were transfected from low passage SH-SY5Y parental cell line using xtreme GENE HP DNA transfection reagent (generated by Dr. Matthew Gegg, Department of Clinical and Movement Neurosciences, UCL). Briefly, 2 x 10^5 cells/ml were seeded in complete culture medium, transfected with a mix of 1 µg plasmid DNA and 1 µL of transfection reagent and were passaged 72 hours after transfection. Stable cell lines expressing the constructs were selected by supplementation of culture media with 400 µg/ml G418. Colonies were harvested

and cultured individually and positive clones were analyzed for the presence of *GBA* by mRNA analysis and western blot.

2.1.5 Growing Parenteral SH-SY5Y, (O/E wt/wt *SNCA*), (O/E A53T *SNCA*), (O/E wt/wt *GBA*) and (O/E wt/L444P *GBA*)

The two SH-SY5Y lines C205 (O/E wt *SNCA*) was kindly provided by Dr. Mark Cooper (Department of Clinical and Movement Neurosciences, UCL) and have been described elsewhere (Chau et al., 2009).

All undifferentiated SH-SY5Y lines were cultured in DMEM: F12 (1:1) growth medium supplemented with 10% (v/v) fetal bovine serum, Sodium Pyruvate (1mM final concentration), (50U/ml Penicillin and 50 µg/ml streptomycin) antibiotics, and NEAA: (0.1 mM of: glycine, L-alanine, L-asparagine, L-aspartic acid, L-glutamic acid, L-proline and L-serine) at 37°C and 5% CO_2. Each line was grown in 10cm plate, and was passaged at 80% confluency via trypsinization. Cells were washed once with 1X PBS and incubated 1ml of trypsin (0.25% trypsin in Versene) for 1-2 minutes at 37°C and plates were gently tapped to encourage mechanical detachment. After neutralizing trypsin with growth media, Cells were centrifuged at 200 xg for 5 minutes at room temperature (RT) to pellet cells. After discarding supernatant, pellet was resuspended in either fresh media and re-plated accordingly (usual dilution was 1:3) or in freezing medium (1/3 of 80% confluent plate in 90% (v/v) FBS, 10% (v/v) DMSO) and cryopreserved in a stepwise manner starting first with -80°C then transferred to Liquid Nitrogen for maintaining cell line stock.

2.1.6 Differentiation of Parenteral SH-SY5Y, (O/E wt/wt *SNCA*), (O/E A53T *SNCA*), (O/E wt *GBA*) and (O/E wt/L444P *GBA*)

The current PD research is mostly performed on SH-SY5Y cells due to the challenges in obtaining dopaminergic neurons and maintaining them as a primary cells. In addition, SH-SY5Y cells are human in origin, easy to maintain and have neuronal preparties. Therefore, different differentiation protocols have been applied to establish a permanently neuronal cultures from these cells (Xicoy et al., 2017, Sidell, 1982). The rapid and simple procedure presented herein, for generating a fully differentiated dopaminergic SH-SY5Y cell model, was based on modifying previous old protocol reported in (Farooqui, 1994). We determined an optimization of the seeding density for at least 10 days of both the parental SH-SY5Y line and those overexpressing wild-type and mutant proteins. Such a procedure yields a 100% homogenous cell population with a neuron–like phenotype, little proliferation and increased tyrosine hydroxylase (TH) expression (both mRNA and protein). Prior to differentiation, either 6 well plates or 60mm dishes were coated first with 1 ml/well of 0.1 mg/ml poly-ornithine solution for an hour. After removing poly-ornithine, each vessel was washed with 1 ml 1xPBS and recoated with the extracellular matrix proteins, 2µg/ml fibronectin and 1µg/ml laminin in 1XPBS for another 1 hour. Coating solution was aspirated immediately before seeding cells with no need for another PBS wash and SH-SY5Y lines were harvested by trypsinization as described above. Each SH-SY5Y pellet was resuspend in 1ml of differentiation media comprised of neurobasal media and supplemented with 1X B27, 50U/ml Penicillin and 50 µg/ml streptomycin antibiotics, 30µM retinoic acid (RA), and 10ng/ml of recombinant human brain derived neurotrophic factor (BDNF; R&D Systems, Abingdon, UK). An aliquot of cells was diluted 1:5 in media and mixed with trypan blue in a ratio of 1:1 after

which cells of each SH-SY5Y line were counted and seeded at density of 3x 10^5cells/ml in to the previously coated vessels in volume of 1.5 ml/ well in 6-well plate and 4 ml/60 mm plate. The initial density was further optimized for SH-SY5Y (O/E wt/wt *SNCA*) cell line to be 4.5 x 10^5 cells/ml as they developed some cell death between 4 and 7 DIV. During differentiation, media were replaced every 2- or 3-days with all treatments protected from light. The 10 days of culturing SH-SY5Y lines in RA induced a full neuronal differentiation and neurite outgrowth with the simultaneous addition of BDNF to improve the cell survival.

In a parallel culture, we differentiated parenteral SH-SY5Y line using the old method (n=1). The 60mm culture plate was not coated prior to seeding and no BDNF was used. Additionally, seeding density was as low as 0.4 x 10^5 cells/ml and cells were cultured instead in DMEM/F-12 nutrient supplemented with 10 % (v/v) fetal calf serum as outlined in (section 2.1.5) with retinoic acid (RA) added in a concentration of 30µM for ten days. The different neuronal morphology between the new and older method is shown in (Figure 0.8).

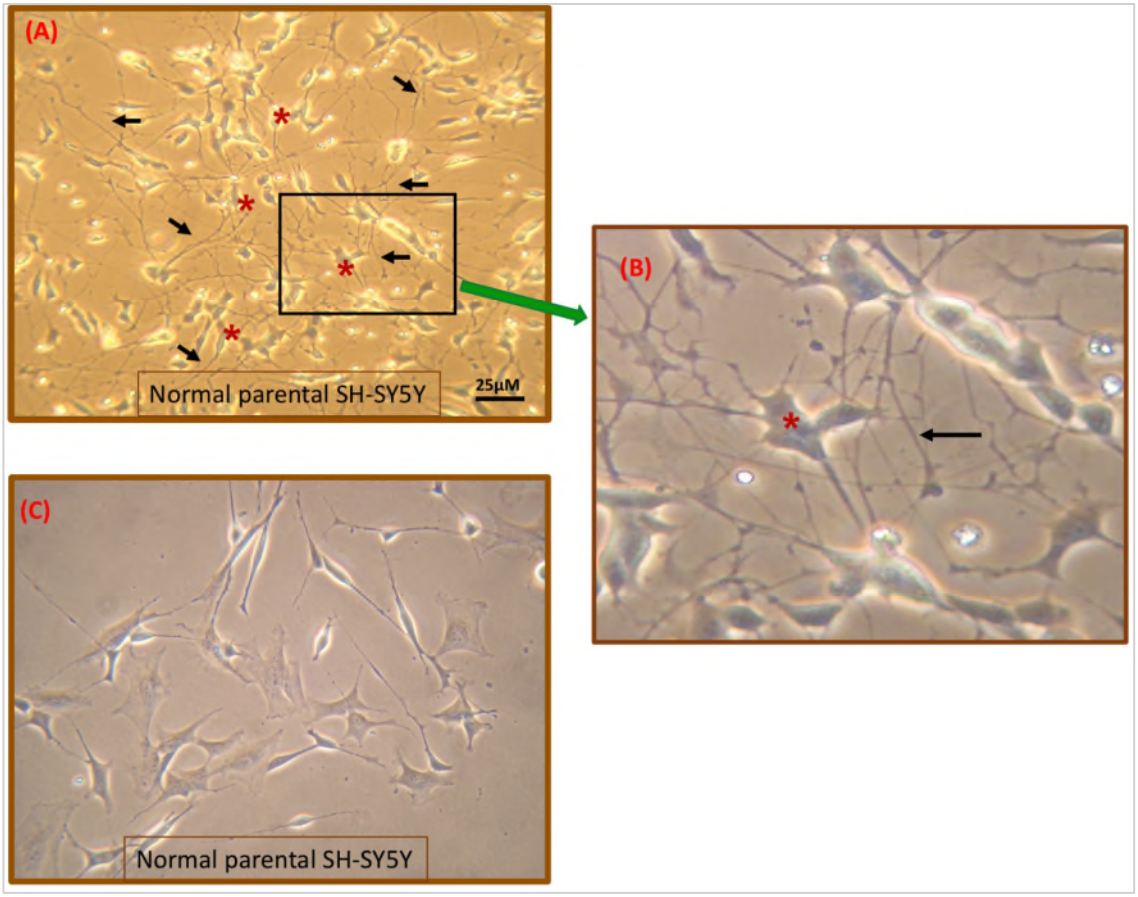

Figure 0.8 Differentiation of SH-SY5Y cell lines (new vs old method). (A, B): Light microscopic images of differentiated of SH-SY5Y cell lines (new vs old method), pictures taken on 10DIV; (A) Effects of (30 µM RA + 10 ng/ml BDNF) treatment in differentiating normal parental SH-SY5Y cells for 10 days showing complex neuronal morphology and no longer divide (×10, Scale bar represents 25 µM), black arrows indicate neurites and red asterisks indicate cell bodies. (B): The boxed region in (A) is shown on the right at higher magnification (×10). (C) Differentiated normal SH-SY5Y cells cultured for 10 days using the old method (×20); DMEM: F12 media supplemented with 10% FCS and 30 µM RA was unsuitable for the complete acquisition of complex neuronal network, cell islets were sparse showing less neurites extension and apparently retaining higher proportion of morphologically distinct substrate adherent (S) type cells.

2.1.7 Pharmacological Treatment Invitro

2.1.7.1 Bafilomycin A1 treatment

Upon harvesting either fibroblast or MCN cultures, 0.2µM of Bafilomycin A1(Sigma) was added to plate to measure macroautophagy flux. treated cells were incubated for 4 hours (fibroblasts) and 6 hours (MCN) at 37°C incubator until the time of collection.

2.1.7.2 Epoxomicin Treatment

Sub-confluent human skin fibroblasts, grown on 10cm plates, were treated with 25nM of proteasomal inhibitor Epoxomicin 24 hours prior to collection. Following this step, the obtained cell lysates were subjected to Endo-H assay and western blot analysis as described in (section 2.5.12).

2.1.7.3 GW4689 Treatment of Mouse Cortical Neurons

2.5mM/well of neutral sphingomyelinase inhibitor (GW4689) was used to treat mouse cortical neurons cultured in 12 well plate 24hours prior to collection. At time of collection, the obtained conditioned media were stored at -80°C until the time of downstream analysis by dot blot.

2.2 Immunocytochemistry Staining of Cultured Mouse Cortical Neurons

MCN were prepared and cultured as described above on poly-ornithine coated glass coverslips for 10 days. coverslips following three PBS washes were first fixed by applying 4% (w/v) fresh paraformaldehyde (Santacruz) in 1xPBS for 15 minutes at room temperature (RT) and permeabilized with 0.1% (v/v) TX-100 in 1xPBS for another 10 minutes. Cells were then blocked with 150µL of (5 % v/v) of normal goat serum (Sigma) in 1xPBS with 0.1% (v/v) TX-100 for 30 minutes at 37°C in a humidified atmosphere. Subsequently, slips were drained and incubated with 150 µL of diluted primary antibody in the dilutions specified in

(Table 0.5) with1x PBS+0.1% (v/v) TX-100 for 45 minutes at 37°C in a humidified atmosphere. Following this, cells were incubated with 100 µl of 1:200 diluted secondary antibody tagged with an Alexa® fluorophore (Table 0.5) in 1xPBS + 0.1% (v/v) TX-100 for 30 minutes at 37°C in a humidified atmosphere. Coverslips were washed 3 times with 1xPBS between each step. Finally, cover slips were mounted in Citifluor/PBS/glycerol supplemented with 2 µg/ml of DAPI (4',6-diamidino-2-phenylindole, Sigma) and cells were visualized using a Zeiss Axioplan fluorescent microscope using a 40X objective. Images were acquired using a CoolSNAP MYO digital camera (Photometrics, Tuscon, AZ, USA) and processed using Image J software (NIH, Bethesda, MD, USA).

2.3 Genotyping of Mouse tissues and human fibroblasts

Unless otherwise stated, chemicals were obtained from Sigma or ThermoFisher Scientific.

2.3.1 Mouse Tissue Digestion

Samples (cerebellar tissue) were collected for genotyping and digestion mix was made Direct PCR lysis buffer (Viagen) supplemented with 1mg/ml proteinase K. Digestion was carried out in 200 µL overnight at 58°C followed by 85°C for the last 45minutes.

2.3.2 Polymerase Chain Reaction (PCR) for Mouse Genotyping

GoTaq PCR kit was supplied by Promega. This ready-to-use, optimized kit includes everything required for high-fidelity PCR except primers and dNTP mix. Both were purchased from euro-Fins for amplification of wt/L444P in mice transcripts. Sequence of each primer is displayed in (Table 0.4).

Briefly and as per manufacture instructions, PCR mix/sample was made of (0.4 µL 40 mM dNTP mixture, 0.2 µL taq polymerase (0.4 units), 1µL of each forward

and reverse primer (0.5 µM final concentration), 4 µL 5X GoTaq buffer, 1-2µL of DNA, and 12.25 µL of RNAse/DNAse free H_2O). PCR was set with an initial activation step at 95°C for 2 minutes. This was followed by 35 cycles of complete denaturation of all double stranded DNA at 98°C for 15 seconds, primer annealing at 58°C for 60 seconds and extension at 72°C for 60 seconds after which a final extension step was set at 72°C for 5 minutes, (Figure 0.9). Correct DNA product (550 bp) was assessed by running on 2% agarose gel electrophoresis.

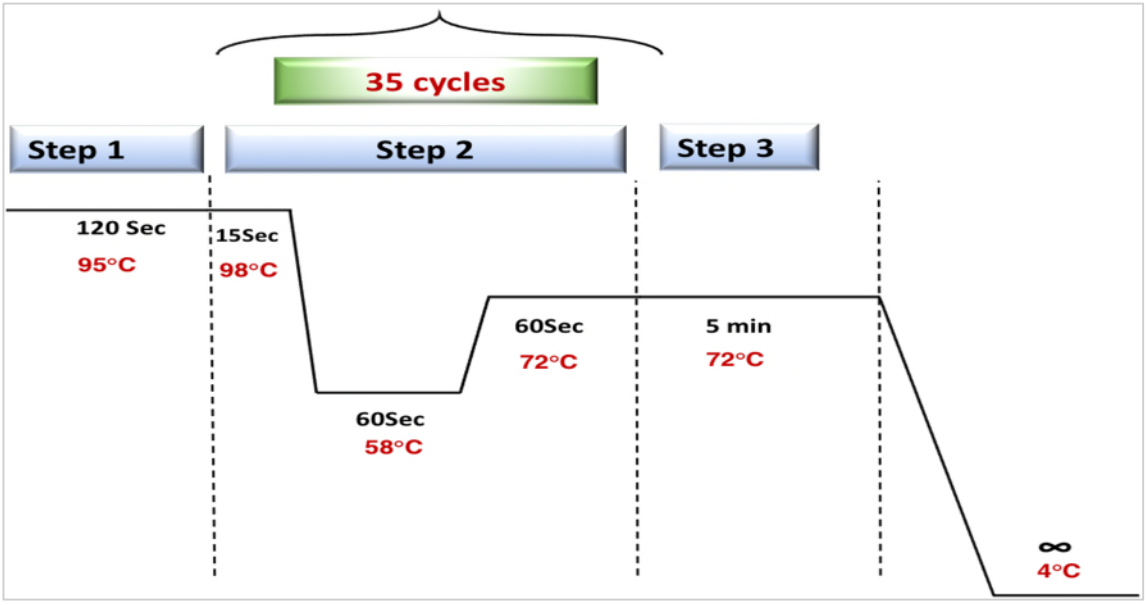

Figure 0.9 PCR cycle steps for amplifying wt/L444P of mice transcript.

2.3.3 Agarose Gel Electrophoresis

2 % (w/v) of Agarose (Bioline) was added to 1x TAEbuffer (comprised of 40 mM Tris, 20 mM acetate and 1 mM EDTA at pH 8.6) and dissolved in a microwave. Once cooled, 10 µL of SafeView DNA/RNA stain (NBS Biologicals) was added to the solution which was then poured into a gel compartment and allowed to set. The gel was submerged in a 700ml of 1xTAE buffer and loaded with 5µL of each PCR sample with water blank included as a negative control. Electrophoresis ran at 100 V for 30 minutes and nucleic acids were visualized with GelRed program on ChemiDoc imaging system (BioRad) using Hyper ladder 1Kb (Bioline). Visualization of single band about 550Kb in size was considered positive for heterozygous L444P mutant. Remainder of samples were sent for Sanger sequencing at Source Bioscience (Cambridge, UK) using L444P forward and reverse primers in (Table 0.4) and sequences were checked using Genome Compiler software.

2.3.4 Sequencing Protocol for Fibroblasts

Qiagen RNeasy kit was used for RNA isolation and nanoScript2 reverse transcription kit (PrimerDesign) was used for cDNA synthesis as per manufacturer's instructions. RNA, isolated from homogenized fibroblasts cell pellets, was eluted in RNase and DNase free water and its concentration was calculated using a Nanodrop (ThermoScientific). 500ng of RNA was converted to cDNA using nanoScript2 reverse transcription kit (PrimerDesign). Briefly, RNA was annealed to oligodT and random nonamer primers for 5 minutes at 65°C. Each sample was then mixed with 1X reaction buffer, 0.5 mM dNTPs and 1µL of reverse transcriptase and incubated at 25°C for 5 minutes, 42°C for 20 minutes and 75 °C for 10 minutes.

PCR master mix for genotyping was prepared using 0.2 µL Phusion Green HS II HF PCR Taq polymerase (2U/µL), 1µL 40 mM dNTP mix), 1µL of each Primer (GP551/552,10 µM each), 4 µL 5X Phusion Taq buffer, 1µL of cDNA and 12.25 µL of RNase/DNase free H_2O). PCR was set with an initial activation step at 98°C for 30 seconds. This was followed by 35 cycles of complete denaturation of all double stranded DNA at 98°C for 10 seconds, primer annealing at 63°C for 30 seconds and extension at 72°C for 30 seconds after which a final extension step was set at 72°C for 10 minutes (Figure 0.10). Correct DNA product was assessed by running on 2% agarose gel using Hyper ladder 1Kb **(Bioline)** and visualization of single band about 550Kb in size was considered positive for *GBA* amplicon. Samples were sent for Sanger sequencing at Source Bioscience using GP551 and GP552, (Table 0.4). Sequences were checked using Genome Compiler software, (Figure 0.11).

Table 0.4 Nucleotide sequences of primers used to amplify DNA from mouse tissue and human *GBA* L444P. GP551 and GP522 primers were used for human dermal fibroblast sample sequencing whereas L444P primers used for sequencing mouse samples.

Primer	Sequence
L444P F	CCCCAGATGACTTGATGCTGG
L444P R	CCAGGTCAGGATCTCTGATGG
GP551	5′- CAACACCATGTCCTTTGCCTC -3′
GP552	3′- CGCCACAGGTAGGTGTGAATG -5′

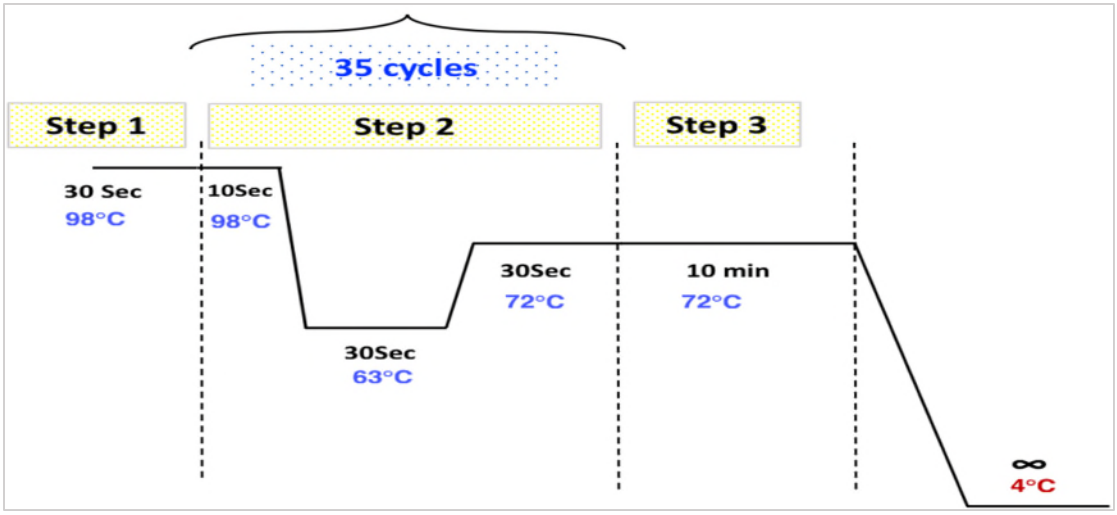

Figure 0.10 PCR cycle steps for amplifying human *GBA* L444P.

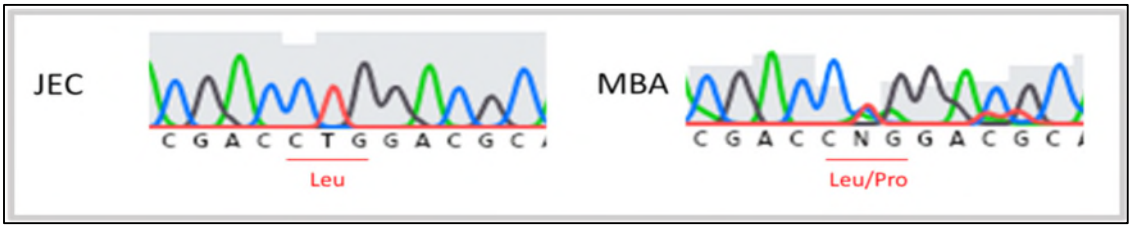

Figure 0.11 DNA sequences results of wildtype and L444P heterozygous human dermal fibroblasts. Sequences are showing WT codon (CTG, Leu; underlined in red) in control fibroblasts (JEC) and WT codon (CTG, Leu) or mutant codon (CCG, Pro) in WT/L444P mutant patient derived fibroblast line.

2.4 Treatment of Cultured SH-SY5Y and Mouse Cortical Neurons with Preformed Alpha-Synuclein Fibrils (PFFs)

Alpha-synuclein (A-SYN) in its fibrillar form (PFFs) has been shown to induce the conversion of endogenous soluble a-synuclein into insoluble forms which aggregate and become phosphorylated at Ser129, (Grassi et al., 2018, Tapias et al., 2017). Animal models have shown that the A-SYN fibrils, but not monomeric forms, can cause spread of Lewy body-like pathology in mouse brain and is associated with cell death of particular neuronal populations (Luk et al., 2012). The fibrils used in the project have been made and extensively characterized by the laboratory of Professor Vittorio Bellotti (UCL Amyloidosis Centre). Members of Department (Dr M Gegg and Dr M Di Stefano) have shown that these fibrils can induce aggregation of A-SYN in control neurons within 10 days of treatment (unpublished data). Also, the same source of PFFs also induces A-SYN pathology in vivo following striatal injection of mice (Izco et al., 2019). Different differentiated SH-SY5Y cell lines and cultured mouse cortical neurons treated with PFFs were investigated for downstream events such as formation of insoluble/aggregated/phosphorylated A-SYN, cell death, and or mitochondrial dysfunction.

Briefly, cells were cultured in respective media until they were ready for treatment. In case of MCN, neurons were treated with PFFs on 4 or 5 DIV whereas differentiating SH-SY5Y cells were seeded with PFFs on 3 or 4 DIV when cells were beginning to show neuronal morphology and not noticeably proliferating.

To improve seeding activity and normalize fibril size/length, 50 µL of PFFs stock (2mg/ml in PBS) was aliquoted in to Eppendorf and fragmented to smaller size through sonication for 5 seconds with some foam and aerosol forming in tube.

Sonicated PFFs were then diluted in to previously prepared respective culture media with all supplements added with final concentration of 5µg/ml. Cultures were treated for 3 days with PFFs (1.5 ml/6well and100µL/96 well plates).

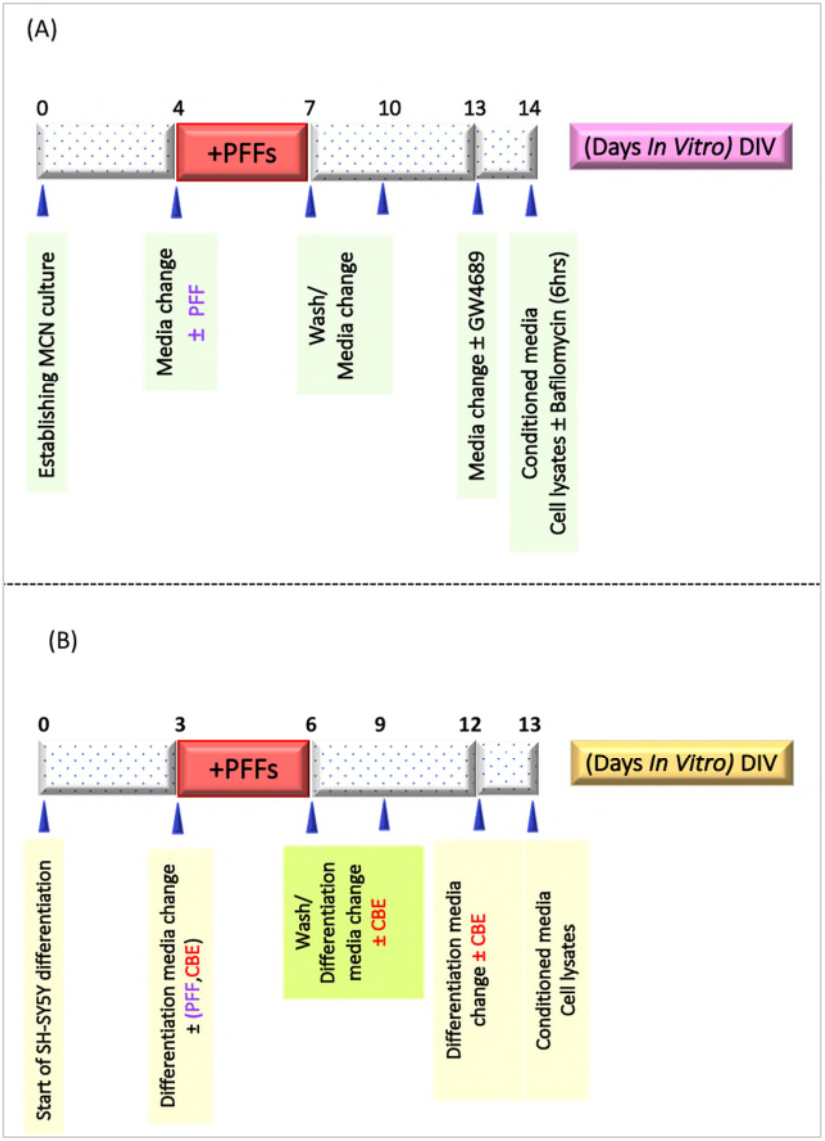

Figure 0.12 Time line guide of culturing mouse cortical neurons and differentiation of SH-SY5Y cell lines. (A): Culturing and collecting mouse cortical neurons ± PFFs seeding. (B): Differentiation of different SH-SY5Y cell lines ± CBE and PFFs treatment.

An equivalent volume of monomeric A-SYN species at a final concentration of 5 µg/mL of monomer was added initially on 6-well plates. However, as there was no accumulated insoluble phosphorylated A-SYN or HMW species observed in this case, we continue our downstream experiments treating cells with only PFFs. Culturing continued with regular media changes for at least 10 days (3 days in presence of PFFs and then at least another 7 days of media changes). Furthermore, during differentiating SHSY5Y cell lines, GCase activity was modulated by a 10 days course of continuous treatment with 10µM of conduritol-b-epoxide (CBE), (sigma). Treatment commenced on 3DIV and was repeated every 3 days to maintain complete inhibition of the enzymatic activity, (

Figure 0.12). Cells were harvested as described in (section 2.1.3) and upon harvesting MCN and differentiated SH-SY5Y cultures, 1ml of conditional media was collected from each sample, centrifuged at 200 xg for 10 minutes and supernatant was stored at -80°C until time for dot blot analysis.

2.5 Tissue Processing, Western Blotting and Biochemical Assays

2.5.1 Reagents Used in Cell/Tissue Homogenizing

All chemicals used in tissue processing were obtained from SigmaThermoFisher Scientific Unless otherwise stated.

2.5.2 Lysis Buffer Recipes

RiPA (radioimmunoprecipitation assay) lysis buffer: 20 mM Tris-HCl (pH 7.5), 150 mM NaCl, 1 mM Na_2EDTA, 1 mM EGTA, 1% (v/v) Triton X-100, 2.5 mM sodium pyrophosphate, 1 mM beta-glycerophosphate, 1 mM Na3VO4, 1 µg/ml leupeptin}, (Cell Signaling), HEPES lysis Buffer: 50mM HEPES, 5mM Na_2EDTA, 150 mM NaCl and 1% (v/v) Triton X-100 used for lysing fibroblast cell pellets before conducting proteasomal assay.

2.5.3 Detergent Used in Preparation of Triton X-100 Soluble and Insoluble Fractions of A-SYN

Used in sequential lysis of both SHSY5Y cell lines and MCN cultures: Triton X-100 buffer:50 mM Tris, pH 7.5, 750 mM NaCl, 5 mM EDTA in 1% (v/v) Triton X-100. Urea-SDS buffer: 10 mM Tris, pH 7.5, 8 M urea in 2% (w/v) SDS, RQ1 DNase 10x Reaction buffer Ref (Promega, Southampton, UK), RQ1 RNase-free DNase (Promega), 1xPhosphatase inhibitors and 1xHalt™ Protease Inhibitor Cocktail, (ThermoFisher scientific).

2.5.4 Reagents and Buffers Used in Western Blotting

10x LDS reducing agent (NP0009), 4x LDS sample buffer (NP0007), 20X MES(NP0002) or MOPS (NP0001) running buffers,12% NuPage Bis-Tris gel (NP034) and 4-12% NuPage Bis-Tris gel gradient (NP032) were all supplied by life Technologies. Pageruler prestained protein ladder (ThermoFisher) used to measure protein size, immobilon®-P transfer membrane PVDF (IPVH00010)

used for transfer and either Amersham ECL (RPN2209) or immobilon Forate, western HRP substrate (WBLUF0100) reagents were used for western blotting detection.

2.5.5 Antibodies Used in WB, Dotblot and ICC

All antibodies applications and dilutions used in this project are displayed in (Table 0.5).

Table 0.5 Antibodies used in this project

Antibody	supplier	Host Species	dilution used	Application
Anti-beta Actin antibody (ab8227)	Abcam	rabbit	1/5000	WB
Recombinant Anti-GAPDH antibody [EPR6256] - Loading Control (ab128915)	Abcam	rabbit	1/2500	WB
Anti-Alpha-synuclein filament antibody ab209538	Abcam	rabbit	1/500	Dot blot/ICC
Anti-Tyrosine Hydroxylase antibody - Neuronal Marker (ab112)	Abcam	rabbit	1/1000	WB
Anti-GAPDH antibody [6C5] - Loading Control (ab8245)	Abcam	mouse	1/2500	WB
LC3B Antibody#2775	Cell signalling	rabbit	1/1000	WB
Recombinant Anti-LIMPII antibody [EPR12080] (ab176317)	Abcam	rabbit	1/1000	WB
CD63 Antibody (H-193): sc-15363	Santa Cruz Biotechnology	rabbit	1/1000	WB
Anti-GRP78 BiP antibody (ab21685)	Abcam	rabbit	1/1000	WB
Anti-COX IV antibody (ab14744)	Abcam	mouse	1/1000	WB
Anti-Cathepsin D antibody [CTD-19] (ab6313)	Abcam	mouse	1/2000	WB
Anti-GBA antibody (ab55080)	Abcam	mouse	1/2000	WB
Anti-Flotillin 1 antibody (133497)	Abcam	rabbit	1/1000	WB
Purified Mouse Anti-Rab11 Clone 47/Rab11 (RUO)	BD Transduction Laboratories	mouse	1/1000	WB
Anti-SQSTM1 / p62 antibody - Autophagosome Marker (ab56416)	Abcam	mouse	4/5000	WB
Anti-Alpha-synuclein antibody [4D6] (ab1903)	Abcam	mouse	1/1000	WB
Antiglial fibrillary acidic protein Ab, clone GA5, (636513)	Merck	mouse	1/500	ICC
Anti-Neuron specific beta III Tubulin antibody ab229590	Abcam	rabbit	1/200	ICC
Anti-LAMP1 antibody - Lysosome Marker (ab24170)	Abcam	rabbit	1/4000	WB
Recombinant Anti-Iba1 antibody [EPR16588] (ab178846)	Abcam	rabbit	1/500	ICC
Polyclonal Goat Anti-Rabbit Immunoglobulins P0448	Dako	goat	1/1500	WB
Polyclonal Goat Anti-Mouse Immunoglobulins P0447	Dako	goat	1/2500	WB
Anti-Rabbit IgG (H+L) Highly Cross-Adsorbed Secondary Antibody, Alexa Fluor 488Cat#A32731	Thermofisher	goat	1/200	ICC
Chicken anti-Mouse IgG (H+L) Cross-Adsorbed Secondary Antibody, Alexa Fluor 594	Thermofisher	Chicken	1/200	ICC
Anti-AIP1/ALIX , Cat. No. ABC40,	Merck	rabbit	1/500	Dot blot
Anti-Glucocerebrosidase (C-terminal) antibody produced in rabbit	Merck	rabbit	1/1000	ICC
Recombinant Anti-Hsc70 antibody [EP1531Y] (ab51052)	Abcam	rabbit	1/1000	WB
Anti-LAMP2A antibody (ab18528)	Abcam	rabbit	1/1000	WB
Recombinant Anti-Alpha-synuclein (phospho S129) antibody [EP1536Y] (ab51253)	Abcam	rabbit	1/1000	WB
eIF2α (D7D3) XP® Rabbit mAb #5324	Cell signalling	rabbit	1/2000	WB
Phospho-eIF2α (Ser51) (D9G8) XP® Rabbit mAb #3398	Cell signalling	rabbit	1/1000	WB
Anti CHOP antibody (GADD153 antibody, GTX116032)	GeneTex	rabbit	1/500	WB
Anti SDHA1 antibody (ab14715)	Abcam	mouse	1/5000	WB

2.5.6 Lysate Preparation (Cell Lysis), Preparation of Protein Extracts and Conditioned Medium

Defrosted cell pellets were lysed in the appropriate lysis buffer to yield between 0.5 and 3 mg/ml of protein concentration (see respective methods). Briefly, 50 and 75 µL were used to lyse neurons in 6 well plate and fibroblast from ¾ 10 cm plate respectively whereas ~30µL was used for lysing differentiated SH-SY5Ycells sequentially. Pellets were resuspended in lysis buffer and incubated on ice for 30 minutes with vortexing every 10 minutes. Lysate was then transferred to microcentrifuge tubes and centrifuged at 17,000 xg for 15 minutes at 4°C. Supernatant was kept for downstream assays and all preparations were performed in the presence of 1x protease inhibitor cocktail.

2.5.7 Bicinchoninic Acid Assay (BCA) for Determining Protein Concentration,

Protein concentration was measured using Pierce® BCA assay kit. The principle of this reaction is based on the colorimetric detection of the total protein amount present in the lysate. This assay relies on the conversion of copper ions to the reduced form (Cu^{+}) by protein present in the solution and the subsequent bonding of bicinchoninic acid Cu^{+} to form a complex with purple color. The absorbance of this complex was measured at a wavelength of 562 nm using BioTek Synergy HT multi-mode Microplate reader.

Briefly, in a 96 well plate, 2.5µL of each sample lysate was dispensed in duplicates and diluted with 22.5µL of dH_2O. Working solution was prepared in (50:1) ratio of reagent A: reagent B. 200µL of working solution was then applied to each sample followed by incubation for 15 minutes at 37°C incubator. To calculate the standard curve, serial dilutions of Bovine Serum Albumin (BSA), (ThermoFisher) were loaded as a standard (0 to1000µg/ml). After blotting the

standard curve, all absorbance measurements were translated to protein concentrations using the standard curve line equation.

2.5.8 Homogenizing Adult Mice Brain Tissue

Midbrain and cortex were dissected from adult Wt/L444P mice following schedule 1 methods by Dr M Gegg and stored at -80 ºC. Adult mice brain tissue samples (22-131mg) were weighed in microfuge tubes and each 10 mg of tissue was extracted in 100µl of 1%(v/v) TX-100 supplemented with 1x protease/phosphatase inhibitors. Samples were incubated on ice for 15 minutes after which homogenate was centrifuged at 17,000 xg for 10 minutes at 4 ºC. Supernatant was placed in fresh tube and protein concentrations were determined using BCA.

2.5.9 Gel Electrophoresis and Western Blot

10 or 20µg of protein depending on the protein of interest (18 µL final volume) was mixed with 2 µL of 10x LDS reducing agent and 6µL of 4x LDS sample buffer. Samples were heated at 70°C for 10 minutes (except urea-SDS fractions) to ensure complete denaturation of protein prior to running on either gradient (4-12%) or 12% Bis_Tris NUPAGE gels at a voltage of 200v for 45 minutes. Following running gels, separated proteins were transferred to immobilon®-P transfer membrane PVDF (IPVH00010) where the transfer unit was assembled as shown in (Figure 0.13) with all layers soaked in towbin buffer (0.025M Tris, 0.192 mM glycine, 20% (v/v) methanol) and transferred at 30V for 60 minutes.

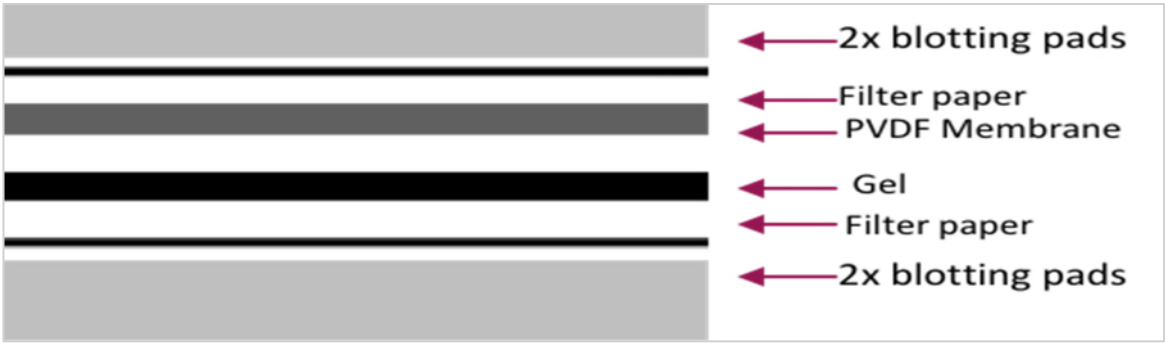

Figure 0.13 Assembling of transfer unit.

Following the transfer, blot was blocked for 60 minutes in 5 ml of 10% (w/v) skimmed milk in 1x PBS and incubated with primary antibody at dilution specified in (Table 0.5) and in incubation buffer (0.4% (v/v) Tween-20, 5% (w/v) skimmed milk powder in PBS) either for 60 minutes at RT or overnight at 4°C. Subsequently, respective secondary antibodies (Table 0.5) conjugated to horseradish peroxidase was applied for 45-60 minutes at RT. Blots were washed between and after antibody incubations with 0.4% (v/v) Tween-20 in 1xPBS as follows; briefly for 2 times followed by two longer washes, each of which for 5 minutes. Protein bands were visualized by enhanced chemiluminescence using either of western blotting detection reagents mentioned in (section2.5.4). Band densitometry was performed using Image-lab software and the volume of each protein was quantified relative to that of either βactin or GAPDH (loading controls) to measure the amount of protein of interest. As A-SYN monomers can easily detached from the transferred membranes during incubation with primary antibody, we applied the method reported by (Sasaki et al., 2015) for better detection of A-SYN, in both phosphorylated and nonphosphorylated state. After transfer, cut was made at 25kDa region and the bottom part of the blot was fixed with 4% paraformaldehyde (Santa-Cruz, CA, USA) containing (0.01v/v) glutaraldehyde for 30 minutes. Following fixation, the blot was washed 3times

with 0.4% (v/v) Tween-20 in 1xPBS for 5 minutes. Next, both fixed and non-fixed parts of the membranes were blocked and processed the same way as above.

2.5.10 Sequential Extraction of Cell Cultures

The detergent Triton X-100 is a good general-purpose detergent for preparing lysates. However, it cannot solubilize lipid rafts, proteins that have aggregated and become insoluble, or lysed nuclei. Therefore, to investigate insoluble proteins such as A-SYN, in its insoluble or aggregating forms, we needed to solubilize material with the chaotropic reagent urea and the anionic detergent sodium dodecyl sulphate (SDS).

Either fresh or defrosted differentiated SH-SY5Y and cortical neurons cell pellets were prepared for sequential extraction of soluble and insoluble fractions of A-SYN. Briefly, pellets were first lysed in the appropriate volume of high salt 1% (v/v) TX-100 buffer (30µL for SH-SY5Y and 50µL for MCN) supplemented with 1X protease and 1X phosphatase inhibitor cocktails,10% (v/v) of RQ1 DNase buffer and 4 units of DNase per sample (Promega). Suspended cells were kept on ice for 15 minutes with vortexing every 5 minutes and cleared by centrifugation at 17,000xg at 4 °C for 20 minutes yielding soluble proteins in the supernatant. The pellets containing nuclei, cell debris and insoluble proteins were then solubilized in 8M urea and (2% w/v) SDS, 1X protease and phosphatase inhibitors and 4 units of DNase/sample. Resuspended pellets were kept at room temperature for 15 minutes with vortexing every 5 minutes and cleared by centrifugation at 17,000xg at 4 °C for 20 minutes. Both fractions were then separated by SDS-PAGE and western blotted for protein(s) of interest (section 2.5.9).

2.5.11 Quantification of Lysosomal Hydrolases Enzymatic Activity

For GCase assay, 10mM of fluorogenic substrate, (4–methyl umbelliferyl–β–D–glucopyranoside (MUGLc) was assayed in the presence of 149mM sodium taurocholate, (NaT). Fluorogenic substrates 4-methyl-umbelliferyl-N-acetyl-glucosaminide (8mM) and 4-methylumbel-liferyl-b-D-galactopyransoside (1mM) were used in β-hexosaminidase and β-galactosidase enzyme assays respectively. In all experiments, 5μM of 4-methylumbelliferone was used as a standard and all enzymatic activities were measured in duplicates for each sample.

2.5.11.1 GCase Assay

The general principle of adding sodium taurocholate (NaT) is to inhibit the cytosolic glucocerebrosidase (GBA2) and activate lysosomal associated glucocerebrosidase (GBA1), (Wenger et al., 1978). At acidic pH, β-glucocerebrosidase hydrolyses the substrate MUGLc to 4–methylumbelliferone and glucose. Adding alkaline buffer stops the enzymatic reaction and causes 4–methylumbelliferone to fluoresce at a different wavelength. When setting up GCase assay, 5μL McIlvaine citrate–phosphate buffer (MV; 0.1 M citric acid, 0.2M Na_2HPO_4, pH 5.4) and 3μL 149mM NaT were mixed and dispensed into 96-well plate with 2.5 μL protein lysate (1-4 mg/ml) and the reaction started by adding 10μL of 10mM MUGLc substrate. Following this, 2.5μL H_2O blank and 240μL of 1nmol standard solution were added to separate wells and plate was sealed and incubated at 37°C for 60 minutes. The reaction was stopped by adding 220 μL of the stop solution (0.25M Glycine, pH10.4) and the fluorescence was measured at 360nm excitation /460 emission ($360_{Ex}/460_{Em}$) using a Bio Tek Synergy HT multi-mode Microplate reader. H_2O blank was used to calculate the background and

enzymatic activity was measured in cells in nanomolar concentration of cleaved substrate per µg protein per hour).

2.5.11.2 Lysosomal Hydrolases (β hexosaminidase and β Galactosidase) Assays

For β-hexosaminidase assay, 20µL of McIlvaine citrate–phosphate buffer (MV, pH 4.2) was dispensed into 96-well plate with 2.55µL protein lysate (0.11-0.44mg/ml) and the reaction started by adding 10 µL of 8mM 4-methylumbelliferyl-N-acetyl-glucosamide. For β-galactosidase assay, 20µL of McIlvaine citrate–phosphate buffer (MV, pH 4.1) was dispensed into 96-well plate with 2.5µL protein lysate (0.1-0.4 mg/ml) and the reaction started by adding 10µL of 1mM 4-methylumbelliferyl- β-D-galactopyranoside. To calculate the background, 2.5µL H_2O, instead of protein lysate, was set up and 240µL of 1nmol standard solution was added to separate wells. Following this, the sealed plate was incubated at 37°C for 30 minutes and the reaction was stopped by adding 220µL of the stop solution (0.25M Glycine, pH 10.4). Fluorescence was measured at (360_{Ex}/460_{Em}) using a Bio Tek Synergy HT multi-mode Microplate reader and each enzymatic activity was calculated in nanomolar concentration of cleaved substrate per µg protein per minute).

2.5.12 Endoglycosidase-H (Endo-H) Assay

2.5.12.1 Proteasomal Inhibition

Epoxomicin is a potent and selective proteasomal inhibitor that primarily inhibit the chymotrypsin-like activity of 20S subunit without affecting other nonproteasomal proteases, (Meng et al., 1999). Sub-confluent human dermal fibroblasts, cultured in 10cm plates, were treated with 25nM of Epoxomicin. Twenty-four hours later, fibroblasts were harvested by trypsinization and pelleted at 17,000 xg. Protein lysates were prepared by lysing cells in 60µl of 1% (v/v) TX-100 in 1xPBS supplemented with 1xprotease inhibitors cocktail.

2.5.12.2 Endo-H and PNGase-F Treatment

in an effort to follow the intracellular fate of glucocerebrosidase, we monitored the processing of its N-glycans in both N370 and L444P heterozygous and GD fibroblasts. Protein concentration was first measured in the lysate using BCA kit (section 2.5.7). According to the manufacturer's instructions, diluted samples of lysates, containing 20µg of total protein were denatured with 1X of denaturing glycoprotein buffer at 100°C for 10 minutes. To each tube of the denatured protein sample, 10µl of reaction mixture was added and two experimental conditions were set up for each enzymatic treatment as shown in (Table 0.6). Following this, samples were subjected to 2 hours incubation with Endo-H and/or PNGase.

2.5.12.3 Western Blotting

Western blotting of all samples was performed following the protocol outlined in (section 2.5.9) except for using 4-12% gel and MOPS running buffer, to improve resolution of bands.

Table 0.6 Reaction mixtures of Endo-H assay

(A)

Endo-H	Without Endo-H	With Endo-H
10X G5 reaction buffer 3	2µL	2 µL
Endo-H (1000 units)	0 µL	2 µL
H_20	8 µL	6 µL

(B)

PNGase	Without PNGase	With PNGase
10X G5 reaction buffer 2	2µL	2 µL
NP-40 (10%)	2µL	2µL
PNGase (1000 units)	0 µL	1 µL
H_20	6 µL	5 µL

2.6 Proteasomal Assay

2.6.1 Regents Preparation for Proteasomal Assay

The 20S proteasomal assay kit was purchased from Merck Millipore (APT280).

Table 0.7 Set up of proteasomal assay

	Test sample	H_2O	Master Mix	Total Volume (µL)
Test sample	10	0	90	100
Test sample +inhibitor	10	0	90	100
Substrate blank	0	10	90	100

Table 0.8 Dilutions of AMC standard used in proteasomal assay.

	[AMC] mM	ml AMC	ml 1X reagent buffer
A	12.5	25 (125 mM stock)	225
B	4.17	100 (A)	200
C	1.38	100 (B)	200
D	0.46	100 (C)	200
E	0.15	100 (D)	200
F	0.05	100 (E)	200
G	0	0	120

2.6.2 Proteasomal Assay Procedure

The basal activity of proteasome was assayed in fibroblast and MCN lysate as compared to control. 20S proteasome, the catalytic subunit of the UPS, is therefore considered as a marker of proteolytic activity and homeostasis. The general principle of this assay was based on measuring the cleavage of an artificial substrate LLVY-7-amino-4-methylcoumarin to LLVY+7-amino-4-methylcoumarin (AMC) standard. As per manufacture instruction and in a 96 well plate, a master mix comprised of 10µL of 10X reagent buffer,10 µL diluted proteasome substrate (10 mM final concentration) and 70µL dH_2O was applied as 90µL/well to either test sample, test sample plus the inhibitor or to the substrate blank reaction. Each sample was measured in duplicate and the assay was set up as shown in (Table 0.7). Inhibition of proteasomal activity was performed by incubating 10µL of test sample with 1µL of diluted Lactacystin (0.25 mM final concentration) for 15 minutes at RT. Following 1hour incubation at 37°C, and just before measurement, serial dilutions of AMC (0.05 to 12.5µg/ml) were loaded as 100µL/well and used to plot a standard curve, (Table 0.8). Fluorescence was measured with excitation at 360nm and emission at 460nm using a Bio Tek Synergy HT multi-mode Microplate reader. By using the AMC standard curve and the protein concentration of lysates, proteasome activity was calculated in µM of AMC per µg protein per hour.

2.7 Citrate Synthase (CS) Activity

Citrate synthase (CS) is a mitochondrial marker/protein and measurement of its level of activity gives an indication of the number of mitochondria within a sample. Citrate synthase catalyzes the reaction between oxaloacetate (OAA), the substrate, and acetyl CoA resulting in the production of citrate and liberation of "free" thiol groups (CoA-SH).

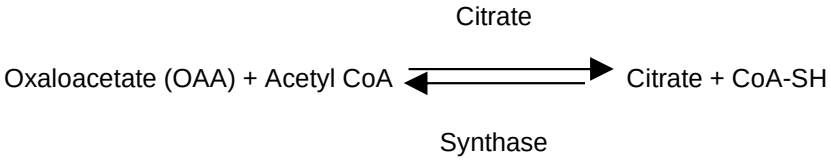

DTNB ("Ellmans reagent"-5,5'-dithio bis-2-nitrobenzoid acid) binds free thiol groups to produce DTNB-CoA which is yellow and absorbs at 412nm.

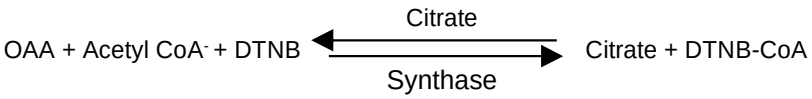

To calculate citrate synthase activity, 10µg protein was added in to a tube of reaction mixture made of 5 reagents, common to both test and reference, as indicated in (Table 0.9) making a total volume of 1ml. In this assay, the reference cuvette contained everything except the substrate (OAA) used as a blank. The solutions were mixed and then oxaloacetate was added to start the reaction after which 240µl of reaction mixture was quickly transferred in to 96 well plate and loaded as 4 wells/reaction. CS activity was measured on microplate at 412nm for 10 minutes at 30 ºC to get the rate (DTNB extinction coefficient 13.6×10^3 $M^{-1}cm^{-1}$ and Path length is 0.85cm), and the reaction was calculated using the Beer

Lambert Law: A = ECL where A= absorbance/min, E=extinction coefficient, C = concentration, L = pathlength.

C (Mol/min/ml) = (A (A412/min/ml)/13.6x10^3(Mol/cm) x 0.85 (cm)) *100.

The enzyme activity was normalized to protein concentration in samples and blotted as Mol/min/mg protein, (Figure 0.14).

Table 0.9 Setting up CS reaction.

Reagents	Ref Eppendorf	Test Eppendorf
Tris Buffer	500µl	500µl
Acetyl CoA	20µl	20µl
DTNB	20µl	20µl
Triton-X100	10µl	10µl
dd H_2O	450µl	430µl
Mito-Prep Susp	-	10µl
Oxaloacetate	-	10µl
TOTAL VOL	1ML	1ML

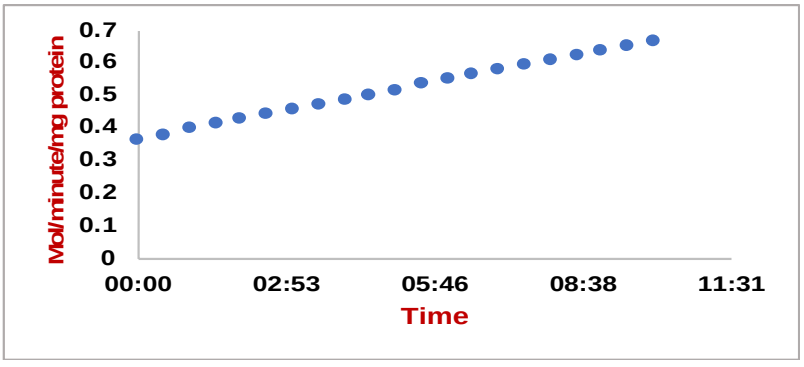

Figure 0.14 Citrate synthase rate.

2.8 Fluorometric Measurements of Cell Viability (CTB) Assay

The CellTiter-Blue® reagent was supplied by (Promega) and the assay is a single step rather than kinetic pathway. We used this quick and convenient method as a screening test for cytotoxicity. It is used to enumerate the number of live and dead cells present in multi well plates. Metabolically active cells retain the ability to reduce blue colored resazurin into highly fluorescent pink colored resorufin by the aerobic respiration. However, nonviable cells rapidly lose their metabolic capacity and don't reduce resazurin and thus no fluorescent signals will be generated. In a precoated 96 well plates, differentiated SH-SY5Y cell lines and mouse cortical neurons were cultured as normal and subjected to treatment of preformed a-synuclein fibrils (PFFs) with and without CBE treatment. Upon harvesting cultures, 20µl of indicator dye (resazurin) was added to 100µl respective media of each well and plates were incubated for 2 hours. The assay was performed in duplicates with 100µl of fresh media used as blank. Following incubation, the fluorescence was measured using a Bio Tek imark Synergy HT multi-mode Microplate reader at (530_{Ex}/590_{Em}) and was proportional to the number of viable cells in culture.

2.9 Dot Blot Analysis

2.9.1 Materials and Reagents Used

0.45µm PROTRAN Nitrocellulose membrane (NBA085A001EA) by (Perkin Elmer, Beaconsfield, UK), 1X Sterile phosphate buffered saline (PBS) and BlockACE (BioRad, Eugene, OR, USA).

2.9.2 Procedure

The Bio-Dot microfiltration apparatus (BioRad) allows the measurement of proteins in cell culture media and the detection of proteins in their native form. We used dot blot apparatus to analyze conditional media collected from either SH-SY5Y or primary neuronal cultures treated with PFFs. The apparatus was first assembled as per manufacture instructions after which 11.2cm x 7.5cm nitrocellulose membrane (Perkin Elmer), previously wet in 1xPBS, was placed on top of sealing gasket of the apparatus under vacuum. Before loading media, 1xPBS was loaded twice into each well with multi-channel pipette to wash the membrane. Following this, 100–400µl of respective culture media containing protein of interest was added to each well, filtered through the membrane by gentle vacuum. The blot was washed again twice with 1xPBS and stained with Ponceau red for a minute to view wells. Cuts were then made as required and the blot was washed 2-3 times with PBS until Ponceau stain was removed. Following this, the experiment continued following the protocol specified previously in western blotting technique (section 2.5.9) with blot blocked first in 20ml of BlockACE (BioRad) for 1 hour followed by incubation with antibodies of choice specified in (Table 0.5).

2.10 Measurement of O2 Consumption Rate and Citrate Synthase Activity

2.10.1 Seahorse for MCN

Cellular oxygen consumption rate (OCR) was measured in selected cultures from two independent wt/L444P MCN using an Agilent Seahorse XF Mito stress test (Stockport, UK).

Seahorse analyzer assay allows the measurement of both basal and maximal mitochondrial respiration in a non-invasive way and after injection of drug compounds through a specific portal system. Cortical neurons were grown in XF24 plates precoated with 100µl of 0.1mg/ml poly-ornithine solution and culture continued for 10days with growth media changed on day 7 in vitro. We used a seeding density of $1.2x10^4$ cells/200µl /well of XF24 plate, allowing five wells per embryo and leaving the sixth well as a blank filled only with fresh media (Figure 0.15).

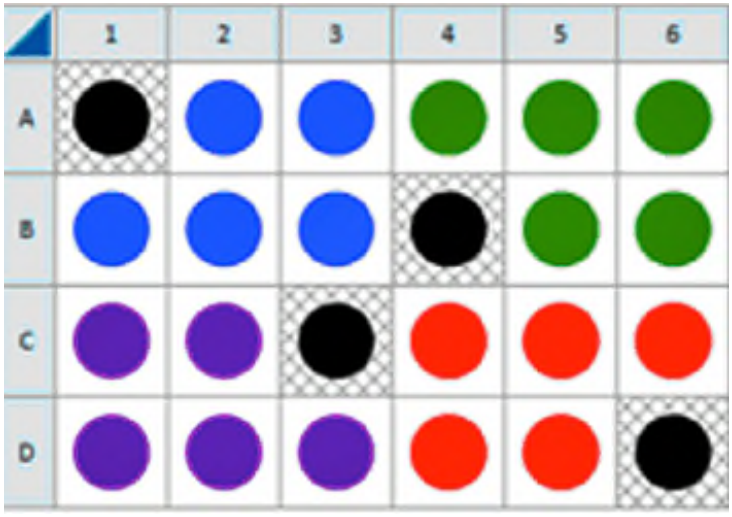

Figure 0.15 Layout and loading pattern in seahorse XF24 plate.

One day prior to analysis, each well of XF24 calibration plate was filled with 1ml of XF Calibrant (pH 7.4) after which sensor cartridge was submerged carefully into the plate and incubated overnight at 37°C with no CO_2. On the same day of measurement (10DIV), the confluency of neurons in each well was checked and only those showing apparent blank patches were labelled to exclude them from the measurement as this will affect the accuracy.

Following this step and immediately before metabolic flux measurement, XF24 plate was washed and culture media were replaced with 525µl of freshly made XF-seahorse DMEM supplemented with 2mM Glucose, 2mM Glutamine, and1mM pyruvate and prewarmed to 37°C. The plate was then placed in non-CO_2 incubator and allowed to equilibrate in the new media with the adjusted pH to 7.4 for an hour. Meanwhile, XF24 extracellular flux assay kit was prepared by making a stock solution of Oligomycin, CCCP and Antimycin A to target mitochondrial respiration. 2ml of assay DMEM media was prepared containing 10µM of each of these three compounds and 60µl/well of each was loaded into the appropriate port of the cartridge as port A for Oligomycin, B for CCCP and C for Antimycin A, leaving D port empty as a blank.

Setting up seahorse assay was done by loading assay template correctly in the Seahorse XF24 software and defining the cell name in wells and the three injections with names (Figure 0.16). Following this, the sensor cartridge was placed with the calibration plate into instrument tray to initiate calibration and equilibrate sensors. After initiation step, calibration plate was replaced with cell culture plate without the lid and the assay ran following the instruction in the software. Once the basal OCR was measured, the compounds were added sequentially and the effects on OCR was measured. After the assay, culture plate

was placed on ice and cells were lysed in 100µl of 1%TX-100 in 1xPBS for 15 minutes with protein concentration in each well quantified by BCA as in (section2.5.7).

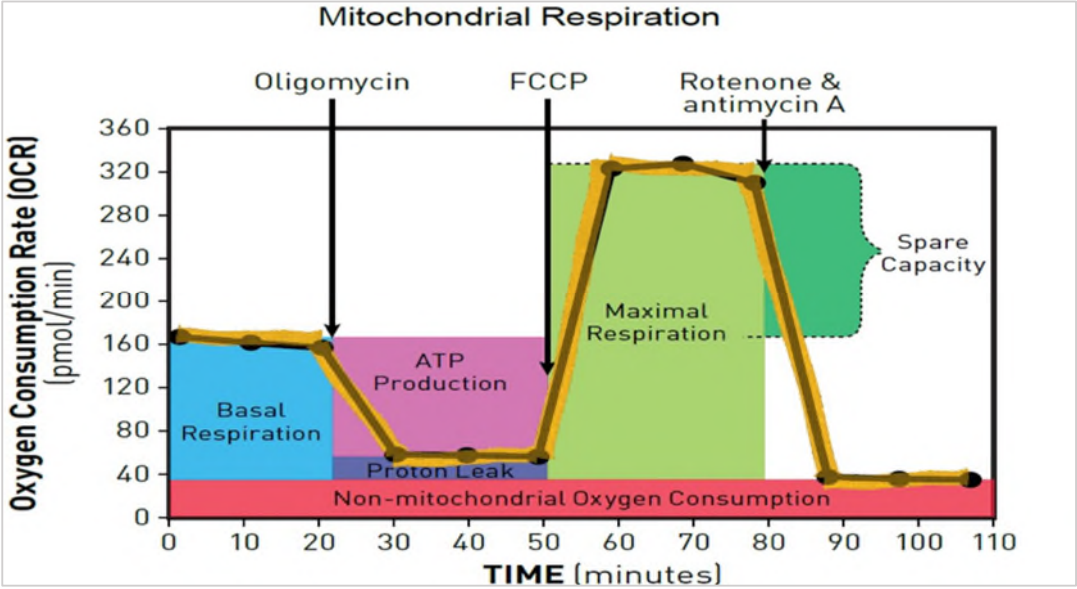

Figure 0.16 Agilent Seahorse XF Cell Mito Stress Test profile. To show the key parameters of mitochondrial function.

2.11 ELISA

2.11.1 Mouse Cortical Neurons

We used sandwich enzyme immunoassay for quantitative measurement of A-SYN release in to conditional media collected from mouse cortical neuronal cultures. Reagents were prepared as per manufacturer's instructions and kit protocol was followed exactly as described (Cat # RDR-SNCa-Mu; Reddot Biotech Inc, Canada). Briefly, 100µL of each dilution of standard (0-1500 pg/ml), blank, and samples (1:50 and 1:100 dilutions) were loaded into the appropriate wells after which the plate was covered with sealer and incubate for 2 hours at 37°C. Following this step, the liquid was removed from each well with no wash and a 100µL of detection reagent A working solution was dispensed into each well followed by incubating the plate for another 1 hour at 37°C. The solution from each well was then aspirated and the plate was washed 3 times with 350µL of 1x wash solution and tapped onto absorbent paper to remove any remaining liquid from all wells completely. After the last wash and decanting, a 100µL of detection reagent B working solution was added into each well and the plate was incubated for another 1 hour at 37°C followed by repeating the same aspiration and washing process for a total of 5 times. TMB substrate solution (90µL) was added after into each well to turn liquid in to blue color and plate was incubated for 15-25 minutes at 37°C. Lastly, 50µL of stop solution loaded into each well in which the liquid turned to yellow and the measurements was performed using the microplate reader at 450nm immediately. Absorbance data was then normalized to pg/ml using the standard curve and normalized to protein content of the well.

2.12 Differentiated SH-SY5Y Cells

We used Human α-Synuclein ELISA Kit supplied by BioLegend to quantify the monomeric A-SYN release in to culture media collected from differentiated SH-SY5Y cell lines treated with PFFs, and CBE.

2.12.1 Preparing Reagents used for Human A-SYN ELISA

As per manufacture instructions, all kit components were brought to RT before use, and 1x wash buffer was made by diluting 5x wash buffer in distilled water.

The standard Intermediates and curve were prepared as illustrated in (Table 0.10) and (Table 0.11) respectively.

Samples were then diluted in 1x reagent diluent in duplicate (1:5 and 1:10 dilutions) and each dilution was mixed well by vortexing 3 x 2 seconds.

Biotinylated primary antibody made of by adding 6µL of the primary antibody stock to 6mL of 1x reagent diluent. Streptavidin HRP an “HRP Intermediate” was made first by mixing 10µL of Streptavidin-HRP stock with 990µL of 1x reagent diluent after which 150µL from the HRP Intermediate was added to 22.35mL of 1x reagent diluent.

Table 0.10 Preparation of Standard Intermediates.

Volume of Standard (µL)	Volume of 1X Reagent Diluent (µL)	Final Concentration (pg/mL)
40µL intermediate #2	1280	1500
550µL of#1	825	600
550µL of#2	825	240
550µL of#3	825	96.0
550µL of#4	825	38.4
550µL of#5	825	15.4
550µL of#6	825	6.1
0	825	0

Table 0.11 Preparation of standard curve

Total number	Volume of Standard	Volume of 1X Reagent Diluent (µL)	Final Concentration (ng/mL)
Intermediate #1	10µL of reconstituted standard	990	5,000
Intermediate #2	10µL of intermediate #1	990	50

2.12.2 Running Human A-SYN ELISA

Preparation of all components as per instruction manual is described above. The assay was conducted in two consecutive days and it started by washing the plate 4 times with 300µL/well of 1x wash buffer after which 200µL of each standard and another 200µL of each sample dilution were added to the plate. After loading, the plate was covered and incubated overnight at 4°C while shaking. After incubation, 50µL/well of the biotinylated primary antibody added and plate was incubated for 2 hours followed by adding 200µL/well of diluted streptavidin HRP with another hour of incubation, all at RT. The same process of 4 times washing and drying of plate was repeated after each incubation throughout the assay and the final step included mixing up 5.5mL of each of chemiluminescent substrates and adding 100µL of mixture per well immediately before reading plate. The total concentration of monomeric A-SYN release was presented as pg/mg of protein.

2.13 Statistical Analysis

Data were displayed as normal distribution and all values were represented as mean **±** standard error of the mean from the number of independent cell cultures or preps (n). Statistical significance tested using either unpaired T test or one-way ANOVA with multiple comparison test carried out between different experimental groups using Graph- Pad Prism Software.

Levels of significance were set to $*p < 0.05$, $**p < 0.01$, $***p < 0.001$ and P value < 0.05 was considered significant.

3 Human Dermal Fibroblasts as a model of *GBA*-linked PD

3.1 Introduction

The use of cellular cultures has an advantage over studying Parkinson disease directly on patients or animal models. It is able to explore the two main alterations that occur in dopaminergic neurons during PD pathogenesis. Previous published work supported the usefulness of fibroblasts model as a powerful and non-invasive way to investigate PD pathogenesis. Patients derived fibroblasts from idiopathic PD (Ambrosi et al., 2014) or monogenic disease phenotypes such as PINK1-PD (Abramov et al., 2011), LRRK2 mutation (Juárez-Flores et al., 2018) and ATP13A2 loss of function mutation (Dehay et al., 2012) exhibited ALP impairment, and bioenergetic deficits similar to those found in postmortem PD brain and other neuronal models.

Many studies have utilized human dermal fibroblast as a model to investigate *GBA*-linked PD molecular mechanisms. Reduced enzymatic level and activity were detected in fibroblasts derived from GD, PD with a variety of *GBA* mutations and non-manifesting carriers, such a reduction resulted from a combination of arrested enzyme in the ER and lower *GBA* transcript level (de la Mata et al., 2015, Sanchez-Martinez et al., 2016, McNeill et al., 2014, Collins et al., 2017). ER stress and UPR have been implicated to play fundamental role in the pathogenesis of PD (Remondelli and Renna, 2017). Thus, mutant protein trapped in ER is identified as misfolded and will start initiating ER stress and UPR in an attempt of the cell to refold this protein by ER resident chaperon such as BiP/Grp78. Failure to restore the proper folding will result in retro-translocation of misfolded protein to the cytosol and elimination by the ubiquitin proteasomal system (UPS) through endoplasmic reticulum associated degradation (ERAD)

process. Given that evidence, enhanced expression of BiP was found in patient derived fibroblasts with a pool of *GBA* mutations in order to reduce the protein burden in ER (McNeill et al., 2014, Ron and Horowitz, 2005, Mu et al., 2008). In contrast to mature cytosolic protein, misfolded GCase trapped in the ER contains N-linked glycans which are sensitive to cleavage by endoglycosidase-H (endo-H) and detected by western blotting as lower molecular weight band. Thus, the appearance of such a band following endo-H treatment is indicative of GCase arrest in the ER. Many studies have reported increased level of this band, detected by western blotting, in fibroblast from both GD patients and non-manifesting mutation carriers (Bendikov-Bar et al., 2011, McNeill et al., 2014, de la Mata et al., 2015, Mu et al., 2008) reaching at least 50% of the enzyme in homozygous L444P mutation. Similarly, dysregulation of calcium (Ca^{2+}) homeostasis, increased vulnerability to stress responses and neurodegeneration have been observed in patients derived fibroblast with *GBA* N370S mutation which, although was beneficial for protein folding, it could render the cell sensitive to apoptotic stimuli (Kilpatrick et al., 2016). As both ALP and UPS represent the two main cornerstone pathways of protein and organelle catabolism, they were implicated in a wide spectrum of pathological states, among which were neurodegeneration and aging (Rubinsztein, 2006). Defective GCase activity leads to alteration in the lysosomal dependent processes such as ALP which further implicates the role of autophagy in *GBA* linked PD. It was shown that GCase deficient fibroblast exhibited compromised autophagy lysosomal reformation, a cellular process controlled by mTOR (Magalhaes et al., 2016). Additionally, De La Mata et al. group showed how the GD L444P mutation can lead to alteration in autophagy and impairment of autophagic flux which

subsequently leads to accumulation of autophagic substrates (de la Mata et al., 2015). Such an impairment of protein degradation contributed to biochemical abnormalities in primary fibroblast derived from GD patients including ROS production, impaired mitochondrial flux and mitophagy activation.

While *GBA* mutations are numerically the most important predisposing factor for devolving PD, the genotype-phenotype association have been previously stratified to categories L444P mutation as severe mutation. This mutation leads pathologically, when in homozygosity state, to an extensive ERAD and clinically is predictive of neuropathic type 3 of GD (Hruska et al., 2008). Despite this notion, the majority of *GBA* mutation-linked risk is represented by the heterozygous state (Sidransky et al., 2009). Carriers of these mutations have been reported to have higher odd ratio of developing PD and 5 years younger age of onset (Gan-Or et al., 2015). However, in the existing literature, studies have mainly focused on the effect of homozygous L444P state in the context of *GBA*-linked PD using patients derived fibroblast model (Bendikov-Bar et al., 2011, de la Mata et al., 2015). Therefore, due to the relative paucity of work specifically related to heterozygous L444P mutation, we have started studying the pathophysiology of this mutation in primary cultured fibroblasts derived from mutation carriers with and without PD.

3.2 Experimental Aims

The central aim of this chapter is to investigate the impact of heterozygous L444P mutation in the context of PD in human-derived fibroblast model. Objectives

A. Characterization of fibroblasts by measuring activities and expression of GCase and other lysosomal enzymes and proteins.
B. Detection of trapped GCase in ER of wt/L444P fibroblast.
C. Investigating UPS and ALP protein degradation pathways in wt/L444P fibroblast

3.3 Fibroblast Cultures

Fibroblast cultures in this chapter were established using donor samples from the Lysosomal Storage Disorder Unit at the Royal Free London NHS Foundation Trust. Two groups were used:

(1) heterozygous *GBA* mutation positive carrier.

(2) genetically unrelated controls (spouses/partners).

They were identified by taking a detailed family history from each GD patient, and recruited with consent by clinical colleagues from the Lysosomal Storage Disorder Unit. The diagnosis of PD was made according to the UK Parkinson's Disease Society Brain Bank Criteria. All biopsies were obtained following informed patient consent following Hampstead Research Ethical committee approval (10/H0720/21/21). The methods were carried out in accordance with the relevant guidelines in the above-mentioned ethics approval and punch biopsy was taken from each patient (5 wild type and 5 L444P heterozygous mutants with and without PD). The genotype and PD association of the patient cohort is given in (Table 0.1).

The establishment of cultures was done previously by members of our laboratory and samples were sent for Sanger sequencing (see section 2.3.4) and they were all confirmed to be wild type or wt/L444P mutants (also referred to as wt/Δ in Table 0.1).

Table 0.1 Characteristics of human-derived fibroblast cultures.

Patient	Age at time of Biopsy (years)	Gender	Genotype	+/- PD
Ctl9	52	F	wt/wt	—
EOR	50	F	wt/wt	—
JEC	82	F	wt/wt	—
JER	52	F	wt/wt	—
MCL	59	M	wt/wt	—
CHM	72	M	wt/△	+PD
TCH	45	F	wt/△	—
MBA	67	M	wt/△	—
BSL	85	M	wt/△	+PD
PJR	62	M	wt/△	—

3.4 Results

3.4.1 GCase Activity and Protein Expression level in wt/L444P Human Dermal Fibroblasts

From previous work done in our laboratory (McNeill et al., 2014), both GCase activity and protein levels were significantly reduced to the same extent in non-manifesting heterozygote *GBA* carriers (NMC) and heterozygote *GBA* carriers with PD as compared to control. This study contained a mix of *GBA* mutations including N370S and L444P. Furthermore, it cannot be excluded that some of the NMC will develop PD later in their life. Therefore, in our study we have decided to pool the data from wt/L444P cell lines with PD (n=2) and wt/L444P NMC (n=3) that are listed in (Table 0.1). Wt/wt and KO mouse embryonic fibroblasts (MEF) were used as positive and negative controls respectively. GCase activity was 1.60nmol/hr/µg in wt/wt MEF whereas GBA KO MEF presented minimal activity (2% residual activity). We also found that GCase activity was significantly reduced by 34.7 % (*p =0.014) in heterozygous mutants (0.978 ±0.070) as compared to control (1.50 ±0.15), (Figure 0.1,B), (n=5).

To confirm the previous findings of (McNeill et al., 2014), when GCase activity was split in to NMC and GBA carriers with PD, GCase activity was 1.03±0.110 nmol/h/µg protein (n=3) and 0.900 ± 0.050 nmol/h/µg protein (n=2) respectively with no significant difference found between these two groups (p>0.999). Therefore, we decided to pool the WT/L444P fibroblasts in all experiments as planned, (Figure 0.1, A).

To determine if the decrease in GCase activity was due to decreased protein levels, cell lysates were subjected to western blotting. Densitometric analysis results showed a nonsignificant reduction in GCase protein expression level by

30.32% in mutant fibroblast when compared to control (*p*= 0.134), (n=4) (Figure 0.2).

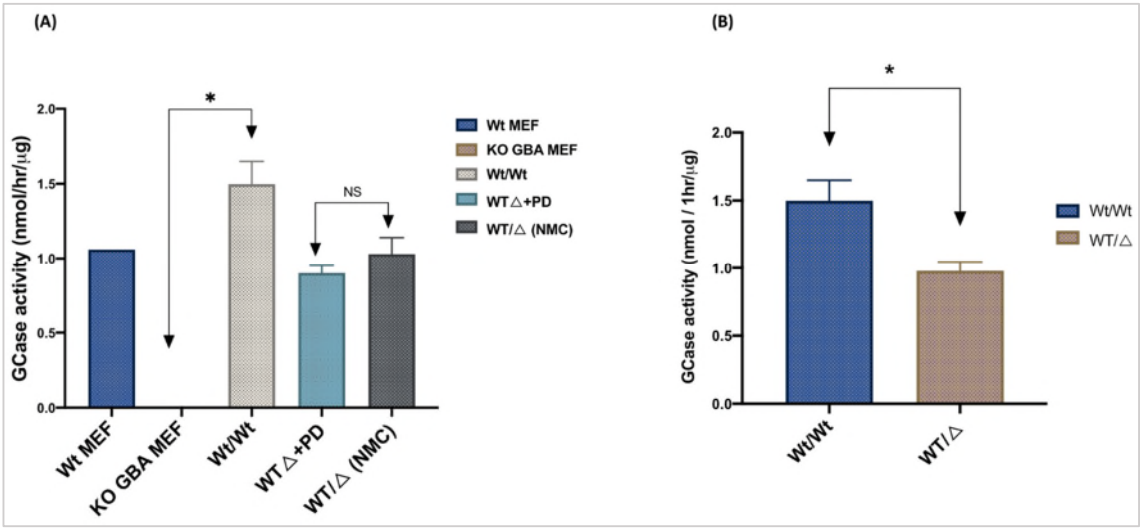

Figure 0.1 GCase activity in wt/L444P fibroblast. (A): Bar chart summarizing GCase activity in (nmol of fluorescence/hr/µg of protein) in different study groups; positive control (wt/wt MEF=1.06nmol/hr/µg, n=1) and wt/wt human derived fibroblast (mean=1.50 ±0.151, n=5), negative control (GBA KO MEF=0.008 ,n=1) representing significant 98% drop of GCase activity when compared to wt/wt group (*p=0.017), and the two other groups of *GBA* heterozygous mutation; one with PD=0.900±0.050,n=3, and the other group without PD, NMC=1.03±0.110, n=2, no significant alteration in GCase activity found between NMC and wt/L444P+PD group (p>0.999). (B) GCase enzyme activity was 34.7% significantly lower in fibroblasts from wt/L444P mutation carriers (0.9780 ±0.07003) than control (1.50 ±0.15, n=5, *p=0.014). Each bar represents mean GCase activity (nmol/hr/ug protein) with error bars representing the standard error of the mean.

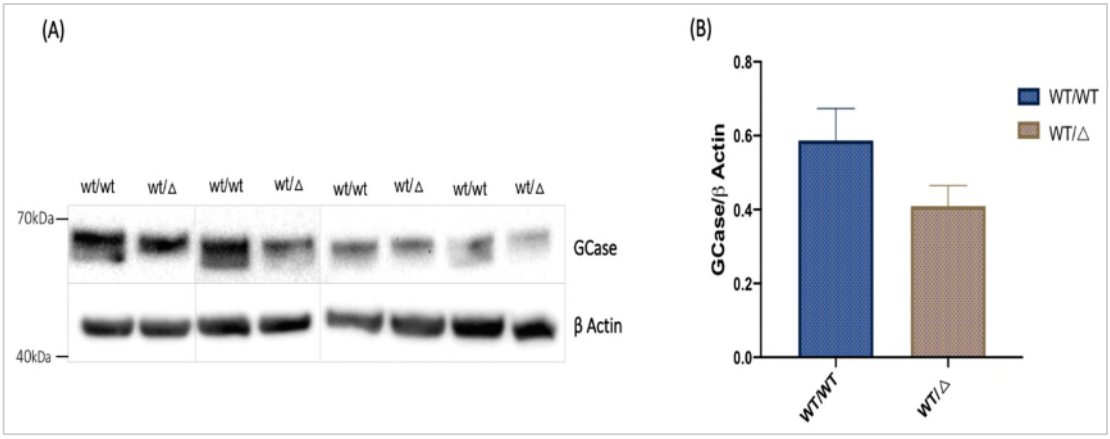

Figure 0.2 GCase protein expression level in wt/L444P human dermal fibroblast. (A): Representative western blot image showing reduced level of GCase protein in heterozygous L444P mutant fibroblasts (n=4wt/wt and 4wt/L444P); β Actin was used as loading control and vertical line denotes where blots have been cropped to remove air bubbles (B): Bar chart representation of western blot showing statistically non-significant 30.32% reduction in GCase band density of wt/L444P mutant fibroblast when compared to healthy controls, (*p*=0.134). Each bar represents mean of GCase protein relative expression to housekeeping protein (β actin) from 4 independent fibroblasts cultures in one group ± SEM

3.4.2 Investigating Lysosomal Biochemistry in wt/L444P Human Dermal Fibroblast

The level of lysosomal membrane integral protein 2 (LIMP2) was quantified in human dermal fibroblasts, both in L444P mutant and the control group. LIMP2 functions as a carrier protein to translocate GCase in to the lysosome. In mannose phosphate receptor (MPR) double KO MEF, GCase sorting and activity was not affected indicating that the enzyme is trafficked to the lysosome by LIMP2 and not via MPR dependent manner (Reczek et al., 2007). Our results did not show any significant alteration (p=0.591) in the level of LIMP2 in wt/L444P mutant fibroblasts (0.476± 0.112) when compared to control (0.569±0.123), (Figure 0.3 A and B), n=5.

LAMP1 is one of the most abundant lysosomal membrane proteins (LMPs) that resides mainly on the lysosomal limiting membrane (Saftig and Klumperman, 2009). We found comparable levels of the mean LAMP1 protein expression between control group (1.69±0.244) and wt/L444P fibroblasts (1.58±0.279), (p=0.776, n=5), (Figure 0.3 A and C).

Protein level of mature Cathepsin D (27kDa) was also measured by western blot in control and mutant fibroblasts. Cathepsin D act as a principle lysosomal protease responsible for the degradation of many proteins. It was reported that CathD functions to enhance the activity of GCase (Ambrosi et al., 2015, McGlinchey and Lee, 2013). Our results showed a slight but not significant elevation in Cathepsin D level in the wt/L444P fibroblast (0.852±0.194) with respect to control (0.666±0.103), (p=0.421, n=5), (Figure 0.3 A and D).

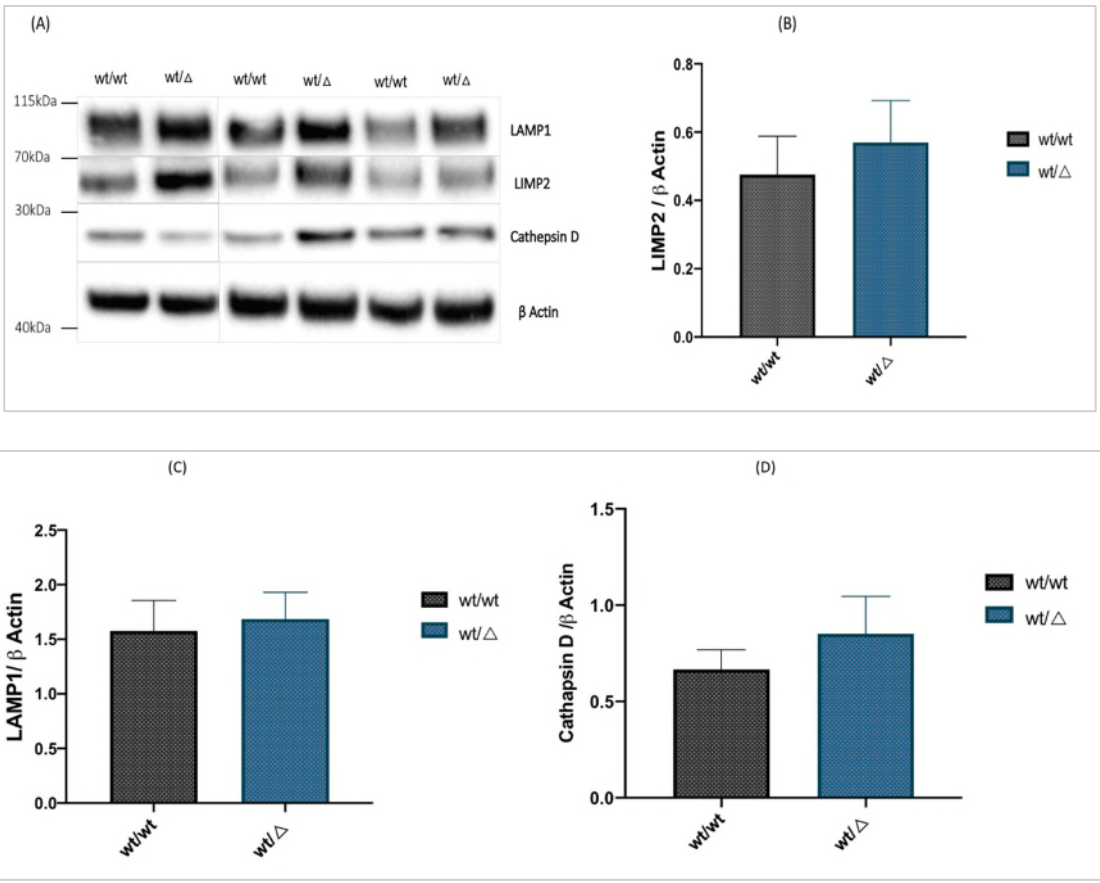

Figure 0.3 Analysis of lysosomal markers in wt/L444P human dermal fibroblast. (A): Representative western blots image demonstrating unchanged levels of LIMP2 and LAMP1 in wt/L444P fibroblast when compared to control (upper two panels) with a trend of increased Cathepsin D expression level in mutant lines (lower panel), β Actin was used as loading control and the vertical line drawn in blot images denotes the site of cut to remove air bubble. (B, C): Bar chart analysis of western blot bands densities of both LIMP2 and LAMP1 lysosomal markers, (n=5wt/wt, 5wt/L444P). For all sample measured, there was no evidence of significant change in both markers; LIMP2 (*p*=0.591) and LAMP1 (p=0.776) mean values±SEM in the wt/L444P fibroblasts were 0.476± 0.112 and 1.69±0.244 against wt/wt group 0.569±0.123 and 1.58±0.279 respectively. (D): Bar chart analysis showing a slight but not significant elevation (*p* =0.421) of Cathepsin D expression level in wt/L444P fibroblast (0.852±0.1935) when compared to control (0.666±0.1026). All data were expressed as the mean density of the target protein expressed against the density of the housekeeping protein (β actin) from 5 independent fibroblast cultures ±SEM of the blots shown.

These findings were in line with unchanged activities of the other lysosomal hydrolases, β-galactosidase and β-hexosaminidase, in which no significant change in the activity of these lysosomal hydrolases against healthy controls. Hexosaminidase activity was 0.486 ±0.028 in wt/wt and 0.452±0.019 in mutant group, whereas β-galactosidase activity was 0.078±0.007 in wt/wt and 0.080±0.005 in wt/L444P fibroblast, (n=5), (Figure 0.4).

Collectively, this was suggesting that the reduced GCase activity was simply due to mutation and not secondary to alteration of lysosomal mass in mutant fibroblast.

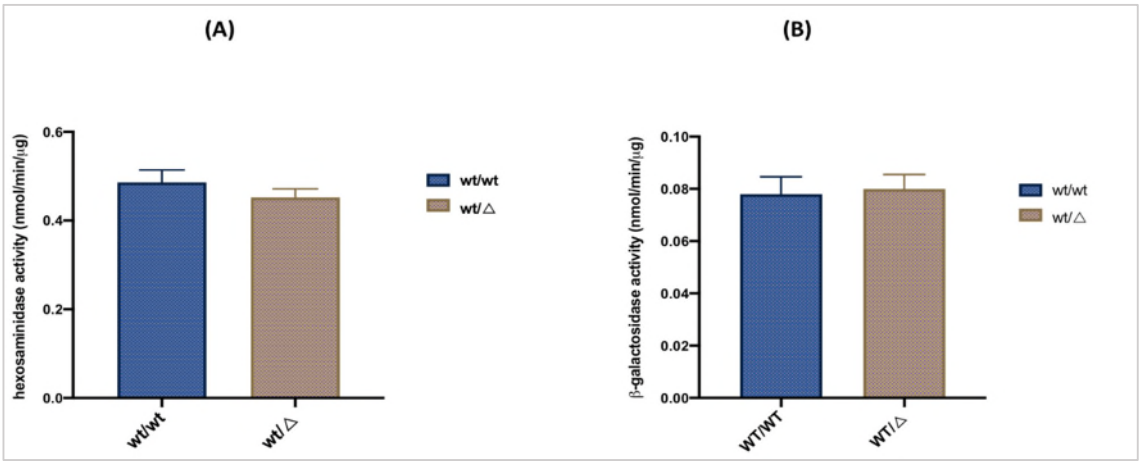

Figure 0.4: lysosomal hydrolases activities in wt/L444P human dermal fibroblast: Bar chart representation of (A) β-hexosaminidase and (B) β-galactosidase activities in fibroblasts from controls & L444P mutation carriers. Enzymatic activity was measured in nmol of fluorescence/minute/μg of protein and revealed no significant change of activity in mutant groups when compared to healthy controls; hexosaminidase activity was 0.486 ±0.028 in wt/wt and 0.452±0.019 in mutant group, whereas β-galactosidase activity was 0.078±0.007 in wt/wt and 0.080±0.005 in wt/L444P fibroblast, each bar represents mean of activity in all cell lines per group ± SEM, (n=5).

3.4.3 Autophagic Defect in L444P Mutant Fibroblast

Since GCase deficiency has been linked with impairment of MA, we measured the flux through this pathway. To do this we used two markers of MA, LC3-II, and p62, which both help recruit to autophagosomes, which then fuses with lysosomes, and degrades cargo. LC3-II levels are considered to represent the number of autophagosomes in the cell, while p62 reflects how much cargo is present within these autophagosomes as it helps bind cargo to the LC3-II on autophagosomes. Under untreated conditions (ut) the amount of p62 and LC3-II were unchanged between wild type and wt/L444P groups suggesting that autophagosome number (LC3-II) and autophagosome cargo (p62) are unaffected by the L444P mutation, (mean values of LC3II in both untreated wt/wt and wt/△ groups were 0.061±0.0115 and 0.071±0.017 whereas the mean values of P62 in the same untreated groups were 0.326±0.036 and 0.274±0.042 respectively), (Figure 0.5). To understand the MA flux (e.g. the rate of autophagosome synthesis and degradation), cells were treated with 0.2 μM of specific inhibitor of vacuolar (H+) V-ATPases, bafilomycin A1 (Baf) for 4 hours, which de-acidifies lysosomes, and therefore are unable to fuse with autophagosomes and degrade them. Therefore, over the four-hour time point, all the autophagosomes made during this period accumulate within the cell. As expected, Baf treatment significantly increased both LC3-II levels (***P*=0.001) and p62 (**P*=0.034) compared to untreated (ut) cells. However, the accumulation of p62 and LC3-II was similar between wt/wt cells and wt/Δ showing that the presence of L444P did not affect the rate of synthesis of autophagosomes, (Figure 0.5 B,C) (mean values of LC3-II in both bafilomycin treated wt/wt and wt/Δ groups were 0.618±0.0102 and 0.749±0.013; *P*=0.815 whereas those of P62 in

the same groups were 0.497±0.043 and 0.544±0.029; *P*=0.947 respectively), (Figure 0.5). Furthermore, since the number of autophagosomes formed was the same between wt/wt and wt/△ cells. These observations suggested that there is no accumulation of LC3-II or p62 under untreated condition and that the rate of autophagosome degradation was also the same. To conclude, MA flux does not appear to be affected in fibroblasts with heterozygote L4444P mutations.

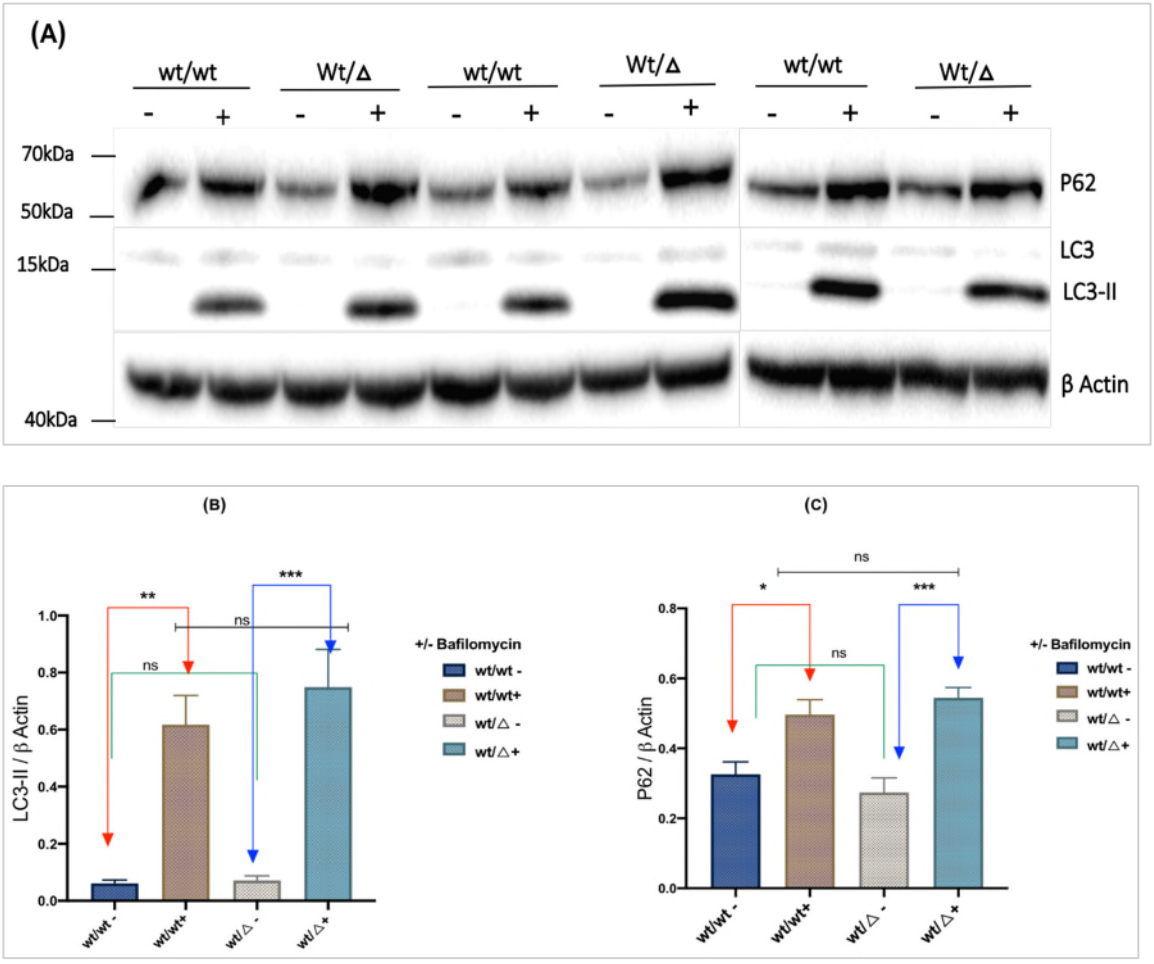

Figure 0.5 Investigating MA flux in wt/L444P fibroblast: MA flux does not appear to be affected in fibroblasts with heterozygote L4444P mutations. (A): Representative western blot images showing no evident change in P62 level (top panel) or the LC3-II level (middle panel) between the basal condition (-) and following BafA1 treatment (+) in heterozygous L444P mutant fibroblasts. β Actin was used as loading control. (B): Analysis of LC3-II densities showing that under basal condition (ut) the amount of LC3-II was unchanged between wild type and wt/△ groups; LC3-II untreated

wt/wt=0.061±0.012; untreated wt/△ group= 0.071±0.017, *P*>0.999. However, bafilomycin treatment significantly increased LC3-II levels in wt/wt (*P*=0.001) and wt/△ fibroblast (****P*=0.0002) against their respective untreated groups; LC3-II in +baf wt/wt=0.618±0.102 whereas in +baf wt/△=0.749±0.133. More importantly, there was no significant change detected in LC3-II level in wt/△ fibroblast cells with (*P*=0.815) and without (*P*>0.999) bafilomycin treatment, when compared to their respective wt/wt groups; LC3-II untreated wt/wt= 0.061±0.011 and wt/△ groups= 0.071±0.017, while in both bafilomycin treated wt/wt and wt/Δ groups, LC3-II= 0.618±0.010 and 0.749±0.0133 respectively. All data were expressed as the mean density of LC3-II expressed against the density of the housekeeping protein (β actin) from 5 independent fibroblast cultures ±SEM (n=5). (C): Bar chart analysis of western blot P62 densities showing no significant alteration in p62 level between wt/wt and wt/Δ groups; P62 untreated wt/wt= 0.326±0.035, untreated wt/△=0.274±0.042, (*P*=0.920). Bafilomycin treatment however significantly increased P62 levels in both wt/wt (**P*=0.034) and wt/△ group (****P*=0.0007) as compared to the respective untreated groups. Also, P62 level did not significantly change between wt/wt and wt/△ fibroblast groups in the presence (*P*=0.947) and absence (*P*=0.920) of bafilomycin treatment; P62 untreated wt/wt= 0.326±0.036 and wt/△ group= 0.274±0.042 while in both bafilomycin treated wt/wt and wt/Δ groups P62= 0.497±0.0429 and 0.544±0.029 respectively. All data were expressed as the mean density of P62 protein expressed against the density of the housekeeping protein (β actin) from 5 independent fibroblast cultures ±SEM (n=5).**

3.4.4 Investigating Chaperone-Mediated Autophagy (CMA) in wt/L444P Fibroblast

Another pathway for cytosolic protein clearance through lysosomes is chaperone-mediated autophagy (CMA). Substrate proteins in this pathway are characterized by the presence of motif in their amino acid sequence (Dice, 1990, Massey et al., 2004). This motif is recognized by a cytosolic chaperone, the heat shock protein of 70 kDa (Hsc70).

When bound to hsc70, the substrate protein is unfolded and the chaperon-substrate complex then docks at the lysosomal membrane by binding to the cytosolic tail of a single transmembrane protein receptor called lysosome-associated membrane protein 2A (LAMP2a) and delivers cargo into the lysosomal lumen for degradation by hydrolases and proteases (Salvador et al., 2000). It has previously observed that the levels of hsc70 and LAMP2a decreased in sporadic PD brains (Alvarez-Erviti et al., 2010). To investigate if CMA pathway is compromised in affected fibroblast, we assessed its activity by measuring LAMP2a and HSC70 protein expression levels. Our results showed that the level HSC70 marker was comparable between control and wt/L444P fibroblasts (P=0.676); mean expression level of HSC70 in wt/wt fibroblast was 0.426±0.067 whereas in wt/△ group it was 0.445±0.084, (Figure 0.6 C). Likewise, LAMP2a protein level did not significantly change (P=0.997) between wt/△ fibroblast (1.62±0.138) and wt/wt group (1.62±0.098), (Figure 0.6 D). These observations concluded that there was no defective CMA pathway associated with heterozygous L444P mutation.

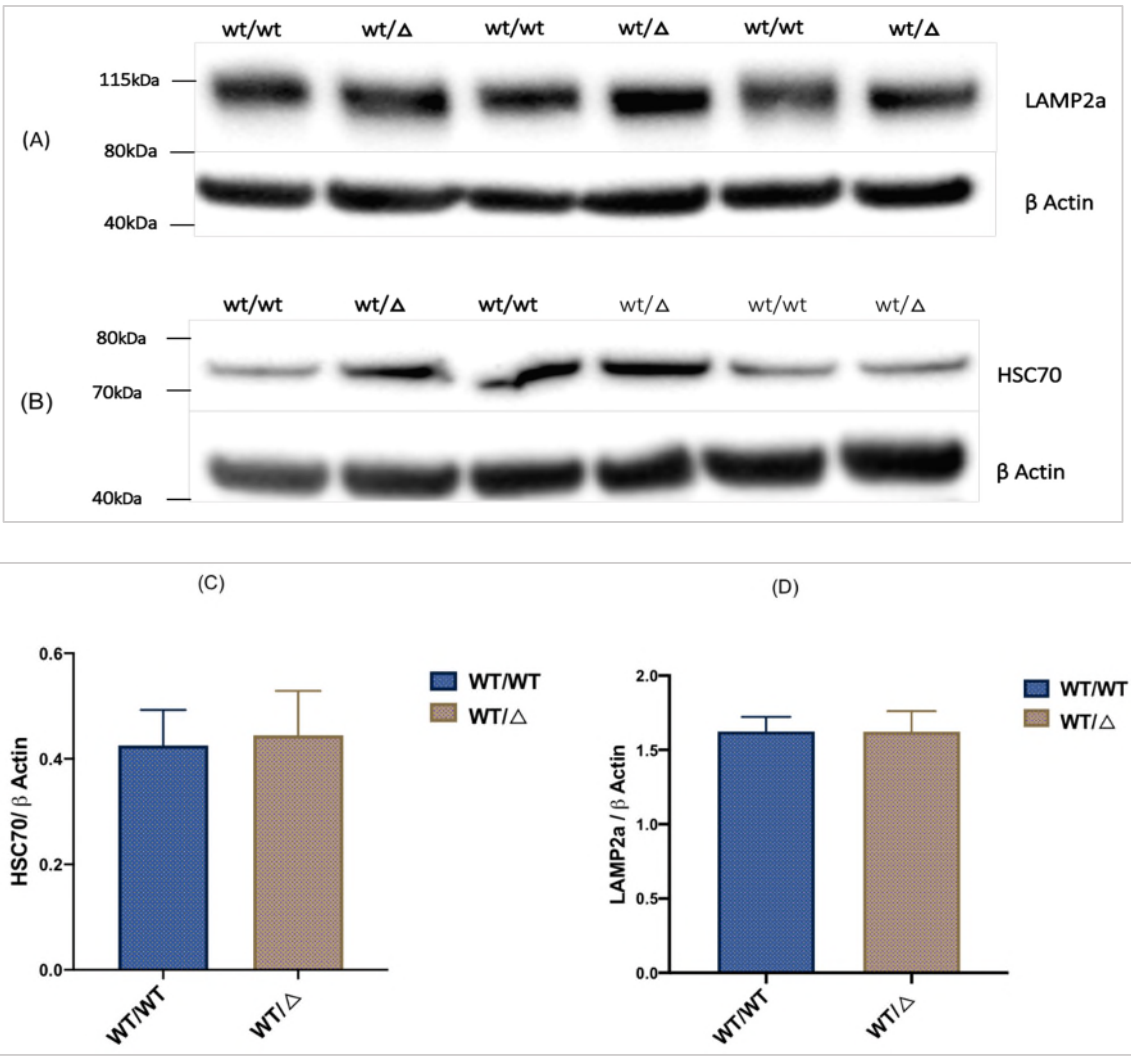

Figure 0.6 CMA in wt/L444P patient derived fibroblast: No defective CMA pathway was seen in fibroblasts with heterozygote L444P mutations. (A, B): Representative western blot images showing no evident change in LAMP2a (top blot) and HSC70 (bottom blot) markers of CMA in wt/△ fibroblasts when compared to wt/wt groups, β Actin was used as loading control. (C): Bar chart analysis showing comparable HSC70 between wt/wt (0.426±0.067) and wt/△ fibroblast (0.445±0.084), *P*=0.676. (D): Bar chart representation showing no significant change in LAMP2a level between wt/△ fibroblast (1.62±0.138) and wt/wt group (1.62±0.098), *P*=0.997. All data were expressed as the mean density of target proteins (LAMP2a and HSC70) expressed against the density of the housekeeping protein (β actin) from 5 independent fibroblast cultures ±SEM, (n=5).

3.4.5 Proteasomal activity in Fibroblasts

Although ALP is considered as one of the major protein degradation pathways in the cell, it is not only the pathway involved in the cellular quality control. UPS also contributes to this phenomenon by the turnover of proteins such as monomeric alpha-synuclein and the removal of unfolded protein by ERAD. Therefore, we measured the basal activity of the 20S catalytic subunit of the proteasome. There was not significant change in proteasome activity in dermal fibroblast cells with L444P mutation (0.053±0.005) when compared to wt/wt group (0.047±0.004), (*P*=0.423). (n=5wt/wt and 4 wt/△). As a control, fibroblast lysates were incubated with 0.25mM of the specific proteasome inhibitor, Lactacystin. When incubated with Lactacystin, proteasomal activity dropped by 98% (n=1) to confirm that what we have measured was 20S activity (Figure 0.7 B).

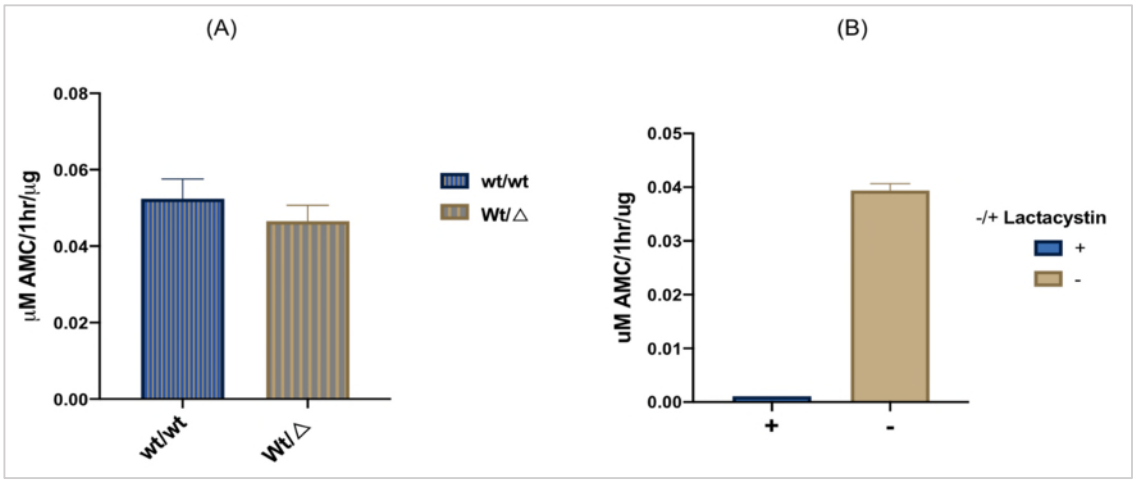

Figure 0.7. 20S proteasomal activity in wt/L444P fibroblasts: under basal condition and after treatment with Lactacystin. (A): Bar chart summarizing 20S proteasomal activity in human dermal fibroblast; 20S reaction rate was calculated in μM of AMC/1hr/μg of protein (n=5 wt/wt and 4 wt/△) and data shown represent mean ± SEM. The chart shows no evidence of alteration in 20S activity in wt/△ (0.053±0.005) against wt/wt group (0.047±0.004), (*P*=0.423). (B): Bar chart representation of inhibited proteasomal activity following treatment with 0.25mM of the proteasomal inhibitor, Lactacystin, in fibroblasts (n=1) indicating the specificity of the reaction measured.

3.4.6 ER stress &UPR (Control)

ER stress and UPR are discussed in details in (section1.8). The most immediate response in ER stress is upregulation of Bip/GRP78 level due to its release from ER sensors and subsequently turning them to the active state. We first did a preliminary pilot study (n=1) to investigate if the induced ER stress and UPR in fibroblast result in elevated BiP level and higher Phospho-elf2α/elf2α ratio. As expected, control fibroblasts treated with 1μM of Thapsigargin for 24 hours before harvesting showed upregulation of Bip/GRP78 level and increased Phosphorylation of elf2α, (Figure 0.8).

We also assessed the survival of GCase deficient fibroblast through measuring the expression level of apoptotic marker (CHOP) by WB in the wt/wt and wt/L444P fibroblasts (n=4). However, this marker was not detectable in cells (data not shown).

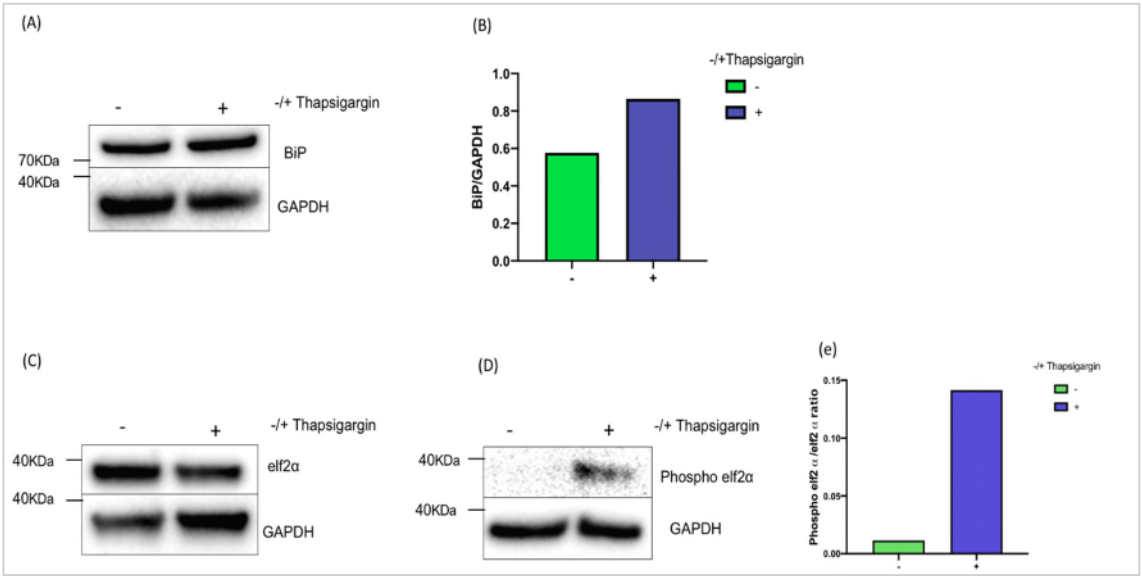

Figure 0.8 inducing ER stress in wt/wt fibroblast (positive control): (A, B): Representative western blot image and bar chart showing increased Bip/GRP78 level upon Thapsigargin treatment (induction of ER stress). (C, D, E): Western blots images and bar chart showing increased level of phosphorylated elf2α in Thapsigargin treated wt/wt fibroblasts (UPR), (n=1). GAPDH was used as a loading control. UPR in wt/L444P Fibroblast model.

It was documented that not only wild type misfolded but also mutant proteins are tapped in the ER inducing UPR (Kopito, 1997). Reduced GCase protein in wt/Δ cells was previously reported and linked to activation of UPR (Bendikov-Bar et al., 2011, Bendikov-Bar et al., 2013, McNeill et al., 2014, Sanchez-Martinez et al., 2016, Braunstein et al., 2018). We therefore analyzed the expression of the unfolded protein response marker BiP/GRP78 in wt/L444P fibroblasts. Western blot analysis of this ER-resident chaperone showed comparable level between the wt/L444P (0.334±0.0345) and wt/wt group (0.342±0.076) suggesting that the mutant GCase retained in ER of the fibroblast, did not induced stress, (*P*=0.926), (Figure 0.9 A and B).

We also extended that to the analysis of PERK arm of UPR through measurement of phosphorylated elf2α/ elf2α in the corresponding cell lines. We detected no significant change (*P*=0.806) in the ratio between the wt/wt (0.345±0.055) and wt/Δ group (0.378±0.118), (Figure 0.10 A and B). The lack of alteration in phosphorylated elf2α/ elf2α ratio in wt/L444P fibroblasts fits with BiP level being not upregulated in these cells.

To conclude, wt/L444P did not induce ER stress and UPR in human dermal fibroblast model.

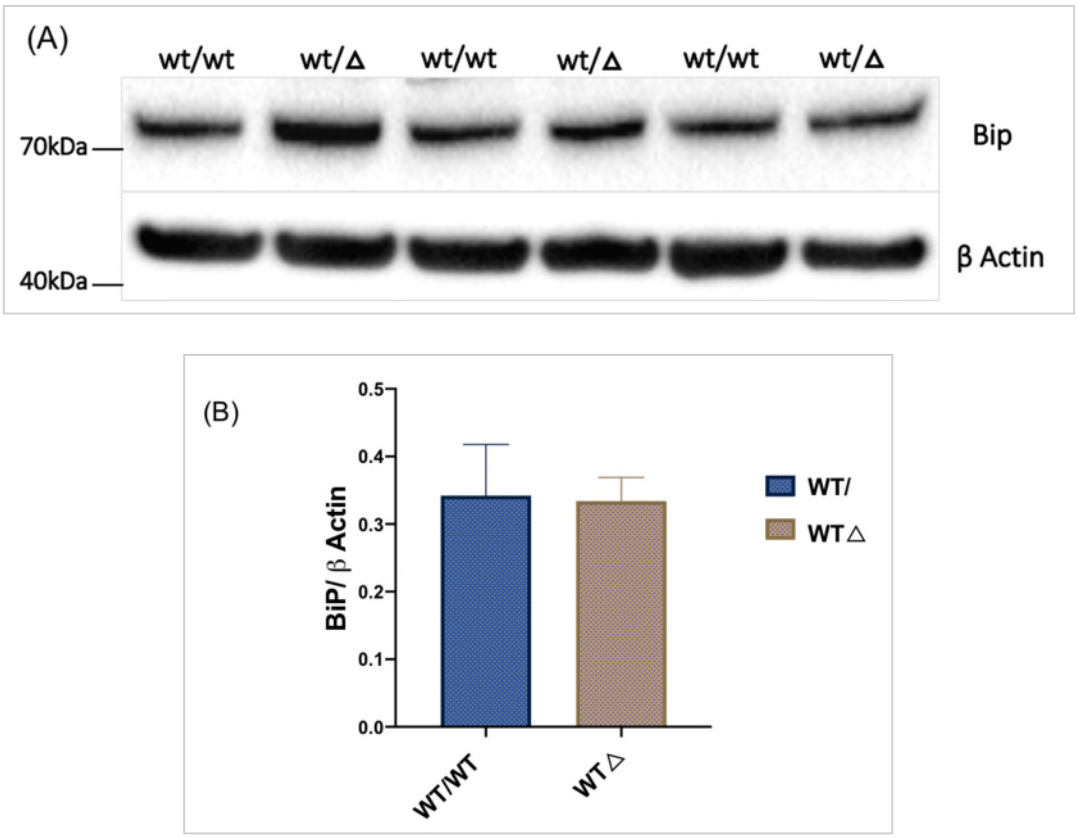

Figure 0.9 BiP expression in wt/L444P fibroblast. (A): Representative western blot image of BiP showing relative comparable densities of protein bands between the control and wt/L444P fibroblasts groups; despite the slightly apparent variability in BiP expression in few lines seen, that could be cell line specific, the overall expression was similar between groups, β Actin was used as a loading control (B): Bar chart summarizing the mean BiP protein level in fibroblast with no significant change (*P*=0.926) between groups; BiP wt/wt =0.342±0.076 and wt/△ =0.334±0.0345. All data represent the mean density of target protein expressed against density of housekeeping protein (β actin) from 5 independent fibroblast cultures ±SEM, (n=5).

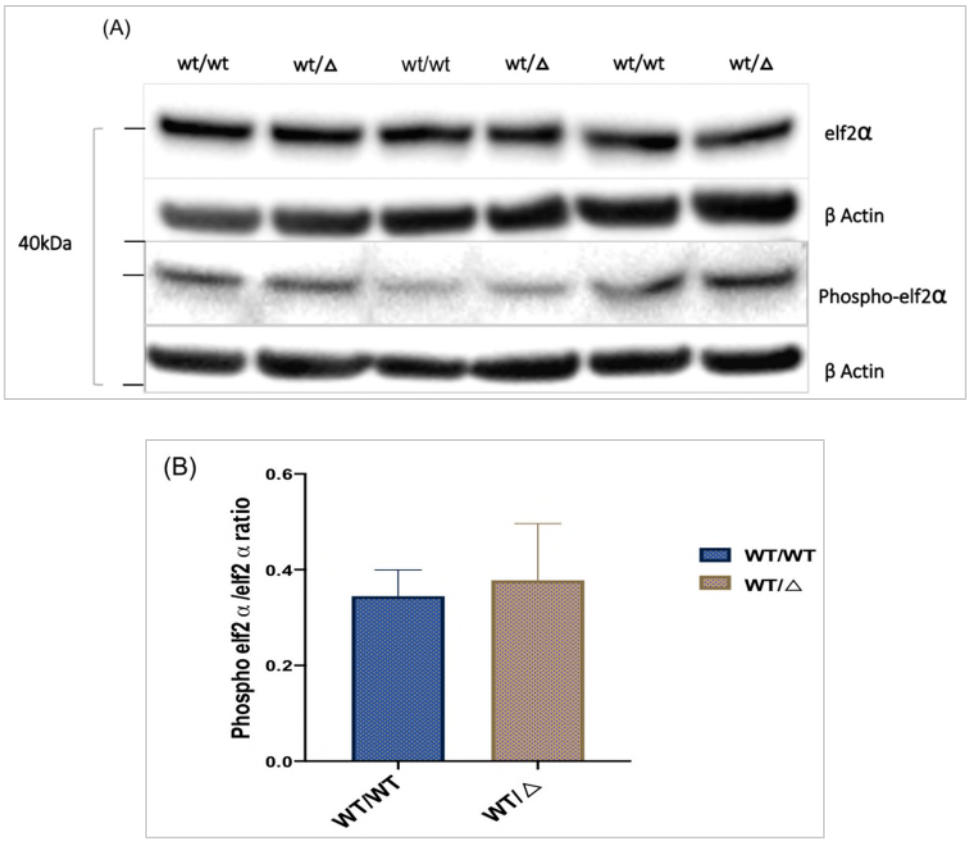

Figure 0.10 Phosphorylation of elf2α; no ER stress and induction of UPR in GCase deficient fibroblasts. (A): Representative western blot image of elf2α (top blot) and phosphorylated elf2α (bottom blot) showing no apparent alteration between the control and wt/△fibroblast, β-Actin was used as a loading control (B): Bar chart summarizing the mean value of phosphorylated elf2α/ elf2α ratio in wt/wt (0.345±0.055) and wt/△ cells (0.378±0.118) with no significant change between the two groups (n=5, *P*=0.806).

3.4.7 ER trapped GCase (Endoglycosidase-H Assay)

We, and in an effort to verify the proportion of trapped mutant enzyme in the ER, we used the glycosylation status of GCase. Endo-H enzyme deglycosylates GCase in the ER and cleaves the bond between the first and second mannose sugar residues. Additionally, GCase is only sensitive to Endo-H cleavage while trapped in the ER whereas mature enzyme is resistant to cleavage because of the mannose residue attached to it. It therefore allows us to distinguish between the enzymes that have not reached the mid-Golgi and the folded, processed, and mature glycoproteins. Also, another enzyme we used called peptide N-glycosidase F (PNGase-F) which removes all the N-linked carbohydrate resulting in complete deglycosylation (Figure 0.11).

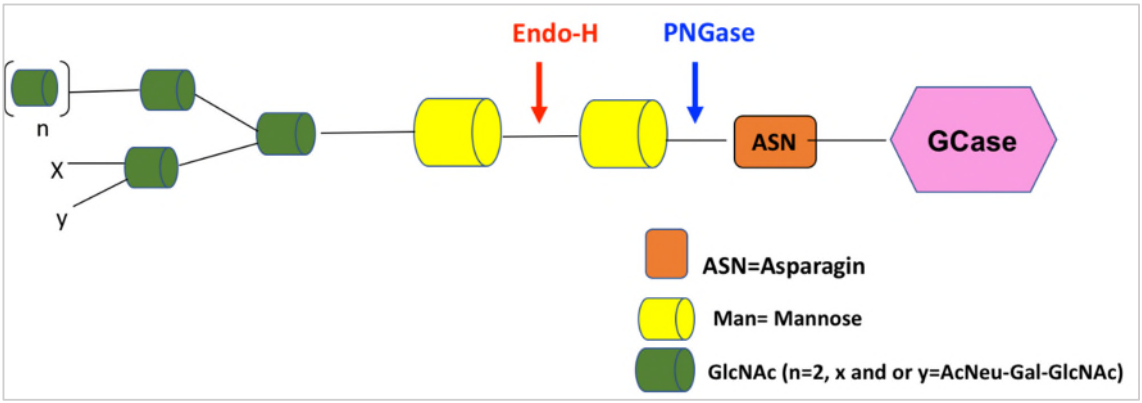

Figure 0.11 Illustrative diagram showing the site, in GCase, of cleavage of both Endoglycosidase-H and PNGase F enzymes. Endo-H only cleaves high mannose structures (red arrow) whereas PNGase F hydrolyses nearly all types of N-Glycan chains from the glycoprotein (blue arrow).

In SDS– PAGE, both Endo-H sensitive and PNGase treated fractions migrated as a low molecular weight bands, which confirmed that any detected changes in GCase protein bands is due to glycosylation and not from changes in amino acid sequence. Cell lysates prepared from homozygous L444P GD fibroblast lines were subjected to PNGase F treatment for 2 hours according to manufacture

instructions. As PNGase cleaves all sugar residues of GCase next to asparagine (Figure 0.11), western blotting and interaction with anti-GCase antibody showed that following PNGase F treatment, a small molecular weight band of GCase appeared migrating from 70kDa to ~50kDa region as indicated by the blue arrow in (Figure 0.12 A and B). When these cell lysates were treated with Endo-H enzyme for two hours, a small amount of GCase enzyme bands was present in the mature state at the region of 70kDa. However, the majority of GCase from Endo-H treated lysates were present at 50kDa region and having similar size to that treated by PNGase denoting trapped enzyme in the ER, red arrow in (Figure 0.12 A). Similar findings were reported previously by (Bendikov-Bar et al., 2011) and (Ron and Horowitz, 2005).

To assess if the degree of ER retention acts as a factor that determine GD severity, we assessed the heterozygous state of L444P mutation using the same approach. We found that in the heterozygous L444P fibroblasts, and following Endo-H treatment, the vast majority of GCase enzyme was in the mature lysosomal state and only when we overexposed the blot, a small portion was found trapped in the ER and appeared at ~50kDa region (yellow arrow in Figure 0.12 B). We also detected similar bands, quantitively confirmed at ~ 50KDa region, in the wild type cells treated with endo-H enzyme (red arrow in Figure 0.12 B). The presence of this trend in both heterozygous and wild type group indicated that most of the protein already passed the mid-Golgi (i.e. mature lysosomal) and only small proportion was retained in the ER. Similar findings were reproduced previously by other groups (Ron and Horowitz, 2005, Bendikov-Bar et al., 2011) pointing out to the presence of variable levels of ER retention among different genotypes including wildtype. Nevertheless, even with the

minimal degree of ER retention, the intracellular localization tests in theis studies showed that most of wild type GCase localized in punctate lysosomal structures, with no calnexin colocalization. On the other hand, all mutants exhibited major colocalization with calnexin, indicating that most of the mutated GCase were retained in the ER inducing ER stress and UPR.

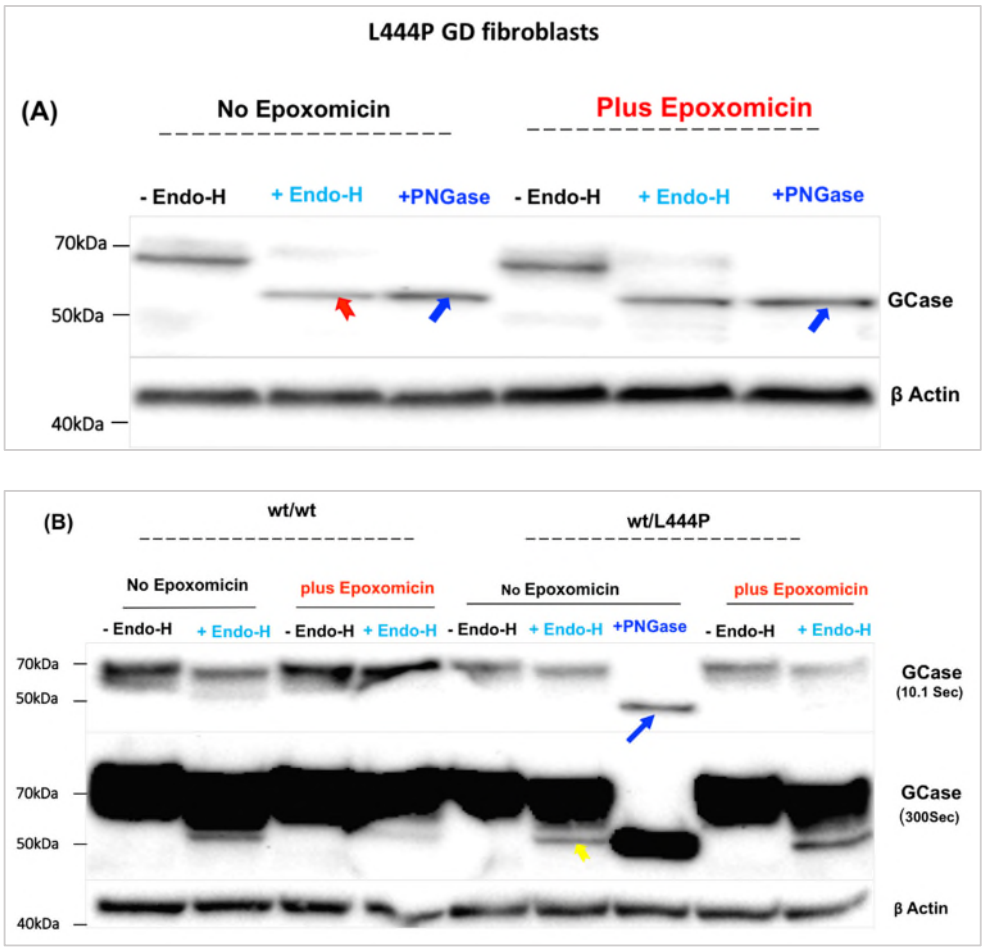

Figure 0.12 Evidence of ER retention of GCase in wt/L444P fibroblast. 20µg protein lysates of both GD L444P fibroblasts (A) and wt/L444P group (B) were incubated for 2 hours with Endo-H and PNGase F enzymes and immunoblotted with anti- GCase and anti β Actin antibodies. Note appearance of low molecular weight band (~ 50kDa) in Gaucher disease samples incubated with PNGase (blue arrows in A, B), which represents complete deglycosylation of GCase. (A): Following Endo-H treatment, an ER retained GCase fractions started to appear at 50kDa region in GD L444P fibroblasts (red arrow) leaving only a small portion of the enzyme in the mature state at 70kDa region. (B): In heterozygous L444P state, the vast majority of the enzyme was present in mature state and only with overexposure of the blots, a small fraction of the trapped enzyme in the ER appeared at ~ 50kDa region (yellow arrow) which was present also in the wild type group (red arrow). The presences of similar Endo-H sensitive bands in wild type group was also reported in other studies (Ron and Horowitz, 2005, Bendikov-Bar et al., 2011). Epoxomicin treated lanes show apparent increase in GCase protein (due to inhibition of proteasomal degradation by UPS).

For purposes of comparison and to further confirm the above findings, we treated N370S mutant fibroblast cells with Endo-H and the result data showed the same trend as L444P mutation state (Figure 0.13 A and B).

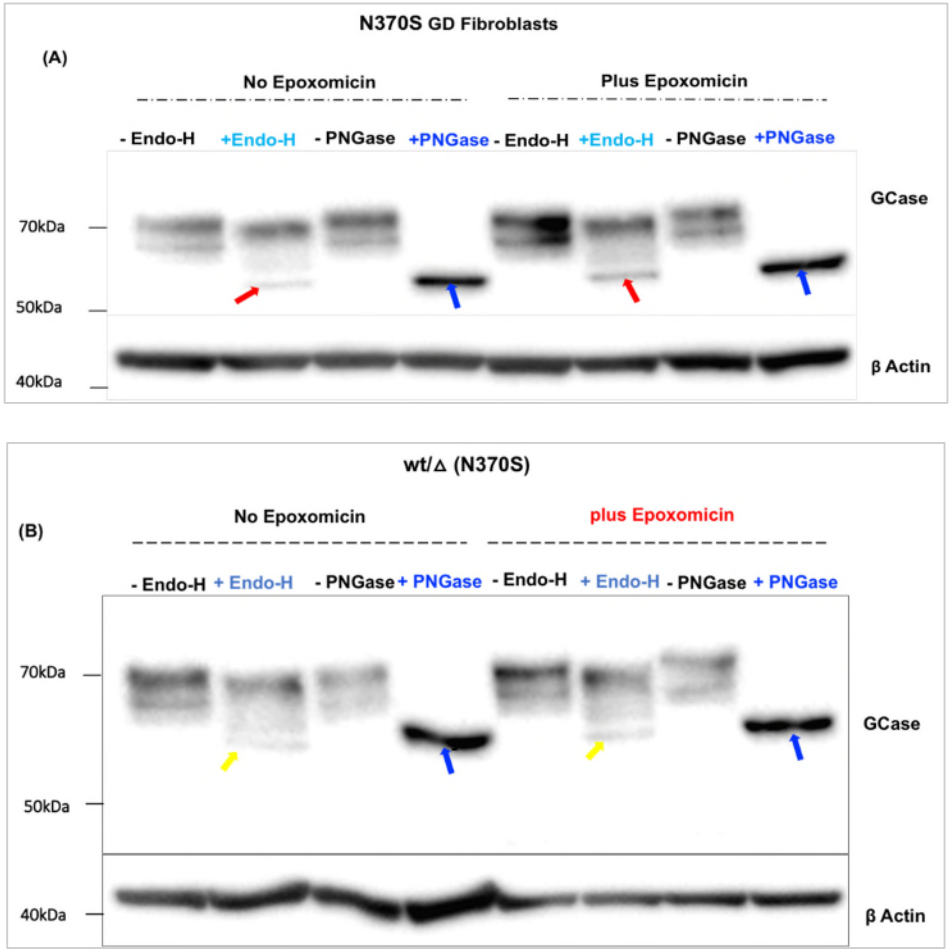

Figure 0.13 ER retention of GCase in GD and heterozygous N370S fibroblast. The trend of ER retention here was similar to that detected in L444P mutant fibroblasts. (A): Following PNGase F treatment, GCase was completely deglycosylated and appeared as lower molecular weight bands at 50kDa region (blue arrow), (also present in B). However, Endo-H treatment retained a large portion of GCase in the ER which appeared at 50kDa region (same as that treated with PNGase F (red arrow) and left only a small portion in the mature state at 70kDa region. (B): In heterozygous N370S state, most of GCase enzyme was lysosomal and only a small fraction appeared at 50kDa region (yellow arrow). Epoxomicin treated lanes show apparent increase in GCase protein (due to inhibition of proteasomal elimination by UPS).

Furthermore, the reduction in GCase protein level observed in the mutant L444P variant raised our suspicion that it could be due to elimination of the misfolded mutant protein by proteasome during the process of ERAD. We therefore monitored the fate of GCase protein by incubating fibroblast lines derived from wild type, both N370S and L444P GD patients, and the corresponding heterozygous lines with 26 nM of proteasomal inhibitor Epoxomicin. (see page 68). Epoxomicin treatment inhibits proteasome and hence prevents the disposal of mutant enzyme by UPS pathway during the later stages of UPR. Although not evident in wt/wt fibroblasts as most of GCase was mature (i.e. lysosomal), all Epoxomicn treated L444P GD fibroblasts and to lesser extent the heterozygous state blot showed increased protein levels indicating stabilization of GCase protein through proteasomal inhibition as they were no longer degraded by UPS (Figure 0.12) and (Figure 0.13).

We also wanted to asses if the trapped GCase has induced UPR and whether it is gene dosage dependent, limited to homozygous mutations, due to greater ER-trapping. We analyzed BiP levels in the same cells used for ER trapping above (Figure 0.14). Our results showed no significant difference in BiP levels (P>0.999) between wildtype (0.303, n=1), GD fibroblasts (0.202±0.044), and heterozygous mutant lines (0.243±0.068). This suggested that in wt/L444P fibroblast model, the trapped GCase in the ER was not sufficient to induce UPR.

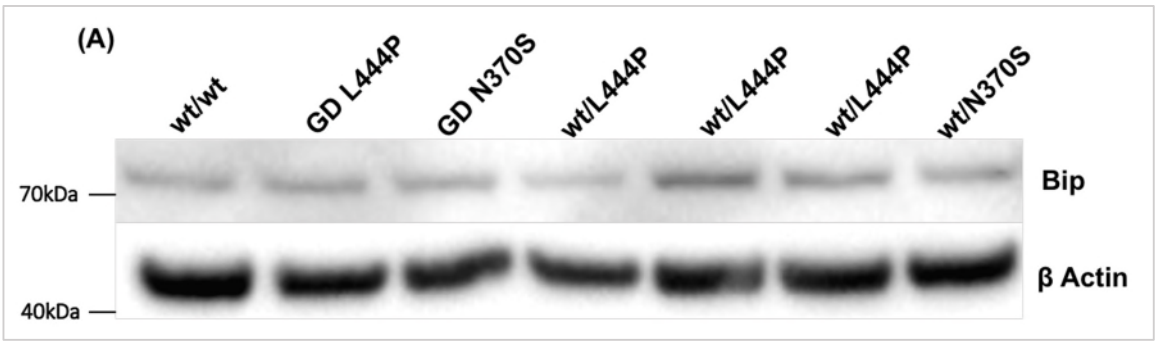

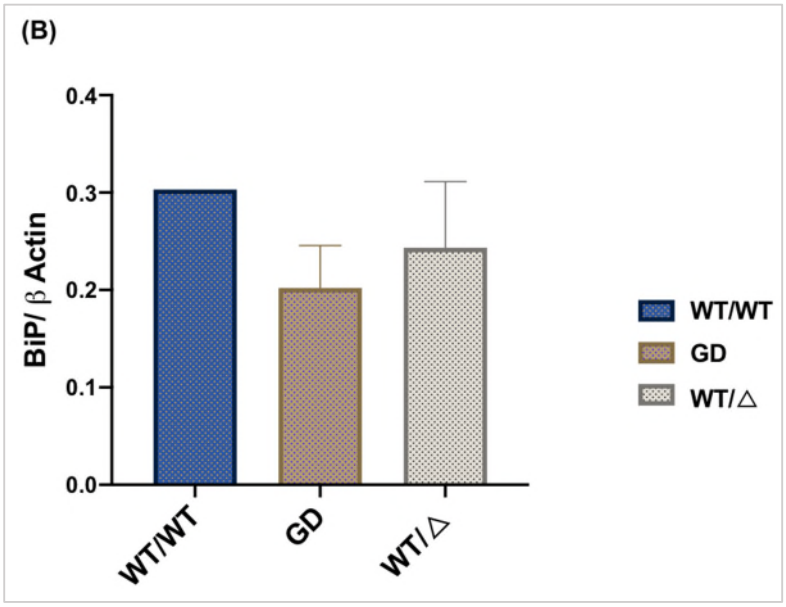

Figure 0.14 Comparing BiP expression level between GD, heterozygous N370S and L444P mutations: (A): Representative western blot image of BiP showing overall comparable levels of the BiP protein between the control and GD homozygous and heterozygous L444P and N370S fibroblasts, β Actin was used as a loading control (B): Bar chart analysis showing no significant change in BiP expression between the groups (P>0.999) in wt/wt (0.303, n=1); GD fibroblasts (0.202±0.044, n=1GDL444P, 1GD N370S; and wt/△ lines (0.243±0.068, n=1wt/N370S and 3wt/L444P). All data were expressed as the mean density of target protein expressed against the density of the housekeeping protein (β actin) from each independent fibroblast cultures ±SEM, analysis done using Kruskal-Wallis test.

3.5 Discussion

This work has started to study the pathophysiology of the L444P mutation in primary cultured fibroblasts derived from heterozygous mutation carriers with and without Parkinson's disease. Results of biochemical alterations associated with GD L444P and heterozygous mutations are summarized in (Table 0.2).

Table 0.2 Comparison of results obtained in fibroblasts model of L444P GD and heterozygous mutant states.

Disease phenotype	Heterozygous L444P	GD L444P
GCase activity	34.7% reduction	Not investigated
GCase protein expression level	Non significant reduction in GCase protein level	Not investigated
Lysosomal contents (LIMP2, LAMP1 Cathepsin D)	Not significantly changed	Not investigated
BiP level	Not significantly changed	Not significantly changed
Phosphorylation of elf2a	Not significantly changed	Not investigated
ER trapping	+	+++
MA	Not significantly changed	Not investigated
CMA	Not significantly changed	Not investigated
UPS	Not significantly changed	Not investigated

We first confirmed 34.7% significantly lower GCase activity in the wt/L444P fibroblasts against control (*P=0.014). In addition, western blotting of these cells showed a ~30% concomitant but nonsignificant reduction in GCase protein level. Reduced enzymatic activity, mRNA and protein levels have been reported

previously by other groups investigating patient derived fibroblast with a variety of *GBA* mutations (de la Mata et al., 2015, McNeill et al., 2014, Sanchez-Martinez et al., 2016, Ambrosi et al., 2015, Collins et al., 2017, Ron and Horowitz, 2005). However, it should be noted GCase activity is considered as more accurate quantitative measure than the assessment of protein expression level.

Due to lower GCase protein level in wt/L444P fibroblasts, we assumed that it is most likely that mutant enzyme trapped in the ER and induces UPR leading at later stages to its elimination by the process of ERAD resulting eventually in loss of function and reduced protein level. The most important question we therefore aimed to answer in this chapter, is whether heterozygous L444P is an ER retention mutation when using human derived fibroblast model. Although it is established that ER stress, retention and proteasomal degradation are well-correlated with GD severity (Ron and Horowitz, 2005), they were not documented before in heterozygous L444P fibroblasts, and for this reason we sought to investigate them on the heterozygous mutation state. To do so, we first went for assessing the level of ER resident chaperon BiP/Grp78 and the ratio of phosphorylated elf2α in L444P mutant fibroblasts. Surprisingly, we found that both BiP level and elf2α phosphorylation were unchanged in mutant lines with respect to control. However, other groups showed significant upregulation of BiP and calnexin levels in GD fibroblasts and to lesser extent in PD derived cells with *GBA* mutations (McNeill et al., 2014). This was indicating that ER stress is secondary to trapped mutant enzyme. Additionally, dysregulation of Ca^{2+} homeostasis and increased vulnerability to stress responses and neurodegeneration has been observed in patients derived fibroblast with *GBA* mutation (Kilpatrick et al., 2016). Although McNeill et al. group has pooled a

variety of homozygous and heterozygous mutations together, the discrepancy between our findings and the above studies is less likely to be due to loss of function since ER stress and Ca^{2+} level perturbation in Kilpatrick et al. work was independent of GCase pharmacologically induced loss of activity in heterozygous N370S fibroblasts.

We then looked at the intracellular processing and trafficking of the mutant enzyme by conducting endo-H assay with and without proteasomal inhibition by Epoxomicin treatment. GCase that unfolds and becomes trapped in the ER contains N-linked glycans which are sensitive to cleavage by endo-H. Our results showed evidence of ER retention in L444P homozygous state in which the vast majority of GCase was Endo-H sensitive, and only a small amount was lysosomal and present in the mature form. On the contrary, and in wild type and heterozygous L444P, a small residual fraction of Endo-H sensitive GCase started to appear after prolonged exposure of the blot to provide us an evidence of ER retention in these cells but was less extensive than GD fibroblasts. Many observations were reported previously using fibroblast carrying different GD and *GBA* heterozygous mutations, and are corroborated to our findings (de la Mata et al., 2015, McNeill et al., 2014, Bendikov-Bar et al., 2011, Ron and Horowitz, 2005, Mu et al., 2008). In addition, the increased protein level after Endo-H treatment in the presence of Epoxomicin further confirmed that the mutant variant is retained in ER and degraded and thus leading to reduced GCase level observed in the mutant variant. However, despite the evidence that L444P and N370S mutations are usually associated with decrease in protein expression due to ERAD (Gegg and Schapira, 2018), there was no alteration in UPS function in our heterozygous L444P fibroblast model. Additionally, the ER trapped fraction

of mutant GCase in our model was not sufficient to induce ER stress and UPR as evident by normal BiP level in heterozygous lines (n=5) and GD fibroblasts (n=2). Perhaps western blotting is not sensitive enough to detect upregulated BiP level since such an increase was very small in Thapsigargin treated control fibroblasts. Alternatively, More sensitive approaches such as Ca^{2+} release studies like in (Kilpatrick et al., 2016) or immunofluorescence measures of calnexin ER stress marker in (Garcia-Sanz et al., 2017) are better required to investigate ER stress and thus could be considered as future prospective. The altered Ca^{2+} signalling in Kilpatrick et al. study was observed in some but not all primary fibroblasts cultures with N370S GD/ heterozygous mutations. Likewise, there was some variability in BiP expression among both normal and mutant fibroblasts lines used in our study which once again, rises the possibility that UPR is cell lines specific or is even activated differently in various cell type.

We next wanted to investigate that if the reduced level of GCase protein was not due to defective trafficking of the enzyme from the ER to the lysosome by measuring LIMP2 protein level by western blot. As expected, LIMP2 level did not differ between the wt/L444P fibroblasts and the control (n=5, p=0.591) suggesting that GCase sorting was not abrogated in these cells. This was consistent with the previous observation of (McNeill et al., 2014, Ambrosi et al., 2015, Magalhaes et al., 2016). In fact, Reczek and collaborators have shown that GCase/LIMP2 complex formation, in mannose-6-phosphate independent manner, and the subsequent sorting of to the lysosome were still preserved even in the most common GD mutant fibroblasts, namely L444P and N370S mutations (Reczek et al., 2007).

In addition, the activities of β-hexosaminidase and β-galactosidase enzymes were not altered between mutant and control groups. This further confirmed that the reduced GCase activity was due to mutation and not due to defective lysosomal biochemistry, and the only lysosomal enzyme affected by *GBA* mutation is GCase enzyme. Similar results were reported previously by groups such as (Tatti et al., 2012, Collins et al., 2017, Kilpatrick et al., 2016, Ron and Horowitz, 2005) using larger cohorts of L444P, N370S NMC and GD-derived fibroblast. Despite that, a subtle alteration in lysosomal biochemistry was found in (McNeill et al., 2014) work. They reported an increased β-hexosaminidase and β-galactosidase activities in GCase deficient fibroblast. However, with the given evidence of elevated lysosomal hydrolyses activity in different tissue homogenates derived from GD patients regardless of their normal protein levels (Moffitt et al., 1978), the enhanced enzymatic activity in above study could be explained as a compensatory mechanism to catabolize the glucosylceramide substrate accumulating in GD cells.

We also screened for other potential aspects of physical and chemical alteration in lysosome associated with wt/L444P mutation by measuring the basal level of cleaved/mature enzyme Cathepsin D, and the late endosomal/lysosomal marker LAMP1. No significant change in LAMP1 level between mutant cells and control, which was consistent with the lack of defect in β-hexosaminidase and β-galactosidase enzymes activities in these cells. However, despite being statistically non-significant, there was a tendency of increased Cathepsin D expression in L444P heterozygous fibroblasts with respect to control. The same finding previously was reported by other groups in GCase deficient fibroblasts (McNeill et al., 2014, Tatti et al., 2012, de la Mata et al., 2015, Kilpatrick et al.,

2016). Although there was no associated alteration or increased lysosomal mass, as evident by normal LAMP1 protein level, Cathepsin D activity or protein expression level went up significantly in some of these studies (Tatti et al., 2012). Therefore, one would speculate that the increased protein level or activity of Cathepsin D acts a defensive cellular response to decrease GCase activity in far sever bi-allelic mutations such as GD L444P. Another difference between our study and that of Ambrosi and collaborators who reported reduced Cathepsin D level is that they pooled N370S and L444P cells in their study. Thus, it is not clear if this experimental approach concealed a possible upregulated level of cathepsin D. Despite that fact that increased expression of cathepsin D was always present in areas of the brain where gliosis is profound, extensive expression and altered cellular distribution of cathepsins predispose to apoptosis and cellular loss through activation of caspases. To further support this notion, elevated mRNA and increased activities of Cath B /Cath D were also reported in more relevant disease model such as GD mice cortex. In this study and in agreement with our findings, all lysosomal protein including LAMP1 were not affected. This once again might suggest that the compensatory protein upregulation in GD is only confined to a subset of lysosomal proteins, particularly Cathepsin D protease. Even other lysosomal storage diseases were associated with elevated mRNA of cathepsin D and/or B and all of which were characterized by neuronal cell loss (Vitner et al., 2010).

Dysfunction of autophagy lysosomal pathway plays an important role in the pathogenesis of PD (Dehay et al., 2013). With the given evidence of defective lysosomal function associated with GCase deficiency, we further characterized our fibroblasts model and measured the effect of heterozygous L444P mutation

on the MA pathway. To do this, we used two markers of MA, LC3-II, and p62, both of which help recruitment of autophagosomes, which then fuse with lysosomes, and the cargo is degraded. Both LC3-II and P62 levels did not significantly differ between experimental groups under basal conditions. In addition, although Bafilomycin A1 treatment increased both LC3-II and p62 as expected, their levels were the same in both wt/L444P mutant and control cells. These findings suggested that there is no evidence of defective of MA in wt/L444P fibroblast. The same findings have been reproduced in heterozygous and GD patients-derived fibroblasts (McNeill et al., 2014, Tatti et al., 2012) and even in GBA KO MEF (Magalhaes et al., 2016). However, it must be noted that in McNeill et al. work, only the basal levels of autophagic markers LC3-II and P62 were assessed without measuring flux. Therefore, a subtle alteration in the pathway cannot be excluded. Alternatively, the homozygous GD state and/or the type of mutation including the two common mutations N340S and L444P, recombinant alleles or null mutations, could have a noticeable impact on the degree of MA flux impairment. Defective flux was apparent in three L444P GD fibroblasts (de la Mata et al., 2015) and in a variety of PD and/or GD patients derived fibroblast harboring either homozygous or recombinant mutations (Collins et al., 2017, Garcia-Sanz et al., 2017). Intriguingly and corroborating our results, we noticed when dissecting Collins et al. cohort that N370S mutations either in GD homozygous state or heterozygous mutation carriers with PD exhibited defective MA flux whereas fibroblasts derived from PD patients with heterozygous L444P mutation showed preserved MA flux. Furthermore, it was Cathepsin D downregulation in Sap C deficient fibroblasts that resulted in altered lysosome function compared with that observed in examined GCase-deficient

cells, even those homozygous for the two most common mutations, N370S and L444P (Tatti et al., 2012). More importantly, in (Mazzulli et al., 2011) study, they analysed the proteolysis of long-lived proteins in GCase KD living neurons by pulse-chase experiment in an attempt to assess ALP in these cells. As a result, they reported 40% significant reduction in the rate of proteolysis which was concomitantly associated with accumulation and enlargement of LAMP1-positive puncta in immunofluorescence analysis. Similar observation reported in other cellular models such as wt/N370S fibroblast in (Garcia-Sanz et al., 2017) in which image analyses detected increased lysosomal mass, dispersed distribution of lysosome inside the cytoplasm and accumulated autophagosome which were all indicative of impaired lysosomal function and MA flux. Therefore, the defective flux observed in these studies could suggest that more sensitive methods rather than western blotting are needed to investigate ALP in fibroblasts. Among these methods, immunofluorescence measures could be addressed in our future work as fibroblasts are not neuronal cells and presents undetectable level of A-SYN substrate to trace its degradation.

In addition to MA, chaperon mediated autophagy (CMA) is involved in the pathogenesis of PD. Importantly. It is considered as the main degradative pathway for A-SYN, the major constituent of Lewy bodies in PD (Sala et al., 2016). Dysfunction of both ALPs was implicated in accumulation, aggregation, and cell to cell propagation of A-SYN (Gegg and Schapira, 2018). During CMA, all substrate proteins are characterized by the presence of a pentapeptide motif that binds to a cytosolic chaperone, the heat shock protein of 70 kDa (Hsc70) docks at the lysosomal membrane by binding to lysosome-associated membrane protein 2A (LAMP2A) delivering the target into the lysosomal lumen for

degradation by hydrolases and proteases (Cuervo et al., 1999). Our results showed no evident change in LAMP2A and HSC70 markers in the wt/L444P fibroblasts when compared to control indicating intact basal activity of CMA pathway in these cells. On the contrary, compromised CMA was reported in *GBA* KO MEF as evident by decreased level of GAPDH substrate in the wild type cells but not in *GBA* heterozygous and KO MEF after cycloheximide (CHX)-induced protein synthesis inhibition, However, both LAMP2A and HSC70 markers were not changed in these cells (Magalhaes et al., 2016). One main function of CMA is to recycle non-essential substances under cellular stress and protein synthesis shutdown (Sala et al., 2016), and it is possible that the subtle alteration observed here in CMA of *GBA* KO MEF was due to its compensatory upregulation in the wild type MEF under CHX treatment and not due to far sever loss of GCase activity in KO state since similar effect was encountered in *GBA* heterozygous MEF.

We also investigated if there is any UPS alteration associated with L444P mutation by measuring the catalytic activity of 20S subunit proteasome. In 5 wt/wt and 4 wt/L444P fibroblasts lines, the reaction rate was calculated in μM of AMC/1hr/ug of protein and our result showed comparable activity between L444P/wt fibroblast and the control group. This was in line with finding reported by (Ambrosi et al., 2015), in which no change in 20S proteasomal activity was found even in far more severe mutations such as N370S and L444P GD fibroblasts. On the contrary and in the same study, fibroblast derived from iPD showed lower basal level of UPS than the control together with association of a slight but not significant increased ubiquitinated proteins level. This observation, with another previously reported by the same group (Ambrosi et al., 2014), were

consistent with McNaught et al. findings (McNaught et al., 2003). It possible as speculated before by (Ambrosi et al., 2014) that the absence of such a deficit reported in *GBA*-linked PD fibroblasts was due to compensatory activation of UPS during the process of ERAD which facilitates clearance of misfolded mutant variant retained in the ER.

Ambroxol hydrochloride is a known cough expectorant and well-established chaperon molecule which can bind unfolded mutant GBA protein and helps its trafficking to the lysosome. Among 1040 drug screened in the national institute of neurological diseases (NINDS) library (Maegawa et al., 2009), Ambroxol was Identified as a potential pharmacological chaperon that can be used effectively for *GBA* mutant variant cases. Furthermore, many studies have previously used fibroblast model as a target for Ambroxol (Sanchez-Martinez et al., 2016, McNeill et al., 2014, Ambrosi et al., 2015, Bendikov-Bar et al., 2011). They confirmed that Ambroxol administration in mutant cells, improved the lysosomal biochemistry by upregulating genes involved in Coordinated Lysosomal Expression and Regulation (CLEAR) network, rescues the GCase activity, enhance its trafficking to the lysosome and reducing ER stress. This signifies its use as a potential therapeutic agent in neurodegenerative diseases associated with proteinopathy such as *GBA*- linked PD.

3.6 Conclusion

In this chapter, we showed that heterozygous L444P mutant GCase has 37.4 % lower enzymatic activity and almost 30% reduced protein expression level with respect to control. This was associated with no concomitant deficits of either ALP or UPS protein degradation pathways. The no apparent change in MA flux might be attributed to either the cellular robustness or the lower energy requirements of fibroblasts, when compared to iPSc-derived dopaminergic neurons, where inhibition of MA flux has been showed in heterozygous *GBA* mutations (Fernandes et al., 2016, Schondorf et al., 2014). However, there was evidence of slight ER trapping of mutant enzyme in heterozygous state which was not enough to induce unfolding response as explained by unchanged BiP level. This can finally suggest that fibroblasts cannot reproduce all the biochemical abnormalities encountered in *GBA*-linked PD, and this might raise the concern about its physiological relevance as a cell models studied.

4 L444P heterozygous *GBA* Mutation in Mouse Cortical Neuronal Model

4.1 Introduction

This chapter provides an insight into the negative impact of heterozygous L444P heterozygous mutation on primary and adult mice cortical neurons. We worked to identify the pathological findings associated with *GBA* mutation such as lysosomal dysfunction, mitochondrial impairment and A-SYN dysmetabolism. We also utilized A-SYN preformed fibrils (PFFs) seeded MCN model to demonstrate how *GBA* mutations in these neurons can worsen handling A-SYN fibrils. *GBA* mutations was shown to play a substantial role as a genetic etiology of dementia of Lewy body (DLB) and PD with dementia with odds ratios of 8.3 and 6.5 respectively (Nalls et al., 2013, Goker-Alpan et al., 2006, DePaolo et al., 2009). The pathological background of *GBA*-PD appeared to be identical to that of idiopathic disease with accumulation of alpha synuclein (A-SYN) in LB as a crucial pathognomonic event not just in PD but also in LBD. The existence of such intracytoplasmic inclusions in *GBA*-PD strengthen the relationship between A-SYN pathology and *GBA* mutations (Schapira, 2015, Goker-Alpan et al., 2006). Previous study of post mortem brain tissue of individuals with LBD reported GCase protein colocalized with A-SYN in LB inclusions (Goker-Alpan et al., 2010). Interestingly, almost all of the cases in this study were carrying *GBA* mutations with an extensive cortical involvement. This could signify the role of *GBA* mutations in A-SYN aggregation and the biogenesis of LB in vivo, possibly through gain of function mechanism. However, it does not exclude the fact that mutant GCase enzyme could contribute to defective clearance and aggregation of A-SYN as evidenced by its colocalization with LAMP1 protein. For this reason,

the loss of function hypothesis might be also implicated in such pathological event. Although dopaminergic neurons are the most vulnerable spot affected in the pathogenesis of PD, dementia emerges as one of the most debilitating complication when cortical tissue succumbs throughout the ascending course of the disease (Liu et al., 2016). The abundant LB pathology in the neocortical and limbic tissue and its frequent association with a spectrum of LBD with *GBA* mutations, shed the light on the sequential biochemical and pathological alterations in cortex with such mutations (Goker-Alpan et al., 2010). Additionally, TH-positive neurons of primary mesencephalic culture might be diluted or their effect is often cancelled by the presence of other non-dopaminergic neurons as they only make up 1 to 5% of the midbrain tissue (Falkenburger and Schulz, 2006, Braak et al., 2003). We therefore selected heterozygous L444P mutant mouse primary cortical neurons as a relevant cellular PD model as judged by cognitive decline associated with the mutation.

Previous studies have established the relationship between GCase activity and A-SYN utilizing cortical neurons; complete knock out of *GBA* resulted in accumulated A-SYN in mouse cortical neurons (Osellame et al., 2013). Instead of manipulating the gene, pharmacologically induced loss of GCase activity in 10 days CBE treatment of primary mouse cortical neurons compromised the lysosomal recycling and function resulting in increased accumulation of A-SYN in the treated neurons (Magalhaes et al., 2016). Alternatively, the accumulated glucosylceramide substrate in *GBA* knockdown (KD) cortical neuronal culture stabilized the oligomeric intermediates of A-SYN leading to further defect in lysosomal function (Mazzulli et al., 2011). Also, an age-dependent progressive decline in GCase activity was observed in the SNpc and putamen regions of

postmortem samples of healthy individuals. The observed reduction was comparable to GCase activity in both *GBA*-mutation carriers and sporadic PD patients and coincided with accumulated glycosphingolipid (GluSph) substrate. (Rocha et al., 2015a, Huebecker et al., 2019). The inhibition of glucosylceramide synthesis reduced level of hippocampal A-SYN aggregates and alleviated the associated cognitive deficits seen in synucleinopathies mouse models, including D409V *GBA* mutants (Sardi et al., 2017). Similarly, augmented GCase activity, mediated by its overexpression in this model and in CNS of A53T synuclein mouse model, has helped to modulate A-SYN process and acted as a therapeutic strategy that may prevent the progression of the disease (Sardi et al., 2011, Sardi et al., 2013). Correspondingly, increased A-SYN level in twenty-month-old A53T transgenic mice were associated with significant reduction in GCase activity throughout different parts of the brain including cerebral cortex (Migdalska-Richards et al., 2016). Therefore, the resulting positive feedback loop between A-SYN and GCase might be representing a combination of both loss and toxic gain of function resulting from the overexpressed mutant enzyme hence this relationship could induce a self-propagation of the disease.

In addition, treatment of rat midbrain dopamine neurons with A-SYN preformed fibrils (PFFs) has previously induced a time and dose dependent accumulation of insoluble synuclein species which underwent phosphorylation at Ser129 and mitochondrial dysfunction (Tapias et al., 2017, Grassi et al., 2018).

Additionally, we limited our investigations in wt/L444P MCN to PFFs as those forms have been shown to be the only A-SYN species that trigger aggregation of endogenous synuclein both invitro and in vivo, (Luk et al., 2012, Luk et al., 2009).

Defective GCase activity was also found to enhance the nigral cell loss induced by A-SYN overexpression in heterozygous L444P aged mice (Migdalska-Richards et al., 2017). However, with the given evidence of special and temporal pathology spread of LBs and Lewy neurites in PD, reaching the cortex at the final stage of PD and the paucity of dopaminergic neurons, it might represent an inevitable obstacle when protein aggregation, viability and biochemical assays in disease model is the frequently considered outcome.

Effective mitochondrial quality control and lysosomal clearance of damaged organelles and cellular materials are essential for maintaining cellular homeostasis particularly in post mitotic cells such as neurons (Osellame et al., 2013). Mitochondrial dysfunction has been greatly implicated in familial PD, with mutations in PINK1, Parkin and DJ-1 (Schapira, 2008). Defective NADH-ubiquinone reductase (Complex I) activity was observed in the substantia nigra of sporadic PD patients (Schapira et al., 1990, Schapira et al., 1989). In PD, perturbation of mitophagy, accumulation of A-SYN, defective calcium homeostasis and build-up of oxygen free radical species are all implicated in the pathogenesis and cell death, (Gegg and Schapira, 2018). It was also proposed that *GBA* mutations increase the risk for PD by inducing the same pathology as in sporadic PD brain (Schapira, 2015). Due to the dependence of neurons on mitochondrial activity, we sought in this chapter to assess whether deficient GCase activity leads to accumulation of bioenergetically compromised mitochondria in wt/L444P primary mouse cortical neurons.

4.2 Experimental Aims

The central aim of this chapter is to investigate the impact of heterozygous L444P mutation in the context of PD in utilizing mouse cortical neuronal model.

4.3 Objectives

A. Characterization of mouse cortical neuronal (MCN) cultures by measuring activities and GCase and other lysosomal enzymes.
B. Investigating UPR in MCN and adult mice cortical brain regions.
C. Assessment of any defect in the protein's degradation machineries associated with L444P mutation by characterizing autophagy flux, markers of CMA and UPS in the MCN.
D. With the given evidence that A-SYN is degraded by the above-mentioned degradation pathways, investigating its metabolism in mouse neurons as pathological consequence of L444P mutation is crucial outcome of this chapter; the effect of PFFs seeding on the basal level of A-SYN and the proportion of soluble and insoluble protein fractions in both control and L444P MCN will be investigated.
E. Assessment of mitochondrial respiratory function using Seahorse technology and mitochondrial content in primary cortical neurons and brain tissues of WT/L444P adult mice.

4.4 Experimental Design

As homozygous L444P mutation is lethal in mice, the designed experimental work was performed on the heterozygous mutant state. Mice were treated in accordance with local ethical committee guidelines and the UK Animals (Scientific Procedures) Act 1986. The colony was maintained under project license 70/7685 issued by the UK Home Office. B6;129S4-Gbatm1Rlp/Mmnc

(000117-UNC) mice expressing heterozygous knock-in L444P mutation in the murine *GBA1* gene (L444P/+ mice) were purchased from the Mutant Mouse Regional Resource Centre (MMRRC), (Liu et al., 1998).

Mouse cortical neuronal cultures were prepared from E16 embryos following the standard procedures as described in (section 2.1.3) of materials and methods chapter. Briefly, dissociated cortical neurons were cultured in a polyornithine coated 6 well plates, or XF 24 wells seahorse plate for investigating mitochondrial function, with regular media changes until they were harvested on10 DIV. For downstream experiments, cultures were either treated with 0.2µM of Bafilomycin A for 6hours to inhibit macroautophagy or 2.5 µM of GW4689 for 24hours to inhibit exosome release prior to harvesting. Cell pellets were frozen at -80°C until time of experiment. For PFFs seeding, neurons were treated with a final concentration of 5 µg/mL per well in 4 or 5 DIV. Cultures were maintained for 10 days (3 days in presence of PFFs and then at least another 7 days of media changes) as illustrated in (

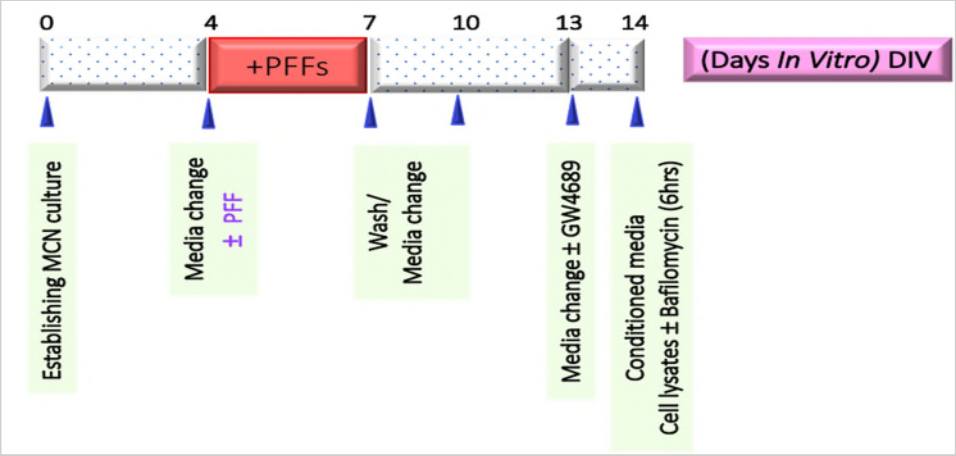

Figure 0.1). Upon harvesting,1ml of conditional media was collected from each sample for downstream analysis such as dot blot and ELISA.

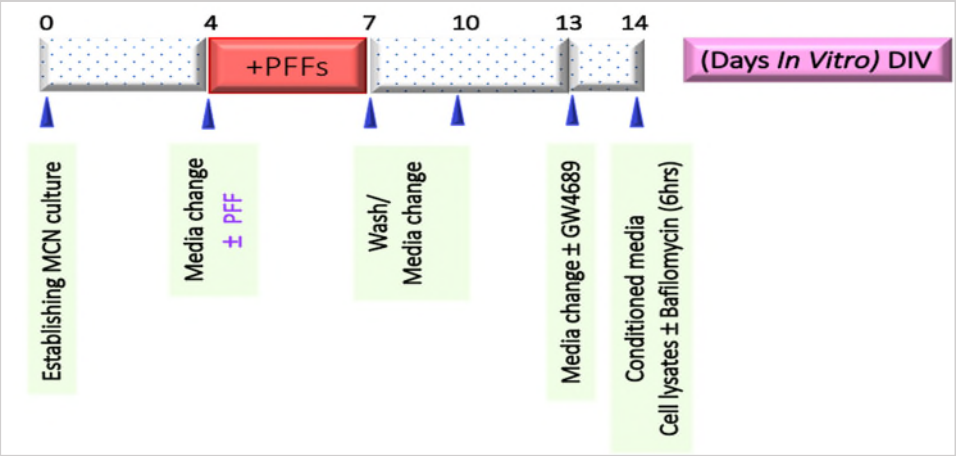

Figure 0.1 Timeline of culturing, GW4689 treating and PFFs seeding of mouse cortical neuronal (MCN).

4.5 Results

4.5.1 Immunocytochemistry of Mouse Cortical Neurons

Prior to investigating the effect of heterozygote L444P mutation in MCN, the purity of these primary cultures was assessed. Immunocytochemistry staining was performed to prove that these are neurons with a very little glia contamination. E16 mouse cortical neurons harvested on day 10 in culture were immunostained using Anti-GFAP (Glial fibrillary acid protein) for labelling Astrocytes, and Anti β III Tubulin to label neurons. Cells were counterstained with DAPI (4',6-diamidino-2-phenylindole) to visualize DNA in the nuclei. The majority of MCN culture was neuronal as shown in the merged image (Figure 0.2, D). Immunostaining for the microglia marker Iba1 was negative and to further confirm these findings, western blotting of MCN preps showed expression of β III Tubulin protein at the expected size in neurons, but not Iba1. The rat BV2 microglia cell line was used as a positive control for Iba1 (Figure 0.2).

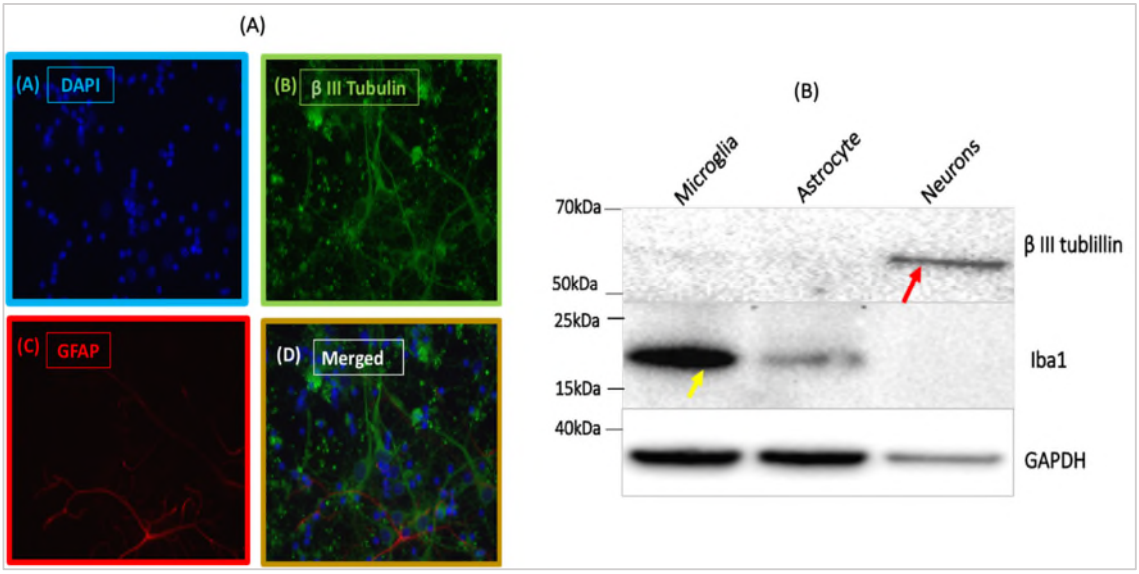

Figure 0.2 Immunocytochemistry analysis of mouse cortical neurons. A): Imaging was performed using a 40 X objective; (A) counterstain of nuclei with 4',6-diamidino-2-phenylindole (DAPI). (B) Anti β III tubulin labelling of neurons. (C) Astrocytes labelled with anti-GFAP (Glial fibrillary acid protein) antibody. (D) Merged image shows that the culture is mostly neuronal. (B): Western blot representative image of BV2 microglia cell line, primary mouse astrocytes and neuronal cultures, (n=1); β III tubulin is only expressed in neurons (red arrow) whereas Iba1 (microglial activation marker) is expressed in microglia (yellow arrow), GAPDH was used as loading control.

4.5.2 GCase activity in mutant mouse cortical neurons

Results showed that GCase activity in heterozygous mutants was 37.6 % significantly lower than the control, (**p*=0.031, n=4), (Figure 0.3). However, with the low yield feature of post mitotic MCN, it was challenging to detect GCase protein expression in these cells. The antibody that detects mouse GCase (Sigma G4171) requires 80µg of protein for a valid western blot analysis of GCase expression in MCN lysate and still gives a very weak signal, (Dr. Matthew Gegg, personal communication). To address this issue, we tried IF but this was also negative and we were not able to detect endogenous GBA protein in mouse

cortical neurons (Figure 0.4). Thus, the available data was limited to the GCase enzymatic activity which was expectedly reduced in wt/ △ neurons.

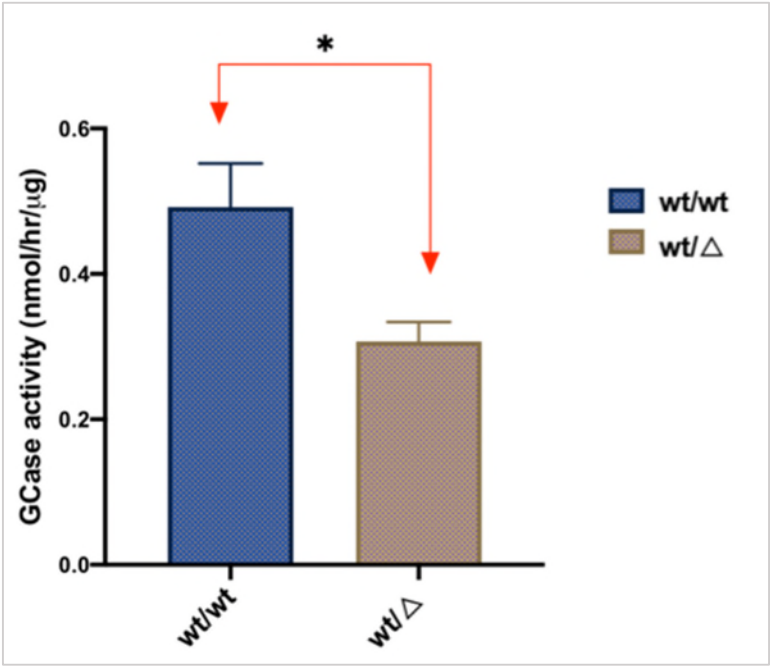

Figure 0.3 GCase activity in wt/△ mouse cortical neurons. GCase enzyme activity was significantly %37.6 lower in wt/△ neurons (mean= 0.307 ±0.027) as compared to control (mean=0.492±0.060). Data represent the mean GCase activity expressed as nmol/hr/µg protein ± the standard error of the mean from 4 independent MCN cultures (n=4 and *p=0.031).

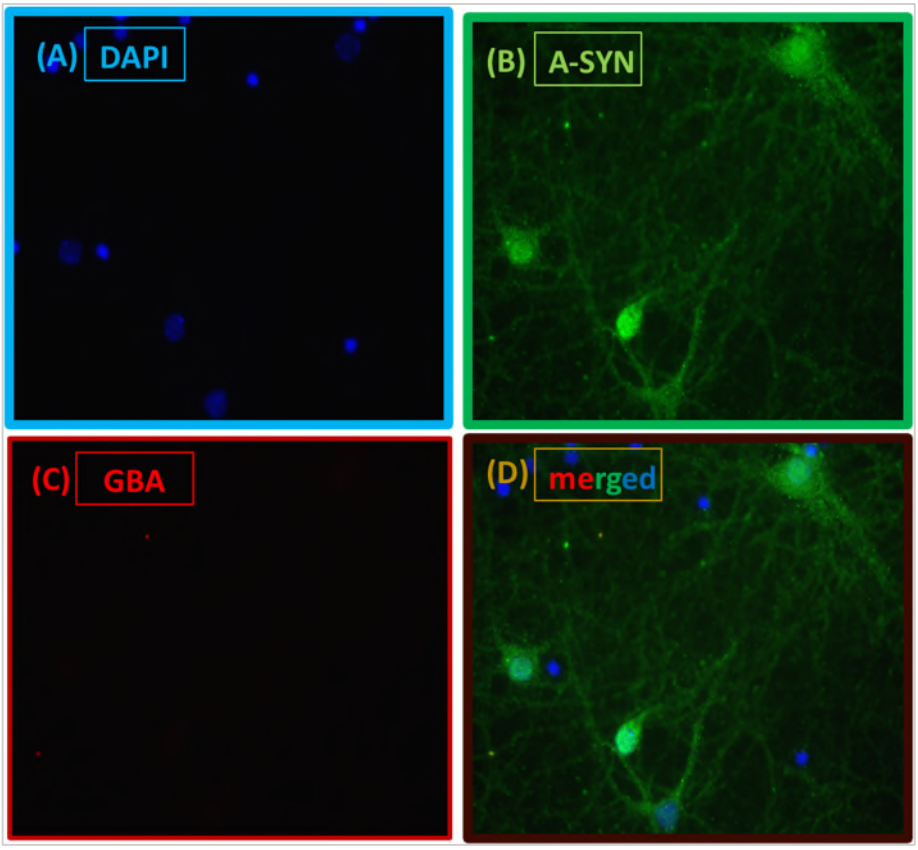

Figure 0.4 Immunocytochemistry analysis of mouse cortical neurons. (A): counterstain of nuclei with DAPI. (B): Positive immunoreactivity of A-SYN using Anti mouse A-SYN labelling (C): MCN labelled with rabbit anti-GBA antibody (red channel) showing no GCase protein immunoreactivity. (D): Merged image confirming no endogenous GCase protein expression detected.

4.5.3 Assessment of Other Lysosomal Hydrolases Activities and Lysosomal Contents in wt/△ MCN Model

In contrast to GCase, no significant alteration of β-hexosaminidase (p=0.905) and β-galactosidase (p=0.576) activities was observed in wt/△ neurons against control groups (n=4), (Figure 0.5).

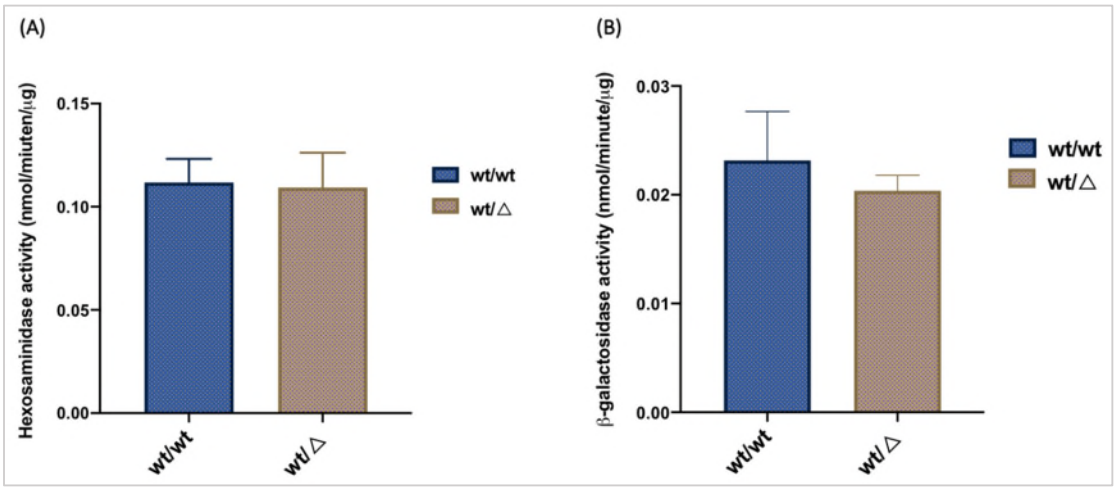

Figure 0.5 Summarization of β-hexosaminidase and β-galactosidase activities in wt/△ MCN. Enzymatic activity was measured in nmol of product/minute/µg protein, there was no significant change of either enzymatic activities between experimental groups. (A): The mean hexosaminidase activity in wt/wt group= 0.112± 0.011 and in wt/Δ group =0.109± 0.017, (p=0.905, n=4) whereas in (B): β-galactosidase activity = 0.023± 0.004 and 0.020± 0.001 in control and wt/Δ groups respectively, (p=0.576, n=4). Each bar represents mean of enzymatic activity from 4 independent MCN cultures ± SEM, (n=4).

To determine whether *GBA* mutation has an impact on the lysosomal content, we also assessed the level of lysosomal associated membrane protein 1 (LAMP1) (n=8wt/wt, 11 wt/△), integral membrane protein 2 (LIMP2), (n=10wt/wt, 12 wt/△) and mature cathepsin D, (n=10wt/wt, 12 wt/△) in wt/△ MCN and their corresponding wild type control groups. However, no statistically significant changes were observed in lysosomal protein markers between experimental

groups (Figure 0.6). These observations were coupled with the unchanged activities of the for-mentioned lysosomal hydrolases and collectively supported the notion that the reduction in GCase activity was due to *GBA* mutation and not due to altered lysosomal mass.

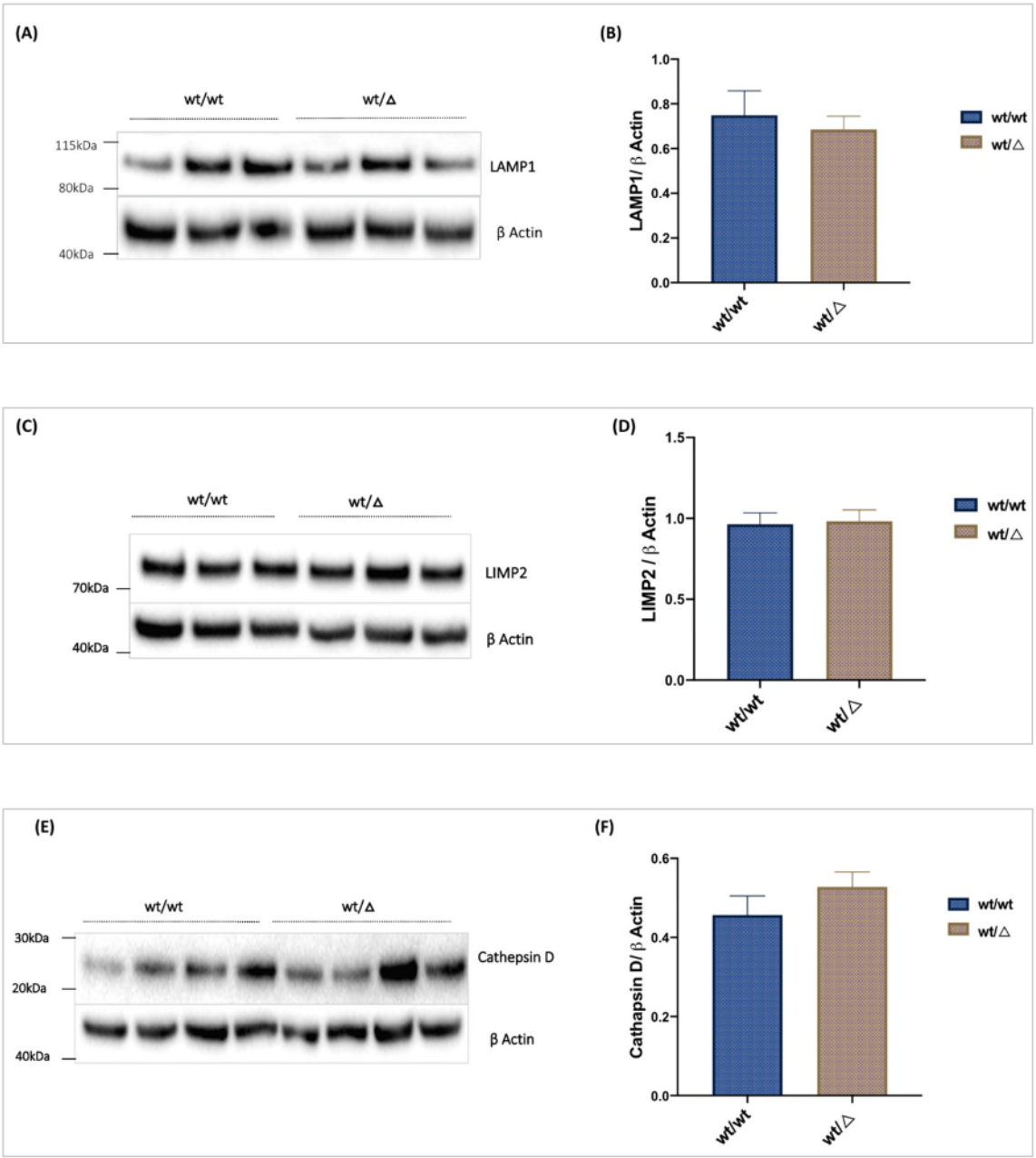

Figure 0.6 Effect of heterozygous L444P mutation on lysosomal contents in mouse cortical neurons. (A, C and E): Representative western blot images of (A) LAMP1 endolysosomal marker (C) LIMP2, (E) Mature cathepsin D showing apparently comparable band densities of each protein between wt/△ neurons and their

corresponding wildtype control groups, β Actin was used as loading control. (B): Bar chart quantification showing no significant alteration (*p*=0.587) in LAMP1 mean expression level between wt/△(0.685±0.059) and wt/wt (0.749±0.110) groups, (n=8wt/wt and 11 wt/△). (D): Bar chart summarizing LIMP2 expression level and showing no significant change (*p*=0.960) between wildtype (0.982± 0.148) and wt/△(0.973± 0.072) groups, (n=10wt/wt, 12 wt/△). (F): Bar chart quantification of cathepsin D protein showing comparable levels (*p*=0.256) of protein expression between wt/△ neurons (0.528± 0.016) and wildtype control group (0.468± 0.085), (n=10wt/wt, 12 wt/△). All data represented the mean density of target protein expressed against the density of the housekeeping protein (β actin) of MCN cultures from 3 independent preps.

4.5.4 Effect of L444P Heterozygous Mutation (wt/△) on Autophagy Lysosomal Pathway (ALP) and Ubiquitin Proteasomal System (UPS)

4.5.4.1 Effect on Macroautophagy (MA) Pathway

We have previously found normal autophagic flux with heterozygous L444P mutation in human dermal fibroblasts (Figure 0.5). Thus, we investigated whether this mutation can promote defect in autophagic machinery in mouse primary cortical neurons. Our results were obtained from several independent cell cultures and were similar to those observed in fibroblasts as illustrated in (section 3.4.3). We used two markers of MA, LC3-II, and p62 to investigate autophagy flux, both under basal condition and when treating cells with 0.2 μM of bafilomycin (BAF) A1 for 6 hours. During autophagy, LC3II is recruited to autophagosomal membrane to fuse with the lysosome in which intra-autophagosomal contents are degraded by lysosomal hydrolases. Detection of LC3-II level by immunoblotting is considered as reliable method for monitoring the number of autophagosomes in the cell, while p62 reflects how much cargo is present within these autophagosomes as it helps bind cargo to the LC3-II on autophagosomes. Our results showed that under basal conditions (ut), the amount of LC3-II and p62 were unchanged indicating that both autophagosome number (LC3-II) and cargo (p62) were unaffected by mutation; (mean LC3-II level in both untreated wt/wt and wt/Δ group was 0.547 ±0.059 and 0.562±0.090 respectively whereas the mean P62 level in the respective group was 0.262±0.068 and 0.321±0.073), (Figure 0.7). After six- hours blockade of autophagy flux, there was a significant increase in LC3-II (***P=0.0003) and p62 (****P<0.0001) levels of bafilomycin-treated neurons against untreated control groups. However, this increment was similar between wt/wt cells and wt/Δ groups showing that the presence of

mutation did not affect the rate of synthesis of autophagosomes (LC3-II in both treated wt/wt and wt/Δ groups =1.251±0.124 and 1.074±0.114 respectively whereas P62 levels in the corresponding groups = 0.940±0.081 and 0.830±0.086 respectively), (Figure 0.7 B, C). In light of this, MA flux was found unaffected in mouse cortical neurons with L444P heterozygous mutation.

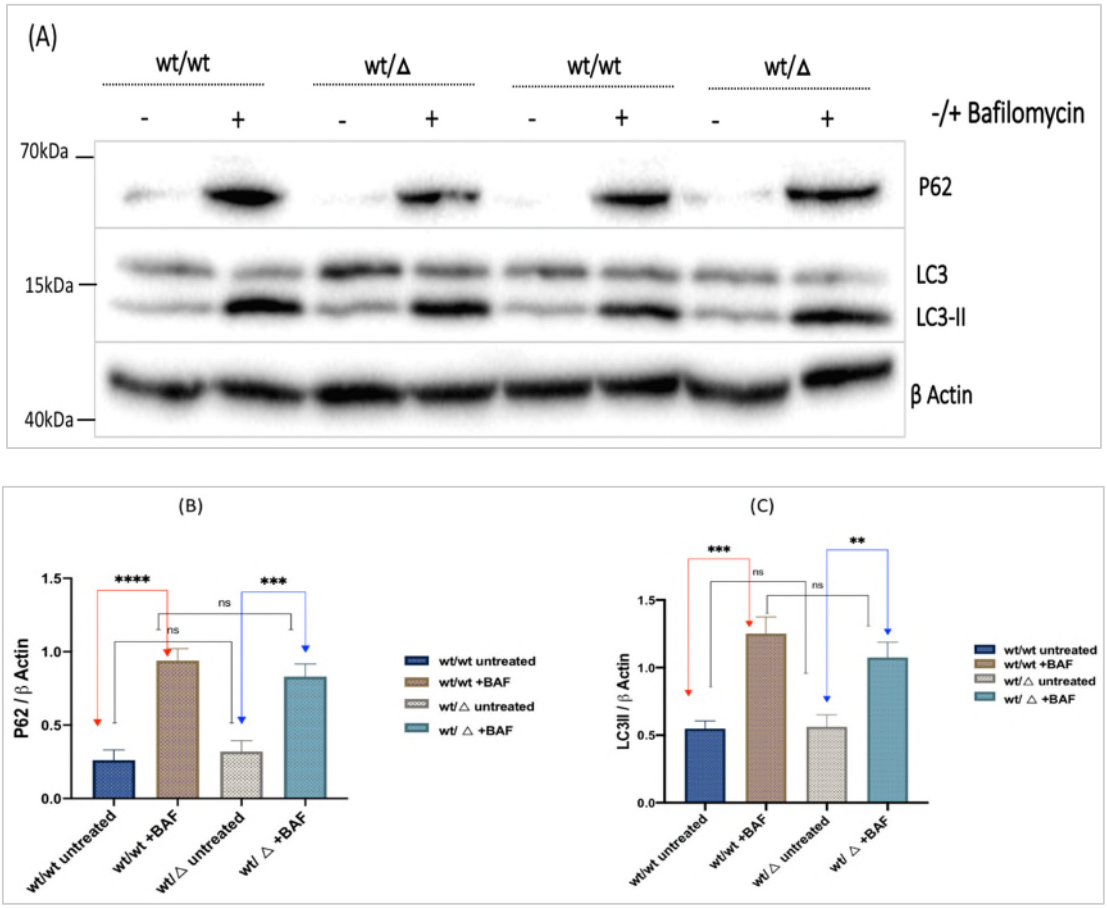

Figure 0.7 Evidence of no impairment of macroautophagy flux with heterozygous L444P mutation in mouse cortical neurons. (A): Representative western blot images showing no evident change in P62 level (top panel) or the LC3-II level (middle panel) between wt/wt and wt/△ groups, both under basal condition (-) and following bafilomycin (BAF) treatment (+), β Actin was used as loading control. (B): Bar chart analysis of autophagic protein (P62) densities showing that BAF-treatment significantly increased P62 level in wt/wt (*****P*<0.0001) against their corresponding untreated group; P62 untreated =0.262± 0.068; +BAF =0.940± 0.081. Also, a similar trend of increased P62 level was detected in wt/△ neurons following autophagy blockade; bafilomycin significantly increased P62 level in wt/△ (0.830± 0.0.086),**

(*P=0.0003) against wt/wt control group (0.321±0.073). Despite that, there was no significant change in P62 between wt/wt and wt/△ neurons with (P=0.789) and without (P=0.973) bafilomycin treatment, (n=10 wt/wt, 9wt/△). (C): Bar chart summarizing LC3-II expression level and showing bafilomycin significantly increased LC3-II in both wt/wt (****P<0.0001) and wt/△ (**P=0.003) groups. Similar to P62, there was no significant change LC3-II level in wt/wt and wt/△ regardless of the presence (P=0.623) or absence (P>0.999) of BAF treatment; mean LC3-II level under basal condition was 0.547± 0.059 in wt/wt and 0.562±0.090 in wt/△ groups whereas following bafilomycin treatment, LC3-II in wt/wt=1.251± 0.124 and in wt/△=1.074± 0.114. Data represent the mean density of the LC3-II and P62 proteins expressed against the density of the housekeeping proteins (β actin or GAPDH) of MCN cultures from three independent neuronal preps± SEM.**

4.5.4.2 Effect on Chaperone Mediated Autophagy (CMA)

Under physiological condition, monomeric A-SYN can also be trafficked via CMA and ultimately degraded by lysosomes, (Cuervo et al., 2004). Given the encountered defects in CMA pathway in PD brain (Alvarez-Erviti et al., 2010), we assessed the protein levels of two key mediators of this pathway, LAMP2a and HSC70 proteins, as manipulating this pathway could be crucial therapeutic target in PD. Our result was similar to those found in fibroblasts model; it showed no significant alteration in both LAMP2a (P=0.776) and HSC70 (P=0.522) markers between wt/△cortical neurons and control groups; LAMP2a in wt/△ mouse neurons= 0.656±0.080 and in wt/wt= 0.698±0.121whereas HSC70 =0.609±0.119 in wt/wt and 0.719±0.115 in wt/Δ group, (n=7wt/wt, 8wt/△ from two independent MCN preps). This suggests that CMA is unaffected in mouse cortical neurons with wt/△ mutation, (Figure 0.8).

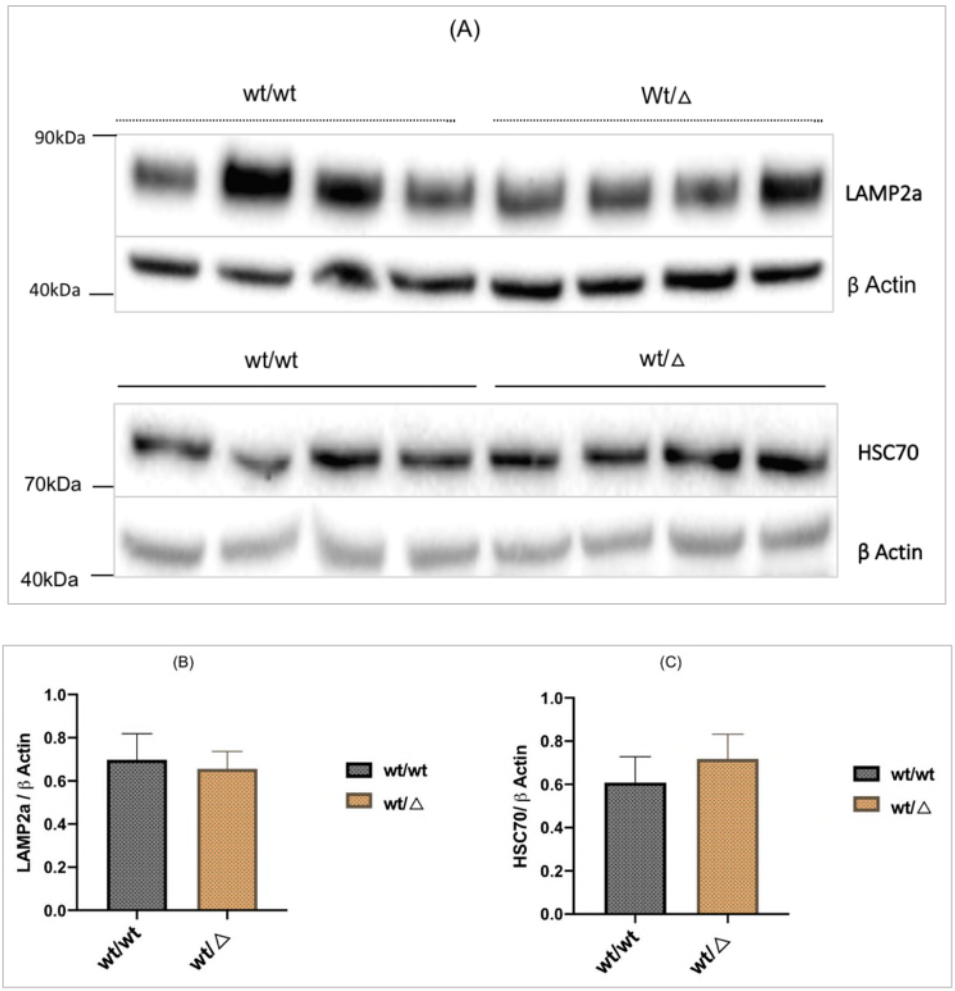

Figure 0.8 Analysis of chaperon mediated autophagy (CMA) related proteins in wt/△ mouse cortical neurons. (A, B): Representative western blot images showing no evident change in LAMP2a (top blot) and HSC70 (bottom blot) markers of CMA in wt/△ MCN when compared to wt/wt control, β Actin was used as loading control (C): Bar chart quantification showing comparable LAMP2a levels between wt/△ mouse neurons (0.656±0.080) and control (0.698±0.121), (n=7wt/wt, 8wt/△, *P*=0.776). (D): Bar chart quantification showing no significant change in HSC70 level between wt/wt (0.609±0.119) and wt/△ MCN (0.719±0.115), (n=7wt/wt, 8wt/△, *P*=0.522). Data represent the mean density of LAMP2a and HSC70 proteins expressed against the density of housekeeping protein (β actin) of cultures from two independent preps± SEM.

4.5.5 Ubiquitin Proteasomal System (UPS) in wt/△ MCN

UPS also contributes to the phenomenon of unfolded A-SYN turnover. The previous finding of defective UPS in both iPD brains and in *GBA* knock out (K/O) mouse mixed cortical neuronal culture provided direct link to A-SYN pathology (McNaught et al., 2002, McNaught et al., 2003, Osellame et al., 2013). Therefore, we measured the basal activity of the 20S catalytic subunit of proteasome and our results showed no significant alteration in activity in wt/ △ MCN (mean=0.0671±0.008) when compared to control (0.057±0.015), 20S activity was calculated in µM of AMC/1hr/µg of protein (n=5wt/wt and 11 wt/△, *P*=0.554), (Figure 0.9).

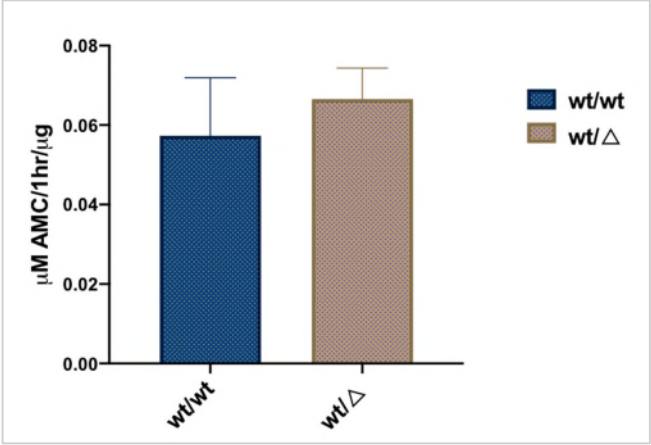

Figure 0.9 Investigating UPS activity in wt/L444P MCN model. Bar chart summarizing 20S proteasomal subunit activity (chymotrypsin like) measured in wt/△ neurons; the activity was analyzed using Chemicon's assay which is based on detecting the fluorophore (AMC) after cleavage from the substrate LLVY-AMC. The reaction rate was measured in duplicates, normalized to protein concentration and calculated in µM of AMC/1hr/µg protein. Analysis showed no significant change in the activity (*P*=0.554) in wt/△ MCN (0.067±0.008) when compared to wildtype group (0.057±0.015). Data analyzed represent the mean of 5wt/wt and 11 wt/△ cultures derived from 2 independent neuronal preps± SEM, (n=5wt/wt and 11 wt/△).

4.5.6 Analysis of ER stress and UPR in wt/△ mouse cortical neurons and adult mice brain tissue

We assessed how wt/△neurons handle misfolded mutant enzyme by measuring the level of ER chaperone binding immunoglobulin protein (BiP), also known as GRP78, by western blot (Figure 0.10 A, B). We found that wt/△ neurons are showing similar levels of BiP (0.784±0.074) when compared to their control littermates (0.830±0.084), (n=7, *p*=0.682).

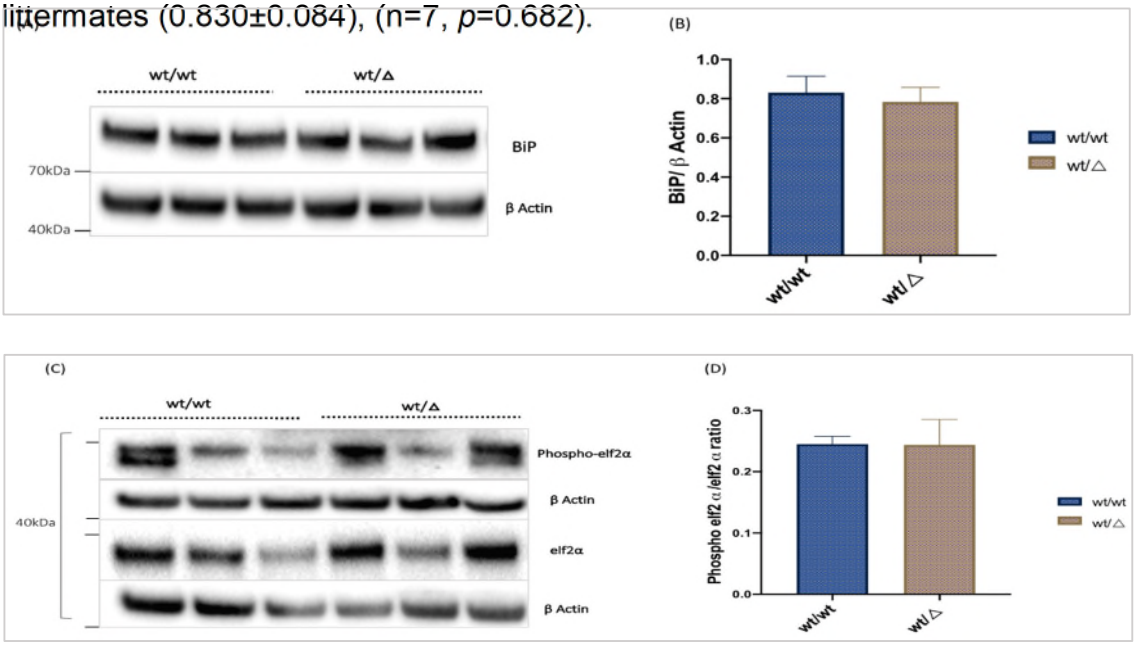

Figure 0.10 The lack of ER stress and unfolded protein response (UPR) in L444P mutation. (A,C): Levels of ER proteins BiP/GRP78 and elf2a phosphorylation were determined in wt/△mouse cortical neurons and compared to control showing apparently comparable levels of the two markers between the two experimental groups, β Actin was used as loading control. (B): Bar chart analysis of BiP/GRP78 band intensity normalized to β Actin and showing no significant alteration in wt/△ neurons (0.784±0.074) when compared to control (0.830±0.084), (*p*=0.682, n=7), data represent the average of 7 cultures taken from two independent MCN preps and expressed as mean ± SEM. (D): The intensities of elf2α and phospho-elf2α were normalized to β Actin and expressed as a ratio of phospho-elf2α/elf2α; densitometric analysis showed comparable ratios between wt/△neurons (0.784±0.074) and control (0.830±0.084), (*p* =0.682), data represent the average of 4 independent MCN cultures ± SEM.

consistent with this finding, levels of phosphorylated elf2α were not significantly changed (*p*=0.68, n=4) between wt/△ (0.784±0.074) and control group (0.830±0.084) suggesting that PERK branch of UPR was not activated in wt/△ neurons (Figure 0.10 C, D). These observations were coupled with absence of MA impairment (Figure 0.7) and A-SYN accumulation (see section 4.5.7). Therefore, to assess if the apparent lack of UPR response is a feature of cortical neurons as a whole or MCN only, we analyzed BiP expression in cortex of 3-months old mice with wt/L444P mutation (Figure 0.11 A, B). We were not able to detect any significant up or downregulation in BiP expression level in wt/△ 3 months old adult mice cortex (0.793± 0.040) against the corresponding wildtype control littermates (0.733 ±0.131), (*P*=0.636). We also compared the endogenous A-SYN levels in the cortex of the same mice and found no significant change (*p*=0.590) between wt/△ group (1.37±0.196) and their wt/wt control littermate (1.196±0.091), (Figure 0.11 C, D).

Due to selective vulnerability of dopaminergic neurons in substantia nigra pars compacta (SNpc) of the midbrain in PD (Surmeier et al., 2017), we compared BiP and A-SYN levels in the midbrain of wt/△ 3 months old mice. Similar to the cortex, we observed no significant change (*P*=0.496) in BiP between wt/△ midbrain (0.957± 0.158) and wt/wt control group (1.102 ±0.124), (Figure 0.12 A, B). Despite that, there was a subtle increase in A-SYN level in wt/△ mice midbrain (1.37±0.196) against wt/wt group (0.994±0.218) which did not reach statistical significance (*p*=0.479), (Figure 0.12 A, C).

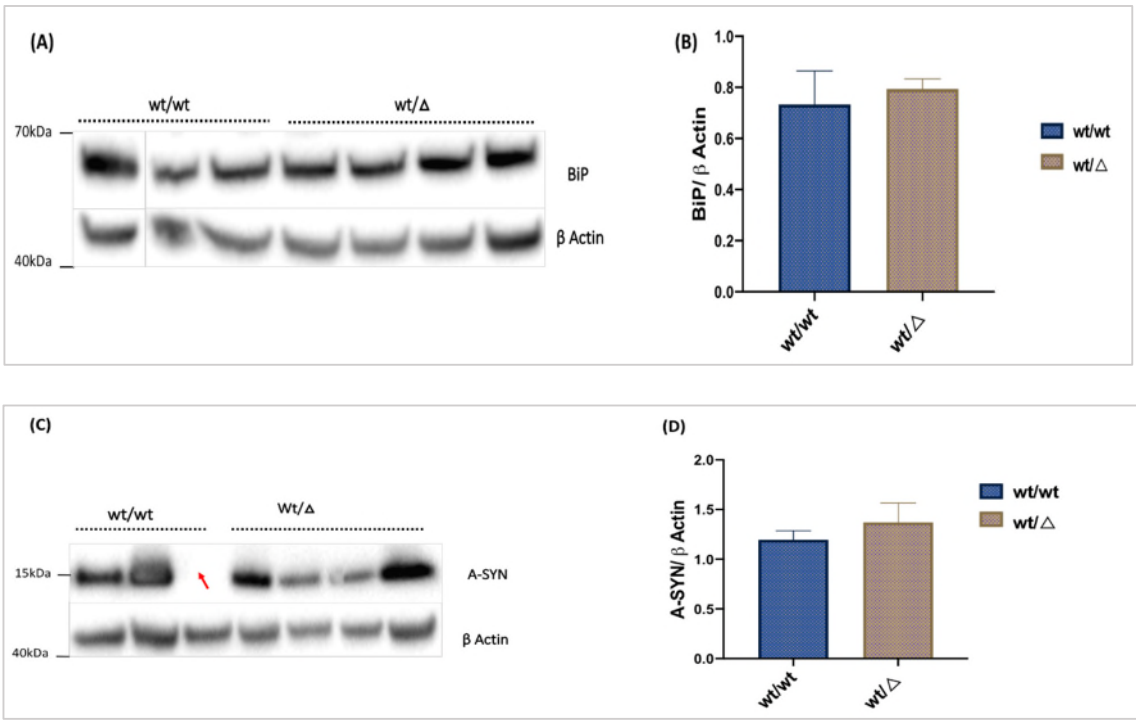

Figure 0.11 ER stress and A-SYN level in wt/L444P 3mo old adult mice cortex. (A): Western blotting image for ER resident chaperon (BiP) in the cortex of 3 months old mice showing apparently comparable levels of BiP expression between wt/△mutant mice and their control littermates, β Actin used as loading control. (B): Bar chart quantification showing no significant change (*P*=0.636) in BiP level between wt/△ group (0.793± 0.040) and control (0.733 ±0.131), data represent the average of 3wt/wt and 4 wt/△ cortex samples ± SEM, (n=3 wt/wt and 4 wt/△). (C): Representative western blot image of A-SYN expression relative to β Actin (loading control) showing no evident change in A-SYN between wt/△ and wt/wt groups. One wild type cortex was lacking detectable A-SYN expression (red arrow). (D): Quantification of intracellular A-SYN level in wt/△ 3 months old adult mice cortex showing no statistically significant (*p*=0.590) changes in A-SYN of wt/△mice cortex (1.37±0.196) against their wt/wt control littermates (1.196±0.091). Data represent the average of 2wt/wt and 4 wt/△ cortex samples ± SEM, (n=2 wt/wt and 4 wt/△).

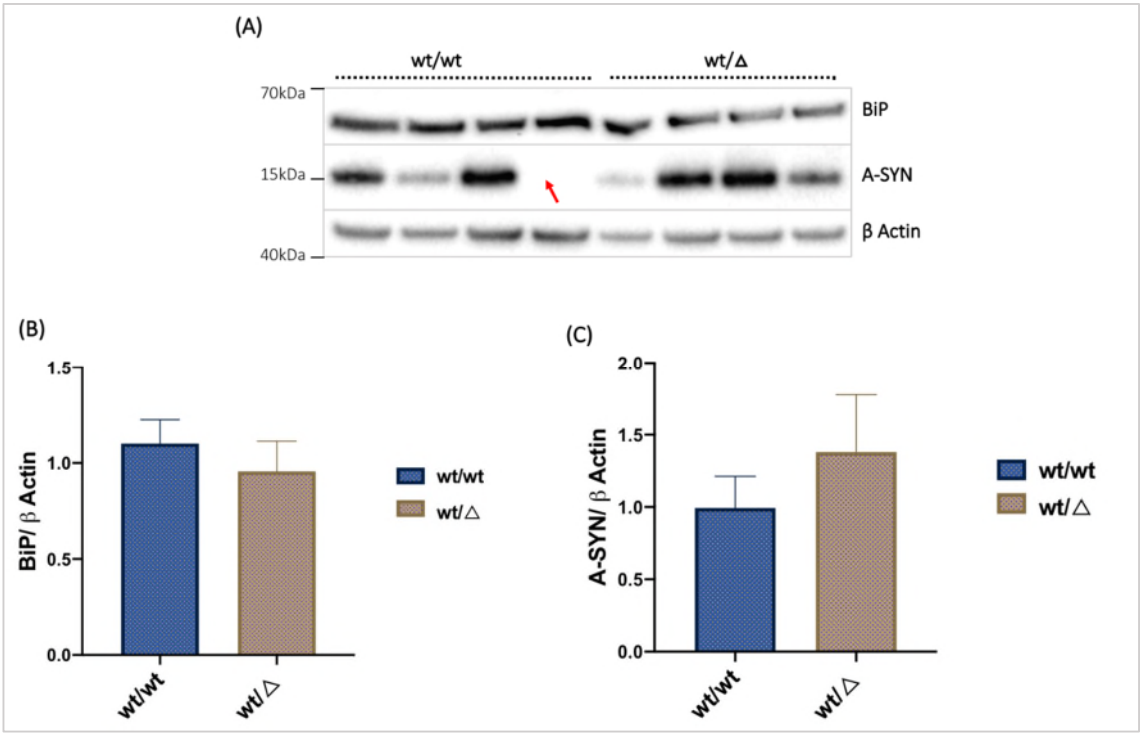

Figure 0.12 ER stress and A-SYN level in midbrain tissue of wt/L444P 3mo old adult mice. (A): Representative western blot image for BiP and A-SYN showing apparently comparable levels of both proteins between midbrain of wt/△ 3 months old mice and their corresponding wt/wt littermates, β Actin was used as loading control and one wild type midbrain was lacking detectable A-SYN expression (red arrow). (B):Bar chart quantification showing no significant change (*P*=0.496) in BiP level between wt/△ midbrain (0.957± 0.158) and wt/wt control group (1.102 ±0.124), data represent the average of BiP expression relative to housekeeping protein (β Actin) from 4wt/wt and 4 wt/△ midbrain samples ± SEM, (n=4). (C): Quantification of intracellular A-SYN level in midbrain of wt/△ 3 months adult mice showing non-significant trend of increased A-SYN (*p*=0.479) in wt/△ midbrain neurons (1.380±0.398) with respect to wt/wt control group (0.994±0.218). Data represent the average of A-SYN expression relative to housekeeping protein (β Actin) from 3wt/wt and 4 wt/△ midbrain samples ± SEM, (n=3wt/wt, 4 wt/△).

Furthermore, we used 8-months old mice in our analysis to detect if BiP level changes with time in mutant mice. Compared to 3-month-old mice (0.669± 0.076), there was no significant change (*P*=0.296) of BiP expression level in cortex of 8-month-old adult mice (0.96 ±0.153), (Figure 0.13 A, B). This finding was coupled with comparable levels of endogenous A-SYN both in 8-month old

cortex (1.69±0.275) and 3-month adult mice group (1.468±0.203), (*p*=0.568), (Figure 0.13 A, C). Taken together, these findings suggest the lack of ER stress and UPR in MCN and brain tissues of adult mice with heterozygous L444P mutation.

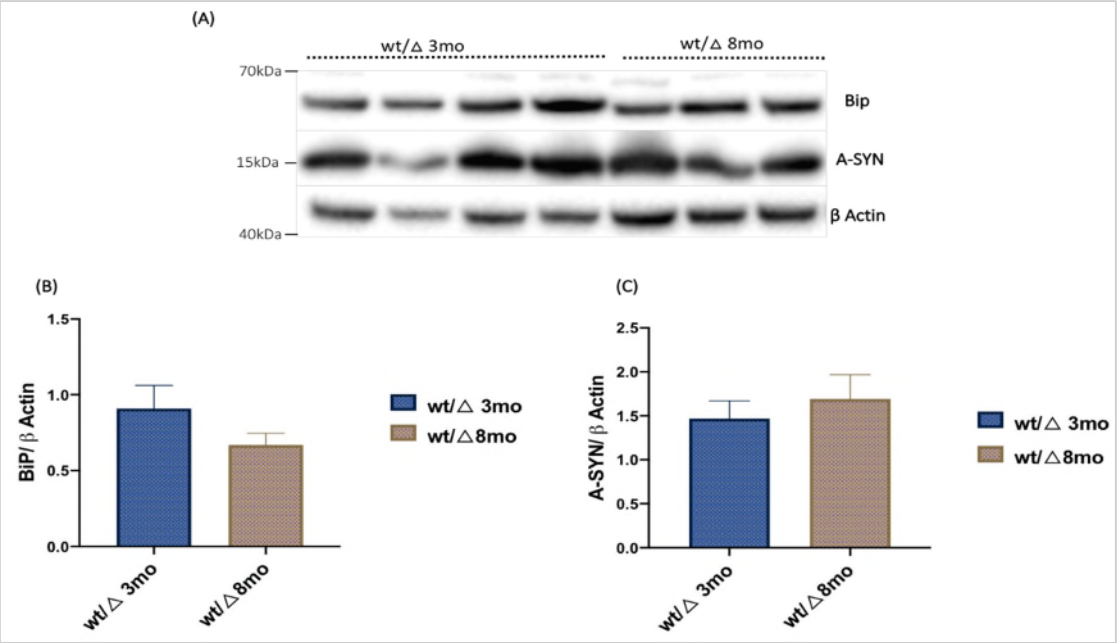

Figure 0.13 ER stress and A-SYN level in wt/△3-mo vs 8-mo old adult mice cortex. (A): Representative western blot image showing no evident change in BiP or A-SYN expression levels in wt/△ 8mo old adult mice cortex as compared to 3mo old mice, β Actin was used as loading control. (B): Bar chart quantification showing no significant change (*P*=0.296) of BiP expression in cortex of 8-month-old adult mice (0.96 ±0.153) against that of 3-month old (0.669± 0.076). Data represent the average of 4 wt/△ 3months old- and 4 wt/△ 8 months old-adult mice cortices ± SEM, (n=4 3-month, 3 8-month). (C): Bar chart quantification of A-SYN showing no significant alteration in endogenous A-SYN level in 8-month old cortex (1.69±0.275) with respect to 3-month adult mice group (1.468±0.203), *p*=0.568 and data represent the mean expression level of A-SYN normalized to β Actin (loading control) ± SEM, (n=4 of 3-month and 3 of 8-month adult mice).

4.5.7 Effect of Heterozygous L444P mutation on Alpha Synuclein (A-SYN) Metabolism in Mouse Cortical Neurons

A-SYN accumulation and Lewy body formation are hallmarks of *GBA*-PD. We investigated the metabolism of A-SYN in MCN model to find if the partial loss of GCase enzymatic activity in mouse cortex exhibited the same pathology reported previously by several study groups using different models (Mazzulli et al., 2011, Rocha et al., 2015b). We first measured intracellular A-SYN protein level in primary neuronal cultures by western blot and noticed first variability in A-SYN bands intensities within cultures. Although similar pattern of expression found in (Li et al., 2019) study, WB analysis did not show any increased A-SYN level in the mutant neurons (0.542±0.147) when compared to wt/wt group (0.527±0.146) (P =0.947), (Figure 0.14). This finding was further supported by the absence of defective ALP or UPS in mouse cortex (Figure 0.7, Figure 0.8, Figure 0.9) which if were downregulated would have predisposed to accumulation and phosphorylation of A-SYN as reported by (Magalhaes et al., 2016, Osellame et al., 2013, Alvarez-Erviti et al., 2010, Mazzulli et al., 2011, Cullen et al., 2011).

We then looked at the basal release of A-SYN in to MCN culture media, both under basal condition and upon treating cells with GW4689, the neutral sphingomyelinase (nSMases) inhibitor. GW4869 is known to inhibit ceramide-mediated inward budding of intraluminal vesicles (ILV) in to lumen of multi-vesicular bodies (MVBs) to prevent the release of exosomes from cells (Phuyal et al., 2014).

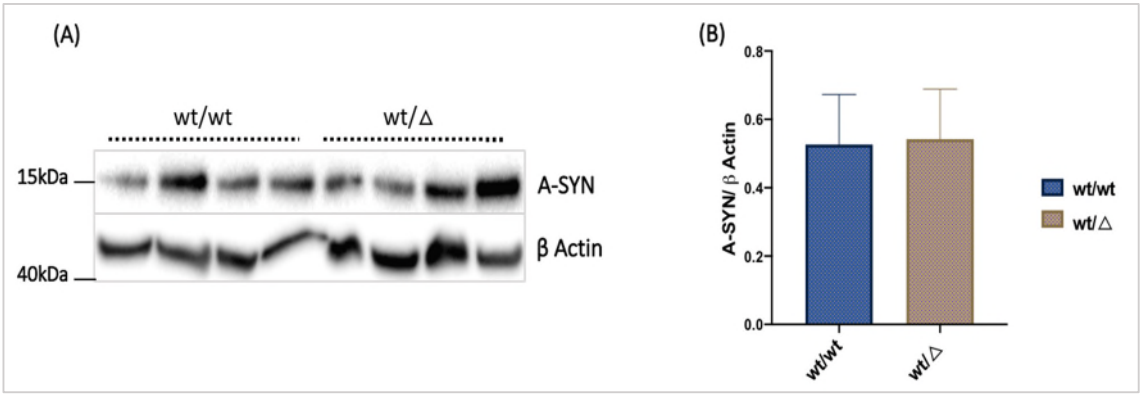

Figure 0.14 A-SYN intracellular level in the wt/L444P MCN. (A): Western blot representative image for A-SYN expression relative β Actin (loading control). Although there was variability in A-SYN bands intensities between cultures which was consistent with those of (Li et al., 2019) work, bar chart quantification in (B) showed comparable levels of A-SYN between wt/△cells (0.542±0.147) and their wt/wt control (0.527±0.146), (*p* =0.947). Data represent the average of 5wt/wt and 9wt/Δ cultures from 3 independent MCN preps ± SEM.

We chose to use GW4869 here to investigate if inhibiting nSMases and the subsequent blocking of exosomes secretion would alter the release of monomeric A-SYN species from the cell. Blocking exosomes secretion In LUHMES neurons using 5μM GW4869 has been shown to exacerbate A-SYN induced cell death (Fussi et al., 2018). We therefore sought to detect first the optimum inhibitory concentration of GW4689 we should use. In a wild-type primary neuronal cultures, we inhibited exosomal secretion by treating cells with two different concentrations of GW4689 (2.5, 5 and 10μM) for 24 hours prior to harvesting. We found that only neurons treated with 2.5μM inhibitory concentration showed no apparent neurotoxicity whereas those treated with 5μM exhibited clear cell death with fewer cell bodies associated with retraction/degeneration of neurites (Figure 0.15, black arrow) and 10μM completely killed them (data not shown). Consequently, we excluded higher doses from further analysis and decided to continue treating neurons with 2.5μM GW4689.

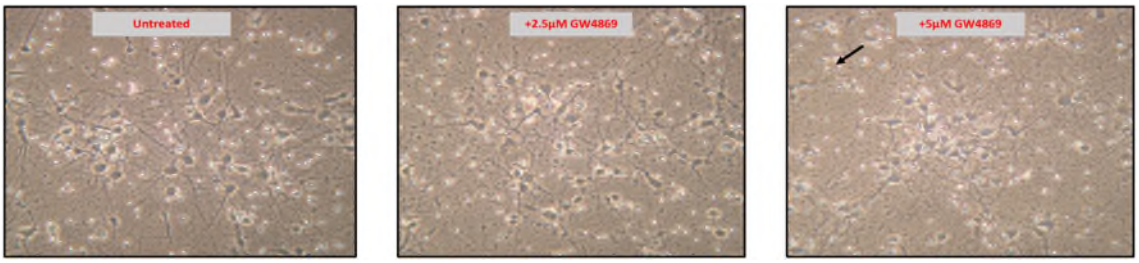

Figure 0.15 Effect of different doses of sphingomyelinase inhibitor (GW4689) treatment on wild type MCN (control). Light microscopic image (40x) of untreated, +2.5µM, and +5µM of sphingomyelinase inhibitor (GW4689) with the apparent cytotoxic effect of 5µM inhibitory concentration of GW4689. The black arrow clearly indicates the site of cell death, fewer cell bodies and retraction/degeneration of neurites.

Following this, the amount of monomeric A-SYN released in to media was measured by ELISA as per manufacturer's instructions, (section 2.12.2), (n=10wt/wt,9 wt/△). We found that under basal condition, the release of monomeric A-SYN did not significantly differ (*P*=0.996) between wt/wt (2661±611.6) and wt/△ neurons (2859±719.1), (Figure 0.16).Similarly, GW4869 treatment did not significantly alter the secretion of A-SYN between wt/wt (2971±739.5) and wt/△ group (1598±325.4), (P=0.433). These findings collectively indicated that under basal condition, there was no accumulated intracellular A-SYN or increase in its release in to culture media of wt/△ mouse cortical neurons. In addition, GW4869 treatment, at 2.5µM concentration, did not affect the secretion of monomeric A-SYN in cells regardless of genotype.

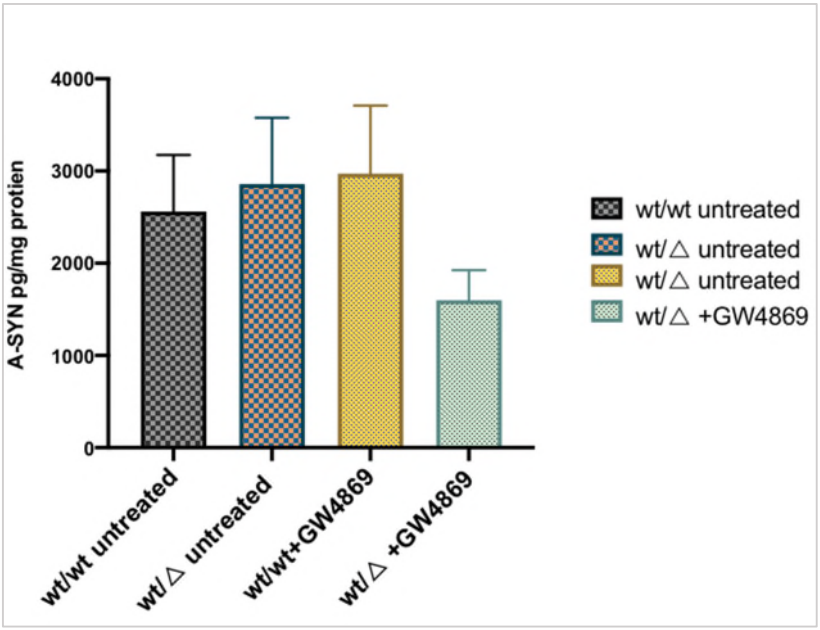

Figure 0.16 Detection monomeric A-SYN release into culture media of wt/△ MCN using Mouse Synuclein Alpha (SNCa) ELISA. The data were expressed as A-SYN pg/mg protein from 10 wt/wt and 9 wt/ wt/△ independent MCN cultures with two separate dilutions per culture, (n=10wt/wt,9 wt/△); under basal condition, the release of monomeric A-SYN did not significantly differ (*P*=0.996) between wt/wt (2661±611.6) and wt/△ neurons (2859±719.1). Also, when cultures were treated with GW4869, no significant difference (*P*=0.433) in monomeric A-SYN exocytosis observed between experimental groups;(wt/wt =2971±739.5, wt/△=1598±325.4).

Furthermore, with the detection of extracellular release of monomeric A-SYN from cells, we investigated the possibility induced exosomal release of A-SYN in to wt/△ MCN media, both under basal condition and upon treating cells with GW4689. The release of exosomes fractions was assessed previously using markers such as flotillin and CD63 that are known to be located solely on the outer surface of the exosomes (Magalhaes et al., 2018).

We first investigated the expression profile of these marker proteins, in wt/wt neurons treated with GW4869. Western blotting confirmed a clear separation for flotillin and CD63, both in untreated lysates and upon treating cells with 2.5 and 5µM of GW4869 (Figure 0.17), (n=1). The increased flotillin at 5µM dose of GW4869 suggests that release of exosomes might be prevented at this dose.

However, this dose was confirmed to be cytotoxic (Figure 0.15). In addition, dot blot analyses of culture media derived from wt/wt and wt/△ neurons were found immune-negative for flotillin and CD63 markers in both genotypes, (data not shown). We therefore proceeded to run dot blot on culture media derived from wt/△ MCN (Figure 0.18 A) and quantified another exosomes-specific protein (Alix) both under basal condition (untreated cells) and with 2.5µM GW4869 treatment (Figure 0.18 B). We found that despite the evidence of exosomes secretion in culture media of wt/△ cortical neurons under basal condition (Alix=1157981±156832), the amount released was not significantly different from that of wt/wt group (Alix=1252183±178220), (*P*=0.992). In addition, when treating neurons with GW4869 at 2.5µM concentration, it did not inhibit exosome release as evidenced by comparable secretion between groups (Alix wt/wt+GW4869=1200726±169720; wt/△+GW4869=1319993±189627, *P*=0.981), (Figure 0.18 B).

Taken together, these findings suggested that there was no accumulated endogenous A-SYN or enhanced exocytosis of either monomeric or exosome associated-A-SYN in media of wt/△ mouse cortical neuron.

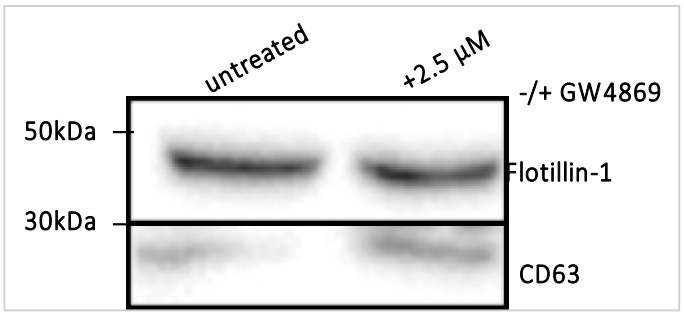

Figure 0.17 Western blotting using exosome specific markers flotillin and CD63 (±GW4689 treatment). Both anti flotillin and anti CD63 antibodies gave positive signals in both untreated and GW4689-treated wildtype MCN, (n=1).

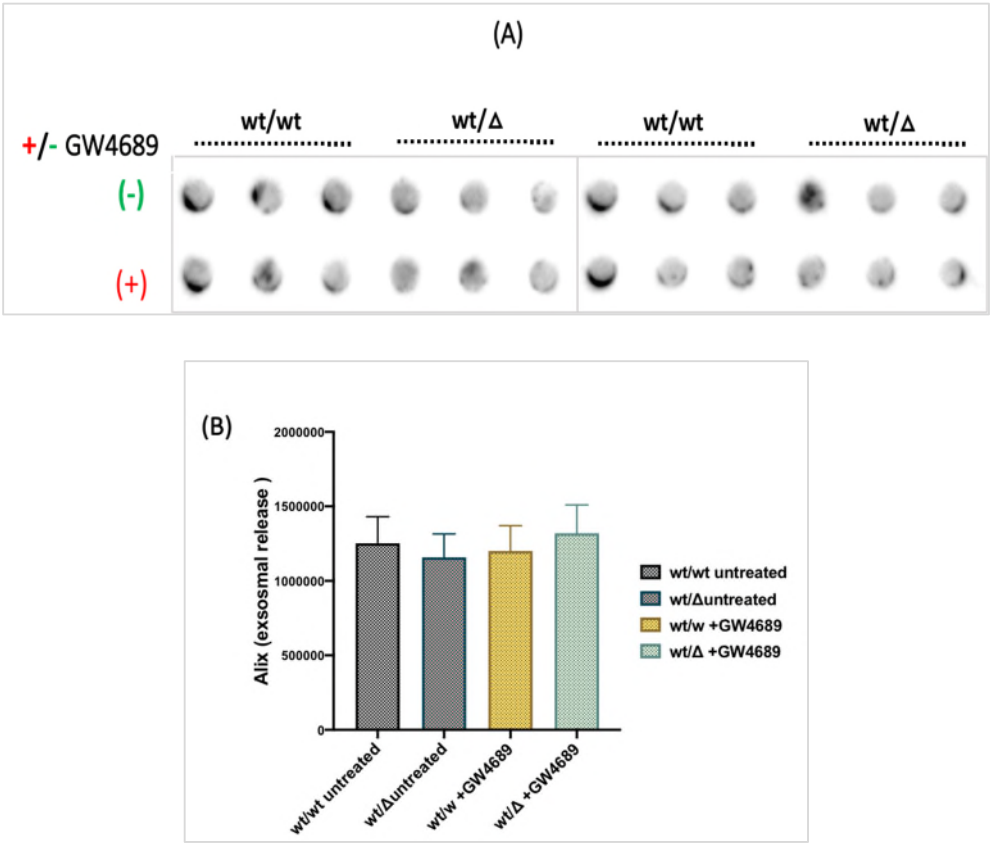

Figure 0.18 Quantification of exosomal release in wt/wt and wt/△neurons ±GW4689. Dot blot image and bar chart quantification of both wt/wt and wt/△neurons, treated GW4689, showing no significant change in the release of exosomes-associated fractions of A-SYN into CM of neurons under both experimental conditions and regardless of the genotype; Alix in untreated wt/△=1157981±156832 which was not significantly different from that of untreated wt/wt group (Alix=1252183±178220), (*P*=0.992). Also, wt/△neurons treated with 2.5µM of GW4869 showed no difference in exosomal release from wt/wt (Alix wt/wt+GW4869=1200726±169720; wt/ △

+GW4869=1319993±189627, *P*=0.981), Data represent the mean ± SEM, (*p*=0.9222), conditional media were collected from 13 individual cultures derived from 3 independent MCN preps (n=13).

4.5.8 Seeding neurons with preformed fibrils (PFFs)

4.5.8.1 Effect of PFFs Seeding in Wild Type Mouse Cortical Neurons

With the growing evidence that pathogenic forms of insoluble A-SYN are likely contributing to LBs and LN pathology, we first sought to investigate whether wildtype cortical neurons are susceptible to preformed fibril (PFFs) treatments leading to accumulation and extracellular release of insoluble A-SYN. The putative effect of fibrillary A-SYN treatment was first investigated on wild type MCN a screening test. It was previously shown in our laboratory that these fibrils can induce aggregation of A-SYN in control neurons within 10 days treatment (unpublished data). After seeding neuronal cultures with monomeric A-SYN species (5µg) and PFFs (5µg) for 10 days (section 2.4), TX-100 and SDS-Urea soluble A-SYN were fractionated and separated by electrophoresis. Our results showed that when treating neurons with monomeric A-SYN species or PFFs, the vast majority of A-SYN remained in TX-100 soluble state and did not significantly (*P*=0.941) differ from control (untreated) when quantified on lower exposure blots (untreated=0.684±0.271;+monomeric=0.731 ±0.242; +PFFs= 0.594±0.321,n=2), (Figure 0.19, B). As previously reported by others (Luk et al., 2012), monomeric A-SYN did not induce endogenous A-SYN to become insoluble. However, a small fraction of insoluble A-SYN was found in PFFs treated neurons (Figure 0.19 A blue arrowhead). In addition, there was evidence of HMW A-SYN species (~30-40kDa) present in PFFs treated MCN (Figure 0.19 A, green arrowhead). Other higher molecular weight species (>115-250kDa in size) appeared as non-specific

bands as there were present in untreated, monomeric- and PFFs treated neurons and in some soluble fractions of the blot (Figure 0.19, A red asterisks).

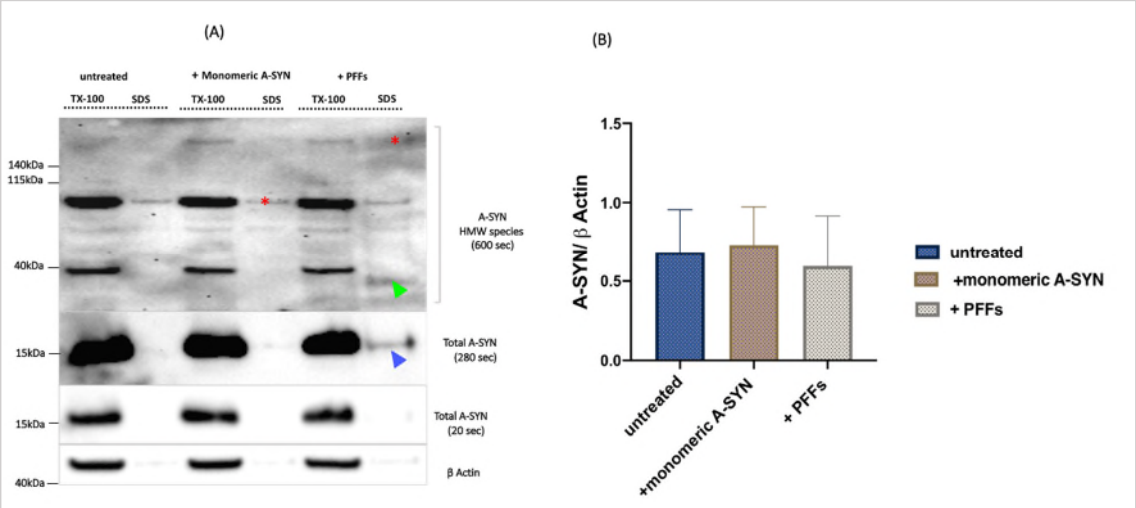

Figure 0.19 Consequence of monomeric A-SYN and PFFs seeding of wild type MCN. (A): Representative western blot image for wildtype MCN culture showing that in untreated neurons or those treated with monomeric A-SYN species or PFFs, most of A-SYN was present in TX-100 fractions. Only small fraction of insoluble A-SYN was found in PFFs seeded neurons (blue arrowhead). HMW A-SYN species (~30-40kDa in size, green arrowhead) were present in PFFs treated neurons. In addition, other HMW species (>115-250kDa) were found as non-specific bands in untreated, monomeric- and PFFs-treated neurons and in some TX-100 soluble fractions, (red asterisk). (B): Bar chart quantification for TX-100 soluble A-SYN expression relative to β Actin showing comparable levels of A-SYN between untreated monomeric- and PFFs treated MCN(*p*=0.941), (untreated=0.684±0.271; +monomeric=0.731±0.242;+PFFs=0.594±0.32). Data represent the mean expression level of TX-100 A-SYN normalized to β Actin (loading control) and derived from two independent wildtype MCN ± SEM, (n=2).

As aggregated A-SYN fibrils might have a prion like mechanism and can be released and spread from one cell to the other (Luk et al., 2012, Lee et al., 2014, Gegg et al., 2020), we conducted dot blot to support the phenomenon of release of A-SYN fibrils from cells. Because the antibody specific to synuclein fibrils (ab209538) is a conformation specific, the protein needs to be in its native form and detected by dot blot rather than denaturing western blotting. In dot blot, cell culture media were spiked with 0-30ng/ml of PFFs (standard curve), and the antibody detected PFFs in a manner proportional to recombinant PFFs dilutions (Figure 0.20, A). Analysis of culture media derived from untreated and monomeric A-SYN treated-wildtype MCN showed no A-SYN fibrils released in the last 24hours. However, media from PFFs-treated cells, (control I and II), were positive for A-SYN fibrils (Figure 0.20, B). When the A-SYN fibrils were normalized to the protein content of the well, the average amount of A-SYN fibrils released in to conditioned media of PFFs-treated MCN was 18.212 in control (I) and 36.097 ng/ml in control (II) wild type neurons. These were 274 and139 fold respectively lower than the PFFs concentration we used to load cultures on 4 DIV.

These findings collectively suggest that treating wt/wt neurons with PFFs induces A-SYN to become TX-100 insoluble and enhances the release of A-SYN fibrils from cells.

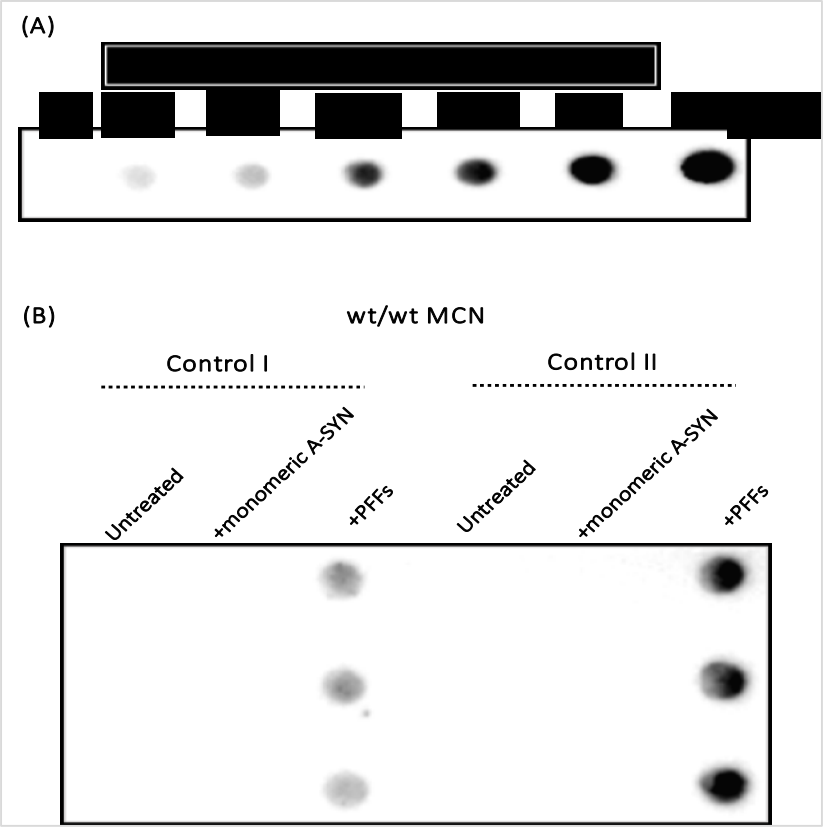

Figure 0.20 Dot blot for the extracellular release of fibrillary A-SYN following PFFs treatment of wild type neurons (control). Representative dot blot image showing release of fibrillary form of A-SYN (ng/mg protein) upon PFFs seeding of wild type (control I&II) MCN. (A): 0-30ng/ml PFFs standard curve measured by dot blot and showing specificity of anti-A-SYN fibrillar antibody (ab209538) for PFFs in a dose dependent manner. (B): Dot blot for A-SYN fibrils in conditioned media derived from untreated, monomeric A-SYN and PFFs-treated wild type mouse neuronal cultures (control I and II). Conditioned media was measured in triplicate and PFFs concentration calculated using standard curve. After normalizing it to protein content of the respective well, the mean concentrations of A-SYN fibrils released from treated cultures were 18.212 in control I and 36.097 ng/ml in control II.

4.5.8.2 Effect of PFFs Seeding in L444P Heterozygous Mouse Cortical Neurons

Having established that PFFs induce insoluble A-SYN in control MCN, we started treating cultured cells with PFFs in the background of heterozygous L444P mutation. This was done in an attempt to unravel the potential increased toxicity of PFFs treatment, not just in term of synuclein protein aggregation and extracellular release but also to asses cellular viability and exocytosis via exosomes through dot blot analysis of L444P MCN culture media. After 10 days of PFFs-seeding, pellets were fractionated sequentially in a high salt + TX-100 and SDS-urea lysis buffers, the example blots are shown in (Figure 0.21).

A summary of increased insoluble monomeric and high molecular weight (HMW) A-SYN species in PFFs- seeded GCase deficient neurons is shown in (Table 0.1), (n=9).

Table 0.1 Effect of PFFs seeding in wt/△L444P MCN

Genotype	Insoluble monomeric A-SYN	Insoluble phospho-A-SYN	HMW
wt/wt	7/9	2/9	6/9
wt/△	7/9	5/9	9/9

Western blot analysis of cell lysates showed that treating wt/△ neurons with PFFs induced significant accumulation of TX-100 soluble A-SYN fraction as compared to control (wt/wt) group; (TX-100 A-SYN: wt/wt=0.372±0.101, wt/△=0.989±0.149, n=6wt/wt, 8 wt/△, $^{**}P$=0.008), (Figure 0.21 A, B, C). Also, a considerable

proportion of A-SYN became TX-100 insoluble (solubilized with SDS-urea) following PFFs treatment (blue arrowhead in Figure 0.21, A, B). When the density of insoluble bands was measured (Figure 0.21, D), there was increased monomeric A-SYN in wt/△ group against control, but this however, did not reach statistical significance (*P*=0.386), (SDS-Urea A-SYN: wt/wt=0.404±0.095, wt/△ =0.736±0.130, n=7). Similar to previous reports (Luk et al., 2012, Gegg et al., 2020, Tapias et al., 2017), ~46% of the accumulated insoluble A-SYN was phosphorylated at Ser 129 (red arrowhead Figure 0.21, A and B, n=5). In addition, there was evidence of HMW insoluble band >250 kDa observed in all blots of PFFs-treated wt/△ groups, (n=9), (Table 0.1, Figure 0.21 A and B black asterisks). Other lower insoluble HMW bands (~30-40kDa) were found in some PFFs treated neurons regardless of the genotype (Figure 0.21 A, B green arrowhead).

Taken together, these observations suggest that PFFs seeding in wt/△ neurons induced A-SYN to significantly accumulate, become TX-100 insoluble and Ser129 hyperphosphorylated.

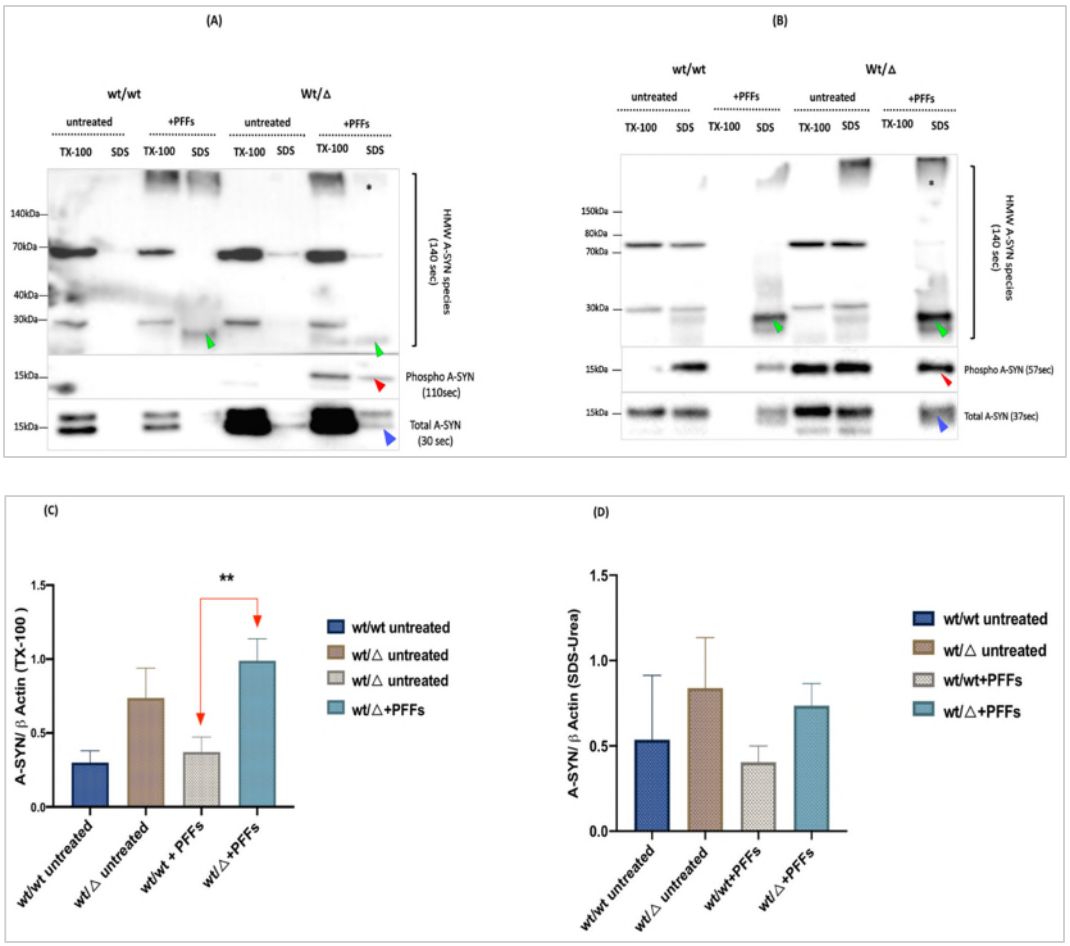

Figure 0.21 Effect of PFFs treatment in wt/L444P mouse cortical neurons. (A,B): Representative western blot image showing increased level of monomeric TX-100-soluble A-SYN in PFFs-treated wt/△MCN with evidence of some fractions turning insoluble (blue arrowhead) and phosphorylated at Ser129 (red arrowheads). Insoluble HMW species band (>250 kDa) appeared in all PFFs seeded wt/△ neurons (black asterisks), (n=9). (C): Quantification of A-SYN TX-100 soluble and insoluble fractions in PFFs-seeded wt/△MCN showing significant accumulation of soluble A-SYN fraction observed in wt/△ treated neurons (0.989±0.149) when compared to wt/wt group (0.372±0.101) wt/△; **P=0.008), data represent the mean expression level of TX-100 A-SYN normalized to β Actin (loading control) and derived from 6wt/wt and 8 wt/△ independent MCN ± SEM. (D): Quantification of insoluble A-SYN fractions showing nonsignificant (P=0.386) increased monomeric A-SYN in wt/△ group against control (SDS-Urea A-SYN: wt/wt=0.404±0.095, wt/△=0.736±0.130), data represent the mean expression level of SDS-urea A-SYN fractions normalized to β Actin (loading control) and derived from 7 independent MCN ± SEM, n=7).

We also ran dot blot to measure fibrillar A-SYN releases in to culture media of wt/△ MCN, both under basal condition (untreated control) and with PFFs treatment, (Figure 0.22 D). Our result showed no signals in untreated MCN regardless of the genotype (Figure 0.22, A). In addition, despite the induced A-SYN fibrillar exocytosis into PFFs- seeded culture media of both wild type and wt/△ neurons, there was no significant difference between experimental groups, (n=8wt/wt, 7wt/△, (*P*=0.387), (Figure 0.22 B, C). The mean A-SYN fibril concentration in PFFs-treated wt/wt MCN, after normalization to protein concentration in well, was 43.24±15.81 ng/ml while that of wt/△ group was 27.48 ±5.012ng/ml. This amount was 181-fold lower than the PFFs concentration used to seed neurons with on

We next investigated the exosomal release to culture media of wt/△ MCN under 4DIV.
basal condition and following PFFs treatment. Our result showed immunopositivity for Alix exosomal marker regardless of the presence and absence of treatment (Figure 0.23 A). However, with the evidence of exosomes released in to media derived from mutant neurons, the quantification showed no significant difference between treated and untreated cultures; (Alix untreated =6.51±3.92; PFFs treated= 5.95±0.690; *P*=0.841; n=2 untreated and 4 PFFs-treated wt/△ MCN), (Figure 0.23 B).
.

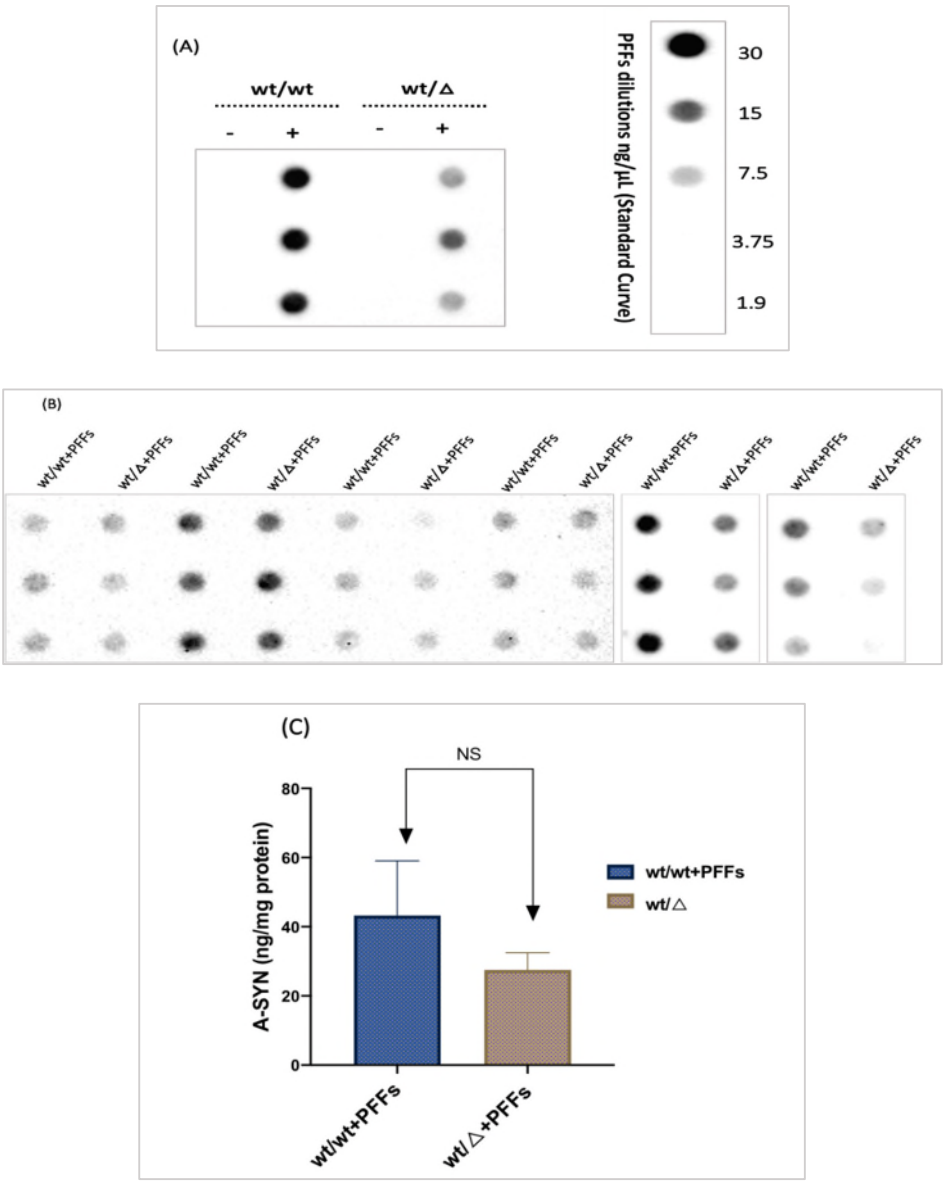

Figure 0.22 Dot blot approach with conditional media derived from MCN. (A): Dot blot image of PFFs-treated MCN showing abolishment of A-SYN immunostaining in media derived from untreated, both wildtype and L444P mutant MCN cultures, (n=3wt/wt, 1wt/△). (B):Probing with anti-fibrillary A-SYN antibody showing induced A-SYN fibrillar release into media of PFFs-seeded wild type and wt/△ neurons. (C): Bar chart quantification of A-SYN release in to CM of MCN seeded with PFFs; A-SYN fibril concentration was expressed as ng/mg protein and normalized to protein concentration in well. The analysis showed nonsignificant change in exocytosis between the treated wt/wt MCN (43.24±15.81 ng/ml) and wt/△ group (27.48 ±5.012ng/ml), (*p*=0.3867). Data represent the average of 3 experimental repeats ± SEM and derived from 8 wild type and 7 wt/△ independent MCN cultures.

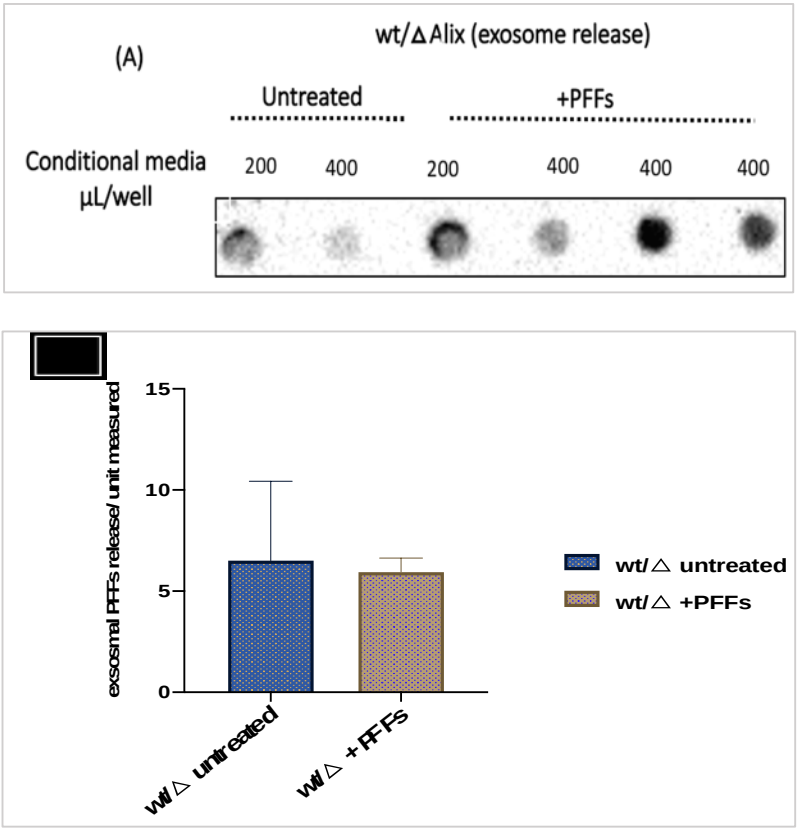

Figure 0.23 Investigating the exosomal release to culture media of wt/△ MCN, under basal condition and following PFFs treatment. (A): 200 or 400 µL of culture media collected from wt/△ cultures were spotted on dot blot and showed immunopositivity for Alix exosomal marker, regardless of the presence and absence of treatment. (B): Bar chart quantification showing no significant difference in exosomal release between treated and untreated groups; (Alix untreated =6.51±3.92; PFFs treated= 5.95±0.690; *P*=0.841). Data represent the average of exosomal released in culture media ± SEM and derived from 2 untreated and 4 treated independent wt/△MCN cultures, (n=2 untreated, 4 PFFs-treated).

4.5.9 Fluorometric Measurement of Cell Viability in Primary Neuronal Culture Seeded with PFFs

The toxic effect of A-SYN accumulation and aggregation is not limited to the donor cells, but also extend to the extracellular space and other recipient cells leading consequently to cell death, (Ahn et al., 2006, Luk et al., 2009). It was previously shown that A-SYN measuring 5-30µM and taken up by the neighboring cells can induce cell death in primary cortical neurons in a dose dependent manner (Sung et al., 2001, Danzer et al., 2012, Desplats et al., 2009). Therefore, we analyzed the cell viability of the primary neuronal cultures seeded with PFFs using CellTiter-Blue® (CTB) viability assay. CTB is briefly a method for estimating the number of viable cells present in a multi-well plate. These cells retain the ability to reduce Resazurin (blue color) into Resorufin which is highly fluorescent. Nonviable cells however, rapidly lose their metabolic capacity, do not reduce the indicator dye, and thereby do not generate fluorescent signal.

The assay was performed as described in (section 2.8) and we found no significant change in the number of viable cells between PFFs-treated and untreated cells regardless of the genotype, (P=0.960), (n=5wt/wt, 10 wt/△). This was suggestive that heterozygous L444P mutation did not affect cell viability. More importantly, the extracellular released of A-SYN fibrils shown above was due to exocytosis and not as a pathological consequence of PFFs-induced cytotoxicity, (Figure 0.24).

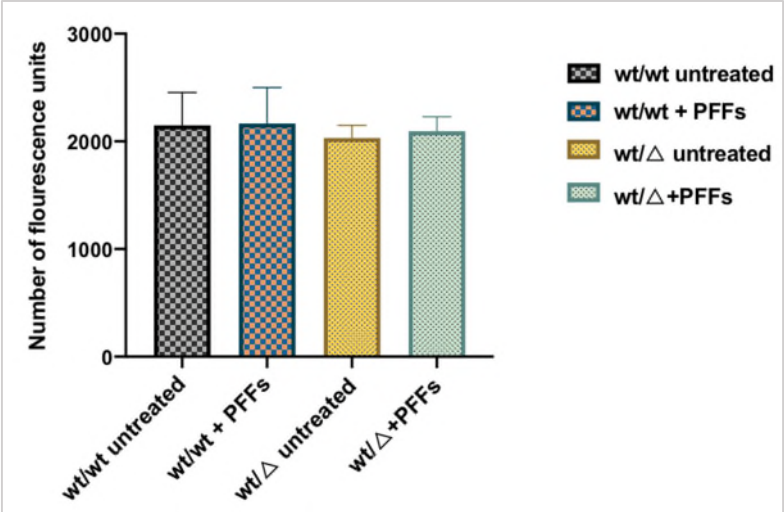

Figure 0.24 Influence of PFFs seeding for 10 days on cell viability of wt/L444P MCN. As determined by the CTB assay, no significant change of viable cell number observed between PFFs-treated and untreated cells regardless of genotype (*P*=0.960). Data was expressed as the mean fluorescence measured from 3 wells ± SEM, (n=5wt/wt, 10 wt/△).

4.5.10 Mitochondrial Function and Contents in wt/L444P MCN and Adult Mice

We next assessed mitochondrial oxygen consumption rates (OCRs) in mouse cortical neurons 10 DIV to investigate if L444P heterozygous mutation is linked to mitochondrial dysfunction. We employed Agilent Seahorse XF technique as described in (section 2.10.1). The basal, maximal, and spare respiratory capacities were measured by additions of oligomycin (ATPase inhibitor), FCCP (uncoupler to show maximal respiration), and antimycin A (to show non-mitochondrial oxygen consumption), (n=4 wt/wt, 7 wt/△). Results showed that oligomycin inhibited respiration coupled to oxidative phosphorylation and FCCP accelerated respiration to maximum capacity in both wildtype and mutant neurons. However, although it did not reach statistical significance, there was a trend of decrease in the basal, maximal respiration and the spare respiratory capacity in wt/△ neurons as compared to wt/wt group and shown in (Figure 0.25); The mean OCR under basal condition in wt/wt=19.60±8.99; wt/△=12.26±3.24, *P*=0.374, whereas the maximal OCR in wt/wt

=21.85±10.73; wt/△=12.36±3.379, *P*=0.3196 (

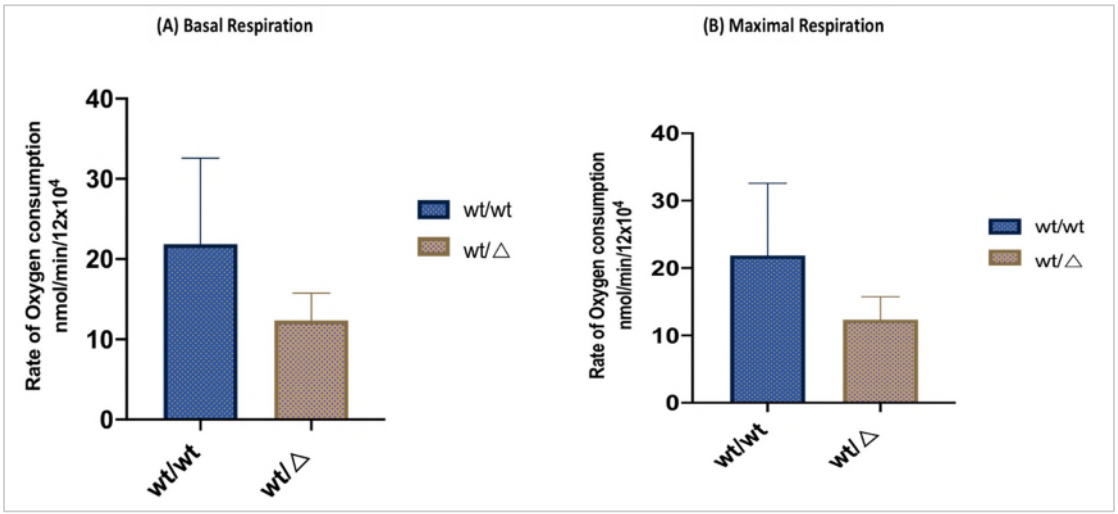

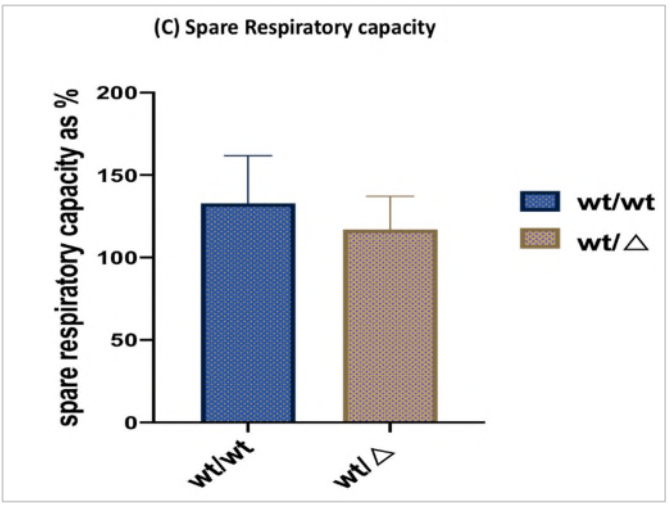

Figure 0.25 A, B). In addition, there was ~12% non-significant reduction in the reserve respiratory capacity in wt/△ neurons as compared to wt/wt group. The spare capacity which represent the difference between the basal and maximal OCRs

was117.1±20.04 in wt/△ MCN and 132.9±28.81 in wt/wt control group, *p*=0.656, (

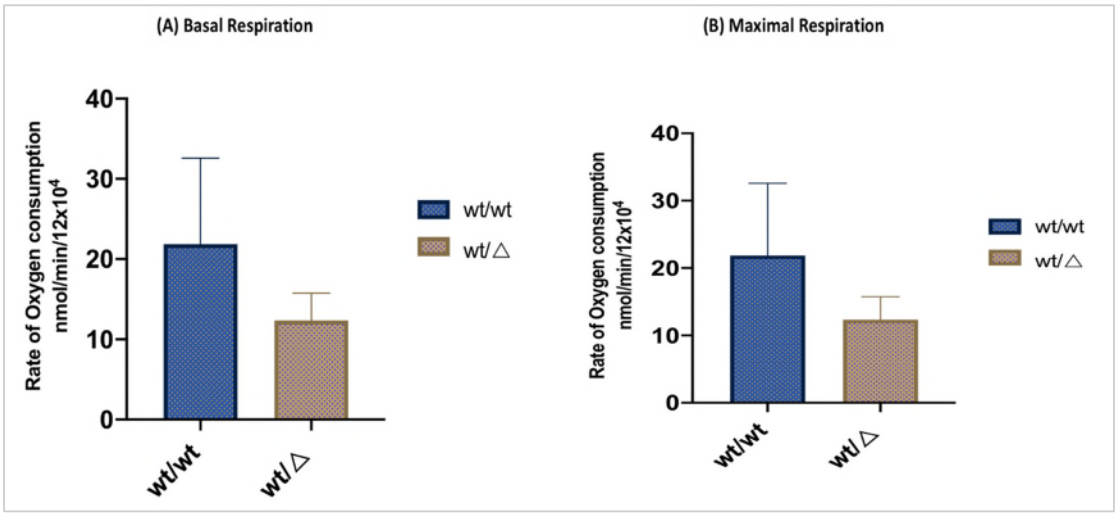

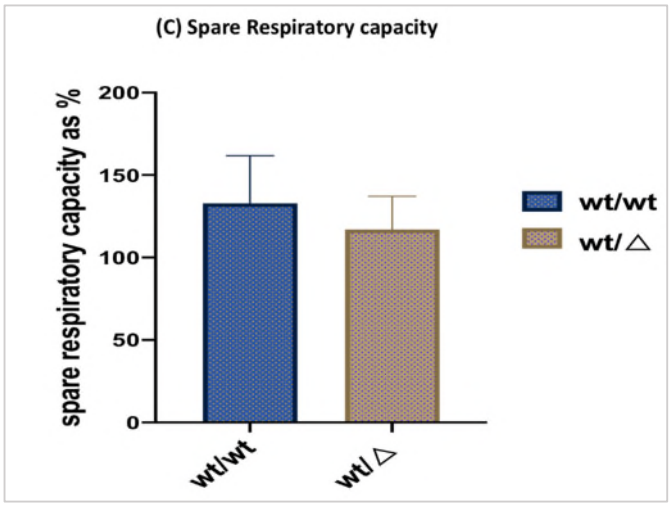

Figure 0.25 C). All data were expressed as the mean values± SEM, derived from 4 wt/wt and 7 wt/△ independent MCN cultures and taken from two separate neuronal isolations.

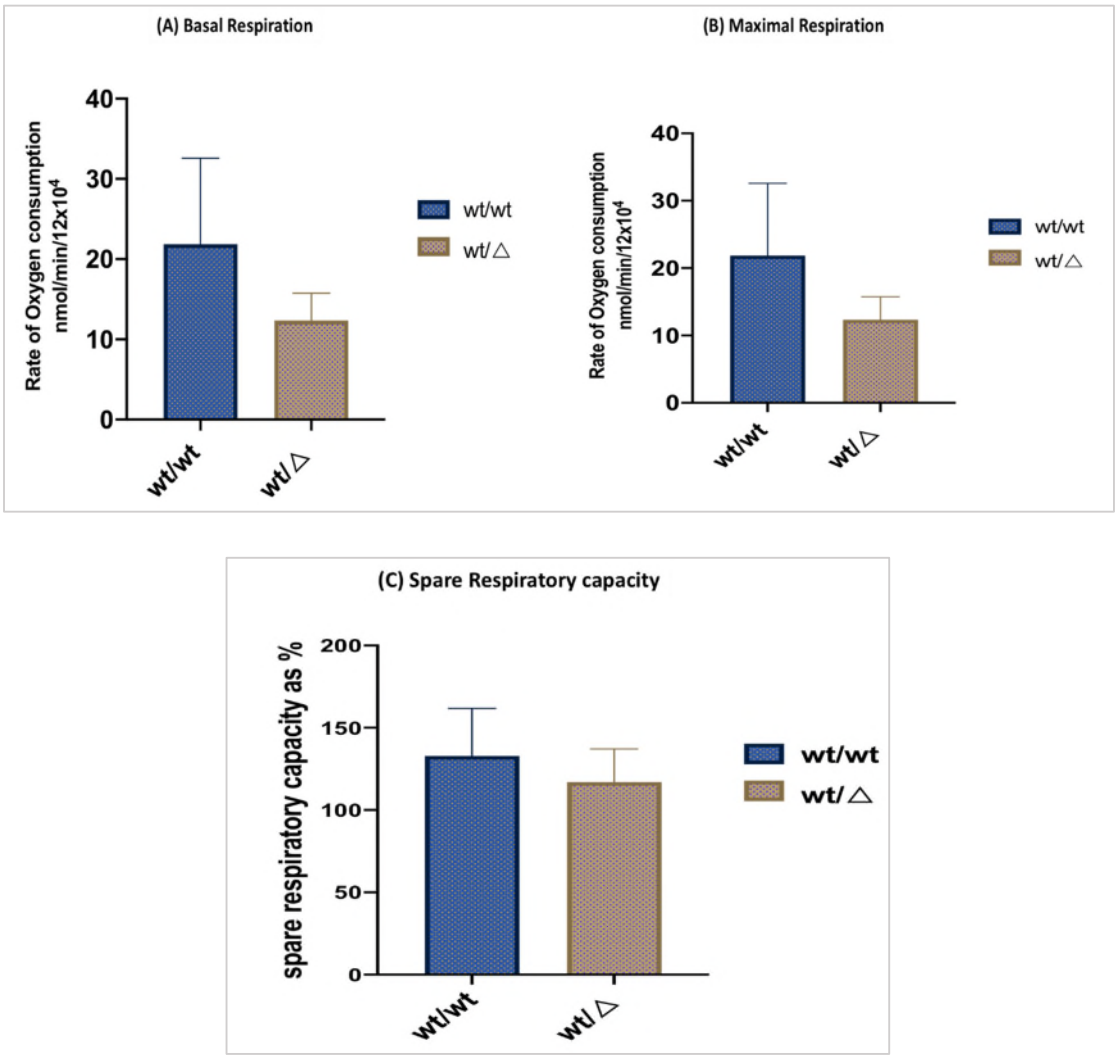

Figure 0.25 Investigating respiratory chain activity in wt/L444P MCN. (A): Oligomycin inhibited respiration coupled to oxidative phosphorylation in control group (19.60±8.995) and to lesser extent in wt/△ neurons (12.26±3.235), *p*=0.374. (B): A statistically non-significant reduction in the maximal (uncoupled) rate observed in mutant neurons as measured via the addition of FCCP (wt/ △ =12.36±3.379, wt/wt=21.85±10.73, *P*=0.3196). (C): The same trend of reduction was reflected on the spare respiratory capacity in the mutant neurons (117.1±20.04) when compared to their wt/wt littermates (132.9±28.81), *p*=0.656. Data = mean ± SEM, n=4 wt/wt and 7 wt/ △ independent MCN cultures.

In addition to bioenergetic function assessment, we investigated the expression levels of two selected mitochondrial respiratory chain proteins, complexes II (SDHA1) and complex IV (Cytochrome c oxidase) via immunoblotting (Figure 0.25 A). Following SDS-PAGE analysis, we found comparable steady-state levels of complex II and IV proteins between wt/wt and wt/△MCN; (SDHA1: wt/△ =1.15±0.109, wt/wt =1.07±0.051, *P*=0.099; Complex IV: wt/△= 0.505±0.083, wt/wt=0.545±0.074, *P*=0.735, n=4). (Figure 0.26 B, C).

We further extended our investigation to quantitatively assess the mitochondria abundance in our sample lysates via spectrophotometric measurement of citrate synthase (CS) activity (Figure 0.26 D). CS is an enzyme presents inside the mitochondrial matrix and its activity, as expressed in mol/min/mg protein, was non-significantly altered in wt/△ neurons (4173±312.2) when compared to wt/wt control (4945±778.7), (n=6, *P*=0.380).

These findings suggest no significant defect in mitochondrial function and mass observed in wt/△ mouse cortical neurons.

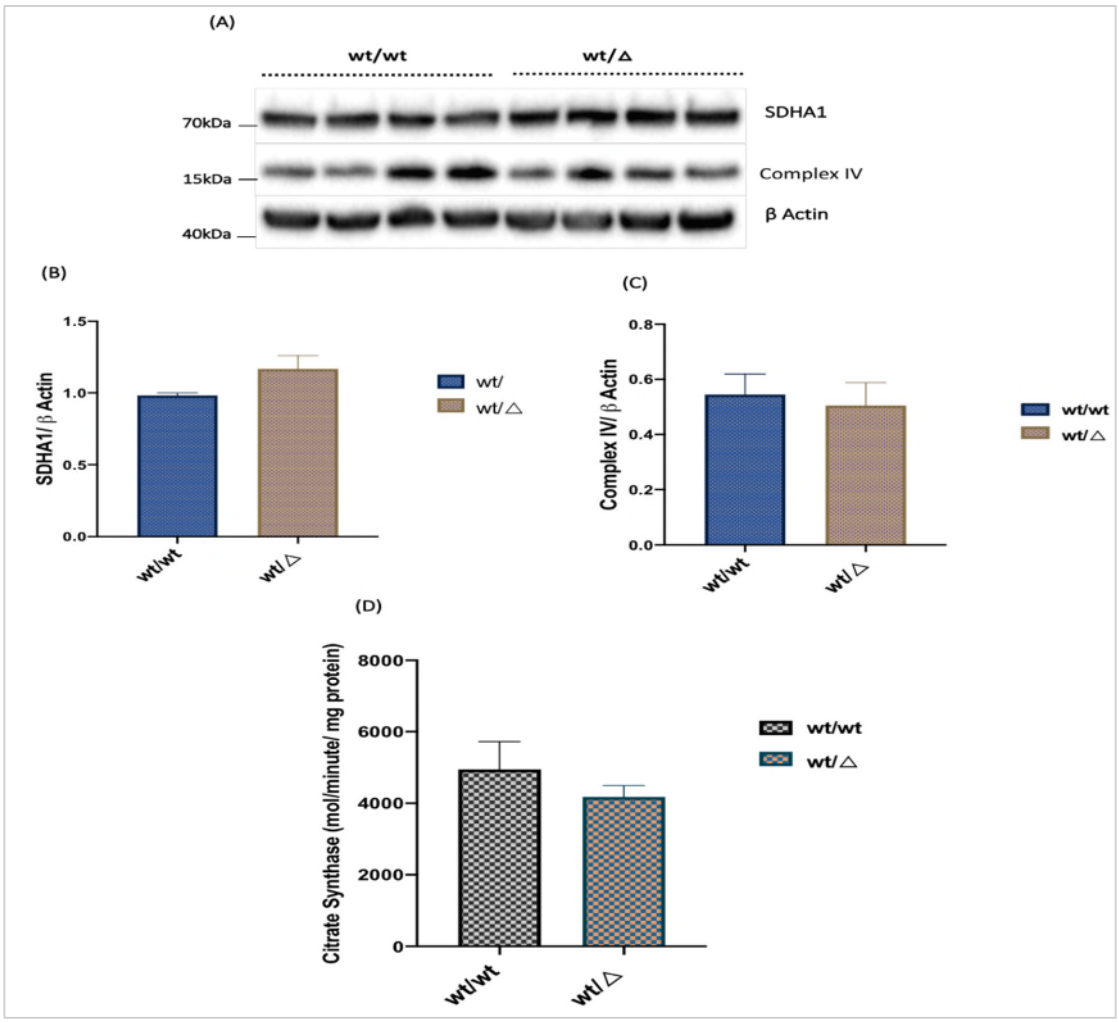

Figure 0.26 Investigating mitochondrial contents in wt/L444P MCN model. (A): Representative western blot image for the relative expression of complex IV and complex II (SDHA1) mitochondrial proteins to β Actin (loading control). (B): Bar chart quantification of complex II (SDHA1) protein showing no significant alteration in the expression level between wt/wt group (0.892 ±0.017) and wt/△ group (1.166±0.0932), (n=4, *p*=0.099). (C): Bar chart quantification of complex IV showing comparable expression levels between wt/△and wt/wt cortical neurons (wt/wt =0.545±0.074, wt/△ = 0.505±0.083), (n=4, *p*=0.735). Data in B and C represent the average of SDHA1 and complex IV expression levels relative to β actin ± SEM and derived from 4 independent MCN cultures, (n=4). (D): Assessment of mitochondrial matrix enzyme citrate synthase (CS) activity in mol/min/mg protein showing no significant alteration of enzyme activity in wt/△ MCN (4173±312.2) as compared to that of wt/wt group (4945±778.7), (n=6, *P*=0.380). Data represent the average of 2 experimental repeats ± SEM and derived from 6 independent MCN cultures.

We next analyzed if there is any reduction in mitochondrial number and respiratory chain proteins in aged mice. Immunoblot analysis of complexes II and IV in the cortex of 3month old mice showed no significant change in both proteins between wt/△ mice and their wt/wt control littermates (Figure 0.27 A, B, C, n=4).

In addition, there was no significant alteration observed in citrate synthase activity of cortical tissue derived from 3 months wt/△ adult mice when compared to control group (Figure 0.27 D, n=4).

Furthermore, we used 8-months old mice to investigate any change in mitochondrial complexes II and IV expression levels, or in CS activity, in aged mice with time. (Figure 0.28, n=4/3mo and 3/8mo). Likewise, we found no significant change in either of these parameters in 8months aged mice against 3month group.

Because dopaminergic neurons in substantia nigra pars compacta (SNpc) of midbrain are the most vulnerable neurons affected in PD (Surmeier et al., 2017), we applied the same paradigm on midbrain tissue derived from 3 months old wt/L444P adult mice. The same trend was observed in the midbrain of 3months old wt/△ mice, with no significant change detected in complex II, IV and CS activity against wt/wt control littermates, (Figure 0.29).

Taken together, these results collectively suggested non-significant change in mitochondrial function and mass detected in wt/L444P MCN or adult mice.

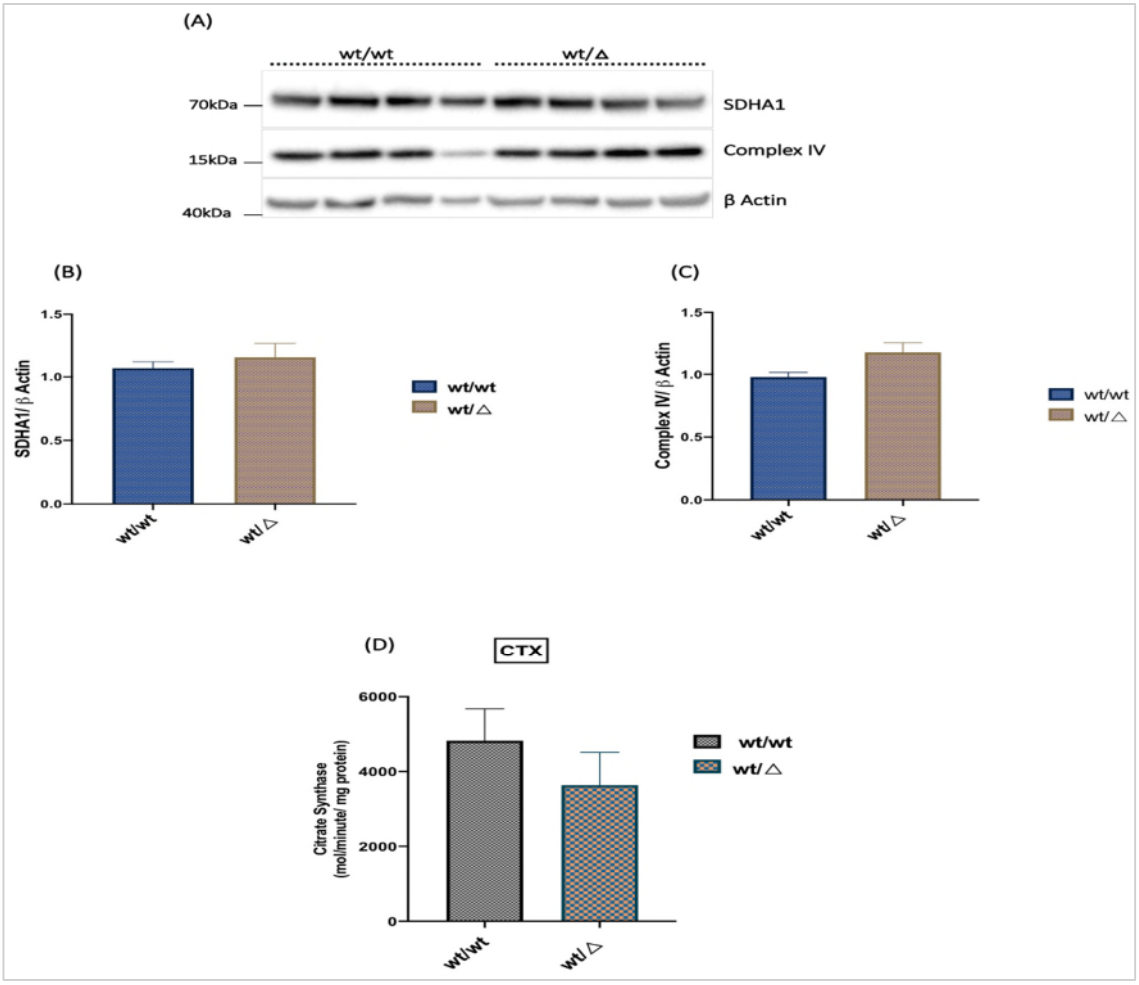

Figure 0.27 Investigating mitochondrial contents and citrate synthase activity in the cortical tissue of 3-month old wt/L444P transgenic mice. (A): Immunoblot image of both complex II (SDHA1) and IV showing comparable levels of markers between wt/△ mice and their wt/wt control littermates, β Actin was used as loading control. (B,C): Bar charts quantifying SDHA1 and complex IV proteins showing no significant alteration between wt/wt and wt/△ mice groups; (SDHA1: wt/△ mice=1.154±0.109 and wt/wt=1.068±0.051, *P*=0.557), (complex IV: wt/wt control= 0.977±0.036 whereas wt/△ mice=1.174±0.076, *P*=0.094). Data in B and C represent the average level of SDHA1 and complex IV relative to housekeeping protein (β Actin) ± SEM and derived from 3wt/wt and 4wt/△ mice, (n=3wt/wt and 4wt/△). (D): Bar chart quantification of citrate synthase activity (measured as mol/minute/mg protein) in cortical tissue homogenate of wt/L444P adult transgenic mice. There was a slight but not significant reduction in CS activity in wt/△ mice (4826±850) with respect to their wt/wt control littermates (3638±877), (*P*=0.369). Data represent the average of 2 experimental repeats ± SEM, (n= 4).

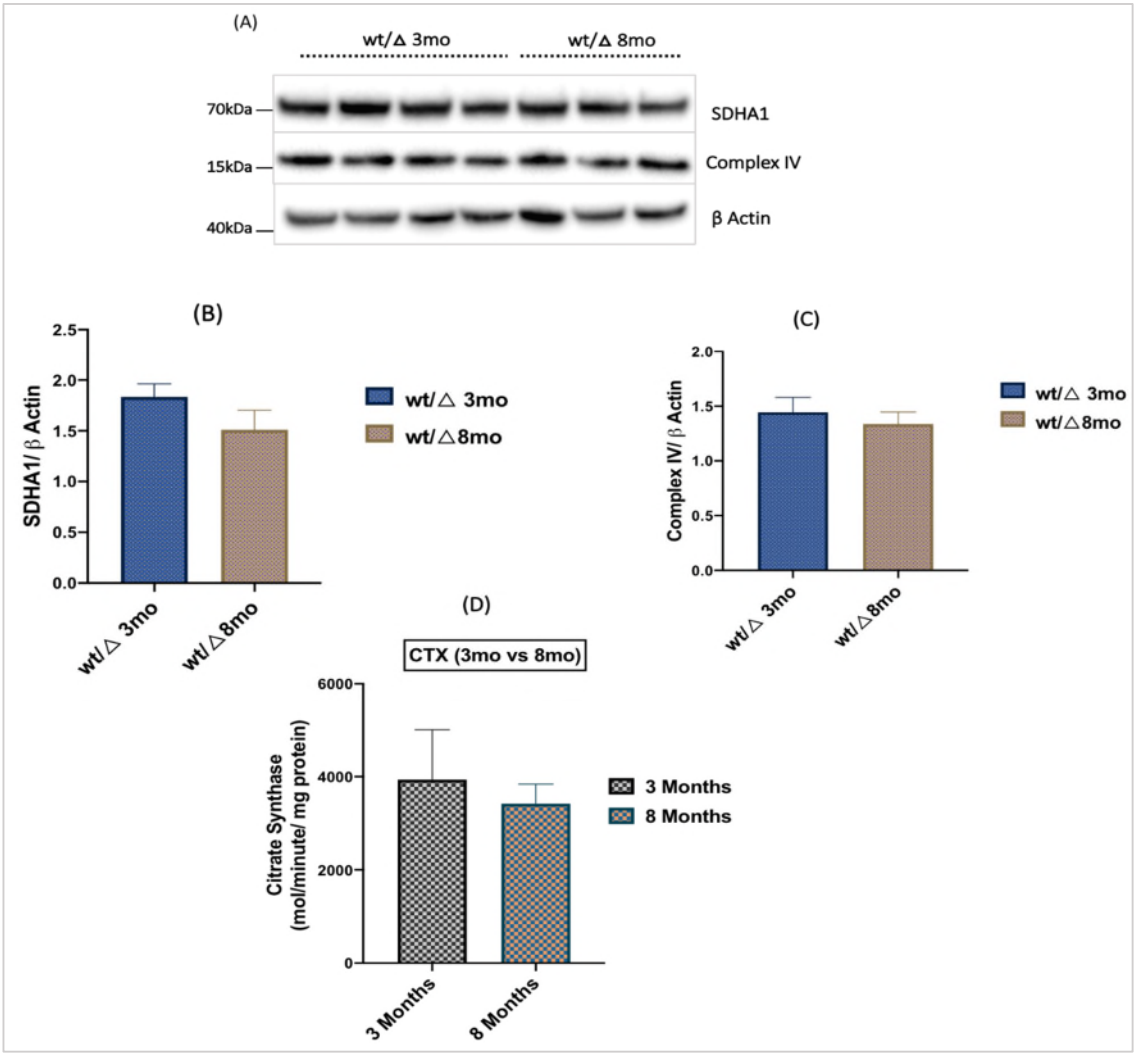

Figure 0.28 Investigating mitochondrial contents and citrate synthase activity in the cortical tissue of 3-month vs 8-month old wt/L444P adult transgenic mice. (A): immunoblot image for both complex II (SDHA1) and complex IV showing no apparent change in both markers between the two experimental groups, β Actin was used as loading control. (B,C): Bar chart quantifications showing no significant change in both markers expression levels between 3 and 8months wt/△ mice groups; (SDHA1:3-month =1.84±0.128, 8-month old =1.51±0.192, *P*=0.201), (complex IV; 3month =1.46±0.135, 8-month=1.34±0.111, *P*=0.579). Data in B and C represent the mean of SDHA1 and complex IV expression levels relative to β Actin± SEM derived from 4 of 3months and 3 of 8months wt/△ mice. (D) Bar chart quantification of citrate synthase activity (measured as mol/minute/mg protein) in cortex of 3-month vs 8-month old wt/L444P transgenic mice. There is no significant alteration of activity in the cortex of 8month mice (3429±421.8) against that of 3month wt/△ group (3937±1070), data represent the average of 2 experimental repeats± SEM derived from 4 of 3-month and 3 of 8-month old mice), (*P*=0.710).

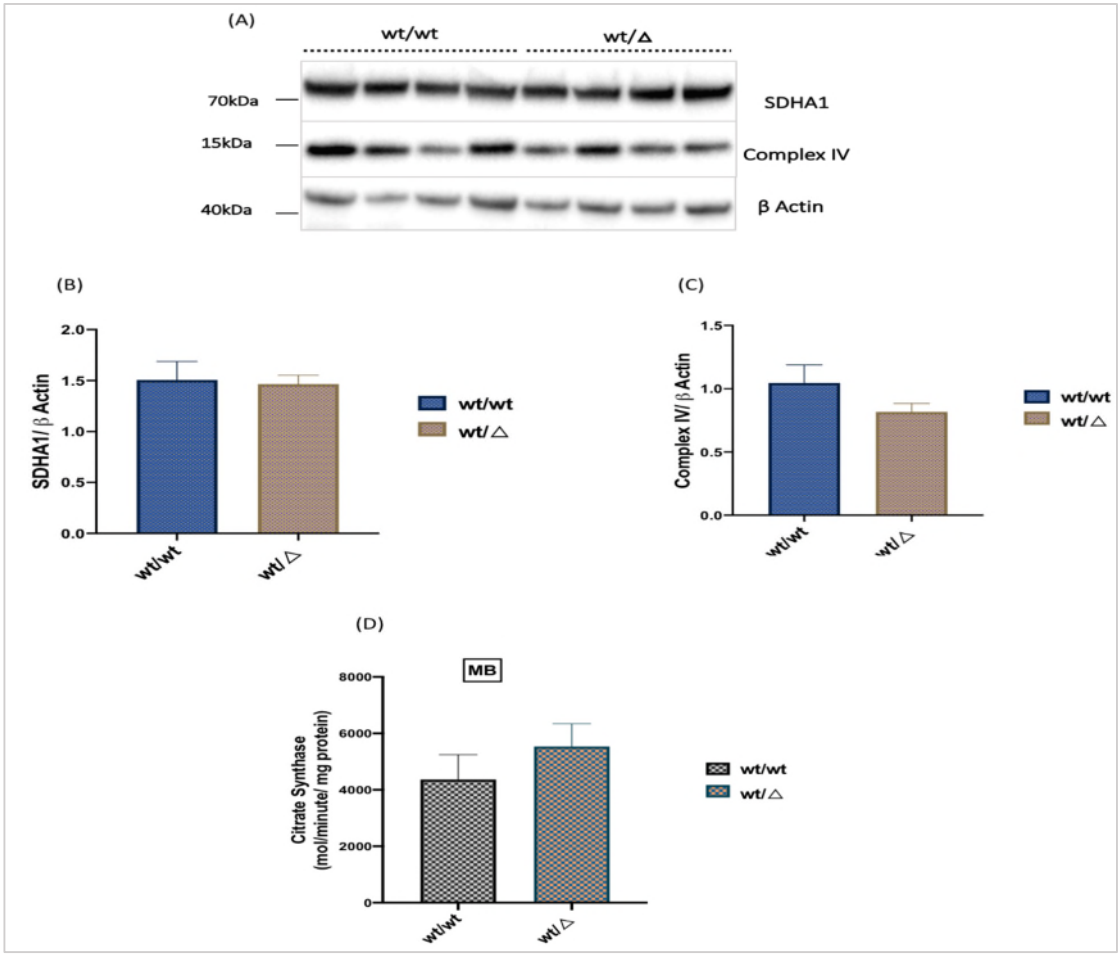

Figure 0.29 Investigating mitochondrial contents and citrate synthase activity in the midbrain tissue of 3-month old wt/L444P transgenic mice. (A): Immunoblot image of both complex II (SDHA1) and complex IV showing no apparent change in both markers between wt/△ mice and their wt/wt control littermates, β Actin was used as loading control. (B, C): Bar charts summarizing the mean expression levels of SDHA1 and complex II in the midbrain of 3-months mice; no significant change in either SDHA1 or complex IV proteins between experimental groups; (SDHA1: wt/△ =1.47±0.090 while that of wt/wt=1.51±0.183, *P*=0.850), (complex IV level in wt/△ mice=0.817±0.664 and in wt/wt control group=1.045±0, *P*=0.197). Data in B and C represent the mean expression levels of both SDHA1 and complex IV proteins relative to β Actin± SEM, n=4. (D) Bar chart quantification of citrate synthase activity (measured as mol/minute/mg protein) in midbrain homogenate of wt/L444P 3 months old mice showing a slight but not significant trend of increase in CS activity in midbrain tissue of wt/△ mice (5531±808.6) with respect to their wt/wt control littermates (4365±881.1), data represent the average of 2 experimental repeats ± SEM, (*P*=0.367, n=4)

4.6 Discussion

In this chapter, we used mouse cortical neurons as a platform to test the biochemical alterations associated with wt/L444P mutation. Summary of the main disease phenotypes associated with L444P mutations in MCN are listed in (Table 0.2).

Table 0.2 Summary of main results obtained using MCN model of L444P heterozygous mutation.

Disease phenotype	Methods	MCN	Adult mice Cortex (3months/8 months)	Adult mice Midbrain (3months)
GCase Activity	Enzymatic assay	37.6 % Significant reduction	not investigated	not investigated
GCase Protein Expression	Immunocytochemistry	no detection of endogenous GBA protein in MCN	not investigated	not investigated
β-hexosaminidase and β-galactosidase activities	Enzymatic assay	not changed	not investigated	not investigated
Lysosomal Contents (LIMP2, LAMP1 Cathepsin D)	Western blotting	no statistically significant changes in lysosomal proteins	not investigated	not investigated
Autophagy Flux	Western blotting	No impairment	not investigated	not investigated
CMA	Western blotting	No impairment	not investigated	not investigated
UPS	Chemicon's assay of 20S subunit activity	No impairment	not investigated	not investigated
BiP level	Western blotting	Not significantly changed	not significantly changed	not significantly changed
Phosphorylation of elf2a	Western blotting	Not significantly changed	not investigated	not investigated
Endogenous A-SYN Level	Western blotting	not significantly changed	not significantly changed	not significantly changed
Extracellular Release of Monomeric A-SYN	ELISA	not significantly altered under basal condition or with 2.5µMGW4869	not investigated	not investigated
Release of Exosomes	Dot blot	not significantly inhibited with 2.5µMGW4869	not investigated	not investigated
Pathological Phenotype with PFFs Seeding **TX-100 vs SDS-urea A-SYN intracellular levels**	Western blotting	-significantly accumulated TX-100 soluble A-SYN -more A-SYN become SDS-Urea soluble and Ser129 hyperphosphorylated -Evidence of HMW A-SYN species	not investigated	not investigated
Release of free fibrillar A-SYN and exosome fractions	Dot blot	not significantly induced A-SYN fibrils (free or exosomes-associated fractions)		
Effect on cell viability	CellTiter-Blue® Cell Viability (CTB) Assay	No effect on cell viability		
Mitochondrial Assessment **(Bioenergetic/complex II and IV levels)**	Agilent Seahorse XF technique	No significant slight reduction in basal and maximum OCRs/ 12% non significant reduction in spare respiratory capacity	not investigated	not investigated
(mitochondrial number /CS activity)	Western blotting analysis of complex II and IV	not significantly changed	not significantly changed	not significantly changed
	CS activity assay	not significantly changed	not significantly changed	not significantly changed

4.6.1 GCase Activity and Integrity of Protein Quality Control are Linked to Defective A-SYN Metabolism

The measured GCase enzyme activity in our wt/L444P primary cortical neurons showed 37.6% significant reduction when compared to wt/wt group. This anticipated finding was previously produced by work on wt/L444P *GBA* knock in aged mice and in the hippocampal and primary cortical neurons derived from mice carrying the same mutation (Fishbein et al., 2014, Migdalska-Richards et al., 2017, Li et al., 2019, Migdalska-Richards et al., 2016).

The significant reduction in GCase activity was even observed in different brain regions of PD patients with and without *GBA* mutations indicating the crucial role of GCase enzyme in the development of iPD (Gegg et al., 2012, Murphy et al., 2014). In contrast to reduced GCase activity, we could not detect any altered activities of lysosomal hydrolases, β-hexosaminidase and β-galactosidase enzymes. Furthermore, no change in lysosomal associated protein level was detected in our wt/△ model. These observations were suggestive that the deficient enzymatic activity was due to *GBA* mutation and not reflected on lysosomal mass. Consistent with our results is the previous finding of normal lysosomal protein markers levels and hydrolases activities in *GBA* K/O and wt/L444P transgenic mice and primary neuronal cultures (Magalhaes et al., 2018, Osellame et al., 2013, Migdalska-Richards et al., 2017).

However, how GCase enzyme when mutated predispose to A-SYN dysmetabolism and PD pathogenesis is still to be fully elucidated. A bidirectional loop between GCase and A-SYN has been previously suggested, when reduced enzymatic activity results in substrate accumulation which intern stabilized the oligomeric species of A-SYN allowing greater GCase dysfunction due to direct

interaction between the two proteins (Mazzulli et al., 2011, Yap et al., 2013). Therefore, it would not surprising to see that in both cellular and animal models whenever there is a reduction in GCase activity, it perturbs lysosomal function and subsequently A-SYN turnover, which predispose to its accumulation and aggregation. Conversely, both in vivo and invitro overexpression of A-SYN are to be associated with reduces GCase activity. With the previous presence of defective proteostasis associated with PD (Dehay et al., 2013) and impediment of A-SYN turnover, the attention was driven to the role of lysosomal dysfunction and altered A-SYN metabolism as a central component of PD pathogenesis, (Cuervo et al., 2004, Mazzulli et al., 2011).

We therefore started to characterize MA flux in wt/L444P neurons to find any concomitant defect in autophagic machinery. Our results showed no evidence of impaired flux in wt/△MCN in comparison to wt/wt control. We also did not detect any increased A-SYN levels in these neurons as compared to wt/wt group (n=5wt/wt, 9wt/Δ), P>0.05.

In contrast to our finding, A-SYN accumulated in severe GD phenotypes such as GCase pharmacological inhibition by CBE (95% loss of activity) in mouse cortical neurons (Magalhaes et al., 2016), and in a *GBA* K/O mouse mixed cortical tissue (Osellame et al., 2013). However, heterozygous L444P *GBA* mutation has been less thoroughly investigated and to our knowledge, only recent work by Li et al. group investigated the effect of wt/L444P mutation in vitro. They confirmed defective induction of autophagy and flux with an increase in the overall steady state level of A-SYN. However, Li et al group used mouse hippocampal neurons to model wt/L444P PD. The established impaired integrity of MA in this work was thought to be through a dual mechanism of loss of GCase activity that impaired

autophagosomes clearance with the mutant enzyme per se impeding autophagic induction (Li et al., 2019). Perhaps the hippocampus is more susceptible to A-SYN accumulation than cortical regions in *GBA* mouse models. Other GD model showing notable A-SYN accumulation and cognitive deficits was reported in a study by Sardi et al. group (Sardi et al., 2011).

In addition to MA flux, we analyzed CMA function in mutant neurons as one of its major roles is to dispose damaged and aggregation prone proteins such as A-SYN (Cuervo et al., 2004, Sala et al., 2016). We therefore hypothesized defective CMA in our model but failed to detect impairment of this pathway as evidenced by comparable protein levels of both HSC70 and LAMP2a between experimental groups. Evidence of reduced levels of CMA markers concomitantly with A-SYN aggregation and LBs formation was reported in SNpc and amygdala of post mortem PD brains, (Alvarez-Erviti et al., 2010).

The absence of defective ALP in our MCN model might imply that longer time point than 10 DIV is needed to induce impairment in either of the above protein clearance pathways. Other possibility is that *GBA* mutations affect MA flux in dopaminergic neurons more than cortical neurons and could explain why particular neuronal populations in PD are more susceptible to neurodegeneration. Impaired autophagy was a major pathological feature in both N370S and L444P iPSc derived dopaminergic neurons (Schondorf et al., 2014, Fernandes et al., 2016) respectively. Furthermore, it is possible that the ~40% reduction in GCase activity associated with heterozygosity for L444P mutation was not sufficient to have any influence on ALP. Aging of wt/L444P mice for 24 months (Migdalska-Richards et al., 2017) resulted in small A-SYN accumulation which suggests that aging was a risk factor for the disease phenotype in this work. Alternatively, the

impaired MA reported specifically in hippocampal neurons in Li et al. study might indicate that the defective MA secondary to heterozygous L444P mutation is possibly tissue specific.

Although MA is particularly omnivorous pathway, it is not the only pathway through which cellular material is degraded; UPS contributes to cellular quality control by degrading soluble and misfolded proteins during the process of ERAD. Most previous studies had focused on the alteration of UPS in iPD and its link to A-SYN pathology (McNaught et al., 2002, McNaught et al., 2003). Furthermore, many but not all studies, that came after McNaught et al. showed how proteasomal inhibition can lead to defective clearance and increased level of A-SYN emphasizing the link between UPS deficit and PD (Bedford et al., 2008, Beal and Lang, 2006). However, there was paucity of published research about the effect of *GBA* mutations on UPS with only one study of impaired UPS in *GBA* KO was performed, however, on a mouse mixed cortical neuronal culture (Osellame et al., 2013). The accumulated A-SYN oligomeric species in this work was observed as a pathological consequence of impaired MA and UPS pathways in *GBA* K/O model. Also, Epoxomicin inducing proteasomal inhibition in SH-SY5Y cell lines was previously detected as a cause of decrease turnover and accumulation of Ser129 phosphorylated A-SYN and thus predisposing to cellular death, (Chau et al., 2009). These findings indicate the inability of neurons to turn over the aggregated A-SYN as a result of complete loss of enzymatic activity and impaired protein quality control. Nevertheless, we were unable to detect any defective UPS associated with L444P mutation in our MCN model. This observation when coupled with the lack of ALP impairment, could be related to the brain region characterized. There are, however, other possible explanations

related to the difference between almost total loss of GCase activity and only one mutant allele as evidence in Osellame et al. work. They reported normal MA flux and UPS pathways under *GBA* heterozygous state of the same neuronal model employed, (Osellame et al., 2013).

A summary of previous studies reporting increased A-SYN in various disease models of *GBA*-linked PD are listed in (Table 0.3).

Table 0.3 Summary of published studies investigating A-SYN metabolism in relation to *GBA*-PD

Study	Mutation	Disease model	A-SYN level
Li et al., 2019	Heterozygous L444P	Hippocampal neurons	↑ A-SYN
Fishbein et al., 2014	Heterozygous L444P+ Overexpression wt and A53T *SNCA*	Primary cortical neurons	↑ A-SYN
Migdalska-Richards A et al., 2017	Heterozygous L444P aged mice >18mo	cortex	↑ A-SYN
Magalhaes J et al., 2016	+CBE (95% loss of GCase activity)	Primary cortical neurons	↑ A-SYN
Gegg et al., 2020	+CBE (95% loss of GCase activity)+PFFs treatment	Primary cortical neurons	↑ A-SYN
Osellame LD et al., 2013	GBA KO	Mixed culture of cortical neurons & Astrocytes	↑ A-SYN

On top of increased A-SYN steady state level due to defective clearance in wt/L444P cultures, it was documented that overexpression of either wt/wt or A53T mutant A-SYN with a background of wt/L444P increasing A-SYN half-life and thus predisposed to its phosphorylation and accumulation in A53T *SNCA* and wt/L444P brain culture of double-transgenic mice (Fishbein et al., 2014). Although previous immunocytochemical analysis of GBA K/O and wt/L444P transgenic aged mice showed similar distribution of accumulated A-SYN in different brain regions with more involvement of hippocampi of *GBA* K/O, these findings were not replicated in the same mice using WB analysis (Migdalska-

Richards et al., 2017). However, A-SYN was found increased by 147% in mouse primary neuronal cultures treated with CBE (Magalhaes et al., 2016). These cultures also exhibited HMW species and 165% increased Ser129 phosphorylated A-SYN as detected by WB. This might indicate that A-SYN accumulation needs total loss of GCase activity in a time and dose dependent manner and the difference in the sensitivity of the two techniques in detecting A-SYN accumulation (Migdalska-Richards et al., 2017). In addition, despite the accumulated A-SYN found in multiple brain regions of wt/L444P aged mice including the cortex and CA3 layer of the hippocampus, there was no aggregated proteinase K resistant A-SYN in the same regions analyzed, (Migdalska-Richards et al., 2017). On the contrary, Sardi et al. experimental approach on mouse model showed progressive accumulation of A-SYN aggregates in the hippocampus coincident with memory deficit in D409V knock-in mice (Sardi et al., 2011). Therefore, it is possible that L444P mutation in mice neurons does not reach the threshold of LBs formation hence it needs further exacerbation of disease phenotype as with overexpression of mutant A53T *SNCA,* (Fishbein et al., 2014). The homozygosity of D409V *GBA* mutation used in Sardi et al., work reduced GCase activity to ~15% and resulted in more pronounced accumulation of ubiquitinated aggregates containing proteinase K-resistant A-SYN in mouse hippocampal neurons. Incorporated in to this is the finding that only heterozygous D409V/+ mutation but not *GBA*-/+ exhibited hippocampal accumulation of A- SYN aggregates despite that both mutations retained similar activity of GCase enzyme, (Sardi et al., 2011). The discrepancy here is related to the mutation type and dosage which are needed to induce misprocessing of A-SYN. Considering the above observations and the given fact that heterozygosity for *GBA* mutation

does not always result in PD but rather increases the relative risk 4-fold, it could be difficult to reproduce PD-related phenotype in a heterozygous state of primary cortical neurons especially in shorter lifespan of mice. Therefore, with time constraints of primary cultures compared even to aged animals, (Migdalska-Richards et al., 2016) or the prolonged culture of iPCs derived neurons (Schondorf et al., 2014), it might prove challenging to detect significant changes in A-SYN metabolism. We therefore chose to first seed wt/wt primary cortical neurons with monomeric A-SYN and PFFs to enhance the phenotypic abnormalities and emulate the pathological scenario occurring in PD brain and start triggering Ser129 phosphorylation of A-SYN. Our result has expectedly showed that treating wt/wt MCN with PFFs but not monomeric A-SYN accumulated A-SYN and enhanced it to become detergent insoluble (SDS-urea soluble). Based on these results, we next analyzed the effect of PFFs seeding in wt/L444P MCN and found that it significantly led to accumulation of TX-100 A-SYN and enhanced more A-SYN to become insoluble and even hyperphosphorylated at Ser129. This was also associated with evidence of >20kDa HMW spices present mostly in all treated mutant neurons, (n=9). These findings strongly indicated that heterozygous L444P mutation was not merely sufficient to induce pathological inclusion similar to LBs and LNs found in PD. Also, on the background of L444P mutation, a PFFs-treated model is needed to enable reproducibility of such pathology.

4.6.2 PFFs Seeding of Primary Cortical Neurons Supports “Trojan Horses" Hypothesis of Neurodegeneration

Given the short time period of MCN experiments and the growing evidence of A-SYN fibrils acting in a prion-like fashion, we utilized PFFs on our wt/L444P model to see if this has an effect on A-SYN metabolism. Overall, wt/L444P MCN tended to show an increased amount of phosphorylated insoluble A-SYN and evidence of more HMW insoluble species, compared to control. These data suggest that *GBA* mutations can affect metabolism of pathogenic A-SYN species. An important aspect of pathogenic A-SYN is the ability to pass from one neuron to another, inducing hfunctional A-SYN in recipient cells to become misfolded and insoluble. The release of monomeric synuclein in CBE treated primary neuronal cultures was significantly increased by 159% when compared to untreated neurons (Magalhaes et al., 2016). We measured monomeric and exosome-associated A-SYN release into culture media by ELISA and dot blotting respectively. However, no significant difference in the release of monomeric or exosomal A-SYN could be detected between wild type and GCase-deficient neurons under basal condition. Furthermore, GW4689 treatment did not inhibit the secretion of either monomeric or exosome-associated A-SYN into wt/L444P condition media. Perhaps a future higher non-cytotoxic inhibitory concentration of GW4689 is needed to detect significant difference in exosomal A-SYN release as SMase was not inhibited with the use of 2.5 µM dose. In addition, investigating Rab11 as another marker of exocytic pathway is a possibly an alternative future plan.

With the evidence that free but not exosome-concealed A-SYN was recovered from the supernatant fractions of A53T *SNCA* overexpressing SH-SY5Y cell,

(Hasegawa et al., 2011), we extended our analysis to investigate the possibility of A-SYN fibrils exocytosis into media of wt/L444P neurons following PFFs treatment. We found that PFFs have equally induced the release of A-SYN fibrils with no significant difference from treated wt/wt control. No change in the release, of otherwise increased, exosome-associated fractions was observed following PFFs treatment regardless of the genotype. The previous observation by (Danzer et al., 2012) showed that inhibiting MA flux in primary neuronal culture, although was accompanied by induced release of free and exosome-associated synuclein, but failed to reach statistical significance which supports of our observation. Alternatively, we could consider future experiment such as exosomes isolation to assess if A-SYN fibrils are free or exosomes associated.

Our study also shed light on the PFFs pathogenicity in the premise of L444P mutation leading cell death and excessive degeneration. The assessment of viability in different cellular models exposed to either synthetic recombinant fibrils or neurons derived synuclein showed signs of cell death. This included nuclear fragmentation, decreased number of proliferating cells and activation of caspases (Desplats et al., 2009, Danzer et al., 2012, Emmanouilidou et al., 2010, Sung et al., 2001, Alvarez-Erviti et al., 2011). Using CTB assay, we found no difference in viable cells count between wild type and mutant MCN cultures seeded with PFFs. This observation indicated that neither L444P mutation nor fibrils seeding is neurotoxic, and A-SYN exocytosis occurred without cell death. Similar observation obtained by (Cleeter et al., 2013) in which even 30 days CBE treatment had no negative impact on cell viability as judged by LDH release. Nevertheless, it was interesting to find that TH+ve dopaminergic neuronal loss is evidently enhanced in the SNpc of wt/L444P aged mice secondary to viral

transduction-induced accumulation of A-SYN, (Migdalska-Richards et al., 2017). The reasons of variability in cell viability among different studies could be related to disease models as cell death was greatly amplified in differentiated SH-SY5Y cells or primary cortical neuron model which has neuronal phenotype (Desplats et al., 2009). Furthermore, it should be taken to consideration that most of these studies were based on over-expression systems which augment the associated pathology especially if they are concomitant with pharmacologically-induced inhibition of protein quality control.

4.6.3 ER stress and UPR in heterozygous L444P cellular and animal models

Assessment of ER stress in the primary cortical neurons did not detect any change in Bip level or phosphorylation of elf2α in the affected cells. These findings were paralleled with normal lysosomal function and normal steady state level of A-SYN. While in contrary to our observation, enhanced expression of ER chaperone was found associated with iPSc-derived dopaminergic neurons carrying either L444P (Schondorf et al., 2014) or N370S (Fernandes et al., 2016) heterozygous *GBA* mutations, and in fibroblast (Bendikov-Bar et al., 2011, McNeill et al., 2014). On the other hand, Kurzawa-Akanbi et al. demonstrated that CBE induced loss of GCase activity results in acute reduction of BiP level in human neural stem cells (Kurzawa-Akanbi et al., 2012), indicating that complete loss of function was affecting UPR. Interestingly, *GBA* heterozygous but not *GBA* KO iPCs-derived dopaminergic neurons showed evidence of triggered ER stress (Schondorf et al., 2018). This discrepancy might be suggesting that BiP is not pivotal to switch UPR in cortical neurons or that the gain of toxic function effect

of heterozygous *GBA* mutation is activated differently in various cell types. In order to further assess if the apparent lack of UPR response was a feature of cortical neurons as a whole, or MCN only, we used the same experimental approach on adult mouse brain tissue homogenates. We found that the lack of ER stress or UPR, associated with no increase in intracellular A-SYN level, was also reflected on midbrain and cortex of aged mice which was in line with Migdalska-Richards et al study (Migdalska-Richards et al., 2017). They did not observe ER stress as normal BiP level was found in the striatum, midbrain and brainstem of aged wt/L444P transgenic mice with evidence of accumulated A-SYN protein in either of these regions. However, decreased Bip chaperon level was found in post-mortem frontal cortex with *GBA* mutation as well as neural crest cell culture pharmacologically exposed to CBE suggesting that the UPR is affected by the reduced enzymatic activity, (Kurzawa-Akanbi et al., 2012). Accordingly, we speculated that in order to detect the effect of loss or gain of function or even both, we might need to completely inhibit GCase activity by CBE like (Kurzawa-Akanbi et al., 2012) work. Alternatively, we could age mice like Migdalska-Richards et al. study in the presence of other aggravating factor like more pronounced A-SYN accumulation that acts in the concert of deficient GCase to show impairment.

4.6.4 Investigating mitochondrial function and mass in wt/L444P in primary cortical neurons and transgenic mice.

The presence of mitochondrial dysfunction characterized by various phenotypic abnormalities such morphological changes, significant reduction in respiratory function and ATP production, oxidative stress and reduced mitochondrial membrane potential (ΔΨm) have been reported in GD fibroblasts harboring L444P mutation (de la Mata et al., 2015). Mitochondrial impairment was also reported with pharmacologically induced inhibition of GCase activity in SH-SY5Y cell lines (Cleeter et al., 2013), in wt/L444P hippocampal neurons (Li et al., 2019) and in iPSc neurons from *GBA*-PD patients and GBA KO mouse neurons (Schondorf et al., 2018, Osellame et al., 2013).

In our wt/L444P primary neurons culture, mitochondrial function was assessed by measuring mitochondrial respiration using Seahorse technology (Agilent). We observed a subtle decline in the basal and maximal respirations with only ~12% non-significant reduction in the reserve respiratory capacity in mutant neurons. On the contrary, defective mitochondrial function with 32.2% and 26.9% reduction in basal and maximal respirations respectively, along with accumulated A-SYN protein were all reported in wt/L444P primary cortical cultures (Yun et al., 2018). The lack of significant bioenergetic deficit detected here in our MCN model was also incorporated with normal complex II and IV protein levels and unaltered CS activity. These findings collectively indicated that it is very unlikely that the mitochondria are not functioning in our model. This could be related to the fact that cortical neurons are possibly operating at higher basal level than other cells to maintain high bioenergetic requirements and only under severe cellular stress such as oxidative stress and deteriorated quality control, significant bioenergetic

deficit could be detected in these cells. Additionally, as mitochondrial quality is under surveillance by autophagy MA which degrades damaged mitochondria during the process of cell recycling, we assessed MA in our wt/L444P neurons but found, however, neither inhibition of such pathway nor accumulated endogenous A-SYN. Our results here suggest that heterozygous L444P mutation alone is not sufficient to derive mitochondrial dysfunction in cortical neurons. The accumulated ASYN levels and impaired protein quality control in CBE treated SH-SY5Y cell lines, *GBA* K/O mixed cortical cultures and in *GBA* K/O iPSc-derived dopaminergic neurons have demonstrated that how the loss of function can cause oxidative stress and accumulation of dysfunctional mitochondrial in these models, (Schondorf et al., 2018, Cleeter et al., 2013, Osellame et al., 2013). In addition to MCN, we also conducted similar analysis of complex II and IV protein levels and CS activity in the cortex and midbrain tissues derived from wt/L444P adult transgenic mice. We found comparable levels of both proteins and unchanged CS activity between wt/L444P and wt/wt control group which indicate an intact mitochondrial mass in all issue homogenates assessed. These findings might be pointing out to further sever associating factors such as complete loss of activity or accumulated A-SYN that are needed until a pathogenic threshold is reached to recapitulate *GBA*-PD phenotype.

4.7 Conclusion

In this chapter, we showed that heterozygous L444P mutant GCase has 37.6 % lower enzymatic activity with respect to control. There was no associated impairment of quality control pathways, mitochondrial dysfunction or ER stress observed in wt/△ neurons. No differences in the basal intracellular level or extracellular release of A-SYN were observed with wt/△ mutation. However, L444P mutant primary cortical neuronsl challenged with exogenous PFFs seeding suggested an increased production of pathogenic A-SYN species. The PFFs model is a useful approach to test the accumulation, release and propagation of neurotoxic inclusions, and how this affects mitochondrial function and ER stress in *GBA*-cell models would be an interesting future direction.

5.Differentiated SH-SY5Y Cells as a Model of PD

5.1. Introduction

As the major pathological events in PD include selective degeneration of SNpc dopaminergic neurons, impaired A-SYN metabolism and formation of intracytoplasmic inclusions (Korecka et al., 2013), it was crucial to employ a permanently established neuronal cell model that is able to recapitulate PD pathology and uncover its underlying mechanisms (Xicoy et al., 2017). Although dermal fibroblast cultures established from GD patients possess human cell origin and amenable for genetic manipulation than other models, these cells do not store lysosomal substrate and the PD-associated *SNCA* gene is barely expressed in them (Auburger et al., 2012). Furthermore, the extensive research conducted on neuronal cell models, such as rodent primary neuronal cultures, wild type neuroblastoma SH-SY5Y cell lines and iPCs derived neurons, was tremendously beneficial in the field of neuroscience research. Therefore, we aimed in this chapter, to provide a preliminary work that could later be transferred to iPCs model use. Using this approach, we sought to manipulate the phenotype of SH-SY5Y neuroblastoma cell line by inducing a program to terminally differentiate these cells toward morphologically and biochemically mature neurons. SH-SY5Y represents the third subclone of SK-N-SH neuroblastoma cells that was first isolated from the bone marrow of 4 years old female patients (Biedler et al., 1973). Continuous proliferation of immortalized cells made SH-SY5Y lineages a great platform for conducting large scale of experiments. In addition, most of PD associated genes remain intact despite the oncogenic nature of SH-SY5Y and the genetic materials could be effectively delivered to these cells via biochemical and physical ways (Falkenburger and Schulz, 2006,

Xicoy et al., 2017). Previous research with a useful outcome on the link between *GBA* mutations and A-SYN metabolism has been carried out on undifferentiated SH-SY5Y cells where GCase enzyme activity was pharmacologically inhibited by CBE treatment (Cleeter et al., 2013, Chu et al., 2009), or via genetic modification of *GBA* gene (Li et al., 2019). However, one of the drawbacks of using immortalized cells is the difficulty to re-produce the same morphology and physiology of a neuronal cell phenotype in continuously dividing cells especially when epigenetic effect ensues. The inability to express synaptic proteins or to differentiate between growth arrest and actual cell death in proliferating cells can also represent an inevitable obstacle when using the undifferentiated cells, (Falkenburger and Schulz, 2006, Lopes et al., 2017a). Another key aspect was the post mitotic feature of neurons and their arrest in cell cycle perhaps render them more sensitive to aggregation-prone proteins such as A-SYN when compared to immortalized cells. This feature became a major contributor to the use of differentiated neuronal model (Hasegawa et al., 2004). Both primary neuronal cultures from mouse and iPCs-derived neurons have been used previously to investigate the effect of *GBA* mutation on mitochondrial function and A-SYN metabolism (Li et al., 2019, Osellame et al., 2013, Magalhaes et al., 2018, Fernandes et al., 2016, Schondorf et al., 2014, Schondorf et al., 2018). However, the main disadvantage of these neuronal cultures is the low cell yield as DAergic neurons make only 20 to 30% of the total cell number in culture which makes it difficult to establish and maintain cultures. We therefore hypothesized that generating a fully differentiated dopaminergic SH-SY5Y cell model, for at least 10 days can provide a 100% homogenous and Tyrosine hydroxylase-positive (TH+) neurons (both mRNA and protein) with neuron–like morphology and of G0

stage of cell cycle. TH has been found in brain and adrenal medulla and is considered as the rate-limiting enzyme of the catecholamine synthesis catalyzing the conversion of L-tyrosine in to L-dopa, the precursor of dopamine (DA) (Nagatsu et al., 1964).

Given that Biedler and his co-workers have identified SH-SY5Y neuroblastoma subclone as a multipotent cells based on their ability to switch between neuronal (N) and epithelioid (S) cell type, deriving dopaminergic neuronal phenotype from these cells depends upon manipulating culture media contents and inducing agents (Biedler et al., 1973, Påhlman et al., 1995). However, the previous studies on the exact SH-SY5Y differentiation methods were contradictory as many previous outcomes have been reported such as dopaminergic, cholinergic, and adrenergic phenotypes. We therefore did systemic review of the available literature to investigate neuroblastoma (NB) cells differentiation and details of both old and recent culture conditions that lead to optimal outcome with minimal limitations. We found that until recently, multiple in vitro differentiation systems have been introduced to obtain the desired DAergic-like neuronal phenotype. Despite that, protocol employed herein was an integration of previous reported modalities of using typically retinoic acid (RA), phorbolester, alone or in combination with neurotrophic growth factors. Furthermore, in the majority of these studies, the differentiated cells were cultured in growth media supplemented with serum and growth factors without the presence of favorable precoating of culture surfaces. Retinoic acid (RA) is a potent agent and is the most commonly used differentiation inducing substance (Kovalevich and Langford, 2013). Many of previous differentiation regimes involved the use of RA in concentrations ranging from 5 to 100μM, for a period of time up to 3 weeks,

with occasional reduction of serum concentration in the media (Xicoy et al., 2017). The first of these studies was reported by (Sidell, 1982) and showed that RA treatment promoted a time and dose dependent-growth inhibition. This was associated with the development of cell processes of LAN-1 neuroblastoma cells reaching the maximum after 4 days of treatment with 1μM RA. These two criteria, despite the fact that they confirmed the morphological differentiation of treated cells, they were not unique to biochemically determine the resulting differentiated phenotype. Additionally, although RA induced increased neuron specific enolase (NSE) relative activity in SH-SY5Y culture, reversibility of the induced growth inhibition was observed 5 days after its removal from the media, (Pahlman et al., 1984). In agreement of this study, culturing SH-SY5Y cells in complete media with RA induced morphological differentiation and growth inhibition of only neuroblast-like (N) cell in 10 days (Encinas et al., 2000, Teppola et al., 2016, Cheung et al., 2009, Presgraves et al., 2004). However, longer period of RA incubation showed increased total number of cells due to the accumulation of S-type cells in culture. It is recommended therefore to differentiate cells with RA for 10 days to avoid the unsuitable side effect of acquiring less homogeneous population of differentiated cells. Furthermore, RA-induced differentiation was shown to increase the expression of TH, dopamine transporter (DAT), and dopamine receptor subtypes 2 and 3 (D2R and D3R), (Farooqui, 1994, Presgraves et al., 2004, Constantinescu et al., 2007, Korecka et al., 2013). With the given evidence that oxidative stress and subsequent cell death due to internalization of 6-hydroxidopamine (6-OHDA) into dopaminergic neurons is a DAT dependent process, differentiated SH-SY5Y cells expressing transporter proteins are sensitive to such parkinsonian neurotoxin-induced insult. On the

contrary, undifferentiated cells expressing only low levels of DAT presented high resistance to this compound (Lopes et al., 2017b). Despite that, incubating cultures with RA, in some case, caused SH-SY5Y cells to differentiate more likely toward cholinergic phenotype when compared to untreated or TPA treated cells, (Adem et al., 1987). It should be considered, however, that RA was typically utilized alone to promote the non-dopaminergic differentiation. Also, only cholinergic or mixed (adrenergic/cholinergic) clones displayed detectable acetylcholine transferase (CAT) enzyme activity (Ross et al., 1981) whereas adrenergic NB subclone such as SH-SY5Y exhibited the highest TH enzymatic activity (Ross and Biedler, 1985). Interestingly, RA induced the expression of full length TrkB receptors that is normally lacked in naïve SH-SY5Y cells, making them responsive to brain derived neurotrophic factor (BDNF) through modulating the expression of neurotrophin receptors (Kaplan et al., 1993). BDNF is an important neurotrohphin factor represents the second member of neurotrophins family and was first purified from pig brain in 1982, (Barde et al., 1982). BDNF gene is expressed in many regions of adult nervous system especially the striatum. It was reported that BDNF acts as a trophic factor for DAergic neurons in the substantia nigra of midbrain, the target cells that degenerate in PD (Hyman et al., 1991). Mesencephalic cultures treated with BDNF showed rescued TH+ DAergic neurons and almost three folds increase in their number which represents only 0.1 to 0.5% of control culture. Interestingly, the more pronounced effect of BDNF was observed when added after 1DIV and replaced every other day to enhance the survival of cells that would have been otherwise lost in the absence of BDNF (Hyman et al., 1991). On the contrary, combined BDNF and RA treatment did not induce morphological differentiation and neurites outgrowth

in SH-SY5Y cultures when BDNF was added on 4DIV (Teppola et al., 2016). In fact, the survival of differentiation cells in culture was dependent on the continuous supply of BDNF hence the removal of such neurotrophin induced apoptosis in an attempt of the cells to re-enter the cell cycle (Encinas et al., 2000). Mature BDNF is best described for its ability to promote cellular mechanisms that maintain the basis of axonal growth and cell survival through binding to TrkB receptors. Such binding is tightly coupled to activity dependent events involving activation of many second messengers such as MAPK-1, P85 and PLC-γ. This signaling event eventually induces an immediate protein synthesis response that influence antiapoptotic survival, cytoskeleton synthesis, dendritic growth and synaptic plasticity enhancement (Deinhardt and Chao, 2014, Palasz et al., 2020). Previous exogenous BDNF supplementation has increased the axonal branching while depletion of this neurotrophin resulted in decreased dendritic density. Therefore, manipulating different amounts of mature BDNF could contribute to different morphological outcome (Deinhardt and Chao, 2014). The second method of choice to differentiate SH-SY5Y cells is treatment with nanomolar concentrations of (TPA), either alone or in combination with RA which induced differentiation of SH-SY5Y cells. Pahlman et al.group induced a protocol of 7 to 10 days of combined TPA and nerve growth factor to differentiate SH-SY5Y and SK-N-SH cells more efficiently to DAergic-like neurons (Pahlman et al., 1981). This was judged by an increased level of NSE activity and expression with almost 40-fold increase in noradrenaline level as compared to control. However, the growth inhibition was partially achieved in cultures and when growth curve was extended in to 4 weeks, a new growth was noted. Also, despite the observation of morphological differentiation evidenced by long process and cell projections,

TPA-treated cultures were sparse in nature whereas differentiated cells tended to aggregate in dense cultures. SH-SY5Y cells have been also driven toward DAergic phenotype by combined treatment of RA and TPA for 10 days. Despite this, the well-developed morphological differentiation and the increased NSE activity observed in this study was not affected by the selective antagonistic effect of RA on TPA-induced noradrenaline synthesis (Pahlman et al., 1984). The sequential exposure of SH-SY5Y culture to 10μM RA, and 10-100ng/mL of BDNF with serum free media was also considered as an induction method of differentiating cells to a homogeneous neuronal population. This outcome was concomitant with the expression of neuronal markers and the absence of any neuronal crest derivatives that normally arise in those cells (Encinas et al., 2000). Recent evidence suggested that finding an optimal coating of culture surface is another essential parameter for cell survival and morphological phenotype of differentiated cells such as neuritis outgrowth, branching and homogenous cell adhesions. SH-SY5Y cells cultured on negatively charged surface tend to lose attachment and eventually become less viable. A variety of coating materials have been widely utilized to improve cellular adhesions into culture surface including extracellular matrix proteins such as (Laminin, Fibronectin, collagen), polymers like polyethyleneimine or polyornithine. Because differentiation is a time dependent process, it is essential to analyze cell morphology few days after seeding cultures to allow time for growth inhibition. SH-SY5Y grown on laminin in serum free DMEM with 50nM IGF-1 for 72 hours exhibited not only morphological but biochemical differentiation phenotypes (Dwane et al., 2013). The effect of Laminin and PEI coating on RA and cholesterol-induced SH-SY5Y differentiation was also evaluated. The morphological analysis of pre-coated

cultures on 10DIV showed the positive impact of laminin on homogenous cellular distributions, adhesion and extension and branching of long neurites with oval nuclei indicating higher level of differentiation (Teppola et al., 2018).

5.2. Experimental Aims

Based on the review of available literature, we aimed to establish a new and potential in vitro system model of previously inaccessible neurons through differentiating SH-SY5Y in to dopaminergic cell model with 100% neuronal characteristics and metabolic machinery for DA synthesis. We also evaluated the validity of such model in PD research by applying multiple modalities of genetic and chemical manipulations on differentiated cells to target pathways linked to *GBA*-PD pathology principally A-SYN dysmetabolism and ER stress.

5.3. Objectives

- To apply a simple 10 days protocol that promote differentiation of SH-SY5Y neuroblastoma cells into 100% dopaminergic neurons.
- To compare old and new protocols on the biochemical differentiation of cells through the measurement of TH- expression and evaluate the effect of applying either of these methods alone on the biochemical and morphological phenotypes of the cells.
- To genetically and chemically modulate GCase activity in these cells either by treating with CBE to completely inhibit GCase, or by over expressing heterozygous L444P mutant *GBA* to mimic the UPR and gain of function pathophysiology.
- To characterize the differentiated cells through the measurement of lysosomal contents and intracellular A-SYN level with the presence and absence of CBE.

- LB is considered as the main pathological hallmark in PD. thus, investigating A-SYN metabolism in differentiated SH-SY5Y cells, either normal or those overexpressing WT *SNCA*, is useful parallel approach. Also, seeding differentiated SH-SY5Y cells with recombinant PFFs may decipher the mechanisms of A-SYN aggregation in neurons known in PD.

5.4. Experimental Design

To investigate biochemical mechanisms that might contribute to DAergic loss observed in PD, we have applied different strategies on differentiated SH-SY5Y based on pharmacological and genetic approaches to manipulate of expression of the candidate gene. SH-SY5Y cell line was obtained from the European Collection of Cell Cultures and all lines used in this project were cultured as illustrated in details in (sections 2.1.5).

Differentiation of different SH-SY5Y lines was carried out using protocol described in (section 2.1.6). Briefly, pre-coated vessels were used for differentiating SH-SY5Y cells at density of 3 x 10^5 cells/ml in a 6-well plates. 30µM RA, combined with 2.5nM of BDNF, was used to induce differentiation in the first 3 days; then the media was replenished with fresh RA+BDNF on 3,6,9 and 12DIV (Figure 0.1). In a parallel culture, parental SH-SY5Y line was differentiated at seeding density of 0.4 x 10^5 cells/ml using the old protocol reported by (Sidell, 1982) and undifferentiated (undiff) SH-SY5Y cells grown as normal were used as control. Assessment of morphological phenotype by light microscopic imaging on10 DIV showed that cells treated with a combination of RA and BDNF were homogenously distributed throughout the culture plate, and have acquired neuronal phenotype characterized by extending and branching neuritic

processes. The biochemical differentiation was confirmed by WB of cell lysates which showed increased TH expression level indicating the dopaminergic lineage of SH-SY5Y cells (Figure 0.3). Detailed differences between new and old differentiation methods are illustrated in (Table 0.1).

Dopaminergic neurons are sensitive to extracellular A-SYN-induced toxicity. Therefore, to enhance its propensity for aggregation, differentiating SH-SY5Y cells were seeded with PFFs on 3 or 4 DIV to ensure cessation of proliferation (section 2.4). Culturing continued with regular media changes for at least 10 days (3 days in presence of PFFs and then at least another 7 days of media changes) and seeded cultures were investigated for downstream pathological events such as formation of insoluble/aggregated/phosphorylated A-SYN and cell death.

Alongside cellular differentiation and in addition to the genetically modified models, we also targeted the impact of GCase loss-of-function on differentiated cells through exposure to pharmacological inhibition of enzyme activity with 10μM of conduritol-b-epoxide (CBE) from 3DIV. Following this, culturing of cells continued for at least 10 days (Figure 0.1), and GCase activity was monitored upon harvesting to check that inhibition was maintained.

Overexpression of WT *SNCA* has been successfully used to model PD (Chau et al., 2009). However, this manipulation needs triggers such as cell differentiation (Xicoy et al., 2017). We therefore differentiated SH-SY5Y lines C205 (overexpressing (O/E) wild-type *SNCA*) to observe A-SYN aggregation in vulnerable cells, undifferentiated C205 was used as control.

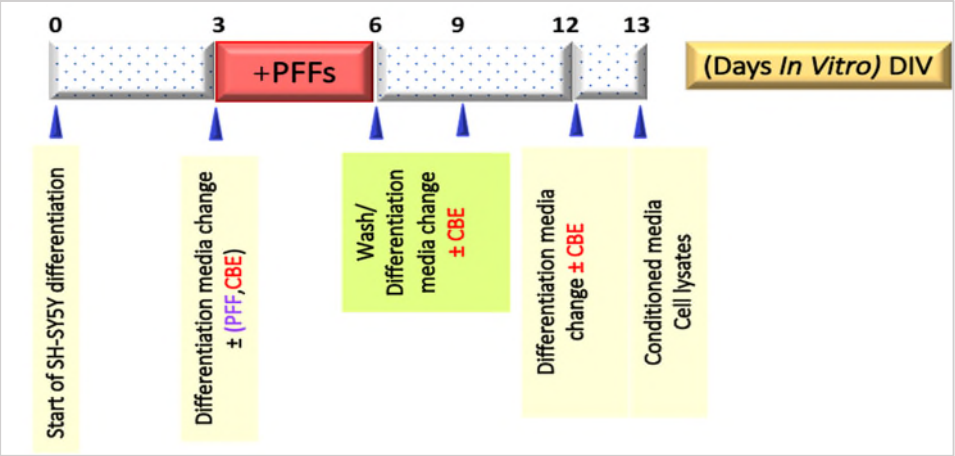

Figure 0.1 Time line guide of differentiation different SH-SY5Y cell lines ± CBE and PFFs treatment.

Table 0.1 Differences between differentiation protocols

Differentiation method	New	Old
BDNF	+ 2.5nM	------
RA	+30µM	+30µM
Seeding density	3 x 10^5 cells/ml (Parental SH-SY5Y) 4.5 x 10^5 cells/ml (SH-SY5Y O/E WT *SNCA)*	0.4 x 10^5 cells/ml
Coating	+++	---------
Differentiation media	Differentiation media (neurobasal media supplemented with 1X B27)	DMEM/F-12 Nutrient (supplemented with 10 % fetal calf serum)
Morphology	complex neuronal network and 100% homogeneous distribution	sparse islets of cells and less neuronal branching /more proportion of (S) type cells
TH expression level	++++	Negligible

5.5. Results

5.5.1. Effect of (RA+BDNF)-Induced Differentiation on Tyrosine Hydroxylase (TH) Level in SH-SY5Y Lines

We demonstrated that SH-SY5Y cells treated with the differentiation agent RA and BDNF exhibited cessation of proliferation rate and acquired neuronal-like morphology. Exogenous administration of BDNF enhances cells survival and contributes to the morphological complexity of neuronal network. In an attempt to assess the validity of RA- treatment in differentiating SH-SY5Y, we analyzed the concomitant change in cellular biochemistry by WB which showed pronounced expression of the DAergic neurons marker (TH) confirming their biochemical phenotype (Figure 0.2). In addition to 100% neuronal morphology (Figure 0.3), differentiated SH-SY5Y O/E WT *SNCA* showed the same increase in TH level as that of the parental line (Figure 0.2). However, TH expression was not further induced by the addition of BDNF nor detected in differentiated cells using RA alone (no BDNF) which was further supportive for the method we used compared to other differentiation protocols (Figure 0.2).

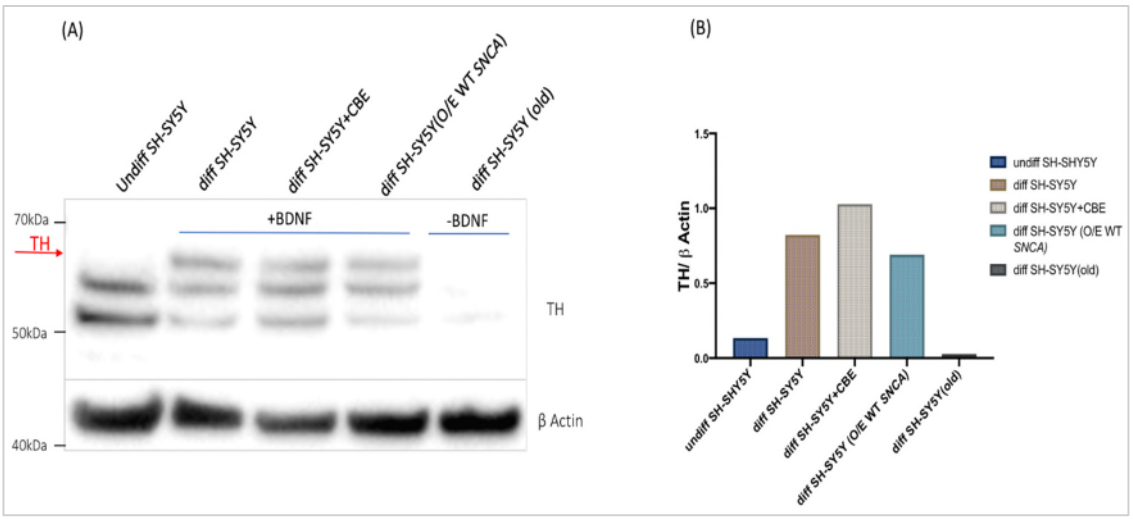

Figure 0.2 Induced expression of TH dopaminergic marker upon SH-SY5Y differentiation. (A, B): Representative image and bar chart summarization of western blot, for normal parental SH-SY5Y and those O/E WT *SNCA*, showing increased TH expression with RA+BDNF treated lines (n=1). Note that TH band of the correct size (~ 60 kDa, red arrow) was not detected in undifferentiated cells (control) or when using the old differentiating protocol (no BDNF), β Actin used as loading control

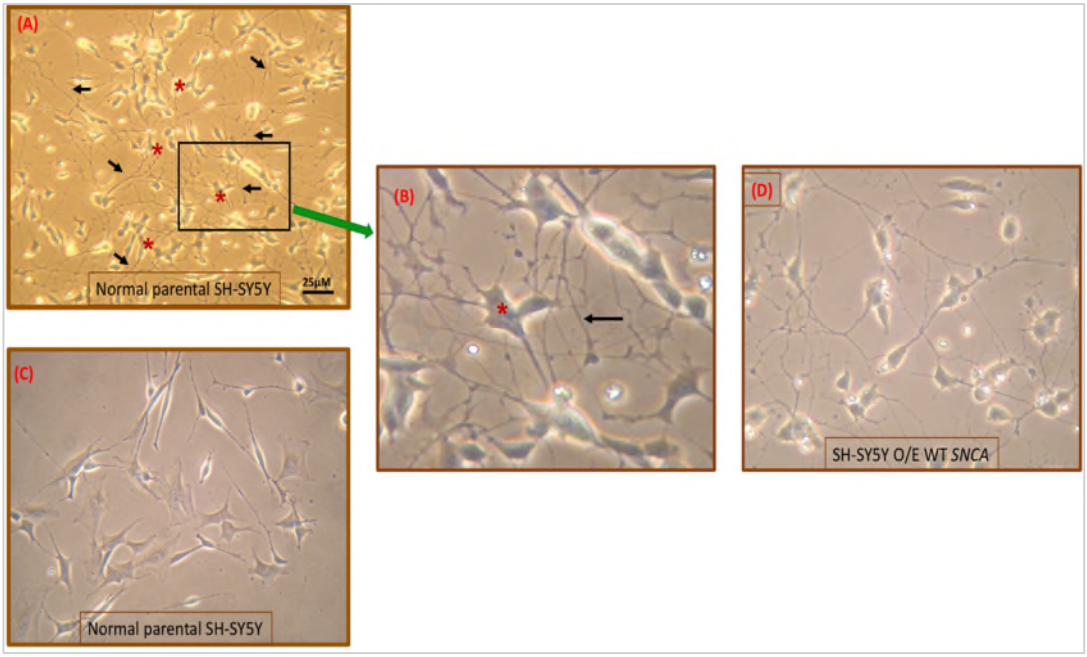

Figure 0.3 Light microscopic images of differentiated of SH-SY5Y cell lines (new vs old method). All pictures were taken on 10DIV; (A): Effects of (30μm RA + 10ng/ml BDNF) in differentiating normal parental SH-SY5Y cells for 10 days showing complex neuronal morphology and no longer division (×10, scale bar represents 25μm), black arrows indicate neurites and red asterisks indicate cell bodies. (B): The boxed region in (A) is shown on the right at higher magnification (×10). (C): Differentiated normal SH-SY5Y cells cultured for 10 days using the old method (×20); the merely administered RA was unsuitable for the complete acquisition of complex neuronal network, cell islets were sparse showing less neurites extension and apparently retaining higher proportion of morphologically distinct substrate adherent (S) type cells. (D): Differentiated SH-SY5Y cells O/E WT *SNCA* cultured for 10 days using RA+BDNF (new method), (×20) showing neuronally differentiated and homogenous cell population with extension of neurites process.

5.5.2. Assessment of GCase and Other Lysosomal Hydrolases Activities in Parental Differentiated SH-SY5Y Model

Total cellular GCase, and other lysosomal hydrolases, β-hexosaminidase and β galactosidase, activities were analyzed in differentiated SH-SY5Y cells. GCase activity was significantly increased in differentiated parental SH-SY5Y (mean=2.16±0.125) when compared to undifferentiated cells (mean=1.31±0.142), (***p<0.05, n=7), (Figure 0.4).

We also confirmed that, in differentiated SH-SY5Y cells, continuous administration 10μM CBE over 10 days dramatically abolished GCase activity by more than 95%. In addition, analysis of other lysosomal hydrolases activities showed significant higher β-hexosaminidase (mean=0.249±0.008, ***p=0.005), and β-galactosidase (mean=0.061±0.005, *p=0.034) when compared to their respective control group, (Figure 0.4). Collectively these findings indicated increased lysosomal mass and further supported the induced expression GCase, LIMP2 and Cathepsin D with differentiation, (Figure 0.5).

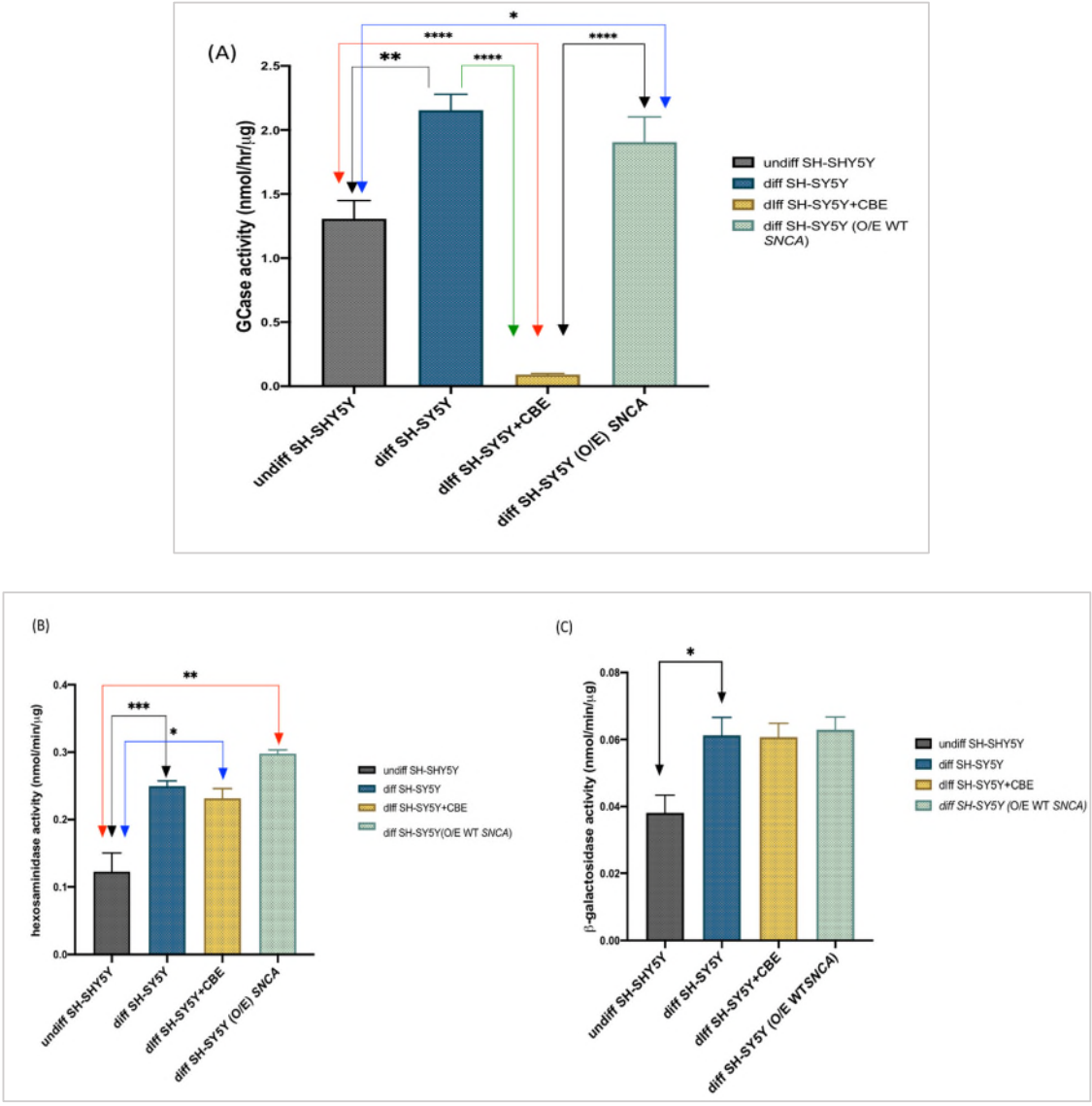

Figure 0.4 Analysis of GCase, β-hexosaminidase and β-galactosidase activities in differentiated SH-SY5Y cell model. (A): Bar charts summarizing for GCase activity measured in nmol of product/hour/µg protein (n=7undiff SH-SY5Y; 7diff SH-SY5Y; 5 diff SH-SY5Y+CBE; 4 diff SH-SY5Y O/E WT *SNCA*): GCase activity significantly (**P*=0.0006) increased following RA+BDNF differentiation of SH-SY5Y cells (mean=2.16±0.125) against control (mean=1.31±0.142). The enzyme activity was also dramatically inhibited following CBE treatment to >95% in treated cells (0.09±0.009) when compared to other untreated SH-SY5Y cell lines (mean undiff SH-SY5Y=1.31±0.142, *****p*<0.0001, diff SH-SY5Y=2.16±0.125 *****p*<0.0001, diff SH-SY5Y O/E WT *SNCA*=1.91±0.198, *****p*<0.0001), data are expressed as mean ± SEM. (B): Bar chart quantification for the mean β hexosaminidase activity measured in nmol of product/min/µg protein, (n=7undiff SH-SY5Y; 8 diff SH-SY5Y; 4 diff SH-SY5Y+CBE;2 diff SH-SY5Y O/E WT *SNCA*); mean activity=0.122±0.028 in control vs 0.249±0.008 in**

diff normal SH-SY5Y cells (*p=0.005); 0.232±0.014 in diff cells exposed to CBE (*p=0.011); and 0.297± 0.006 in diff SH-SY5Y O/E WT *SNCA* (**p=0.002). (C): The mean β-galactosidase activity expressed in nmol of product/min/ µg protein was significantly elevated in diff normal SH-SY5Y (mean=0.061±0.005) against undifferentiated cells (mean=0.063±0.004), (*p=0.034). No significant alteration in β-galactosidase activity observed in diff SH-SY5Y+CBE and diff SH-SY5Y O/E WT *SNCA* with respect to control; (mean activity: diffSH-SY5Y+CBE=0.061±0.004, p=0.101; diffSH-SY5YO/E WT *SNCA*=0.061±0.004, p=0.183), (n=5 undiff SH-SY5Y; 8 diff SH-SY5Y; 4 diff SH-SY5Y+CBE;2 diff SH-SY5Y O/E WT *SNCA*); Each bar represents mean of enzymatic activity from independent cultures ± SEM.**

5.5.3. Characterization of Differentiated SHSY5Y Cells

The change of lysosomal mass following differentiation was investigated in parental normal and WT *SNCA* O/E SH-SY5Y(C2O5) cell lines by western blot. Data were expressed as the mean density of the proteins against the density of the housekeeping protein β actin, from 4 independent cultures± SEM. Our results showed that following differentiating, the amount of GCase protein significantly increased (**p*<0.05) both in the differentiated SH-SY5Y cells (0.881± 0.134) and in respective group treated with CBE (1.26±0.146, ***p*<0.05), when compared to control group (0.083±0.014). Also, GCase amount was found non-significantly increased in differentiated C2O5 cells (0.579±0.435, *p*=0.253) when compared to control group (n=4 undiff SH-S, 2 diff C2O5).

We then explored the effects of differentiation on a major lysosomal protease marker, Cathepsin D, and the GCase transporter LiMP2. The mean expression levels of these proteins, although not reaching statistical significance (*p*>0.05), were found increased in differentiated SH-SY5Y±CBE when compared to control and thus pointing to increased lysosomal contents with differentiation (LiMP2: undiff SH-S=0.418±0.191; diff SH-S=0.759±0.153, diff SH-S+CBE=0.771±0.243; Cathepsin D: undiff SH-S=0.500±0.163; diff SH-S=0.887±0.094; diff SH-S+CBE=0.759±0.105), (

Figure 0.5).

Likewise, LIMP2 expression was induced in differentiated C2O5 cells (0.966± 0.629) as compared to control group, but did not reach statistical significance. Cathepsin D level, however, was similar to that of control group (undiff SH-S=0.500±0.163, diff C2O5=0.511±0.019, p>0.05, n=4 undiff cells, 2 diff C2O5), (Figure 0.5). The increased LIMP2 protein expression in differentiated cells could

be a consequence of CBE treatment. Previous analysis of the interaction of LIMP-2 and mutant GCase showed that L444P mutation did not abrogate it's binding to LIMP-2. However, induced expression of LIMP2 helped to enhance the transport of GCase to lysosomal compartment (Reczek et al., 2007).

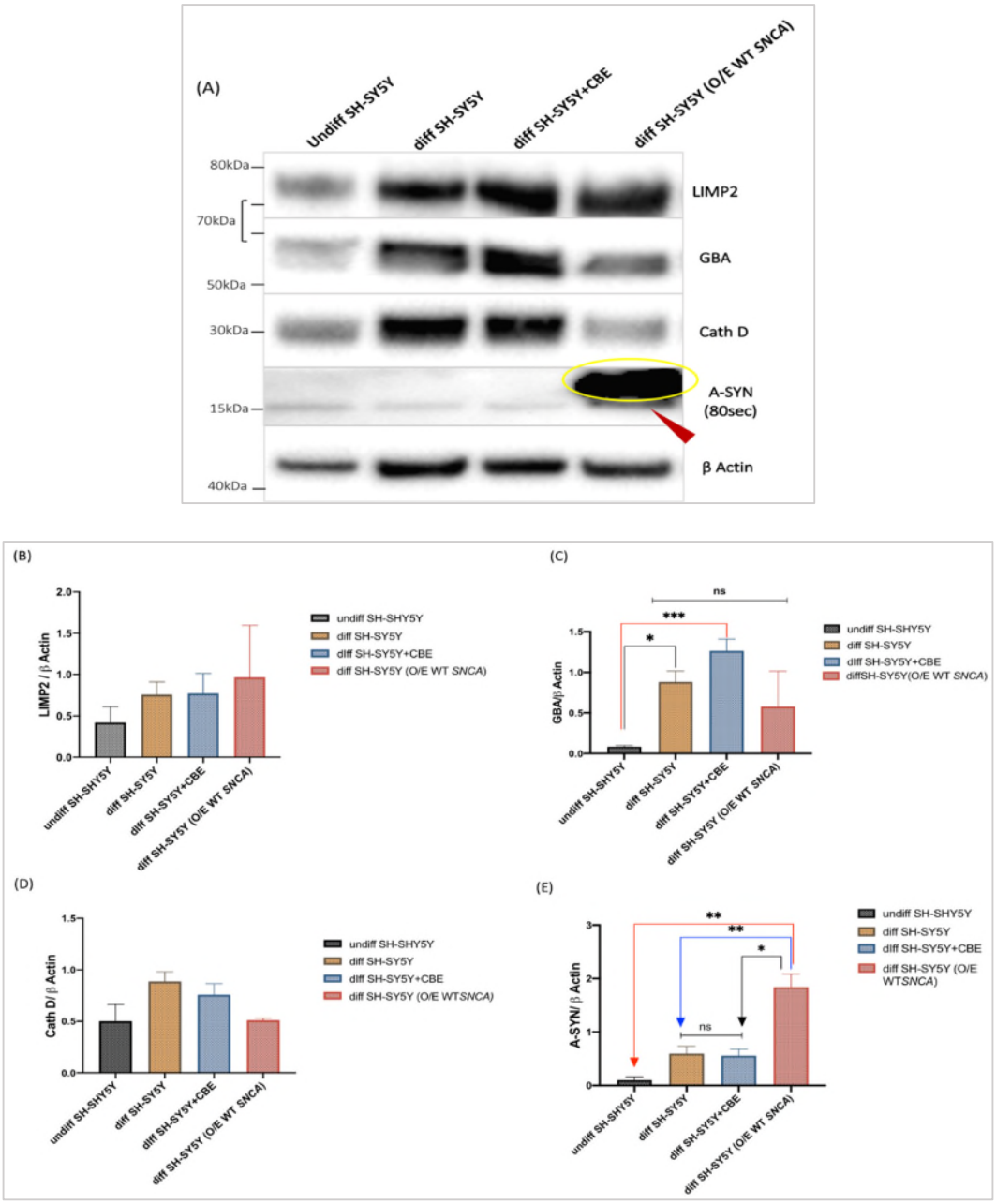

Figure 0.5. Characterization of differentiated SH-SY5Y cells. (A): Western blot image showing increased lysosomal mass upon differentiation as evident by increased GCase, LIMP2, Cath D and A-SYN levels in differentiated SH-SY5Y cells when compared to control group, β Actin used as loading control, (n=4), red arrow is

pointing to endogenous A-SYN running at 15kDa region and yellow circle is showing HA tagged protein migrating at slightly higher size (17kDa). (B): Quantification of mean LiMP2 expression levels normalized to loading control and showing a trend of increased LIMP2 in differentiated SH-SY5Y and C2O5 lines, (Undiff SH-S =0.418±0.191; diff normal SH-S=0.759±0.153; diff SH-S+CBE =0.771±0.243; diff C2O5 =0.966±0.629, *p*=0.741; (n=4 undiff, diff SH-S±CBE and 2 C2O5 lines). (C): Bar charts analysis of western blots showing significantly increased GCase protein, both in the differentiated SH-SY5Y cells (mean=0.881± 0.134, **p*=0.019) and in respective group treated with CBE (1.26±0.146, ***p*=0.001) vs control group (0.083±0.014). The A-SYN overexpression in diff C2O5 cells was associated with nonsignificant reduction in GCase protein level (0.579±0.435) compared to that of normal parental line (0.881 ± 0.134, *p*=0.386); (n=4 undiff, diff SH-S±CBE and 2 C2O5 lines). (D): Bar chart analysis of Cathepsin D protein normalized to β Actin and showing a trend of increased protein expression in differentiated normal SH-SY5Y±CBE when compared to undifferentiated line; Undiff SH-S=0.500±0.163; diff normal SH-S=0.887±0.093; diff SH-S+CBE =0.759±0105, *P*=0.142, (n=4). Differentiated C2O5 cells O/E A-SYN exhibited non-significant reduction in CathD protein (0.511±0.019) vs control group (0.500±0.163), (n=4 undiff normal SH-S and 2 C2O5 lines). (E): Expression level of A-SYN following differentiation showing slight but non-significant increased A-SYN in differentiated parental line and massive elevation of monomeric HA-tagged A-SYN in differentiated C2O5 as compared to all other groups (A-SYN mean; Undiff SH-S =0.099±0.064, ****P*=0.003; diff SH-S=0.593±0.138, ***p*=0.008; diff SH-S+CBE=0.555±0125, **p*=0.014; diff SH-SY5Y O/E WT *SNCA* (C2O5)=1.84±0.246) (n=2 undiff, diff SH-S±CBE and 4 C2O5 lines). All data were expressed as the mean density of the target protein expressed against the density of housekeeping protein (β actin) of cultures derived from independent SH-SY5Y lines ± SEM

Furthermore, we investigated the link between neuronal differentiation and monomeric A-SYN level. We first found nonsignificant elevation of endogenous A-SYN amount in differentiated normal SH-SY5Y cells ±CBE as compared to control (undiff SH-SY5Y line); (control =0.099±0.064, diff SH-S =0.593±0.138, *p*=0.335; diff SH-S +CBE=0.555±0125, *p*=0.545). However, the over-expression of ectopic haemagglutinin (HA)-tagged A-SYN in C2O5 line caused significant increase in A-SYN as compared to control and other differentiated SH-SY5Y lines; (Undiff SH-S =0.099±0.064, ****P*=0.003; diff normal SH-S=0.593±0.138,

**p=0.008; diff normal SH-S+CBE=0.555±0125, *p=0.014; diff C2O5=1.84±0.246); western blotting with anti-total A-SYN antibody showed that these cells exhibited greater proportion of A-SYN band which was migrating slightly slower than that of parental SH-SY5Y at 17kDa region due to HA tagging (Figure 0.5). This expression pattern was similar to that reported in the original work of (Chau et al., 2009) and perhaps it was the reason here of diminished GCase protein level in cells (0.579±0.435) when compared to differentiated parental normal SH-SY5Y (0.881 ± 0.134), (Figure 0.5). This finding has further supported the plausible established link between GCase deficiency and monomeric A-SYN accumulation (Gegg et al., 2012, Mazzulli et al., 2011, Chiasserini et al., 2015, Sardi et al., 2015, Murphy et al., 2014). In addition, it was shown previously that pharmacological inhibition of GCase activity by CBE can lead to increased ASYN levels in dividing SH-SY5Y cells (Cleeter et al., 2013). We therefore investigated the effect of CBE treatment on differentiated normal SH-SY5Y under basal condition and found that in cells challenged with CBE exposure alone, the endogenous monomeric A-SYN level was comparable with that of untreated differentiated cells (diff SH-S =0.593±0.138, p=0.335; diff SH-S +CBE=0.555±0125, p=0.545), (Figure 0.5).

In summary, and at the used cell seeding density, we reported increased levels of GCase, Cathepsin D and LiMP2 proteins in differentiated normal SH-SY5Y in a relative abundance to the undifferentiated cells. However, the over-expression of A-SYN in differentiated C2O5 cells reduced GCase protein level in cells. Also, monomeric A-SYN level was not influenced by almost total loss of GCase activity in differentiated parental cells thus suggesting that an additional stress, rather

than GCase inhibition, is needed to induce A-SYN pathology in differentiated dopaminergic cells.

5.5.4. PFFs Treatment Promotes Insoluble A-SYN Accumulation in Normal Parental and WT *SNCA* Overexpressing Differentiated SH-SY5Y Cells

We used pre-formed recombinant A-SYN fibrils (PFFs) to demonstrate if once taken up by the cells, could promote recruitment of endogenous A-SYN and aggregates formation that are characterized by detergent-insolubility and Ser129 hyperphosphorylation. We have also addressed the impact of loss of GCase activity on A-SYN metabolism by treating differentiated SH-SY5Y cells with PFFs in the presence of 10 µM of GCase inhibitor (CBE). When applying this approach, differentiating parental SH-SY5Y cells were first seeded with 5µg/ml of PFFs as described in details in (section 2.4). Briefly, cells seeded with PFFs for 3 days after which media were changed and cells were incubated for another 7 days with a final media change 24 hours before harvesting cells (Figure 0.1). Ten days after the initial treatment, the proportion of soluble and insoluble A-SYN were assessed by western blotting of Triton X-100 (soluble) vs. urea-SDS (insoluble) fraction, both in the presence and absence CBE. During western blotting, the protein concentration loaded was similar between soluble and insoluble fractions which were probed first for total A-SYN followed by 129Ser phosphorylated form. Our results showed that in any of untreated differentiated cells, no insoluble A-SYN bands were detected (Table 0.2) and all monomeric A-SYN remained in TX-100 soluble fractions (Figure 0.6,B). Also, CBE treatment did not significantly increase TX-100 soluble A-SYN, and only a small proportion of monomeric A-SYN became insoluble and appeared in (SDS-urea) fraction under this condition (yellow arrows Figure 0.6,B and C). As opposed to that and when cells were seeded with PFFs, either alone or combined with CBE, a similar or relatively denser bands ~15kDa appeared as TX-100 soluble state with the vast majority

of A-SYN protein began to accumulate as insoluble (i.e. SDS-Urea-soluble) fractions (red, blue arrows Figure 0.6). Under all experimental conditions, and when the density of the TX-100 soluble and insoluble A-SYN bands was measured, no significant alteration in monomeric soluble A-SYN level was detectable between groups (P=0.104) despite being slightly increased under PFFs±CBE conditions relative to the untreated control, (untreated=0.37±0.098; +CBE=0.60±.111; +PFFs=0.68±0.067; PFFs+CBE=0.84±0.175), (Figure 0.7 A). On the other hand, there was significant increase in insoluble A-SYN fractions in cells following PFFs (0.89±0. 287, *p=0.048) and PFFs+CBE treatment (0.589±0.127, *p=0.019) when compared to untreated group (0.054±0.022). GCase inhibition by itself, was not sufficient to induce significant accumulation of insoluble A-SYN (0.124±0.058, p=0.999) when compared to untreated cells, (Figure 0.7, B).

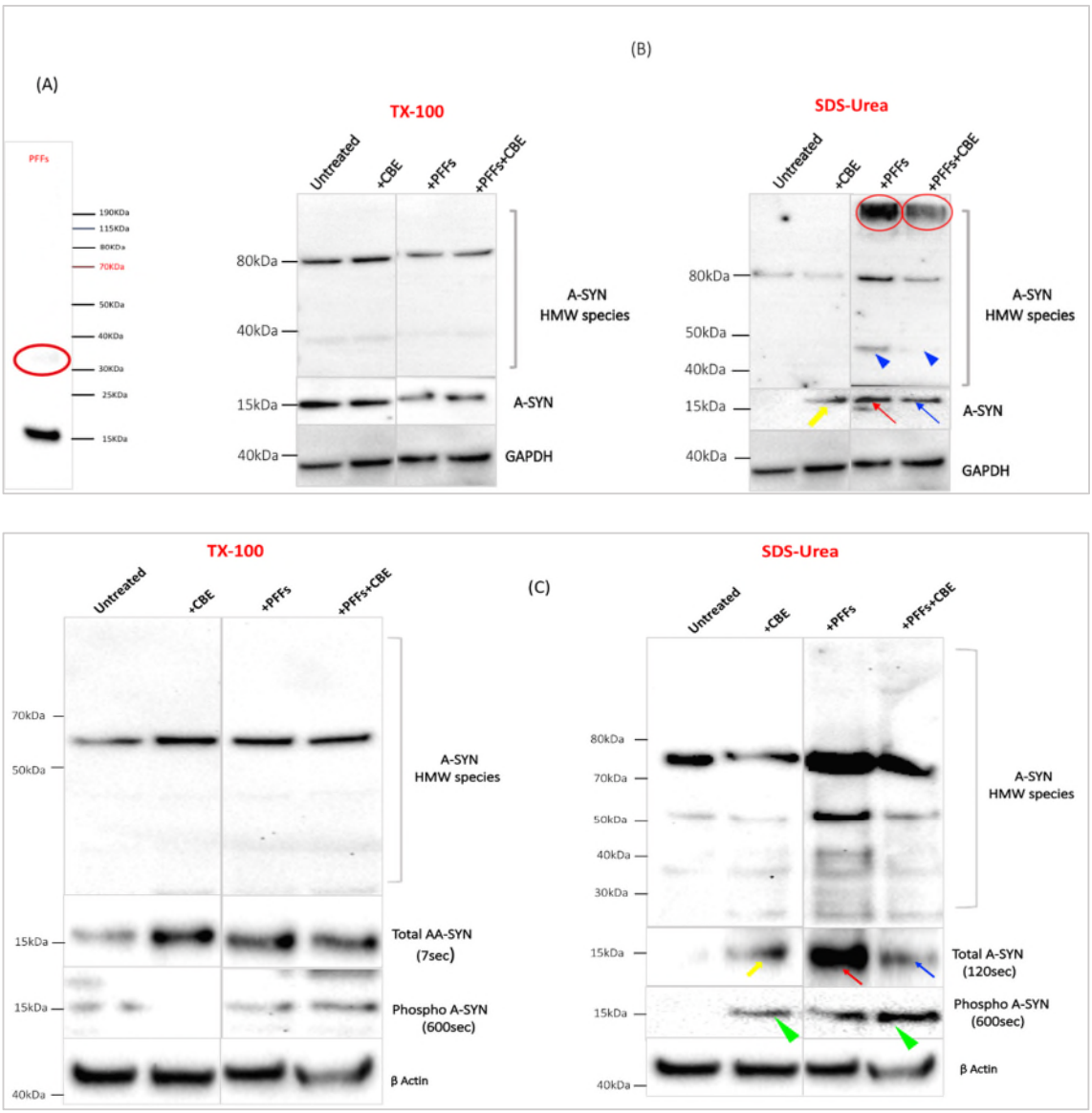

Figure 0.6 Effect of PFFs seeding on differentiated SH-SY5Y dopaminergic neurons. (A): Western blot image for 10 ng recombinant PFFs, mixed with gel loading buffer showing two bands: one at the expected 15 kDa size for monomeric A-SYN, and a faint band at 35 or 40kDa (red circle). (B-D): Representative WB images showing the effect of PFFs seeding on differentiated SH-SY5Y cells 10 days after the initial treatment; the proportion of soluble and insoluble A-SYN were assessed and probed with total and Ser129 phosphorylated anti A-SYN antibodies. There was small fraction of insoluble A-SYN in CBE treated cells (yellow arrows) which became denser in PFFs seeded cells (red arrows) and PFFs+CBE treated (blue arrows). Some of these insoluble fractions were phosphorylated at Ser129 (green arrowheads). Also, there is evidence of HMW species (30-50 kDa, blue arrow heads in B) and (>205kDa, red circles in B) found as insoluble fractions in cells treated with PFFs and PFFs+CBE. β Actin and GAPDH were used as loading controls, (n=6 untreated, 8+CBE, 7+PFFs, 8+CBE+PFFs).

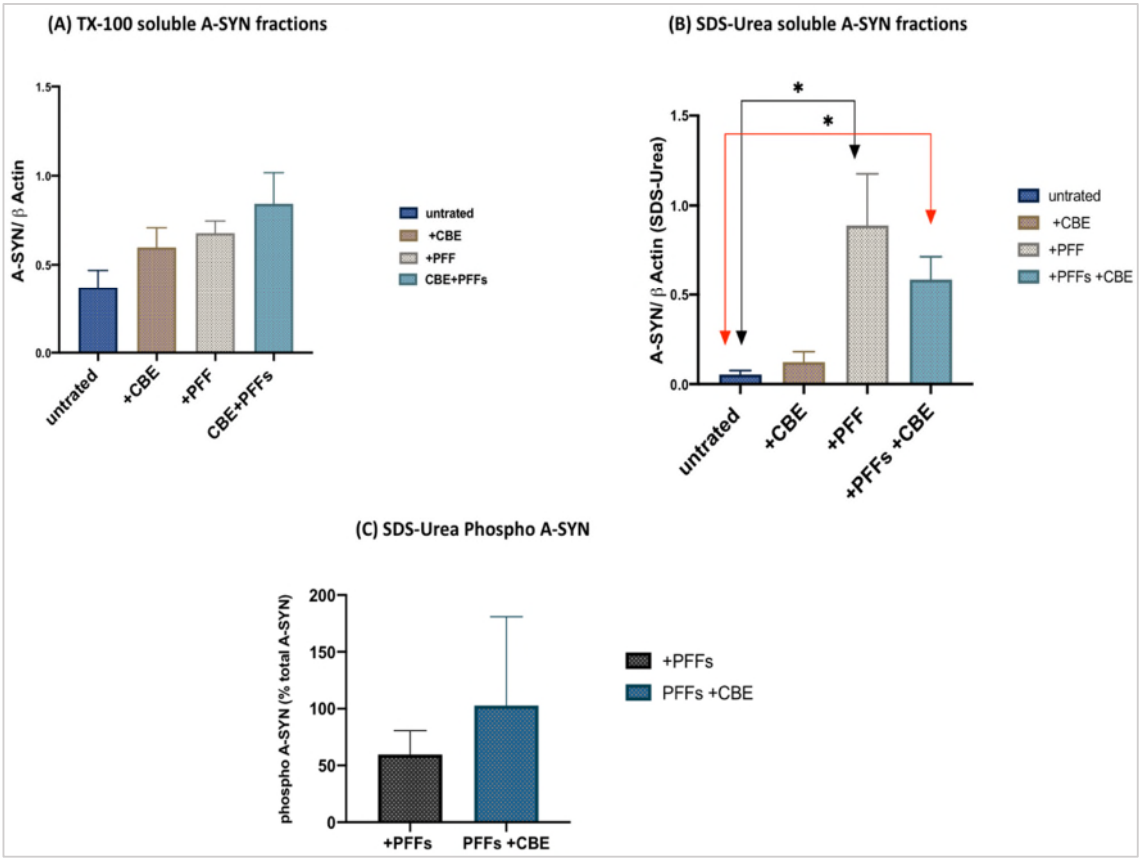

Figure 0.7 Bar chart analysis of western blot of TX-100 soluble vs insoluble A-SYN fractions in differentiated normal SH-SY5Y cells. (A): A non-significant increase in TX-100 soluble A-SYN band densities normalized to that of β Actin or GAPDH in both PFFs (0.679±0.067, n=7) reaching the peak in cells treated PFFs+CBE (0.842±0.175, n=8) against untreated cells (0.370±0.098, n=6) or those treated with CBE (0.580±0.011, n=8). (B) There was significant increase in insoluble A-SYN protein expression in cells following PFFs (0.890±0.287, *p=0.048, n=5) and PFFs+CBE treatment (0.589±0.127, *p=0.019, n=5) when compared to untreated cells (0.054±0.022, n=3). No significant alteration detected between CBE treated (0.124±0.058, n=4) and untreated cells. (C): Bar chart summarizing the proportion of insoluble phosphorylated A-SYN of SDS-soluble fractions relative total insoluble A-SYN and showing no significant (p=0.647, n=2) difference between PFFs (59.62±20.96%) and PFFs±CBE (102.8±78.26%), Data are expressed mean of independent SH-SY5Y cultures± SEM.

Table 0.2 Effect of PFFs seeding on differentiated SH-SY5Y cells

±CBE/ ±PFFs	Insoluble monomeric A-SYN	Insoluble monomeric phospho A-SYN	HMW
Untreated	1/6	0/3	0/5
+CBE	3/6	1/4	0/5
+PFFs	5/6	2/4	6/6
PFFS+CBE	5/6	2/4	5/6

In addition to that, and as a proof of what was measured is most likely the endogenous A-SYN and not just the PFFs added to cultures, we run 10ng of recombinant PFFs mixed with loading buffer on SDS page that showed two bands: one at the expected 15 kDa size for monomeric A-SYN, and a faint band running at 35 or 40kDa, (Figure 0.6 A). By contrast, a high molecular weight (HMW) polypeptide bands (>250 kDa) were specifically detected by antibody against total A-SYN in SDS-urea soluble fractions from cultures seeded with PFFs with and without CBE treatment (red circles in Figure 0.6 B). These bands were remarkably dense in their form (i.e. SDS-stable), corresponding possibly to the aggregated forms of A-SYN and observed in nearly all PFF s seeded blots we analyzed (Table 0.2). This finding was similar to that reported by (Tapias et al., 2017, Grassi et al., 2018). However, no immunoreactivity for such HMW bands was detected in untreated cells or under CBE treatment (Figure 0.6, B and C). Furthermore, there was evidence of an additional minor insoluble HMW bands (~30 and 50 kDa) observed in cultures treated with PFFs with and without CBE treatment (blue arrow heads in Figure 0.6 B). Table 0.2 summarizes the results from several independent PFFs treatments of differentiated SH-SY5Y.

Despite the fact that deposition of the abundant neuronal and glial A-SYN protein as an insoluble fibrillary aggregate is considered as pathognomonic lesion in PD,

A-SYN can undergo post-translational modifications in the brain of PD patients. These modifications include phosphorylation at Ser129 which promote fibrils formation and is thought to be important in Lew pathology (Fujiwara et al., 2002, Anderson et al., 2006, Oueslati, 2016). A-SYN extracted from brains of patients with DLB showed that almost 90% of urea-soluble A-SYN is phosphorylated at Ser129 whereas only 4% of phosphorylated insoluble A-SYN is extracted freshly from normal rat brain (Fujiwara et al., 2002). This observation possibly indicates that phosphorylated A-SYN found in Lewy pathology (LP) might be the real culprit of PD pathogenesis. Importantly, seeding primary neuron cultures with PFFs resulted in accumulation of phospho A-SYN which further confirmed that these species are the key to neurotoxic events in PD (Grassi et al., 2018). To examine the phosphorylation of Ser129 of A-SYN under basal and stress conditions, we used antibody that specifically cross-reacts with 15kDa band corresponding to monomeric phospho-A-SYN. After analyzing differentially solubilized A-SYN blots, we found that although small fraction of monomeric phospho-A-SYN bands remained in TX-100 soluble state, considerable proportion of insoluble monomeric A-SYN was phosphorylated at Ser129 only when cultures were exposed to PFFs (59.62±20.96%) or PFFs±CBE (102.8±78.26%), (green arrow heads Figure 0.6), (Figure 0.7) and were present in two out of four blots (Table 0.2). However, there was no significant difference detected in insoluble phospho A-SYN densities between PFFs and PFFs+CBE groups (n=2, p=0.647).

We also extended our characterization by applying the same experimental paradigm using differentiated SH-SY5Y O/E HA tagged WT *SNCA* (C2O5 cells). This was done to demonstrate that HA tagged A-SYN can show that PFFs treatment can induce the ‘endogenous’ HA-tagged A-SYN to become insoluble

and it is not just PFFs seeded to cells that we are detecting (Figure 0.8 A). First, and as a proof of HA antibody specificity, we included TX-100 soluble lysate of parental normal diff SH-SY5Y in our experiment which, unlike the HA-expressing A-SYN cells, did not detect a band at ~17 KDa. Our results showed that PFFs and CBE treatment, either alone or combined together, did not induce TX-100 A-SYN accumulation in these cells against the untreated control despite high A-SYN expression, (TX-100 A-SYN; untreated =0.930±0.106; +PFFs=0.872±0.168; +CBE=0.961±0.062; PFFs+CBE=1.0001±0.425, *p*=0.983, n=3), (Figure 0.8). However, there was non-significant trend of elevated SDS-Urea soluble HA-A-SYN with the appearances of some 30-50kDa minor HMW species in cells incubated with either PFFs alone or combined with GCase inhibition (SDS untreated=0.273±0.111;+PFFs=0.403±0.222;+CBE=0.189±0.092;PFFs+CBE=0.495±0.222, *p*=0.566, n=3), (Figure 0.8). PFFs treatment by itself was sufficient to induce accumulation of insoluble A-SYN robustly in overexpressing cells when compared to those detected in normal differentiated lines.

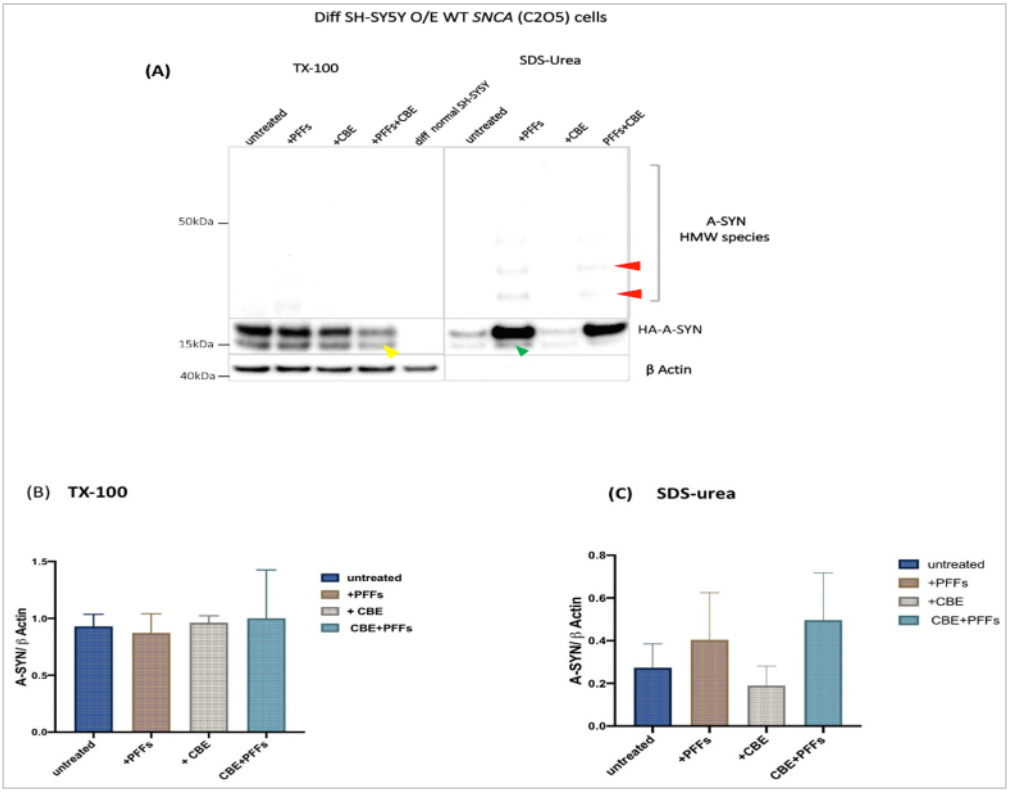

Figure 0.8 Effect of PFFs seeding in differentiated SH-SY5Y O/E WT *SNCA* in the background of GCase inhibition. (A): Representative WB images showing the effect of 10 days long PFFs seeding in differentiated SH-SY5Y O/E WT *SNCA* with and without CBE treatment; the proportion of soluble (yellow arrowhead) and insoluble A-SYN (denoted by the green arrowhead) were assessed and probed with total anti A-SYN antibodies. β Actin used as loading control, (n=3), parental normal differentiated SH-SY5Y (lane 5) was used to show specificity of HA antibody in detecting tagged A-SYN (B) Bar chart analysis of TX-100 soluble A-SYN fractions in differentiated SH-SY5Y cells O/E WT *SNCA* normalized to β Actin; CBE and PFFs treatment, alone or combined, did not induce soluble A-SYN accumulation in cells despite high A-SYN expression,(ASYN;untreated=0.930±0.106;+PFFs=0.872±0.168;+CBE=0.961±0.062;PFFs+CBE=1.0001±0.425, *p*=0.983, n=3). (C): There was small but not significant increase of insoluble A-SYN fraction in PFFs treated with the evidence of 30-50kDa HMW species in cells incubated with either PFFs alone or PFFs combined with GCase inhibition against untreated cells, (SDS-urea ASYN; untreated=0.273±0.111; +PFFs=0.403±0.222; +CBE=0.189±0.092; PFFs+CBE=0.495±0.222, p=0.566, n=3). Data are expressed mean of 3 independent SH-SY5Y cultures± SEM.

5.5.5. Fluorometric Measurement of Cell Viability in Primary Neuronal Culture Seeded with PFFs

The effect of PFFs and CBE treatments on cell viability in differentiated SH-SY5Y was measured (n=5). We observed that treating cells with 5µg/ml of PFFs caused no apparent toxicity. The number of viable cells were comparable between different experimental conditions with and without 10 µM CBE as judged by CTB assay (section 2.8), (Figure 0.9), indicating that PFFs treatment had no effect on cell viability.

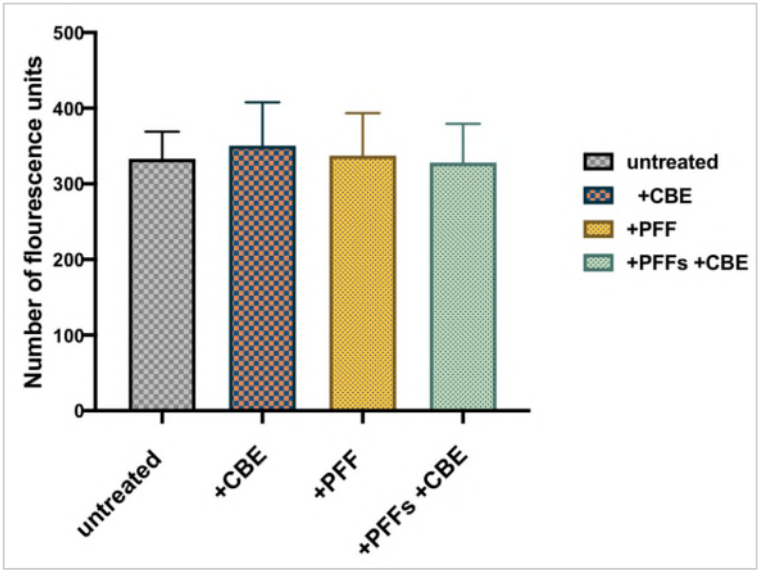

Figure 0.9 Influence of PFFs±CBE on cell viability 10days after the initial treatment of differentiated SH-SY5Y cells. As determined by the CTB assay, no significant change of viable cell number was observed under any experimental condition, (*P*=0.991). Data was expressed as the mean fluorescence and calculated from three wells±SEM, (n=5).

5.5.6. PFFs Induced Extracellular Release of A-SYN From Differentiated Normal SH-SY5Y and Cells O/E WT *SNCA*

There is increasing evidence that aggregated A-SYN fibrils might have a prion like mechanism which contributes to the spread of Lewy body pathology in PD brains (Kim et al., 2019). We therefore continued investigating the extracellular release of A-SYN in differentiated SH-SY5Y cell models by ELISA, both under basal condition and when cells were treated with PFFs ±CBE. Measurement of monomeric A-SYN release into conditional media derived from differentiated normal SH-SY5Y confirmed no significant induction of exocytosis in cultures treated with 10µM CBE for 10 days as compared to untreated group (untreated=1137±97.73, +CBE=1618±600; p>0.999, n=3), (Figure 0.10, A). However, cells seeded with PFFs, either alone or with CBE, showed significant increased extracellular release of A-SYN when compared to control; (untreated=1137±97.73;+PFFs=7638±703;***p=0.008;PFFs+CBE=10178±3186 ; *p=0.039, n=3), (Figure 0.9). The release of A-SYN under PFFs±CBE conditions was even significantly enhanced when compared to CBE treatment alone;(CBE=1618±600.0,+PFFs=7638±703;**p=0.0029;PFFs+CBE=10178±3186, p=0.0576, n=3), (Figure 0.9). This might be indicating that the loss of GCase activity by itself was insufficient to significantly enhance the release of free monomeric A-SYN from cells and an additional stress such as PFFs treatment was needed. However, there was no significant difference in monomeric A-SYN release from cultures treated with PFFs alone and from those treated with PFFs+CBE, (+PFFs=7638±703; PFFs+CBE=10178±3186, p=0.479, n=3), (Figure 0.9).

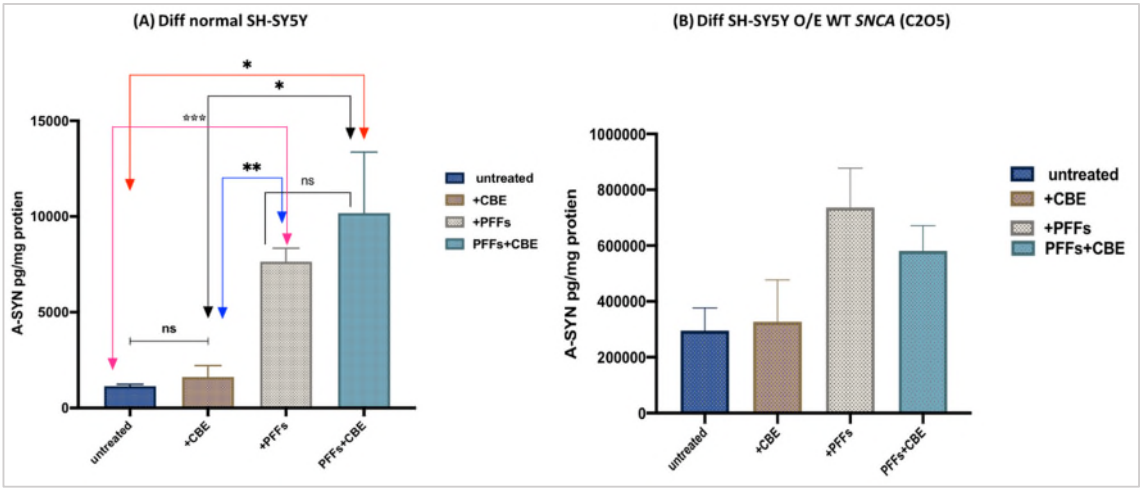

Figure 0.10 ELISA of conditional media derived from differentiated dopaminergic cells, normal parental and over-expressing WT *SNCA* (C2O5). Conditional media was measured in duplicates (A): Bar chart analysis showing no significant induction of A-SYN release in cultures treated with 10μM CBE for 10 days as compared to untreated group (untreated=1137±97.73, +CBE=1618±600; *p*>0.999, n=3). Cultures seeded with PFFs, either alone with CBE, showed significantly increased monomeric A-SYN release into media as compared to control;(untreated=1137±97.73; +PFFs=7638±703; ****p*=0.008; PFFs+CBE=10178±3186; **p*=0.039, n=3). In addition, the release of A-SYN under PFFs±CBE conditions was significantly induced when compared to CBE treatment alone;(CBE=1618±600.0; +PFFs=7638±703; ***p*=0.0029; PFFs+CBE=10178±3186, *p*=0.0576, n=3), there was no alteration in A-SYN release between PFFs alone and PFFs+CBE conditions. (B) Bar chart analysis of monomeric A-SYN release in to media of differentiated SH-SY5Y O/E WT *SNCA* (C2O5) showing that; CBE exposure did not cause further increase in A-SYN release from C2O5 cells when compared to untreated control (untreated=295047±81234, +CBE= 327355±149549, *p*>0.999, n=3). However, the release of A-SYN following PFFs treatment was induced to be 2.5 times more than the control groups (+PFFs= 736433±140951, *p*=0.146, n=3). In addition, PFFs+CBE treatment induced nonsignificant A-SYN extracellular release from cells (PFFs+CBE = 580733±91135, *p*=0.500, n=3). In general, the release of A-SYN in to culture media was much pronounced in cells overexpressing A-SYN than normal parental SH-SY5Y due to higher endogenous A-SYN levels, all presented data were expressed as mean of 2 experimental repeats ± SEM.

We also quantified monomeric A-SYN level released into the conditional media of differentiated SH-SY5Y O/E WT *SNCA* (C2O5) by ELISA. Our results showed that under basal condition, the release A-SYN from C2O5 cells was ~260 times higher compared to that of untreated normal parental SH-SY5Y (ASYN amount in pg/mg protein; untreated diff normal SH-S=1137±97.73; untreated diff C2O5= 295047±81234, n=3) implicating the high level of endogenous A-SYN due to enhanced expression results in more A-SYN being released (Figure 0.10, B). However, CBE exposure did not cause further increase in A-SYN release from differentiated C2O5 cells against untreated control (untreated = 295047±81234, +CBE= 327355±149549, p>0.999, n=3) suggesting that A-SYN release is not dependent on the total loss of GCase activity. Despite that, following PFFs treatment, the release of A-SYN from the same neurons was augmented to be 2.5 times more than that of untreated cultures (+PFFs= 736433±140951, p=0.146, n=3). Furthermore, combined PFFs and CBE induced monomeric A-SYN exocytosis although not reaching statistical significance (PFFs+CBE=580733±91135, p=0.500, n=3), (Figure 0.10). These findings collectively indicated that the released of A-SYN from C2O5 cells was parallel to its overproduction in cells and was even worse by PFFs treatment.

We then extended our analysis to investigate the release of synuclein fibrils into cell culture media in the last 24hrs of the experiment using dot blot. Analysis of culture media from PFFs-treated differentiated normal SH-SY5Y displayed immunopositivity for A-SYN fibrils. However, differentiated normal SH-SY5Y cultures treated with both PFFs and CBE released more A-SYN fibrils, although not reaching statistical significance (+PFFs=87.58±42.69, PFFs+CBE=115.8 ±74.52, P=0.759, n=3), (Figure 0.11, A and B). More importantly, when A-SYN

fibrils were normalized to the protein content of the well, the mean concentration in media was 230.9±69.54 ng/ml in differentiated C2O5+PFFs and 290.6±78.12 in those treated with PFFs+CBE. This amount was more than 2 times higher than that of differentiated parental SH-SY5Y cells (Figure 0.11, A and C). However, we could not estimate if the released A-SYN fibrils were free or exported in exosomes, therefore we used dot blot analysis to further quantify ALIX exosomal marker (Figure 0.12).

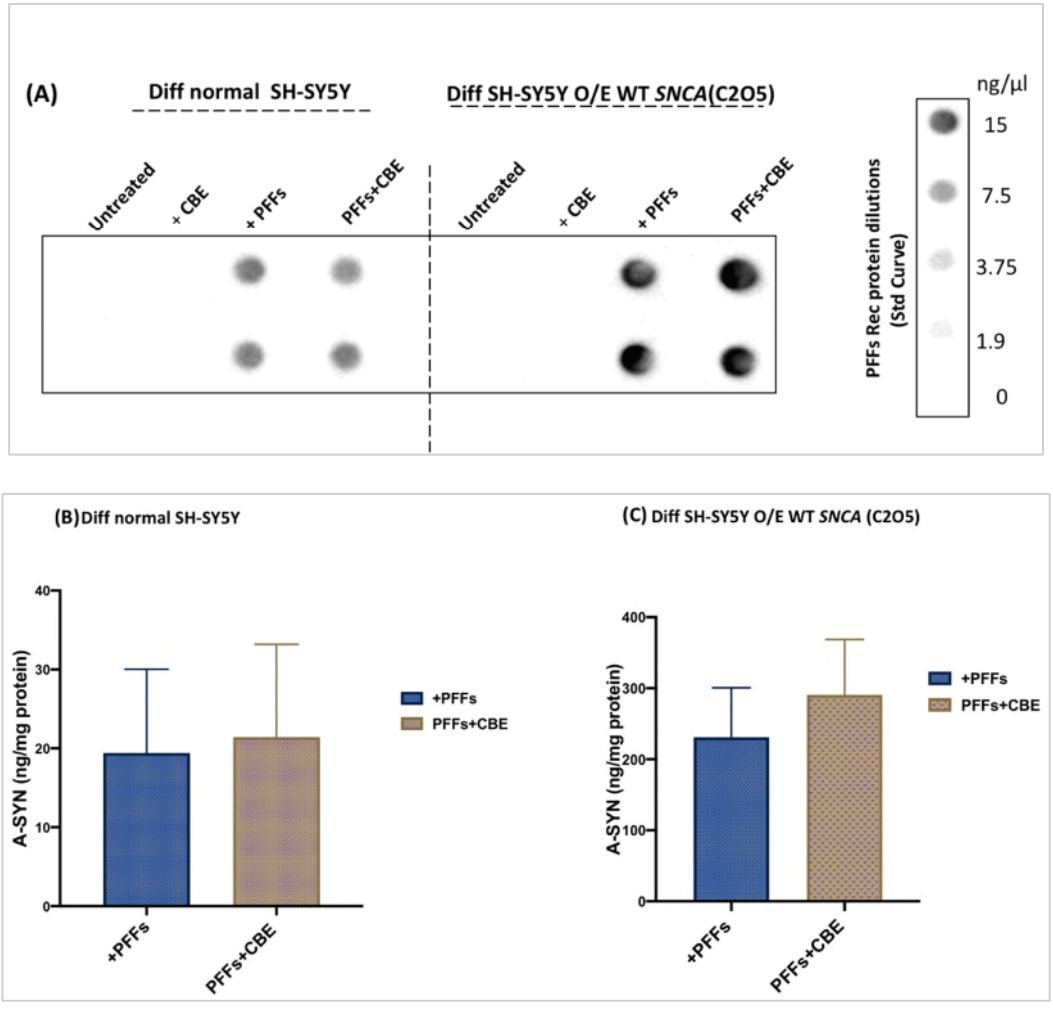

Figure 0.11 Dot blot for A-SYN fibrils in conditioned media from PFFs ±10 µM CBE in differentiated SH-SY5Y cells. (A): Conditional media was measured in duplicates and the PFFs concentration calculated using PFFs standard curve (0-30 ng/ml). The mean was taken and normalized to protein content of the respective well. (B, C): Bar charts showing fibrillar A-SYN release from PFFs±CBE- treated differentiated normal SH-

SY5Y and those O/E WT *SNCA* (n=4 and 3 independent cultures respectively). Data represent the mean ± SEM and show no alteration in the release of A-SYN between PFFs and PFFs+CBE treatment in both normal (+PFFs=19.42±10.6; PFFs+CBE=21.44±11.75; *P*=0.902=, n=4) and cells O/E WT *SNCA* (+PFFs=230.9±69.54; PFFs+CBE=290.6±78.12; *P*=0.599, n=3).

Quantification of number of exosomes released into the media derived from differentiated normal SH-SY5Y cultures showed that it was similar to untreated control whether these cultures were treated with PFFs or not (Alix differentiated normal SH-SY5Y: untreated=615497±327794; +CBE=857033±831833; +PFFs=841057±311588; PFFs+CBE=448145±331674 *P*=0.926, n=3), (Figure 0.12 A and B). This finding demonstrated that although the number of exosomes was not increased, at least part of A-SYN fibrils was present inside exosomes. Likewise, differentiated C2O5 overexpressing A-SYN and treated with PFFs±CBE showed no significance difference in exosomes released when compared to untreated control (Alix differentiated C2O5: untreated=748363±716742;+CBE=1782957±671154;+PFFs=1612306±134481; PFFs+CBE=1635206±716342, *P*=0.856, n=3), (Figure 0.12 A and C). However, due to more intracellular A-SYN being produced in C2O5, cultures treated with PFFs+CBE were releasing nearly 4 times more exosomes than their respective differentiated parental SH-SY5Y cells.

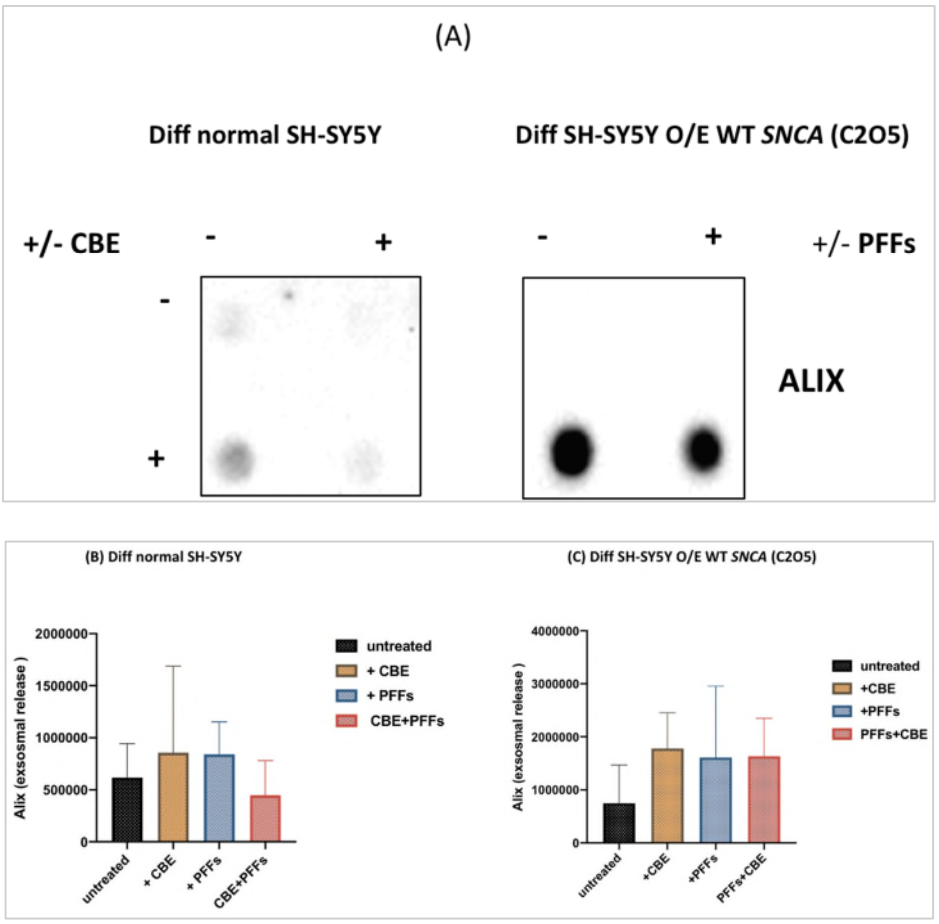

Figure 0.12 Dot blot for the exosome associated release of fibrillar A-SYN into culture media of differentiated SH-SY5Y cells, normal and O/E WT *SNCA* (C2O5). Exosome associated A-SYN fraction from differentiated cells were immunopositive for Alix marker indicating the presence of exosomes in conditioned media (A): Bar chart analysis showing that differentiated normal SH-SY5Y cells treated with PFFs and/or CBE released similar number of exosomes as untreated control (Alix: untreated=615497±327794; +CBE=857033±831833; +PFFs=841052±311588; *P*=0.926, n=3). (C): Quantification of number of exosomes released into culture media of differentiated C2O5 overexpressing WT *SNCA* showing more exosomes in media when compared to differentiated parental SH-SY5Y. However, there was no alteration observed in the release of exosomes under, +PFFs or PFFs+CBE experimental conditions (untreated=748363±716742; +CBE=1782957±671154; +PFFs=1612306±1344831; PFFs+CBE=1635206±716342; *p*=0.269, n=3). Data represent the mean ± SEM.

5.5.7. UPR &ER Stress in Differentiated SH-SY5Y cells O/E WT and L444P *GBA*

Due to the high transfection efficiency with immortalized cells and to remodel *GBA*-PD pathogenic events in dopaminergic system invitro, SH-SY5Y cells were transfected prior to differentiation and using xtreme GENE HP DNA transfection reagent according to the method illustrated in (section 2.1.4). Positive *GBA* L444P colonies (Figure 0.13) were then harvested, cultured individually and analyzed for the presence of *GBA* by mRNA analysis (cells and data generated by David Chau and Dr Gegg, Dept. Clinical and Movement Neurosciences, ION). *GBA* O/E colonies were selected with similar GBA mRNA levels and two clones, over expressing WT *GBA* (clone #4) and L444P (clone #3), were selected established for differentiation. Other clones (WT#3, WT#5 and L444P# 5) were excluded as they died when I started to differentiate them. In addition, despite the complex neuronal morphology of some L444P clones (clone # 6 and 8), their mRNA levels were lower than that of clone L444P #3 and they were therefore not included in my project (Figure 0.13). Therefore, I subsequently chose to characterize clone #4 for WT and clone #3 of L444P SH-SY5Y cells for downstream analysis such as assessing ER stress and UPR.

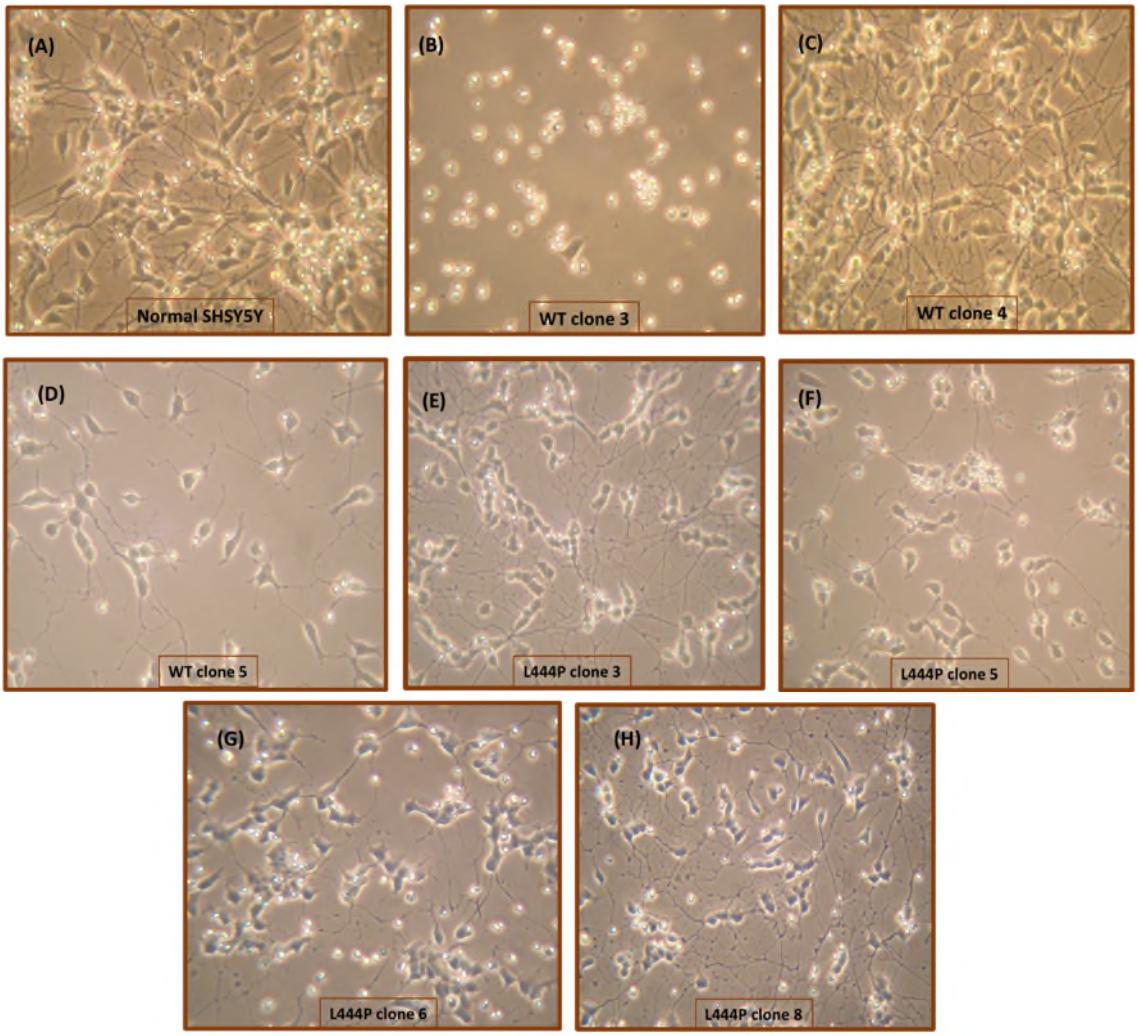

Figure 0.13 Representative photomicrographs of different differentiated SHSY5Y clones (parental, cells O/E WT and L444P *GBA*). (A): Differentiating normal parental SH-SY5Y line. (B, C, D): Different clones (#3, 4 and 5) of differentiating SH-SY5Y overexpressing WT*GBA*. (E, F, G, H): Different clones (#3, 5, 6 and 8) of differentiating SHSY5Y overexpressing L444P *GBA*. All pictures were taken on 10DIV.

Western blot analysis confirmed the increased expression of endogenous GCase in differentiated parental SH-SY5Y cells against undifferentiated control cells (undiff=0.218±0.012, diff=0.342±0.086, *p*=0.835) which was similar to previously shown data (Figure 0.5). Furthermore, this observation was incorporated with a non-significant increase in GCase activity in differentiated normal cells when compared to control (undiff =1.60±0.253 nmol/hr/µg, diff=2.25±1.30 nmol/hr/µg, *p*=0.835, n=3). On the other hand, overexpression of WT *GBA* protein has profoundly increased relative GCase protein level and activity in undifferentiated cells (GCase protein level=1.013±0.092, ***p*=0.006, GCase activity=5.16±0.360, ****p<0.0001, n=3), (Figure 0.14, A and B). However, upon differentiating this line, both parameters were markedly decreased as reflected by drop in total protein level and lysosomal enzyme activity (GCase=0.342±0.086, **p*=0.021, enzyme activity=2.043±0.005nmol/hr/µg, ****p<0.0001, n=3). We also detected that the UPR-inducer, GRP78/BiP, is not significantly altered when the overexpressing cells were differentiated, (BiP: undiff normal SH-SY5Y =0.039±0.011; undiff O/E WT *GBA*= 0.0201±0.063, *p*=0.412; diff O/E WT *GBA* =0.147±0.022, *p*=0.994), (Figure 0.14, D). More importantly, BiP level was significantly upregulated both in un- and differentiated SH-SY5Y O/E L444P *GBA* versus differentiated normal SH-SY5Y (BiP: diff normal SH-SY5Y =0.104±0.034; undiff O/E L444P= 0.579±0.102, ***p=0.0009; diff O/E L444P =0.487±0.064, **p=0.0038). BiP induction was also found higher in these cells as compared to those overexpressing WT *GBA* (diff O/E WT *GBA* =0.1469±0.022; diff O/E L444P =0.487±0.064, **p=0.0047, n=3). As a further support to this finding and the validity of the model (O/E L444P mutation), the upregulated BiP level was coupled to a slight but nonsignificant reduction in GCase protein level against

their respective undifferentiated group (undiff O/E L444P=1.006 ±0214; diff O/E L444P =0.585 ±0.145,**p=0.301) which might indicate that the reduction in protein level was L444P mutation-dependent and resulting from ER retention of mutant enzyme despite the nearly comparable GCase activities within all differentiated SH-SY5Y lines (GCase activity: diff normal cells=2.25±0.130; diff O/E WT=2.043 ±0.005; diff O/E L444P =2.99±0.157, p>0.05, n=3), (Figure 0.14,C). The lack of significant alteration in the activities of other lysosomal hydrolases, namely β-hexosaminidase and β-galactosidase, in differentiated SH-SY5Y O/E L444P *GBA* were also suggestive that our findings were specific to L444P mutation. Furthermore, β-galactosidase activity was only found significantly increased in differentiated normal and O/E WT *GBA* when compared to their respective undifferentiated group. By incorporating this finding with the slight increase in β-hexosaminidase activities in these cells, once again, it was indicative of increased lysosomal mass with differentiation (β-gal in nmol/min/µg; undiff normal=0.046±0.002, diff normal=0.068±0.001, **p=0.009; undiff O/E WT=0.034±0.005, diff O/E WT=0.052±0.0007, *p=0.033), (Figure 0.15).

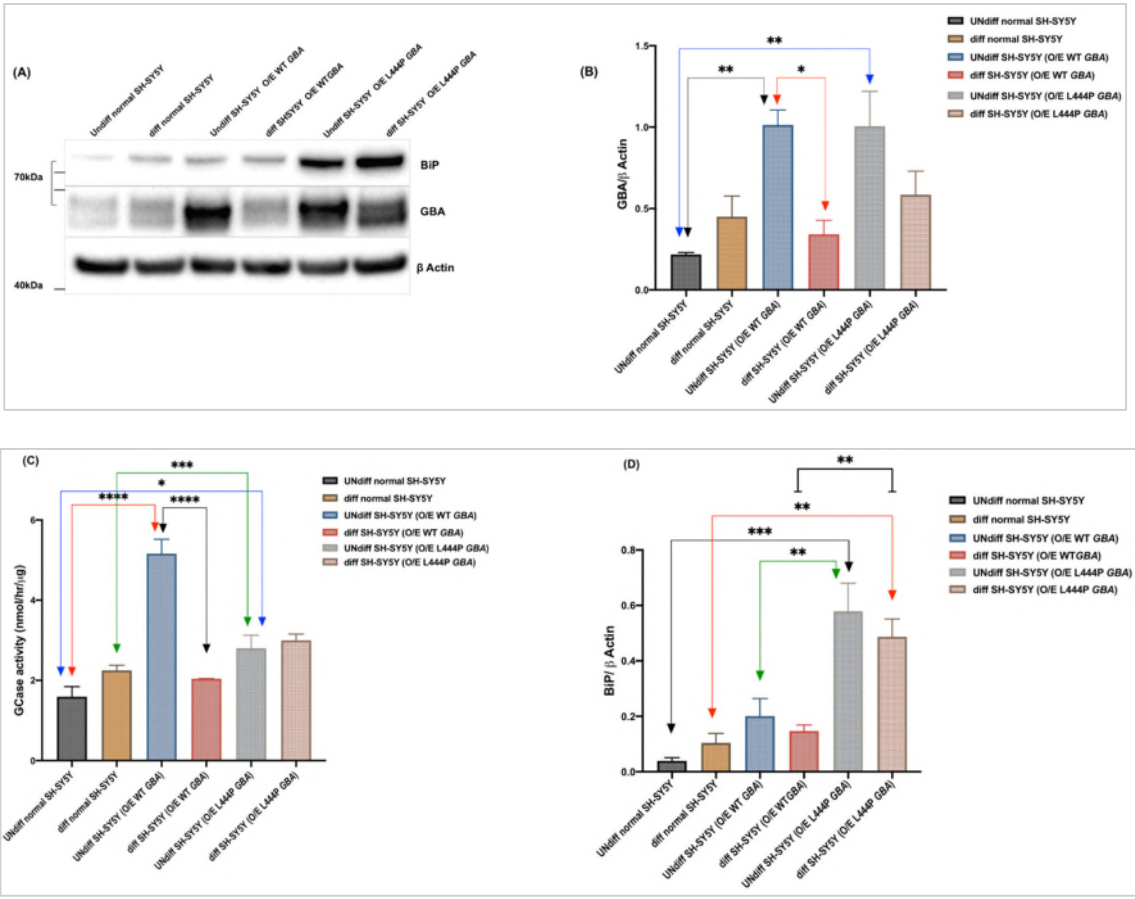

Figure 0.14 Evidence of UPR in differentiated SH-SY5Y O/E and O/E L444P *GBA*. (A): Representative WB images showing BiP and GBA protein expression in differentiated SH-SY5Y normal, O/E WT *GBA* and O/E L444P *GBA*, (β actin was used as loading control and n=3). (B, C): Bar chart quantifying GCase activity and protein level normalized to β actin; it shows nonsignificant increase in both parameters when normal SH-SY5Y is differentiated and compared to control (GCase protein in undiff=0.218±0.012; diff=0.342±0.086, *p*=0.835; enzymatic activity in undiff =1.60±0.253; diff=2.25±1.30, *p*=0.835,). Overexpressed WT *GBA* results in markedly increase GCase amount and activity in undifferentiated line (GCase undiff=1.013±0.092, ***p*=0.006, activity=5.16±0.360 nmol/hr/µg, *****p*<0.0001, n=3). Upon differentiation, both protein amount and activity were markedly decreased (GCase=0.342±0.086, **p*=0.021, enzyme activity=2.043±0.005nmol/hr/µg, *****p*<0.0001, n=3). On the contrary, differentiated cells O/E L444P showed nonsignificant reduction in GCase protein level against their respective undifferentiated group (undiff O/E L444P=1.006 ±0214; diff O/E L444P =0.585 ±0.145, ***p*=0.301). (C): The reduced GCase level was coupled to significant upregulation of ER resident chaperon BiP in diff SH-SY5Y O/E L444P (BiP: diff normal=0.104±0.034; undiff O/E L444P=0.579±0.102, ****p*=0.0009; diff O/E L444P=0.487±0.064, ***p*=0.0038). BiP induction was also increased in L444P differentiated cells when compared to those overexpressing WT

***GBA* (diff O/E WT *GBA* =0.1469±0.022; diff O/E L444P =0.487±0.064, **p=0.0047, n=3). Data represent the mean density of target proteins expressed against the density of the housekeeping protein (β actin) and derived from three independent SH-SY5Y cultures ± SEM.**

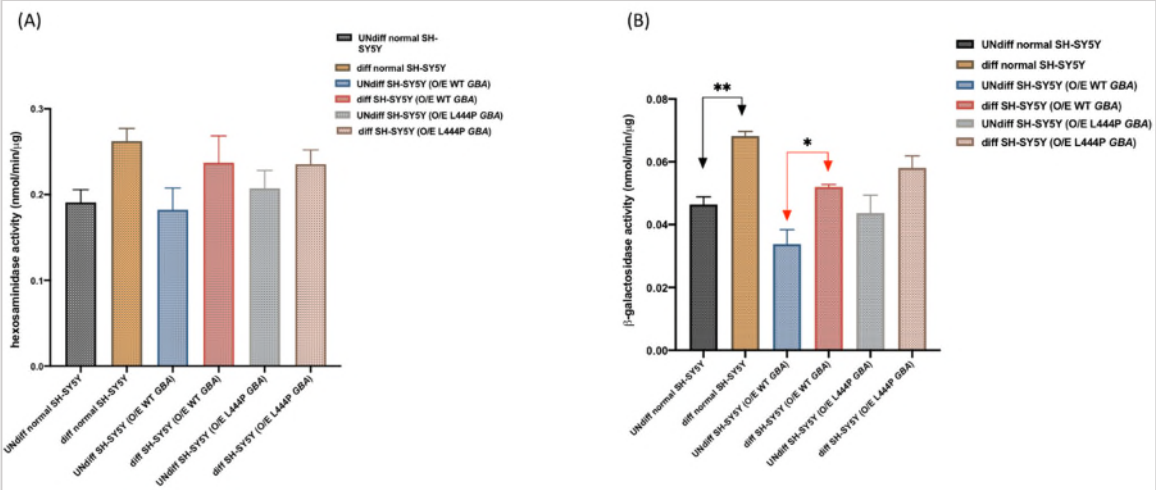

Figure 0.15 Analysis of β-hexosaminidase and β-galactosidase activities in differentiated SH-SY5Y cell models O/E WT and L444P *GBA*. (A): Bar charts summarizing β-hexosaminidase measured in nmol of product/min/µg protein showing a nonsignificant trend of increased activity following (RA+BDNF differentiation) of all SH-SY5Y cell lines against their corresponding undifferentiated groups (undiff normal=0.191±0.015, diff normal=0.262±0.015, p=0.286; undiff O/E WT=0.182±0.025, diff O/E WT=0.237±0.031, p=0.602; undiff O/E L444P=0.207±0.021, diff O/E L444P=0.236±0.016, p=0.984). (B): Bar charts summarizing β-galactosidase measured in nmol of product/min/µg protein showing significant increased activity following differentiation of both normal SH-SY5Y and those O/E WT *GBA* compared to control groups together with a nonsignificant subtle increase in activity in differentiated cells O/E L444P (undiff normal=0.046±0.002, diff normal=0.068±0.001, **p=0.009; undiff O/E WT=0.34±0.005, diff O/E WT=0.052±0.001, *p=0.033; undiff O/E L444P=0.044±0.006, diff O/E L444P=0.058±0.004, p=0.128), each bar represents mean of enzymatic activity from 3 independent SH-SY5Y cultures ± SEM, (n=3).

5.6. Discussion

This chapter investigates the intracellular processing and the release of protopathic A-SYN species using differentiated dopaminergic cells. Utilizing SH-SY5Y cells that were fully differentiated into neurons has also provided us a valid invitro system to explore the relationship between ER stress and L444P mutant GCase in dopaminergic cells. Although modelling SH-SY5Y cells is a common practice, there are still some controversy that the desired differentiation phenotype could recapitulate PD pathogenesis. However, we show in our work that, in addition to exhibiting dopaminergic phenotype, differentiated SH-SY5Y cells could reproduce the same pathological hallmark of PD pathology and act as proof of principal for further in vitro studies of iPCs.

The putative bidirectional link between GCase deficiency and ASYN dysmetabolism, involving impaired lysosomal function and the formation of proteinaceous A-SYN laden inclusions, has been previously linked to PD conferred by *GBA* mutations (Mazzulli et al., 2011). However, and with the implication of both genetic and pharmacological manipulation together with PFFs seeding-based approaches, we noticed that even the persistent profound loss of GCase activity was insufficient to induced *de novo* A-SYN pathology; we observed that 10µM CBE exposure for 10 days' time window did not accumulate insoluble monomeric A-SYN or HMW species in differentiated SH-SY5Y. In accordance with our finding, (Dermentzaki et al., 2013, Cullen et al., 2011, Gegg et al., 2020, Henderson et al., 2020) reported that in differentiated SH- SY5Y cells, HEK293 cells and neurons treated with CBE alone, there was no significant alteration observed in A-SYN level or any impaired clearance of oligomeric A-SYN species. On the contrary, it was previously reported that insoluble A-SYN

accumulates in differentiated SH-SY5Y cells treated with 50μM CBE for 48hrs (Manning-Bog et al., 2009). Moreover, several other studies have reported significant A-SYN accumulation, S129 phosphorylation and the appearance of insoluble HMW species, both in differentiated SH-SY5Y and other cellular models like HEK293, MCN and immortalized normal or A-SYN overexpressing SH-SY5Y cells. In these studies, cell cultures were incubated with various higher doses with longer time exposure to CBE which, in some reports, lasted up to 30 days (Cleeter et al., 2013, Yiğit et al., 2018, Magalhaes et al., 2016, Rocha et al., 2015b, Manning-Bog et al., 2009, Henderson et al., 2020). In addition, A-SYN pathology was enhanced after introducing a non-sense mutation into differentiated SH-SY5Y cells leading to total loss of GCase activity (Bae et al., 2015). These discrepancies could be related to large doses of CBE used to irreversibly inhibit GCase activity by 98%. However, this can jeopardize cell life and reduces viability as indicated by reduced neuronal markers in primary hippocampal neurons in Henderson et al work (Henderson et al., 2020). With the evidence of different disease phenotype following CBE exposure, it is likely that the defective GCase activity in our study was not enough to impair lysosomal function or induce LB pathology over the 10-days' time period. We therefore proposed that perhaps prolonged cell exposure to higher CBE doses or augmented synuclein load in GCase inhibited cultures is needed to act synergistically to induce pathology. In fact, perturbed A-SYN clearance in MCN and differentiated SH-SY5Y, both via pharmacological and genetic methods, was found to not only induce accumulation of insoluble A-SYN, but also increased exocytosis and transmission of A-SYN to promote toxicity of neighboring neurons (Magalhaes et al., 2016, Lee et al., 2013). Nevertheless, how *GBA* mutations can

cause lysosomal dysfunction is not clearly understood but it was previously shown that differentiated SH-SY5Y cells with C-terminal truncation of GCase but intact GCase activity show normal lysosomal function (Bae et al., 2015). It is possible that the loss of function mechanism would result in substrate accumulation and changes in membrane lipid composition (Migdalska-Richards and Schapira, 2016, Magalhaes et al., 2016).

In our model, when cultures were loaded with PFFs, the intracellular A-SYN significantly increased as insoluble fractions which were phosphorylated at Ser129. This was coincident with the appearance of A-SYN positive insoluble HMW species in cells. Similarly, differentiated SH-SY5Y, seeded with PFFs and co-treated with CBE, resulted in significant accumulation of insoluble monomeric and HMW species of A-SYN inside the cells. However, there was no significant difference in insoluble monomeric or Ser129 phospho A-SYN levels between PFFs and PFFs+CBE groups under the 10 days window and may be longer time scale is needed to exacerbate the present pathology. The induced pathology in differentiated SH-SY5Y treated with PFFs±CBE was similar to our previous findings on MCN treated cultured cells with preformed fibrils (PFFs) in the background of heterozygous L444P mutation, (see 172).

With the given evidence that duplications and triplications of the *SNCA* gene are the causes of autosomal dominant PD (Polymeropoulos et al., 1997), we sought to shed light on the effect of high expression of WT A-SYN on differentiated SH-SY5Y neurons (C2O5) and its possible additive effect in promoting cell toxicity and A-SYN accumulation. It was previously reported that the rate of A-SYN phosphorylation and toxicity has been markedly enhanced in undifferentiated C2O5 following proteasomal inhibition and oxidative stress (Chau et al., 2009).

We found that, despite high A-SYN expression levels in these cells, the intracellular TX-100 soluble monomeric HA-A-SYN was not significantly altered between the control and other experimental groups. In accordance with our results, previous induction of human WT ASYN in differentiated SH-SY5Y resulted in accumulated soluble ASYN oligomers, but not aggregates (Vekrellis et al., 2009). We also found that, following CBE treatment, there was no increased insoluble A-SYN detected in differentiated C2O5 cells. It is possible that propensity of ASYN to aggregate was not related to GCase inhibition and thus without adding an additional stress, CBE alone doesn't affect the endogenous A-SYN solubility in the presented time scale. However, other groups have previously reported that overexpressed A-SYN caused accumulation and secretion of insoluble aggregates in differentiated SH-SY5Y cells with genetically induced mutant or inhibited GCase but not in those with intact GCase activity, (Bae et al., 2015, Manning-Bog et al., 2009). In addition, we found that following PFFs loading, differentiated C2O5 cells started to slightly accumulate insoluble A-SYN and 30-50kDa HMW species. This effect was detected under PFFs treatment alone or when combined with CBE indicated that PFFs treatment was enough to induce accumulation of insoluble A-SYN regardless of GCase inhibition. Also, the profound production of A-SYN in C2O5 cells compared to normal differentiated lines would possibly add more A-SYN toxicity and potentiate aggregation particularly with PFFs seeding approach. According to these findings, the previous suggestion of ‘‘double-hit’’ hypothesis of needed aggravating factor, such as chronic exposure to toxins with genetic background, should be considered in order to reproduce PD pathology (Martella et al., 2016, Lopes et al., 2017a).

Having said that exocytosis is enhanced following PFFs seeds are internalized to cells (Kim et al., 2019), we looked at the release of A-SYN, both monomeric and fibrils, into conditional media of differentiated normal and A-SYN overexpressing SH-SY5Y cells (C2O5). The basal level of monomeric A-SYN secretion was 260 times higher in C2O5 than that of normal cells. Furthermore, inhibiting GCase activity in either of these SH-SY5Y lines did not induce further release of monomeric A-SYN. However, PFFs treatment, either alone or combined with CBE, induced significant exocytosis of monomeric A-SYN from differentiated normal SH-SY5Y cells and released 2.5 times more monomeric A-SYN from differentiated C2O5 than parental SH-SY5Y. In line with these findings, differentiated SH-SY5Y cells O/E WT A-SYN and treated with 3-MA, an inhibitor of autophagy, showed increased intracellular levels of insoluble aggregates and enhanced secretion of monomeric A-SYN (Lee et al., 2013). Also, induced exocytosis of both monomeric and exosome aggregated forms of A-SYN either constitutively (Emmanouilidou et al., 2010) or secondary in response to lysosomal, proteasomal and mitochondrial dysfunction was reported in differentiated SH-SY5Y cells O/E WT *SNCA* (Lee et al., 2005, Jang et al., 2010). These findings collectively indicated that the release of monomeric species from C2O5 cells is dependent on the total intracellular A-SYN level and not on GCase functional loss and is further exacerbated by PFFs treatment. We also assessed the release synuclein fibrils into culture media of both differentiated cell types and found that differentiated normal SH-SY5Y treated with both PFFs and CBE released more A-SYN fibrils. Despite that, the amount of released A-SYN fibril was 2 times higher in C2O5 than parental normal cells. To further support our findings, recent study in our laboratory showed that PFFs but not monomeric A-

SYN treatment of both primary neuronal cultures and differentiated SH-SY5Y cells promoted spread of insoluble A-SYN species (Gegg et al., 2020). However, we could not estimate, in our study, if the released A-SYN fibrils were free or inside exosomes and therefore looked at ALIX as a marker of this extracellular vesicles by using dot blot analysis. In both differentiated SH-SY5Y models, ALIX data were similar under all experimental conditions suggesting no change in the number of exosomes released and it was not further affected by GCase inhibition. However, both differentiated cell types were treated originally with the same amount of PFFs (5µg/ml) but the release of fibrils and exosomes was so much more in C2O5 cells under all conditions. This finding suggests that it is possibly the increased seeding inside C2O5 cells due to high intracellular A-SYN levels converts A-SYN to fibrils and so results in more fibrils and ALIX being released. Impaired autophagy in response to *ATG5* knockdown in LUHMES neurons O/E A-SYN has been compensated by the increased exosomal secretion of A-SYN aggregates to cope with excess A-SYN in cells. It was also found that inhibiting the exoxsomal release by sphingomyelinase inhibitor (GW4869), has protected cells against A-SYN induced toxicity (Fussi et al., 2018).

Generally, and even with similar ALIX data we obtained here, the possibility of more A-SYN fibrils could be present in each exosome is not to be excluded. Future experiment such as exosomes isolation is needed to investigate the manner of fibrillar A-SYN release and whether these fibrils are more packed in membrane vesicles or being freely exported from cells. Also, the use of exosomal inhibitors such as GW4689, which block exosomal release and the subsequent spread of A-SYN fibrils, might indicated the amount of synuclein fibrils inside exosomes.

In addition to being exported by tightly regulated cellular pathways, A-SYN aggregated species can be released as a result of cell death (Karpowicz et al., 2019). Additionally, in vitro and in vivo PFFs seeding is known to result in rapid formation of LB inclusions that ultimately leads to cell death (Grassi et al., 2018, Karpowicz et al., 2019, Luk et al., 2009). We therefore examined if PFFs- induced pathological burden results in cell toxicity and loss in differentiated SH-SY5Y cultures. Our results showed that culturing cells in which PFFs were seeded for as long as 10 days had no obvious impact on cell viability regardless of pharmacological GCase inhibition as judged by CBT assay. It was previously reported by (Vekrellis et al., 2009) in which differentiated SH-SY5Y expressing WT ASYN, and not normal parental cells, exhibited evident of caspase dependent non-apoptotic cellular death 6 days after RA-treatment and ASYN overexpression. Also, the neuronal loss observed in Luk et al. work did not differ between PFFs treated and untreated control group at 7 and 9 DIV, but started to appear at 12 DIV (Luk et al., 2009). This might be indicting that the gradual cellular degeneration could be either proportional to the background A-SYN expression in differentiated SH-SY5Y cells or dependent on the doses and time of PFFs exposure in primary hippocampal culture. These observations collectively added to the attractive features of the differentiated SH-SY5Y model we used. Differentiating immortalized *GBA*$^{-/-}$ cortical neuron cultures with 10 μM of RA for 6 days did not result in either endogenous A-SYN protein accumulation or toxicity (Westbroek et al., 2016). Also, the released A-SYN species from cells was not due cell membrane leakage from dead cells as the cell viability assay showed no evidence of cell death in our model.

A-SYN pathology in both differentiated SH-SY5Y lines, challenged with PFFs shows that an additional stress made by PFFs, either alone or combined with CBE, is enough to promote A-SYN becoming insoluble and aggregated (Table 0.2). However, for further deciphering the early process of LBs formation and with the given evidence that both gain of function and loss of function mechanisms are implicated in A-SYN dysmetabolism (Migdalska-Richards and Schapira, 2016), previous work confirmed retained GCase in ER of undifferentiated SH-SY5Y cells O/E L444P *GBA* (Li et al., 2019). More recently, BiP expression was found upregulated following PFFs treatment of differentiated SH-SY5Y cells and thus accounting for the concomitant reduction in GCase level in these cells (Gegg et al., 2020). Previous investigation of ER stress in wt/L444P fibroblast and mouse cortical neuronal models supported the lack of ER stress and UPR despite the evidence of ER trapping of mutant enzyme in fibroblasts. The same findings were encountered in adult mice brain even with subtle alteration in A-SYN level in midbrain of 8-month aged mice (section4.5.6).

In this perspective and based on above results, we sought to establish differentiated SH-SY5Y cells that are stably overexpressing both WT and L444P *GBA* in order to confirm the phenomena of ER stress and UPR that lead to downstream cellular toxicity. We found that BiP level decreased in both normal and differentiated O/E WT *GBA* but was significantly upregulated in cells overexpressing L444P *GBA*. Therefore, UPR following induction of mutation accounted for the reduced GCase level due to impaired trafficking of retained mutant enzyme to the lysosome and thus supporting the toxic gain of function effect of L444P mutation, (Figure 0.14). Previous published studies investigating UPR and ER stress in differentiated neuronal model and in relation to *GBA-PD*

are illustrated in (Table 0.3). In summary, L444P differentiated SH-SY5Y line exhibited ER stress and induced UPR phenotype as marked by upregulation of BiP level.

Table 0.3 summary of published studies investigating ER stress and UPR in PD in vitro models

Study	Disease model	ER Stress and UPR phenotype
(Schondorf et al., 2014)	differentiated from iPS derived from PD patients with L444P *GBA* mutations	Increased release of calcium from the ER
(Schondorf et al., 2018)	differentiated from iPS derived from PD patients with N370S *GBA* mutations and isogenic *GBA* KO neurons	increased BiP and RNA levels of spliced X-box-binding protein-1 (XBP1s) in *GBA*-PD neurons compared to isogenic *GBA* KO neurons (activation of the IRE1 related branch of ER stress)
(Fernandes et al., 2016)	differentiated from iPS derived from PD patients with N370S *GBA* mutations	increased expression of chaperones associated with the UPR, including BiP and calnexin, activation of the IRE arm of the UPR
(Gegg et al., 2020)	differentiated SH-SY5Y cells treated with pathological PFFs seeds	activation of BiP and the UPR following PFF treatment
(Bellucci et al., 2011)	dopaminergic differentiated SH-SY5Y cells subjected to glucose depletion (GD)	GRP78/BiP expression significantly increased in glucose-deprived cells
(Heman-Ackah et al., 2017)	iPS derived neurons with *SNCA* triplication	10-fold increase in IRE1a mRNA levels and the spliced XBP1isoform

5.7. Conclusion

PFFs -seeded differentiated SH-SY5Y can be used as a future powerful platform to recapitulate all the stages of LBs formation and maturation including aggregation, hyperphosphorylation and extracellular release of synuclein in spaciotemporal manner.

Overexpressing L444P in SH-SY5Y cells differentiated into 100% dopaminergic neurons represent a useful and promising experimental paradigm. This supports our proposed hypothesis that; heterozygous L444P mutation is implicated in the pathophysiology of PD through induction of UPR and ER stress which may consequently lead to impairment of A-SYN metabolism, the pathological hallmark in PD. Differentiated SH-SY5Y model could be used as a future valid tool to distinguish the toxic gain of function effect in heterozygous L444P mutation from the total loss of GCase enzyme activity on A-SYN metabolism. This could be the second hit required for more A-SYN toxicity following PFFs treatment. Additionally, it can be useful for exploring the role of not only heterozygous L444P but other *GBA* mutations-linked risk through investigating impaired protein degradation machineries and mitochondrial dysfunction with their potentiality to induce neuronal cells and glial vulnerability and death. The evidence of UPR activation by L444P *GBA* in dopaminergic cells, but not fibroblasts or cortical MCN, suggests the cellular environment among cells that can affect *GBA*-gain of function. It might also explain why some neuronal populations in the brain are more susceptible to neurodegeneration than others.

6.Concluding Discussion

The main findings from studying wt/L444P *GBA* mutations in three cell models were:

1. Limited evidence of lysosomal dysfunction and altered A-SYN metabolism under basal conditions.

2. The use of preformed fibrils Induced perturbed A-SYN metabolism in GCase deficient cells.

3. There was a notable activation of UPR in dopamine containing wt/L444P neuronal models but not in cortical neurons or fibroblasts cell models.

The lack of SNpc phenotypic determinants in the MCN and SH-SY5Y cellular models we utilized made it challenging to recapitulate all aspects of PD pathogenesis in these models. Even with *GBA*-associated higher risk of PD, the selective vulnerability of defined brain regions does not only depend on their expression of wild type or mutation alone (Surmeier et al., 2017, Burbulla and Krainc, 2019). Also, the minority of asymptomatic carriers converts to PD in their lifetime (Avenali et al., 2020, Sidransky and Lopez, 2012, Migdalska-Richards and Schapira, 2016) which adds to the controversy regarding PD with *GBA* mutations and their phenotypic correlation. In fact, advanced ageing still being the commonest risk factor for PD (Reeve et al., 2014), and recent studies suggested that 5% of heterozygous *GBA* mutation carriers gets PD at the age of sixties rising to 15–30% at age eighties. Also, *GBA* mutation prevalence is estimated to be between 2.35% and 9.4% in the PD population, but climbing up to 31.3% in the PD Ashkenazi Jewish populations (Schapira, 2015, Balestrino and Schapira, 2018, Avenali et al., 2020, Sidransky and Hart, 2012, Anheim et al., 2012). Various recent reviews have focused on the potential role of ageing in

the selective vulnerability of SNpc dopaminergic neurons in PD (Zucca et al., 2017, Reeve et al., 2014). Thus, it is likely that an additional factor besides *GBA* mutation, such as age, genetic, epigenetic and environmental events, are needed to derive PD pathogenesis (van Heesbeen and Smidt, 2019, Avenali et al., 2020). Also, with advancing age, many defects accumulate and diminishes the capacity of SNpc DA neurons to successfully cope with stress hence they become vulnerable to the additional insults such as mitochondrial deficiencies, toxic A-SYN species proteostatic dysfunction and telomere shortening (Reeve et al., 2014). We therefore in this project induced aggregating of A-SYN in disease models by seeding cells with PFFs (see page 172 and 224). This was done to trigger a cascade of stressors in MCN and differentiated SH-SY5Y dopaminergic neurons and thus approaching the pathological spectrum of PD. we found that seeding these cells with PFFs resulted increased trend for insoluble phosphorylated A-SYN. Accumulating evidences have collectively indicated that the scheme proposed by Braak et al study (Braak et al., 2003) although impressive, it was not fully dictating the extent and sequence of LBs deposition in susceptible brain regions nor correlating it with neuronal loss. In fact, using assessment of Lewy pathology (LP) alone is not considered as a suitable diagnostic criterion in PD (Surmeier et al., 2017).

It is reported that in preclinical stages of PD, LP appears first in either the olfactory bulb or the dorsal motor nucleus of the vagus (DMV) then preferentially retrogradely spreads from these two regions via synaptically connection to reach the SNpc. LP spreads to SN initiates neuronal loss and symptoms onset then finally reaches the forebrain by the end-stage of PD (Surmeier, 2018, Surmeier et al., 2017, Sulzer and Surmeier, 2013, Brettschneider et al., 2015). Quantitative

pathology mapping and network modelling in mouse brain showed that A-SYN pathology pattern of spread is based on the anatomical connectivity of brain regions and the endogenous A-SYN expression (Henderson et al., 2019).

In addition, Math2^{+} hippocampal neurons were reported to be significantly affected and lost due to PFFs-induced toxicity, in both in vivo and invitro models of synucleinopathies (Luna et al., 2018). The observed toxicity was dependent on the endogenous A-SYN expression. This observation strongly correlated with selective vulnerability of hippocampal neuron subtypes of which Math2^{+} neurons contained the highest amount.

Recent study by our group showed that PFFs treatment of MCN and differentiated SH-SY5Y neurons inhibited lysosomal GCase activity (Gegg et al., 2020). This was coincident with increased extracellular release and spread of pathogenic A-SYN fibrils. This spread, if present in vivo, could result in a greater propagation of LP in *GBA*-PD brains (Gegg et al., 2020). The increased spread from *GBA* mutants' models might as well explain earlier age of onset and cognitive decline in *GBA*-PD. With the evidence that mutation severity can influence PD phenotype profoundly, severe mutations like L444P account for 2- to 3-fold higher risk for developing PDD and DLB than milder mutations (Walker et al., 2019, Avenali et al., 2020, Cilia et al., 2016). In addition, PFFs treated models can be utilized to investigate the propagation of A-SYN via gut-brain axis supporting Braak theory. Recent study by (Kim et al., 2019) reported that PFFs injected into mouse duodenal and pyloric muscularis layer resulted in a spread of pathological A-SYN species in brain regions in a special and temporal manners starting from DMV, the locus coeruleus, and finally reaching SNpc. The spread of A-SYN histopathology to the midbrain was also reported in aged mice in a recent work

by Challis et al. group. In this study, they tested gut-to-brain progression of A-SYN by inoculating the duodenal wall of mice. They also found that over-expressing GCase could reduce the A-SYN pathology spread in gut (Challis et al., 2020).

An additional PD associated insult, such as inhibition of mitochondrial complex 1 by rotenone and/or induction of other mitochondrial stress to deplete mtDNA, might be considered as future work.

PFFs treatment could be useful to bring MCN and SH-SY5Y models phenotypical closer to vulnerable SNpc neurons and hence used as screening tool for future GBA drugs (e.g. Ambroxol). One major obstacle in PD treatment is to consider a specific therapeutic pathway capable of reducing aggregates in human neuronal model systems. During the initial phases of *GBA*-PD, patients show good response to L-Dopa. However, the disease progress is more rapid than that in iPD. In addition to the negative impact of cognitive decline on life of PD and PDD patients; it adds significant burden to patients, care providers and health care systems. To address this, Ambroxol chaperone use in PFFs-seeded cell neuronal models, not only helps to refold GCase and increase GCase levels, but to also limit A-SYN spread. Therefore, it could highlight a future potential therapy for slowing neurodegenerative process. Twelve days treatment of oral Ambroxol was reported to increase GCase activity in the brainstem, midbrain, cortex, and striatum of wild-type as well as wt/L444P transgenic mice (Migdalska-Richards et al., 2016). As A-SYN expression level in different neuronal populations is considered as the primary determinant of its prion-like seeding (Courte et al., 2020), ambroxol treatment reduced A-SYN levels in the brainstem and striatum of transgenic mice overexpressing human *SNCA* when compared to untreated

mice (Migdalska-Richards et al., 2016). These observations support the potentiality of ambroxol as a neuroprotective compound and concur with the outcome of recent single-center open-label clinical trial aimed at 17 PD patients with and without *GBA* mutations (Mullin et al., 2020). In addition to being safe and tolerable drug, this study showed that ambroxol can cross the blood brain barrier, bind to GCase and modulate its activity in CSF during 186 days of escalating exposure period. Increased A-SYN and GCase levels in CSF were also reported in all participants in this work which could be interpreted as an enhanced extracellular transport of A-SYN from brain parenchyma.

Despite the emerging evidence showing the pivotal role ER stress in the pathobiology of PD, few studies have analyzed the link between ER stress and the pathogenesis of *GBA*-PD using dopaminergic neuron (Gegg et al., 2020, Fernandes et al., 2016). Impaired trafficking of GCase from ER to the lysosome has been reported in human midbrain differentiated neurons with triplication of the *SNCA* gene (Mazzulli et al., 2016). Also, treatment of primary neuronal culture with PFFs resulted in recruitment of endogenous A-SYN and its conversion into fibrillar phosphorylated A-SYN aggregates (Grassi et al., 2018). It was also observed in the same study that phosphorylated A-SYN colocalizes with BiP, the master regulator of UPR. Similarly, we reported induced UPR and ER stress in differentiated SH-SY5Y dopaminergic neurons over expressing L444P*GBA* (section 5.5.7). More importantly, the lack of UPR and ER stress in our wt/L444P fibroblast and MCN models (page117 and 198) highlights the apparent susceptibility of differentiated SH-SY5Y cells to L444P mutation insult, relative to other models in our project. In addition, differentiated SH-SY5Y model has an advantage of being 100% dopaminergic whereas iPSc derived-neuronal cultures,

although attractive model, yield only 20– 30% of TH-positive cells (Hartfield et al., 2014, Schondorf et al., 2014). However, it remains unexplained why certain group of neurons such as DMV is relatively resistant and could tolerate LP for years while A9 neurons of SNpc do not. Furthermore, DAergic neuronal loss in some brain regions is not necessarily mirrored by LP and can follow a different pattern of distribution (Surmeier et al., 2017). Regions like ventral tier of SNpc show 10-20% of cells loss in the initial presymptomatic stage (Braak stage I and II) even without LP (Damier et al., 1999). Thus, neurons that die prematurely in PD or manifest LP must share distinguishing features that make them vulnerable cells. Mapping strategies of brain connectome to track the spread of LP through synaptic connections did not detect LP in brain regions strongly innervating the two hotspots in PD, SN and Locus Coeruleus (LC) (Watabe-Uchida et al., 2012). This was suggestive that the selectivity of retrograde spread of LBs and cell loss from the initial seeding sites to other brain regions should have other determinants in addition to spread through brain connectome (Surmeier et al., 2017, Surmeier, 2018). One of the most important features of A9 DA neurons of SNpc is that they have long and highly branched, unmyelinated axons with extraordinary numbers of neurotransmitters release sites. However, the basal mitochondrial stress and ROS production increases in DAergic neurons due to increased oxidative phosphorylation with the absence of ATP demands. This would eventually predispose cells to insult such as genetic mutations and toxins exposure due to compromised mitochondrial function (Sulzer and Surmeier, 2013, Surmeier, 2018, Surmeier et al., 2017, Pacelli et al., 2015, Guzman et al., 2010, Votyakova and Reynolds, 2001). In addition to mitochondrial stress, the large neuronal arborization is associated with elevated level of A-SYN as a

synaptic protein which augment the potentiality of LP (Surmeier, 2018). Another trait of DAergic neuron of SNpc is their distinctive physiology by which they are characterized by a slow and broad action potential (Surmeier et al., 2012). This feature is associated with intracellular slow Ca^2 oscillation generated by Ca^2 driven to cell through plasma membrane channels or from intracellular ER stores (Chan et al., 2007) and the presence of UPR and ER stress by *GBA* mutations will exacerbate this further. This particular combination of autonomous pace-making with the absence of excitatory synaptic input (Nedergaard et al., 1993, Guzman et al., 2009), the broad and slow spikes of action potential and the low intracellular calcium buffering act collectively as key determinants that render SNpc neurons vulnerable cells and distinguish them from the majority of neurons in the brain (Surmeier, 2018, Surmeier et al., 2017). Accordingly, other brain regions such as cortical pyramidal neurons and AM neurons which are not physiologically phenocopied from SNpc DAergic neurons are therefore considerably resistant to LP and cell death in PD (Surmeier et al., 2017). Dopamine is believed to be an additional accomplice in the distinct phenotype of SNpc in PD (Burbulla and Krainc, 2019). Although a significant amount of oxidative stress is generated producing reactive oxygen species within mitochondria, SNpc neurons are believed to be under additional oxidative stress due to the metabolism of dopamine within them (Burbulla et al., 2017). ROS stress eventually leads to a decrease in ATP production and reduction in efficient protein quality control which affect the functioning of neurons (Reeve et al., 2014, Surmeier et al., 2017). This might explain why in experimental modelling *of GBA*-PD, a combination of stress, in addition to *GBA* mutation is needed, to get neuronal death and PD symptoms.

7.References

ABRAMOV, A. Y., GEGG, M., GRUNEWALD, A., WOOD, N. W., KLEIN, C. & SCHAPIRA, A. H. 2011. Bioenergetic consequences of PINK1 mutations in Parkinson disease. *PLoS One,* 6**,** e25622.

ADEM, A., MATTSSON, M. E. K., NORDBERG, A. & PÅHLMAN, S. 1987. Muscarinic receptors in human SH-SY5Y neuroblastoma cell line: regulation by phorbol ester and retinoic acid-induced differentiation. *Developmental Brain Research,* 33**,** 235-242.

AFLAKI, E., BORGER, D. K., MOAVEN, N., STUBBLEFIELD, B. K., ROGERS, S. A., PATNAIK, S., SCHOENEN, F. J., WESTBROEK, W., ZHENG, W., SULLIVAN, P., FUJIWARA, H., SIDHU, R., KHALIQ, Z. M., LOPEZ, G. J., GOLDSTEIN, D. S., ORY, D. S., MARUGAN, J. & SIDRANSKY, E. 2016. A New Glucocerebrosidase Chaperone Reduces alpha-Synuclein and Glycolipid Levels in iPSC-Derived Dopaminergic Neurons from Patients with Gaucher Disease and Parkinsonism. *J Neurosci,* 36**,** 7441-52.

AHN, K. J., PAIK, S. R., CHUNG, K. C. & KIM, J. 2006. Amino acid sequence motifs and mechanistic features of the membrane translocation of alpha-synuclein. *Journal of neurochemistry,* 97**,** 265-279.

ALAEI, M. R., TABRIZI, A., JAFARI, N. & MOZAFARI, H. 2019. Gaucher Disease: New Expanded Classification Emphasizing Neurological Features. *Iran J Child Neurol,* 13**,** 7-24.

ALCALAY, R. N., LEVY, O. A., WATERS, C. C., FAHN, S., FORD, B., KUO, S. H., MAZZONI, P., PAUCIULO, M. W., NICHOLS, W. C., GAN-OR, Z., ROULEAU, G. A., CHUNG, W. K., WOLF, P., OLIVA, P., KEUTZER, J., MARDER, K. & ZHANG, X. 2015. Glucocerebrosidase activity in Parkinson's disease with and without GBA mutations. *Brain,* 138**,** 2648-58.

ALFARO, I. E., ALBORNOZ, A., MOLINA, A., MORENO, J., CORDERO, K., CRIOLLO, A. & BUDINI, M. 2019. Chaperone Mediated Autophagy in the Crosstalk of Neurodegenerative Diseases and Metabolic Disorders. *Frontiers in Endocrinology,* 9.

ALVAREZ-ERVITI, L., RODRIGUEZ-OROZ, M. C., COOPER, J. M., CABALLERO, C., FERRER, I., OBESO, J. A. & SCHAPIRA, A. H. 2010. Chaperone-mediated autophagy markers in Parkinson disease brains. *Arch Neurol,* 67**,** 1464-72.

ALVAREZ-ERVITI, L., SEOW, Y., SCHAPIRA, A. H., GARDINER, C., SARGENT, I. L., WOOD, M. J. & COOPER, J. M. 2011. Lysosomal dysfunction increases exosome-mediated alpha-synuclein release and transmission. *Neurobiol Dis,* 42**,** 360-7.

AMBROSI, G., GHEZZI, C., SEPE, S., MILANESE, C., PAYAN-GOMEZ, C., BOMBARDIERI, C. R., ARMENTERO, M. T., ZANGAGLIA, R., PACCHETTI, C., MASTROBERARDINO, P. G. & BLANDINI, F. 2014. Bioenergetic and proteolytic defects in fibroblasts from patients with sporadic Parkinson's disease. *Biochim Biophys Acta,* 1842**,** 1385-94.

AMBROSI, G., GHEZZI, C., ZANGAGLIA, R., LEVANDIS, G., PACCHETTI, C. & BLANDINI, F. 2015. Ambroxol-induced rescue of defective glucocerebrosidase is associated with increased LIMP-2 and saposin C levels in GBA1 mutant Parkinson's disease cells. *Neurobiol Dis,* 82**,** 235-242.

AMEN, O. M., SARKER, S. D., GHILDYAL, R. & ARYA, A. 2019. Endoplasmic Reticulum Stress Activates Unfolded Protein Response Signaling and Mediates Inflammation, Obesity, and Cardiac Dysfunction: Therapeutic and Molecular Approach. *Frontiers in Pharmacology,* 10.

ANDERSON, J. P., WALKER, D. E., GOLDSTEIN, J. M., DE LAAT, R., BANDUCCI, K., CACCAVELLO, R. J., BARBOUR, R., HUANG, J., KLING, K., LEE, M., DIEP, L., KEIM, P. S., SHEN, X., CHATAWAY, T., SCHLOSSMACHER, M. G., SEUBERT, P., SCHENK, D., SINHA, S., GAI, W. P. & CHILCOTE, T. J. 2006. Phosphorylation of Ser-129 is the dominant pathological modification of alpha-synuclein in familial and sporadic Lewy body disease. *J Biol Chem,* 281**,** 29739-52.

ANHEIM, M., ELBAZ, A., LESAGE, S., DURR, A., CONDROYER, C., VIALLET, F., POLLAK, P., BONAÏTI, B., BONAÏTI-PELLIÉ, C., BRICE, A. & FRENCH PARKINSON DISEASE GENETIC, G. 2012. Penetrance of Parkinson disease in glucocerebrosidase gene mutation carriers. *Neurology,* 78**,** 417-420.

ARAWAKA, S., SATO, H., SASAKI, A., KOYAMA, S. & KATO, T. 2017. Mechanisms underlying extensive Ser129-phosphorylation in α-synuclein aggregates. *Acta Neuropathologica Communications,* 5**,** 48.

ATHANASSIADOU, A., VOUTSINAS, G., PSIOURI, L., LEROY, E., POLYMEROPOULOS, M. H., ILIAS, A., MANIATIS, G. M. & PAPAPETROPOULOS, T. 1999. Genetic analysis of families with Parkinson disease that carry the Ala53Thr mutation in the gene encoding alpha-synuclein. *Am J Hum Genet,* 65**,** 555-8.

ATIK, A., STEWART, T. & ZHANG, J. 2016. Alpha-Synuclein as a Biomarker for Parkinson's Disease. *Brain Pathol,* 26**,** 410-8.

AUBURGER, G., KLINKENBERG, M., DROST, J., MARCUS, K., MORALES-GORDO, B., KUNZ, W. S., BRANDT, U., BROCCOLI, V., REICHMANN, H., GISPERT, S. & JENDRACH, M. 2012. Primary skin fibroblasts as a model of Parkinson's disease. *Mol Neurobiol,* 46**,** 20-7.

AVENALI, M., BLANDINI, F. & CERRI, S. 2020. Glucocerebrosidase Defects as a Major Risk Factor for Parkinson's Disease. *Frontiers in aging neuroscience,* 12**,** 97-97.

BAE, E. J., YANG, N. Y., LEE, C., LEE, H. J., KIM, S., SARDI, S. P. & LEE, S. J. 2015. Loss of glucocerebrosidase 1 activity causes lysosomal dysfunction and α-synuclein aggregation. *Exp Mol Med,* 47**,** e153.

BALESTRINO, R. & SCHAPIRA, A. H. V. 2018. Glucocerebrosidase and Parkinson Disease: Molecular, Clinical, and Therapeutic Implications. *Neuroscientist,* 24**,** 540-559.

BARDE, Y. A., EDGAR, D. & THOENEN, H. 1982. Purification of a new neurotrophic factor from mammalian brain. *The EMBO journal,* 1**,** 549-553.

BEAL, F. & LANG, A. 2006. The proteasomal inhibition model of Parkinson's disease: "Boon or bust"? *Ann Neurol,* 60**,** 158-61.

BEDFORD, L., HAY, D., DEVOY, A., PAINE, S., POWE, D. G., SETH, R., GRAY, T., TOPHAM, I., FONE, K., REZVANI, N., MEE, M., SOANE, T., LAYFIELD, R., SHEPPARD, P. W., EBENDAL, T., USOSKIN, D., LOWE, J. & MAYER, R. J. 2008. Depletion of 26S proteasomes in mouse brain neurons causes neurodegeneration and Lewy-like inclusions resembling human pale bodies. *J Neurosci,* 28**,** 8189-98.

BENCE, N. F., SAMPAT, R. M. & KOPITO, R. R. 2001. Impairment of the ubiquitin-proteasome system by protein aggregation. *Science,* 292**,** 1552-5.

BENDIKOV-BAR, I., MAOR, G., FILOCAMO, M. & HOROWITZ, M. 2013. Ambroxol as a pharmacological chaperone for mutant glucocerebrosidase. *Blood Cells Mol Dis,* 50**,** 141-5.

BENDIKOV-BAR, I., RON, I., FILOCAMO, M. & HOROWITZ, M. 2011. Characterization of the ERAD process of the L444P mutant glucocerebrosidase variant. *Blood Cells Mol Dis,* 46**,** 4-10.

BENTEA, E., VAN DER PERREN, A., VAN LIEFFERINGE, J., EL ARFANI, A., ALBERTINI, G., DEMUYSER, T., MERCKX, E., MICHOTTE, Y., SMOLDERS, I., BAEKELANDT, V. & MASSIE, A. 2015. Nigral proteasome inhibition in mice leads to motor and non-motor deficits and increased expression of Ser129 phosphorylated α-synuclein. *Front Behav Neurosci,* 9**,** 68.

BENTO, C. F., RENNA, M., GHISLAT, G., PURI, C., ASHKENAZI, A., VICINANZA, M., MENZIES, F. M. & RUBINSZTEIN, D. C. 2016. Mammalian Autophagy: How Does It Work? *Annual Review of Biochemistry,* 85**,** 1-29.

BERG, D., POSTUMA, R. B., BLOEM, B., CHAN, P., DUBOIS, B., GASSER, T., GOETZ, C. G., HALLIDAY, G. M., HARDY, J., LANG, A. E., LITVAN, I., MAREK, K., OBESO, J., OERTEL, W., OLANOW, C. W., POEWE, W., STERN, M. & DEUSCHL, G. 2014. Time to redefine PD? Introductory statement of the MDS Task Force on the definition of Parkinson's disease. *Mov Disord,* 29**,** 454-62.

BERG-FUSSMAN, A., GRACE, M. E., IOANNOU, Y. & GRABOWSKI, G. A. 1993. Human acid beta-glucosidase. N-glycosylation site occupancy and the effect of glycosylation on enzymatic activity. *J Biol Chem,* 268**,** 14861-6.

BETARBET, R., SHERER, T. B., MACKENZIE, G., GARCIA-OSUNA, M., PANOV, A. V. & GREENAMYRE, J. T. 2000. Chronic systemic pesticide exposure reproduces features of Parkinson's disease. *Nat Neurosci,* 3**,** 1301-6.

BIEDLER, J. L., HELSON, L. & SPENGLER, B. A. 1973. Morphology and growth, tumorigenicity, and cytogenetics of human neuroblastoma cells in continuous culture. *Cancer Res,* 33**,** 2643-52.

BIEGSTRAATEN, M., VAN SCHAIK, I. N., AERTS, J. M. F. G. & HOLLAK, C. E. M. 2008. 'Non-neuronopathic' Gaucher disease reconsidered. Prevalence of neurological manifestations in a Dutch cohort of type I Gaucher disease patients and a systematic review of the literature. *Journal of Inherited Metabolic Disease,* 31**,** 337-349.

BLUMENREICH, S., BARAV, O. B., JENKINS, B. J. & FUTERMAN, A. H. 2020. Lysosomal Storage Disorders Shed Light on Lysosomal Dysfunction in Parkinson's Disease. *Int J Mol Sci,* 21.

BORGHI, R., MARCHESE, R., NEGRO, A., MARINELLI, L., FORLONI, G., ZACCHEO, D., ABBRUZZESE, G. & TABATON, M. 2000. Full length alpha-synuclein is present in cerebrospinal fluid from Parkinson's disease and normal subjects. *Neurosci Lett,* 287**,** 65-7.

BRAAK, H., DEL TREDICI, K., RUB, U., DE VOS, R. A., JANSEN STEUR, E. N. & BRAAK, E. 2003. Staging of brain pathology related to sporadic Parkinson's disease. *Neurobiol Aging,* 24**,** 197-211.

BRAUNSTEIN, H., MAOR, G., CHICCO, G., FILOCAMO, M., ZIMRAN, A. & HOROWITZ, M. 2018. UPR activation and CHOP mediated induction of GBA1 transcription in Gaucher disease. *Blood Cells Mol Dis,* 68**,** 21-29.

BRETTSCHNEIDER, J., DEL TREDICI, K., LEE, V. M. & TROJANOWSKI, J. Q. 2015. Spreading of pathology in neurodegenerative diseases: a focus on human studies. *Nat Rev Neurosci,* 16**,** 109-20.

BROCKMANN, K., SRULIJES, K., HAUSER, A. K., SCHULTE, C., CSOTI, I., GASSER, T. & BERG, D. 2011. GBA-associated PD presents with nonmotor characteristics. *Neurology,* 77**,** 276-80.

BURBULLA, L. F. & KRAINC, D. 2019. The role of dopamine in the pathogenesis of GBA1-linked Parkinson's disease. *Neurobiology of Disease,* 132**,** 104545.

BURBULLA, L. F., SONG, P., MAZZULLI, J. R., ZAMPESE, E., WONG, Y. C., JEON, S., SANTOS, D. P., BLANZ, J., OBERMAIER, C. D., STROJNY, C., SAVAS, J. N., KISKINIS, E., ZHUANG, X., KRÜGER, R., SURMEIER, D. J. & KRAINC, D. 2017. Dopamine oxidation mediates mitochondrial and lysosomal dysfunction in Parkinson's disease. *Science,* 357**,** 1255-1261.

C‐S, K., EF, S., N, D., WY, L., EJ, C., J‐Y, K. & A, A. 2007. The Ala53Thr mutation in the α‐synuclein gene in a Korean family with Parkinson disease. *Clinical Genetics,* 71**,** 471-473.

CASSARINO, D. S., PARKS, J. K., PARKER, W. D. & BENNETT, J. P. 1999. The parkinsonian neurotoxin MPP+ opens the mitochondrial permeability transition pore and releases cytochrome c in isolated mitochondria via an oxidative mechanism. *Biochimica et Biophysica Acta (BBA) - Molecular Basis of Disease,* 1453**,** 49-62.

CHALLIS, C., HORI, A., SAMPSON, T. R., YOO, B. B., CHALLIS, R. C., HAMILTON, A. M., MAZMANIAN, S. K., VOLPICELLI-DALEY, L. A. & GRADINARU, V. 2020. Gut-seeded α-synuclein fibrils promote gut dysfunction and brain pathology specifically in aged mice. *Nature Neuroscience,* 23**,** 327-336.

CHAN, C. S., GUZMAN, J. N., ILIJIC, E., MERCER, J. N., RICK, C., TKATCH, T., MEREDITH, G. E. & SURMEIER, D. J. 2007. 'Rejuvenation' protects neurons in mouse models of Parkinson's disease. *Nature,* 447**,** 1081-6.

CHAU, K. Y., CHING, H. L., SCHAPIRA, A. H. & COOPER, J. M. 2009. Relationship between alpha synuclein phosphorylation, proteasomal inhibition and cell death: relevance to Parkinson's disease pathogenesis. *J Neurochem,* 110**,** 1005-13.

CHAU, V., TOBIAS, J. W., BACHMAIR, A., MARRIOTT, D., ECKER, D. J., GONDA, D. K. & VARSHAVSKY, A. 1989. A multiubiquitin chain is confined to specific lysine in a targeted short-lived protein. *Science,* 243**,** 1576-83.

CHEN, L., THIRUCHELVAM, M. J., MADURA, K. & RICHFIELD, E. K. 2006. Proteasome dysfunction in aged human alpha-synuclein transgenic mice. *Neurobiol Dis,* 23**,** 120-6.

CHEN, M. & WANG, J. 2008. Gaucher disease: review of the literature. *Arch Pathol Lab Med,* 132**,** 851-3.

CHENG, X.-Y., BISWAS, S., LI, J., MAO, C.-J., CHECHNEVA, O., CHEN, J., LI, K., LI, J., ZHANG, J.-R., LIU, C.-F. & DENG, W.-B. 2020. Human iPSCs derived astrocytes rescue rotenone-induced mitochondrial dysfunction and dopaminergic neurodegeneration in vitro by donating functional mitochondria. *Translational Neurodegeneration,* 9**,** 13.

CHEUNG, Y. T., LAU, W. K., YU, M. S., LAI, C. S., YEUNG, S. C., SO, K. F. & CHANG, R. C. 2009. Effects of all-trans-retinoic acid on human SH-SY5Y neuroblastoma as in vitro model in neurotoxicity research. *Neurotoxicology,* 30**,** 127-35.

CHIASSERINI, D., PACIOTTI, S., EUSEBI, P., PERSICHETTI, E., TASEGIAN, A., KURZAWA-AKANBI, M., CHINNERY, P. F., MORRIS, C. M., CALABRESI, P., PARNETTI, L. & BECCARI, T. 2015. Selective loss of glucocerebrosidase activity in sporadic Parkinson's disease and dementia with Lewy bodies. *Mol Neurodegener,* 10**,** 15.

CHOI, J. M., WOO, M. S., MA, H. I., KANG, S. Y., SUNG, Y. H., YONG, S. W., CHUNG, S. J., KIM, J. S., SHIN, H. W., LYOO, C. H., LEE, P. H., BAIK, J. S., KIM, S. J., PARK, M. Y., SOHN, Y. H., KIM, J. H., KIM, J. W., LEE, M. S., LEE, M. C., KIM, D. H. & KIM, Y. J. 2008. Analysis of PARK genes in a Korean cohort of early-onset Parkinson disease. *Neurogenetics,* 9**,** 263-9.

CHU, Y., DODIYA, H., AEBISCHER, P., OLANOW, C. W. & KORDOWER, J. H. 2009. Alterations in lysosomal and proteasomal markers in Parkinson's disease: relationship to alpha-synuclein inclusions. *Neurobiol Dis,* 35**,** 385-98.

CHUN, Y. & KIM, J. 2018. Autophagy: An Essential Degradation Program for Cellular Homeostasis and Life. *Cells,* 7.

CIECHANOVER, A. 2006. The ubiquitin proteolytic system: from a vague idea, through basic mechanisms, and onto human diseases and drug targeting. *Neurology,* 66**,** S7-19.

CIECHANOVER, A. & KWON, Y. T. 2015. Degradation of misfolded proteins in neurodegenerative diseases: therapeutic targets and strategies. *Exp Mol Med,* 47**,** e147.

CILIA, R., TUNESI, S., MAROTTA, G., CEREDA, E., SIRI, C., TESEI, S., ZECCHINELLI, A. L., CANESI, M., MARIANI, C. B., MEUCCI, N., SACILOTTO, G., ZINI, M., BARICHELLA, M., MAGNANI, C., DUGA, S., ASSELTA, R., SOLDA, G., SERESINI, A., SEIA, M., PEZZOLI, G. & GOLDWURM, S. 2016. Survival and dementia in GBA-associated Parkinson's disease: The mutation matters. *Ann Neurol,* 80**,** 662-673.

CLEETER, M. W., CHAU, K. Y., GLUCK, C., MEHTA, A., HUGHES, D. A., DUCHEN, M., WOOD, N. W., HARDY, J., MARK COOPER, J. & SCHAPIRA, A. H. 2013. Glucocerebrosidase inhibition causes mitochondrial dysfunction and free radical damage. *Neurochem Int,* 62**,** 1-7.

COLLA, E. 2019. Linking the Endoplasmic Reticulum to Parkinson’s Disease and Alpha-Synucleinopathy. *Frontiers in Neuroscience,* 13.

COLLA, E., JENSEN, P. H., PLETNIKOVA, O., TRONCOSO, J. C., GLABE, C. & LEE, M. K. 2012. Accumulation of toxic α-synuclein oligomer within endoplasmic reticulum occurs in α-synucleinopathy in vivo. *J Neurosci,* 32**,** 3301-5.

COLLINS, G. A. & GOLDBERG, A. L. 2017. The Logic of the 26S Proteasome. *Cell,* 169**,** 792-806.
COLLINS, L. M., DROUIN-OUELLET, J., KUAN, W. L., COX, T. & BARKER, R. A. 2017. Dermal fibroblasts from patients with Parkinson's disease have normal GCase activity and autophagy compared to patients with PD and GBA mutations. *F1000Res,* 6**,** 1751.
CONRADI, N. G., SOURANDER, P., NILSSON, O., SVENNERHOLM, L. & ERIKSON, A. 1984. Neuropathology of the Norrbottnian type of Gaucher disease. Morphological and biochemical studies. *Acta Neuropathol,* 65**,** 99-109.
CONSTANTINESCU, R., CONSTANTINESCU, A. T., REICHMANN, H. & JANETZKY, B. 2007. Neuronal differentiation and long-term culture of the human neuroblastoma line SH-SY5Y. *J Neural Transm Suppl***,** 17-28.
COOKSON, M. R. 2012. Parkinsonism due to mutations in PINK1, parkin, and DJ-1 and oxidative stress and mitochondrial pathways. *Cold Spring Harb Perspect Med,* 2**,** a009415.
COURTE, J., BOUSSET, L., BOXBERG, Y. V., VILLARD, C., MELKI, R. & PEYRIN, J.-M. 2020. The expression level of alpha-synuclein in different neuronal populations is the primary determinant of its prion-like seeding. *Scientific Reports,* 10**,** 4895.
COUX, O., TANAKA, K. & GOLDBERG, A. L. 1996. Structure and functions of the 20S and 26S proteasomes. *Annu Rev Biochem,* 65**,** 801-47.
CUERVO, A. M., HILDEBRAND, H., BOMHARD, E. M. & DICE, J. F. 1999. Direct lysosomal uptake of alpha 2-microglobulin contributes to chemically induced nephropathy. *Kidney Int,* 55**,** 529-45.
CUERVO, A. M., STEFANIS, L., FREDENBURG, R., LANSBURY, P. T. & SULZER, D. 2004. Impaired degradation of mutant alpha-synuclein by chaperone-mediated autophagy. *Science,* 305**,** 1292-5.
CUERVO, A. M. & WONG, E. 2014. Chaperone-mediated autophagy: roles in disease and aging. *Cell Research,* 24**,** 92-104.
CULLEN, V., SARDI, S. P., NG, J., XU, Y. H., SUN, Y., TOMLINSON, J. J., KOLODZIEJ, P., KAHN, I., SAFTIG, P., WOULFE, J., ROCHET, J. C., GLICKSMAN, M. A., CHENG, S. H., GRABOWSKI, G. A., SHIHABUDDIN, L. S. & SCHLOSSMACHER, M. G. 2011. Acid beta-glucosidase mutants linked to Gaucher disease, Parkinson disease, and Lewy body dementia alter alpha-synuclein processing. *Ann Neurol,* 69**,** 940-53.
DAMIER, P., HIRSCH, E. C., AGID, Y. & GRAYBIEL, A. M. 1999. The substantia nigra of the human brain. II. Patterns of loss of dopamine-containing neurons in Parkinson's disease. *Brain,* 122 (Pt 8)**,** 1437-48.
DANZER, K. M., KRANICH, L. R., RUF, W. P., CAGSAL-GETKIN, O., WINSLOW, A. R., ZHU, L., VANDERBURG, C. R. & MCLEAN, P. J. 2012. Exosomal cell-to-cell transmission of alpha synuclein oligomers. *Mol Neurodegener,* 7**,** 42.
DAUER, W. & PRZEDBORSKI, S. 2003. Parkinson's disease: mechanisms and models. *Neuron,* 39**,** 889-909.
DAVIE, C. A. 2008. A review of Parkinson's disease. *Br Med Bull,* 86**,** 109-27.
DE LA MATA, M., COTAN, D., OROPESA-AVILA, M., GARRIDO-MARAVER, J., CORDERO, M. D., VILLANUEVA PAZ, M., DELGADO PAVON, A., ALCOCER-GOMEZ, E., DE LAVERA, I., YBOT-GONZALEZ, P., PAULA ZADERENKO, A., ORTIZ MELLET, C., GARCIA FERNANDEZ, J. M. &

SANCHEZ-ALCAZAR, J. A. 2015. Pharmacological Chaperones and Coenzyme Q10 Treatment Improves Mutant beta-Glucocerebrosidase Activity and Mitochondrial Function in Neuronopathic Forms of Gaucher Disease. *Sci Rep,* 5**,** 10903.

DE LA MATA, M., COTÁN, D., VILLANUEVA-PAZ, M., DE LAVERA, I., ÁLVAREZ-CÓRDOBA, M., LUZÓN-HIDALGO, R., SUÁREZ-RIVERO, J. M., TISCORNIA, G. & OROPESA-ÁVILA, M. 2016. Mitochondrial Dysfunction in Lysosomal Storage Disorders. *Diseases,* 4.

DEHAY, B., BOVÉ, J., RODRÍGUEZ-MUELA, N., PERIER, C., RECASENS, A., BOYA, P. & VILA, M. 2010. Pathogenic lysosomal depletion in Parkinson's disease. *J Neurosci,* 30**,** 12535-44.

DEHAY, B., MARTINEZ-VICENTE, M., CALDWELL, G. A., CALDWELL, K. A., YUE, Z., COOKSON, M. R., KLEIN, C., VILA, M. & BEZARD, E. 2013. Lysosomal impairment in Parkinson's disease. *Mov Disord,* 28**,** 725-32.

DEHAY, B., RAMIREZ, A., MARTINEZ-VICENTE, M., PERIER, C., CANRON, M. H., DOUDNIKOFF, E., VITAL, A., VILA, M., KLEIN, C. & BEZARD, E. 2012. Loss of P-type ATPase ATP13A2/PARK9 function induces general lysosomal deficiency and leads to Parkinson disease neurodegeneration. *Proc Natl Acad Sci U S A,* 109**,** 9611-6.

DEINHARDT, K. & CHAO, M. V. 2014. Shaping neurons: Long and short range effects of mature and proBDNF signalling upon neuronal structure. *Neuropharmacology,* 76 Pt C**,** 603-9.

DEPAOLO, J., GOKER-ALPAN, O., SAMADDAR, T., LOPEZ, G. & SIDRANSKY, E. 2009. The association between mutations in the lysosomal protein glucocerebrosidase and parkinsonism. *Mov Disord,* 24**,** 1571-8.

DERMENTZAKI, G., DIMITRIOU, E., XILOURI, M., MICHELAKAKIS, H. & STEFANIS, L. 2013. Loss of beta-glucocerebrosidase activity does not affect alpha-synuclein levels or lysosomal function in neuronal cells. *PLoS One,* 8**,** e60674.

DESPLATS, P., LEE, H.-J., BAE, E.-J., PATRICK, C., ROCKENSTEIN, E., CREWS, L., SPENCER, B., MASLIAH, E. & LEE, S.-J. 2009. Inclusion formation and neuronal cell death through neuron-to-neuron transmission of α-synuclein. *Proceedings of the National Academy of Sciences,* 106**,** 13010.

DÍAZ-VILLANUEVA, J. F., DÍAZ-MOLINA, R. & GARCÍA-GONZÁLEZ, V. 2015. Protein Folding and Mechanisms of Proteostasis. *Int J Mol Sci,* 16**,** 17193-230.

DICE, J. F. 1990. Peptide sequences that target cytosolic proteins for lysosomal proteolysis. *Trends Biochem Sci,* 15**,** 305-9.

DORSEY, E. R., CONSTANTINESCU, R., THOMPSON, J. P., BIGLAN, K. M., HOLLOWAY, R. G., KIEBURTZ, K., MARSHALL, F. J., RAVINA, B. M., SCHIFITTO, G., SIDEROWF, A. & TANNER, C. M. 2007. Projected number of people with Parkinson disease in the most populous nations, 2005 through 2030. *Neurology,* 68**,** 384-6.

DUBNIKOV, T. & COHEN, E. 2017. The Emerging Roles of Early Protein Folding Events in the Secretory Pathway in the Development of Neurodegenerative Maladies. *Frontiers in Neuroscience,* 11.

DUBOIS, C., KONDRATSKYI, A., BIDAUX, G., NOYER, L., VANCAUWENBERGHE, E., FARFARIELLO, V., TOILLON, R.-A., ROUDBARAKI, M., TIERNY, D., BONNAL, J.-L., PREVARSKAYA, N. &

VANDEN ABEELE, F. 2020. Co-targeting Mitochondrial Ca2+ Homeostasis and Autophagy Enhances Cancer Cells' Chemosensitivity. *iScience,* 23**,** 101263.

DURAN, R., MENCACCI, N. E., ANGELI, A. V., SHOAI, M., DEAS, E., HOULDEN, H., MEHTA, A., HUGHES, D., COX, T. M., DEEGAN, P., SCHAPIRA, A. H., LEES, A. J., LIMOUSIN, P., JARMAN, P. R., BHATIA, K. P., WOOD, N. W., HARDY, J. & FOLTYNIE, T. 2013. The glucocerobrosidase E326K variant predisposes to Parkinson's disease, but does not cause Gaucher's disease. *Mov Disord,* 28**,** 232-236.

DWANE, S., DURACK, E. & KIELY, P. A. 2013. Optimising parameters for the differentiation of SH-SY5Y cells to study cell adhesion and cell migration. *BMC Res Notes,* 6**,** 366.

EL-AGNAF, O. M., SALEM, S. A., PALEOLOGOU, K. E., COOPER, L. J., FULLWOOD, N. J., GIBSON, M. J., CURRAN, M. D., COURT, J. A., MANN, D. M., IKEDA, S., COOKSON, M. R., HARDY, J. & ALLSOP, D. 2003. Alpha-synuclein implicated in Parkinson's disease is present in extracellular biological fluids, including human plasma. *Faseb j,* 17**,** 1945-7.

EMMANOUILIDOU, E., STEFANIS, L. & VEKRELLIS, K. 2010. Cell-produced alpha-synuclein oligomers are targeted to, and impair, the 26S proteasome. *Neurobiol Aging,* 31**,** 953-68.

ENCINAS, M., IGLESIAS, M., LIU, Y., WANG, H., MUHAISEN, A., CENA, V., GALLEGO, C. & COMELLA, J. X. 2000. Sequential treatment of SH-SY5Y cells with retinoic acid and brain-derived neurotrophic factor gives rise to fully differentiated, neurotrophic factor-dependent, human neuron-like cells. *J Neurochem,* 75**,** 991-1003.

FAHN, S. & SULZER, D. 2004. Neurodegeneration and neuroprotection in Parkinson disease. *NeuroRx,* 1**,** 139-54.

FALKENBURGER, B. H. & SCHULZ, J. B. 2006. Limitations of cellular models in Parkinson's disease research. *J Neural Transm Suppl***,** 261-8.

FAROOQUI, S. M. 1994. Induction of adenylate cyclase sensitive dopamine D2-receptors in retinoic acid induced differentiated human neuroblastoma SHSY-5Y cells. *Life Sci,* 55**,** 1887-93.

FENG, Y., LIANG, Z. H., WANG, T., QIAO, X., LIU, H. J. & SUN, S. G. 2006. alpha-Synuclein redistributed and aggregated in rotenone-induced Parkinson's disease rats. *Neurosci Bull,* 22**,** 288-93.

FERNANDES, H. J., HARTFIELD, E. M., CHRISTIAN, H. C., EMMANOULIDOU, E., ZHENG, Y., BOOTH, H., BOGETOFTE, H., LANG, C., RYAN, B. J., SARDI, S. P., BADGER, J., VOWLES, J., EVETTS, S., TOFARIS, G. K., VEKRELLIS, K., TALBOT, K., HU, M. T., JAMES, W., COWLEY, S. A. & WADE-MARTINS, R. 2016. ER Stress and Autophagic Perturbations Lead to Elevated Extracellular alpha-Synuclein in GBA-N370S Parkinson's iPSC-Derived Dopamine Neurons. *Stem Cell Reports,* 6**,** 342-56.

FERREIRA, C. R. & GAHL, W. A. 2017. Lysosomal storage diseases. *Transl Sci Rare Dis,* 2**,** 1-71.

FERREIRA, M. & MASSANO, J. 2017. An updated review of Parkinson's disease genetics and clinicopathological correlations. *Acta Neurol Scand,* 135**,** 273-284.

FISHBEIN, I., KUO, Y. M., GIASSON, B. I. & NUSSBAUM, R. L. 2014. Augmentation of phenotype in a transgenic Parkinson mouse heterozygous for a Gaucher mutation. *Brain,* 137**,** 3235-47.

FUJIWARA, H., HASEGAWA, M., DOHMAE, N., KAWASHIMA, A., MASLIAH, E., GOLDBERG, M. S., SHEN, J., TAKIO, K. & IWATSUBO, T. 2002. alpha-Synuclein is phosphorylated in synucleinopathy lesions. *Nat Cell Biol,* 4**,** 160-4.

FUSSI, N., HÖLLERHAGE, M., CHAKROUN, T., NYKÄNEN, N.-P., RÖSLER, T. W., KOEGLSPERGER, T., WURST, W., BEHRENDS, C. & HÖGLINGER, G. U. 2018. Exosomal secretion of α-synuclein as protective mechanism after upstream blockage of macroautophagy. *Cell Death & Disease,* 9**,** 757.

GAN-OR, Z., AMSHALOM, I., KILARSKI, L. L., BAR-SHIRA, A., GANA-WEISZ, M., MIRELMAN, A., MARDER, K., BRESSMAN, S., GILADI, N. & ORR-URTREGER, A. 2015. Differential effects of severe vs mild GBA mutations on Parkinson disease. *Neurology,* 84**,** 880-7.

GAN-OR, Z., GILADI, N. & ORR-URTREGER, A. 2009. Differential phenotype in Parkinson's disease patients with severe versus mild GBA mutations. *Brain,* 132**,** e125-e125.

GARCIA-SANZ, P., ORGAZ, L., BUENO-GIL, G., ESPADAS, I., RODRIGUEZ-TRAVER, E., KULISEVSKY, J., GUTIERREZ, A., DAVILA, J. C., GONZALEZ-POLO, R. A., FUENTES, J. M., MIR, P., VICARIO, C. & MORATALLA, R. 2017. N370S-GBA1 mutation causes lysosomal cholesterol accumulation in Parkinson's disease. *Mov Disord,* 32**,** 1409-1422.

GASSER, T. 2009. Mendelian forms of Parkinson's disease. *Biochim Biophys Acta,* 1792**,** 587-96.

GEGG, M. 2020. *RE: Detection of GBA protein expression in mouse cortical neurons*

GEGG, M. E., BURKE, D., HEALES, S. J., COOPER, J. M., HARDY, J., WOOD, N. W. & SCHAPIRA, A. H. 2012. Glucocerebrosidase deficiency in substantia nigra of parkinson disease brains. *Ann Neurol,* 72**,** 455-63.

GEGG, M. E., COOPER, J. M., CHAU, K. Y., ROJO, M., SCHAPIRA, A. H. & TAANMAN, J. W. 2010. Mitofusin 1 and mitofusin 2 are ubiquitinated in a PINK1/parkin-dependent manner upon induction of mitophagy. *Hum Mol Genet,* 19**,** 4861-70.

GEGG, M. E. & SCHAPIRA, A. H. 2016. Mitochondrial dysfunction associated with glucocerebrosidase deficiency. *Neurobiol Dis,* 90**,** 43-50.

GEGG, M. E. & SCHAPIRA, A. H. V. 2018. The role of glucocerebrosidase in Parkinson disease pathogenesis. *Febs j*.

GEGG, M. E., VERONA, G. & SCHAPIRA, A. H. V. 2020. Glucocerebrosidase deficiency promotes release of α-synuclein fibrils from cultured neurons. *Human Molecular Genetics*.

GHEE, M., FOURNIER, A. & MALLET, J. 2000. Rat alpha-synuclein interacts with Tat binding protein 1, a component of the 26S proteasomal complex. *J Neurochem,* 75**,** 2221-4.

GHIDONI, R., BENUSSI, L. & BINETTI, G. 2008. Exosomes: the Trojan horses of neurodegeneration. *Med Hypotheses,* 70**,** 1226-7.

GOKER-ALPAN, O., GIASSON, B. I., EBLAN, M. J., NGUYEN, J., HURTIG, H. I., LEE, V. M., TROJANOWSKI, J. Q. & SIDRANSKY, E. 2006.

Glucocerebrosidase mutations are an important risk factor for Lewy body disorders. *Neurology,* 67**,** 908-10.
GOKER-ALPAN, O., MASDEU, J. C., KOHN, P. D., IANNI, A., LOPEZ, G., GRODEN, C., CHAPMAN, M. C., CROPP, B., EISENBERG, D. P., MANIWANG, E. D., DAVIS, J., WIGGS, E., SIDRANSKY, E. & BERMAN, K. F. 2012. The neurobiology of glucocerebrosidase-associated parkinsonism: a positron emission tomography study of dopamine synthesis and regional cerebral blood flow. *Brain,* 135**,** 2440-8.
GOKER-ALPAN, O., SCHIFFMANN, R., LAMARCA, M. E., NUSSBAUM, R. L., MCINERNEY-LEO, A. & SIDRANSKY, E. 2004. Parkinsonism among Gaucher disease carriers. *J Med Genet,* 41**,** 937-40.
GOKER-ALPAN, O., SCHIFFMANN, R., PARK, J. K., STUBBLEFIELD, B. K., TAYEBI, N. & SIDRANSKY, E. 2003. Phenotypic continuum in neuronopathic gaucher disease: an intermediate phenotype between type 2 and type 3. *The Journal of Pediatrics,* 143**,** 273-276.
GOKER-ALPAN, O., STUBBLEFIELD, B. K., GIASSON, B. I. & SIDRANSKY, E. 2010. Glucocerebrosidase is present in alpha-synuclein inclusions in Lewy body disorders. *Acta Neuropathol,* 120**,** 641-9.
GOLDIN, E. 2010. Gaucher disease and parkinsonism, a molecular link theory. *Mol Genet Metab,* 101**,** 307-10.
GRABOWSKI, G. A. 2008. Phenotype, diagnosis, and treatment of Gaucher's disease. *Lancet,* 372**,** 1263-71.
GRASSI, D., HOWARD, S., ZHOU, M., DIAZ-PEREZ, N., URBAN, N. T., GUERRERO-GIVEN, D., KAMASAWA, N., VOLPICELLI-DALEY, L. A., LOGRASSO, P. & LASMEZAS, C. I. 2018. Identification of a highly neurotoxic alpha-synuclein species inducing mitochondrial damage and mitophagy in Parkinson's disease. *Proc Natl Acad Sci U S A,* 115**,** E2634-e2643.
GRÜNEWALD, A., KUMAR, K. R. & SUE, C. M. 2019. New insights into the complex role of mitochondria in Parkinson's disease. *Progress in Neurobiology,* 177**,** 73-93.
GUO, J. D., ZHAO, X., LI, Y., LI, G. R. & LIU, X. L. 2018. Damage to dopaminergic neurons by oxidative stress in Parkinson's disease (Review). *Int J Mol Med,* 41**,** 1817-1825.
GUZMAN, J. N., SÁNCHEZ-PADILLA, J., CHAN, C. S. & SURMEIER, D. J. 2009. Robust pacemaking in substantia nigra dopaminergic neurons. *J Neurosci,* 29**,** 11011-9.
GUZMAN, J. N., SANCHEZ-PADILLA, J., WOKOSIN, D., KONDAPALLI, J., ILIJIC, E., SCHUMACKER, P. T. & SURMEIER, D. J. 2010. Oxidant stress evoked by pacemaking in dopaminergic neurons is attenuated by DJ-1. *Nature,* 468**,** 696-700.
HALPERIN, A., ELSTEIN, D. & ZIMRAN, A. 2006. Increased incidence of Parkinson disease among relatives of patients with Gaucher disease. *Blood Cells Mol Dis,* 36**,** 426-8.
HAN, F., GRIMES, D. A., LI, F., WANG, T., YU, Z., SONG, N., WU, S., RACACHO, L. & BULMAN, D. E. 2016. Mutations in the glucocerebrosidase gene are common in patients with Parkinson's disease from Eastern Canada. *Int J Neurosci,* 126**,** 415-21.
HARTFIELD, E. M., YAMASAKI-MANN, M., RIBEIRO FERNANDES, H. J., VOWLES, J., JAMES, W. S., COWLEY, S. A. & WADE-MARTINS, R.

2014. Physiological characterisation of human iPS-derived dopaminergic neurons. *PLoS One,* 9**,** e87388.

HASEGAWA, T., KONNO, M., BABA, T., SUGENO, N., KIKUCHI, A., KOBAYASHI, M., MIURA, E., TANAKA, N., TAMAI, K., FURUKAWA, K., ARAI, H., MORI, F., WAKABAYASHI, K., AOKI, M., ITOYAMA, Y. & TAKEDA, A. 2011. The AAA-ATPase VPS4 regulates extracellular secretion and lysosomal targeting of alpha-synuclein. *PLoS One,* 6**,** e29460.

HASEGAWA, T., MATSUZAKI, M., TAKEDA, A., KIKUCHI, A., AKITA, H., PERRY, G., SMITH, M. A. & ITOYAMA, Y. 2004. Accelerated alpha-synuclein aggregation after differentiation of SH-SY5Y neuroblastoma cells. *Brain Res,* 1013**,** 51-9.

HENDERSON, M. X., CORNBLATH, E. J., DARWICH, A., ZHANG, B., BROWN, H., GATHAGAN, R. J., SANDLER, R. M., BASSETT, D. S., TROJANOWSKI, J. Q. & LEE, V. M. Y. 2019. Spread of α-synuclein pathology through the brain connectome is modulated by selective vulnerability and predicted by network analysis. *Nature Neuroscience,* 22**,** 1248-1257.

HENDERSON, M. X., SEDOR, S., MCGEARY, I., CORNBLATH, E. J., PENG, C., RIDDLE, D. M., LI, H. L., ZHANG, B., BROWN, H. J., OLUFEMI, M. F., BASSETT, D. S., TROJANOWSKI, J. Q. & LEE, V. M. Y. 2020. Glucocerebrosidase Activity Modulates Neuronal Susceptibility to Pathological α-Synuclein Insult. *Neuron,* 105**,** 822-836.e7.

HERSHKO, A. & CIECHANOVER, A. 1998. The ubiquitin system. *Annu Rev Biochem,* 67**,** 425-79.

HETZ, C., ZHANG, K. & KAUFMAN, R. J. 2020. Mechanisms, regulation and functions of the unfolded protein response. *Nature Reviews Molecular Cell Biology,* 21**,** 421-438.

HIDESHIMA, T., BRADNER, J. E., CHAUHAN, D. & ANDERSON, K. C. 2005. Intracellular protein degradation and its therapeutic implications. *Clin Cancer Res,* 11**,** 8530-3.

HIRSCH, E. C. & HUNOT, S. 2009. Neuroinflammation in Parkinson's disease: a target for neuroprotection? *Lancet Neurol,* 8**,** 382-97.

HOCHSTRASSER, M. 1996. Ubiquitin-dependent protein degradation. *Annu Rev Genet,* 30**,** 405-39.

HOEPKEN, H. H., GISPERT, S., AZIZOV, M., KLINKENBERG, M., RICCIARDI, F., KURZ, A., MORALES-GORDO, B., BONIN, M., RIESS, O., GASSER, T., KOGEL, D., STEINMETZ, H. & AUBURGER, G. 2008. Parkinson patient fibroblasts show increased alpha-synuclein expression. *Exp Neurol,* 212**,** 307-13.

HOROWITZ, M., PASMANIK-CHOR, M., RON, I. & KOLODNY, E. H. 2011. The enigma of the E326K mutation in acid beta-glucocerebrosidase. *Mol Genet Metab,* 104**,** 35-8.

HRUSKA, K. S., LAMARCA, M. E., SCOTT, C. R. & SIDRANSKY, E. 2008. Gaucher disease: mutation and polymorphism spectrum in the glucocerebrosidase gene (GBA). *Hum Mutat,* 29**,** 567-83.

HRUSKA, K. S., LAMARCA, M. E. & SIDRANSKY, E. 2006. *Gaucher disease: molecular biology and genotype-phenotype correlations*.

HUEBECKER, M., MOLONEY, E. B., VAN DER SPOEL, A. C., PRIESTMAN, D. A., ISACSON, O., HALLETT, P. J. & PLATT, F. M. 2019. Reduced

sphingolipid hydrolase activities, substrate accumulation and ganglioside decline in Parkinson's disease. *Mol Neurodegener,* 14**,** 40.
HUSE, D. M., SCHULMAN, K., ORSINI, L., CASTELLI-HALEY, J., KENNEDY, S. & LENHART, G. 2005. Burden of illness in Parkinson's disease. *Mov Disord,* 20**,** 1449-54.
HYMAN, C., HOFER, M., BARDE, Y. A., JUHASZ, M., YANCOPOULOS, G. D., SQUINTO, S. P. & LINDSAY, R. M. 1991. BDNF is a neurotrophic factor for dopaminergic neurons of the substantia nigra. *Nature,* 350**,** 230-2.
IKEDA, F. & DIKIC, I. 2008. Atypical ubiquitin chains: new molecular signals. 'Protein Modifications: Beyond the Usual Suspects' review series. *EMBO Rep,* 9**,** 536-42.
ISSA, A. R., SUN, J., PETITGAS, C., MESQUITA, A., DULAC, A., ROBIN, M., MOLLEREAU, B., JENNY, A., CHÉRIF-ZAHAR, B. & BIRMAN, S. 2018. The lysosomal membrane protein LAMP2A promotes autophagic flux and prevents SNCA-induced Parkinson disease-like symptoms in the Drosophila brain. *Autophagy,* 14**,** 1898-1910.
IURLARO, R. & MUÑOZ-PINEDO, C. 2016. Cell death induced by endoplasmic reticulum stress. *Febs j,* 283**,** 2640-52.
IZCO, M., BLESA, J., SCHLEEF, M., SCHMEER, M., PORCARI, R., AL-SHAWI, R., ELLMERICH, S., DE TORO, M., GARDINER, C., SEOW, Y., REINARES-SEBASTIAN, A., FORCEN, R., SIMONS, J. P., BELLOTTI, V., COOPER, J. M. & ALVAREZ-ERVITI, L. 2019. Systemic Exosomal Delivery of shRNA Minicircles Prevents Parkinsonian Pathology. *Mol Ther,* 27**,** 2111-2122.
JANG, A., LEE, H. J., SUK, J. E., JUNG, J. W., KIM, K. P. & LEE, S. J. 2010. Non-classical exocytosis of alpha-synuclein is sensitive to folding states and promoted under stress conditions. *J Neurochem,* 113**,** 1263-74.
JUÁREZ-FLORES, D. L., GONZÁLEZ-CASACUBERTA, I., EZQUERRA, M., BAÑÓ, M., CARMONA-PONTAQUE, F., CATALÁN-GARCÍA, M., GUITART-MAMPEL, M., RIVERO, J. J., TOBIAS, E., MILISENDA, J. C., TOLOSA, E., MARTI, M. J., FERNÁNDEZ-SANTIAGO, R., CARDELLACH, F., MORÉN, C. & GARRABOU, G. 2018. Exhaustion of mitochondrial and autophagic reserve may contribute to the development of LRRK2G2019S-Parkinson’s disease. *Journal of Translational Medicine,* 16**,** 160.
JUSTE, Y. R. & CUERVO, A. M. 2019. Analysis of Chaperone-Mediated Autophagy. *Methods Mol Biol,* 1880**,** 703-727.
KALIA, L. V. & LANG, A. E. 2015. Parkinson's disease. *Lancet,* 386**,** 896-912.
KAPLAN, D. R., MATSUMOTO, K., LUCARELLI, E. & THIELE, C. J. 1993. Induction of TrkB by retinoic acid mediates biologic responsiveness to BDNF and differentiation of human neuroblastoma cells. Eukaryotic Signal Transduction Group. *Neuron,* 11**,** 321-31.
KARPOWICZ, R. J., JR., TROJANOWSKI, J. Q. & LEE, V. M. 2019. Transmission of α-synuclein seeds in neurodegenerative disease: recent developments. *Lab Invest,* 99**,** 971-981.
KASTNER, A., HIRSCH, E. C., AGID, Y. & JAVOY-AGID, F. 1993. Tyrosine hydroxylase protein and messenger RNA in the dopaminergic nigral neurons of patients with Parkinson's disease. *Brain Res,* 606**,** 341-5.
KILPATRICK, B. S., MAGALHAES, J., BEAVAN, M. S., MCNEILL, A., GEGG, M. E., CLEETER, M. W. J., BLOOR-YOUNG, D., CHURCHILL, G. C.,

DUCHEN, M. R., SCHAPIRA, A. H. & PATEL, S. 2016. Endoplasmic reticulum and lysosomal Ca2+ stores are remodelled in GBA1-linked Parkinson disease patient fibroblasts. *Cell Calcium,* 59**,** 12-20.

KIM, S., KWON, S. H., KAM, T. I., PANICKER, N., KARUPPAGOUNDER, S. S., LEE, S., LEE, J. H., KIM, W. R., KOOK, M., FOSS, C. A., SHEN, C., LEE, H., KULKARNI, S., PASRICHA, P. J., LEE, G., POMPER, M. G., DAWSON, V. L., DAWSON, T. M. & KO, H. S. 2019. Transneuronal Propagation of Pathologic α-Synuclein from the Gut to the Brain Models Parkinson's Disease. *Neuron,* 103**,** 627-641.e7.

KITADA, T., ASAKAWA, S., HATTORI, N., MATSUMINE, H., YAMAMURA, Y., MINOSHIMA, S., YOKOCHI, M., MIZUNO, Y. & SHIMIZU, N. 1998. Mutations in the parkin gene cause autosomal recessive juvenile parkinsonism. *Nature,* 392**,** 605.

KLEIN, C. & WESTENBERGER, A. 2012. Genetics of Parkinson's disease. *Cold Spring Harb Perspect Med,* 2**,** a008888.

KLIONSKY, D. J., ABELIOVICH, H., AGOSTINIS, P., AGRAWAL, D. K., ALIEV, G., ASKEW, D. S., BABA, M., BAEHRECKE, E. H., BAHR, B. A., BALLABIO, A., BAMBER, B. A., BASSHAM, D. C., BERGAMINI, E., BI, X., BIARD-PIECHACZYK, M., BLUM, J. S., BREDESEN, D. E., BRODSKY, J. L., BRUMELL, J. H., BRUNK, U. T., BURSCH, W., CAMOUGRAND, N., CEBOLLERO, E., CECCONI, F., CHEN, Y., CHIN, L.-S., CHOI, A., CHU, C. T., CHUNG, J., CLARK, R. S. B., CLARKE, P. G. H., CLARKE, S. G., CLAVE, C., CLEVELAND, J. L., CODOGNO, P., COLOMBO, M. I., COTO-MONTES, A., CREGG, J. M., CUERVO, A. M., DEBNATH, J., DENNIS, P. B., DENNIS, P. A., DEMARCHI, F., DERETIC, V., DEVENISH, R. J., DI SANO, F., DICE, J. F., DISTELHORST, C. W., DINESH-KUMAR, S. P., EISSA, N. T., DIFIGLIA, M., DJAVAHERI-MERGNY, M., DORSEY, F. C., DRÖGE, W., DRON, M., DUNN, J. W. A., DUSZENKO, M., ELAZAR, Z., ESCLATINE, A., ESKELINEN, E.-L., FÉSÜS, L., FINLEY, K. D., FUENTES, J. M., FUEYO-MARGARETO, J., FUJISAKI, K., GALLIOT, B., GAO, F.-B., GEWIRTZ, D. A., GIBSON, S. B., GOHLA, A., GOLDBERG, A. L., GONZALEZ, R., GONZÁLEZ-ESTÉVEZ, C., GORSKI, S. M., GOTTLIEB, R. A., HÄUSSINGER, D., HE, Y.-W., HEIDENREICH, K., HILL, J. A., HØYER-HANSEN, M., HU, X., HUANG, W.-P., IWASAKI, A., JÄÄTTELÄ, M., JACKSON, W. T., JIANG, X., JIN, S. V., JOHANSEN, T., JUNG, J. U., KADOWAKI, M., KANG, C., KELEKAR, A., KESSEL, D. H., KIEL, J. A. K. W., KIM, H. P., KIMCHI, A., KINSELLA, T. J., KISELYOV, K., KITAMOTO, K., KNECHT, E., et al. 2008. Guidelines for the use and interpretation of assays for monitoring autophagy in higher eukaryotes. *Autophagy,* 4**,** 151-175.

KLUCKEN, J., POEHLER, A.-M., EBRAHIMI-FAKHARI, D., SCHNEIDER, J., NUBER, S., ROCKENSTEIN, E., SCHLÖTZER-SCHREHARDT, U., HYMAN, B. T., MCLEAN, P. J., MASLIAH, E. & WINKLER, J. 2012. Alpha-synuclein aggregation involves a bafilomycin A1-sensitive autophagy pathway. *Autophagy,* 8**,** 754-766.

KOMATSU, M., WAGURI, S., UENO, T., IWATA, J., MURATA, S., TANIDA, I., EZAKI, J., MIZUSHIMA, N., OHSUMI, Y., UCHIYAMA, Y., KOMINAMI, E., TANAKA, K. & CHIBA, T. 2005. Impairment of starvation-induced and constitutive autophagy in Atg7-deficient mice. *J Cell Biol,* 169**,** 425-34.

KOPITO, R. R. 1997. ER quality control: the cytoplasmic connection. *Cell,* 88**,** 427-30.

KORDOWER, J. H., FREEMAN, T. B., SNOW, B. J., VINGERHOETS, F. J., MUFSON, E. J., SANBERG, P. R., HAUSER, R. A., SMITH, D. A., NAUERT, G. M., PERL, D. P. & ET AL. 1995. Neuropathological evidence of graft survival and striatal reinnervation after the transplantation of fetal mesencephalic tissue in a patient with Parkinson's disease. *N Engl J Med,* 332**,** 1118-24.

KORECKA, J. A., VAN KESTEREN, R. E., BLAAS, E., SPITZER, S. O., KAMSTRA, J. H., SMIT, A. B., SWAAB, D. F., VERHAAGEN, J. & BOSSERS, K. 2013. Phenotypic characterization of retinoic acid differentiated SH-SY5Y cells by transcriptional profiling. *PLoS One,* 8**,** e63862.

KOROLCHUK, V. I., MANSILLA, A., MENZIES, F. M. & RUBINSZTEIN, D. C. 2009. Autophagy Inhibition Compromises Degradation of Ubiquitin-Proteasome Pathway Substrates. *Molecular Cell,* 33**,** 517-527.

KOVALEVICH, J. & LANGFORD, D. 2013. Considerations for the use of SH-SY5Y neuroblastoma cells in neurobiology. *Methods Mol Biol,* 1078**,** 9-21.

KTISTAKIS, N. T. & TOOZE, S. A. 2016. Digesting the Expanding Mechanisms of Autophagy. *Trends Cell Biol,* 26**,** 624-635.

KUMA, A., HATANO, M., MATSUI, M., YAMAMOTO, A., NAKAYA, H., YOSHIMORI, T., OHSUMI, Y., TOKUHISA, T. & MIZUSHIMA, N. 2004. The role of autophagy during the early neonatal starvation period. *Nature,* 432**,** 1032-6.

KUMAR, K. R., RAMIREZ, A., GOBEL, A., KRESOJEVIC, N., SVETEL, M., LOHMANN, K., C, M. S., ROLFS, A., MAZZULLI, J. R., ALCALAY, R. N., KRAINC, D., KLEIN, C., KOSTIC, V. & GRUNEWALD, A. 2013. Glucocerebrosidase mutations in a Serbian Parkinson's disease population. *Eur J Neurol,* 20**,** 402-5.

KURZAWA-AKANBI, M., HANSON, P. S., BLAIN, P. G., LETT, D. J., MCKEITH, I. G., CHINNERY, P. F. & MORRIS, C. M. 2012. Glucocerebrosidase mutations alter the endoplasmic reticulum and lysosomes in Lewy body disease. *J Neurochem,* 123**,** 298-309.

LANGSTON, J. W. 2006. The Parkinson's complex: parkinsonism is just the tip of the iceberg. *Ann Neurol,* 59**,** 591-6.

LANGSTON, J. W., FORNO, L. S., TETRUD, J., REEVES, A. G., KAPLAN, J. A. & KARLUK, D. 1999. Evidence of active nerve cell degeneration in the substantia nigra of humans years after 1-methyl-4-phenyl-1,2,3,6-tetrahydropyridine exposure. *Ann Neurol,* 46**,** 598-605.

LEE, H. J., BAE, E. J. & LEE, S. J. 2014. Extracellular alpha--synuclein-a novel and crucial factor in Lewy body diseases. *Nat Rev Neurol,* 10**,** 92-8.

LEE, H. J., CHO, E. D., LEE, K. W., KIM, J. H., CHO, S. G. & LEE, S. J. 2013. Autophagic failure promotes the exocytosis and intercellular transfer of α-synuclein. *Exp Mol Med,* 45**,** e22.

LEE, H. J., PATEL, S. & LEE, S. J. 2005. Intravesicular localization and exocytosis of alpha-synuclein and its aggregates. *J Neurosci,* 25**,** 6016-24.

LEE, Y., LEE, S., CHANG, S.-C. & LEE, J. 2019. Significant roles of neuroinflammation in Parkinson’s disease: therapeutic targets for PD prevention. *Archives of Pharmacal Research,* 42**,** 416-425.

LEHTONEN, Š., SONNINEN, T. M., WOJCIECHOWSKI, S., GOLDSTEINS, G. & KOISTINAHO, J. 2019. Dysfunction of Cellular Proteostasis in Parkinson's Disease. *Front Neurosci,* 13**,** 457.

LESAGE, S., ANHEIM, M., CONDROYER, C., POLLAK, P., DURIF, F., DUPUITS, C., VIALLET, F., LOHMANN, E., CORVOL, J. C., HONORE, A., RIVAUD, S., VIDAILHET, M., DURR, A. & BRICE, A. 2011. Large-scale screening of the Gaucher's disease-related glucocerebrosidase gene in Europeans with Parkinson's disease. *Hum Mol Genet,* 20**,** 202-10.

LEVINE, B. & KLIONSKY, D. J. 2004. Development by self-digestion: molecular mechanisms and biological functions of autophagy. *Dev Cell,* 6**,** 463-77.

LEVINE, B. & KROEMER, G. 2008. Autophagy in the pathogenesis of disease. *Cell,* 132**,** 27-42.

LI, D., SHI, J. J., MAO, C. J., LIU, S., WANG, J. D., CHEN, J., WANG, F., YANG, Y. P., HU, W. D., HU, L. F. & LIU, C. F. 2013. Alteration of dynein function affects α-synuclein degradation via the autophagosome-lysosome pathway. *Int J Mol Sci,* 14**,** 24242-54.

LI, H., HAM, A., MA, T. C., KUO, S. H., KANTER, E., KIM, D., KO, H. S., QUAN, Y., SARDI, S. P., LI, A., ARANCIO, O., KANG, U. J., SULZER, D. & TANG, G. 2019. Mitochondrial dysfunction and mitophagy defect triggered by heterozygous GBA mutations. *Autophagy,* 15**,** 113-130.

LI, J. Y., ENGLUND, E., HOLTON, J. L., SOULET, D., HAGELL, P., LEES, A. J., LASHLEY, T., QUINN, N. P., REHNCRONA, S., BJORKLUND, A., WIDNER, H., REVESZ, T., LINDVALL, O. & BRUNDIN, P. 2008. Lewy bodies in grafted neurons in subjects with Parkinson's disease suggest host-to-graft disease propagation. *Nat Med,* 14**,** 501-3.

LINARI, S. & CASTAMAN, G. 2015. Clinical manifestations and management of Gaucher disease. *Clin Cases Miner Bone Metab,* 12**,** 157-64.

LINDHOLM, D., KORHONEN, L., ERIKSSON, O. & KÕKS, S. 2017. Recent Insights into the Role of Unfolded Protein Response in ER Stress in Health and Disease. *Frontiers in Cell and Developmental Biology,* 5.

LIU, G., BOOT, B., LOCASCIO, J. J., JANSEN, I. E., WINDER-RHODES, S., EBERLY, S., ELBAZ, A., BRICE, A., RAVINA, B., VAN HILTEN, J. J., CORMIER-DEQUAIRE, F., CORVOL, J. C., BARKER, R. A., HEUTINK, P., MARINUS, J., WILLIAMS-GRAY, C. H. & SCHERZER, C. R. 2016. Specifically neuropathic Gaucher's mutations accelerate cognitive decline in Parkinson's. *Ann Neurol,* 80**,** 674-685.

LIU, Y., SUZUKI, K., REED, J. D., GRINBERG, A., WESTPHAL, H., HOFFMANN, A., DORING, T., SANDHOFF, K. & PROIA, R. L. 1998. Mice with type 2 and 3 Gaucher disease point mutations generated by a single insertion mutagenesis procedure. *Proc Natl Acad Sci U S A,* 95**,** 2503-8.

LOPES, F. M., BRISTOT, I. J., DA MOTTA, L. L., PARSONS, R. B. & KLAMT, F. 2017a. Mimicking Parkinson's Disease in a Dish: Merits and Pitfalls of the Most Commonly used Dopaminergic In Vitro Models. *Neuromolecular Med,* 19**,** 241-255.

LOPES, F. M., DA MOTTA, L. L., DE BASTIANI, M. A., PFAFFENSELLER, B., AGUIAR, B. W., DE SOUZA, L. F., ZANATTA, G., VARGAS, D. M., SCHONHOFEN, P., LONDERO, G. F., DE MEDEIROS, L. M., FREIRE, V. N., DAFRE, A. L., CASTRO, M. A., PARSONS, R. B. & KLAMT, F. 2017b. RA Differentiation Enhances Dopaminergic Features, Changes Redox Parameters, and Increases Dopamine Transporter Dependency in

6-Hydroxydopamine-Induced Neurotoxicity in SH-SY5Y Cells. *Neurotox Res,* 31**,** 545-559.

LU, J., YANG, C., CHEN, M., YE, D. Y., LONSER, R. R., BRADY, R. O. & ZHUANG, Z. 2011. Histone deacetylase inhibitors prevent the degradation and restore the activity of glucocerebrosidase in Gaucher disease. *Proc Natl Acad Sci U S A,* 108**,** 21200-5.

LUK, K. C., KEHM, V., CARROLL, J., ZHANG, B., O'BRIEN, P., TROJANOWSKI, J. Q. & LEE, V. M. Y. 2012. Pathological α-synuclein transmission initiates Parkinson-like neurodegeneration in nontransgenic mice. *Science (New York, N.Y.),* 338**,** 949-953.

LUK, K. C., SONG, C., BRIEN, P., STIEBER, A., BRANCH, J. R., BRUNDEN, K. R., TROJANOWSKI, J. Q. & LEE, V. M. Y. 2009. Exogenous α-synuclein fibrils seed the formation of Lewy body-like intracellular inclusions in cultured cells. *Proceedings of the National Academy of Sciences,* 106**,** 20051.

LUNA, E., DECKER, S. C., RIDDLE, D. M., CAPUTO, A., ZHANG, B., COLE, T., CASWELL, C., XIE, S. X., LEE, V. M. Y. & LUK, K. C. 2018. Differential α-synuclein expression contributes to selective vulnerability of hippocampal neuron subpopulations to fibril-induced toxicity. *Acta Neuropathol,* 135**,** 855-875.

LUPAS, A., ZWICKL, P., WENZEL, T., SEEMULLER, E. & BAUMEISTER, W. 1995. Structure and function of the 20S proteasome and of its regulatory complexes. *Cold Spring Harb Symp Quant Biol,* 60**,** 515-24.

MAEGAWA, G. H., TROPAK, M. B., BUTTNER, J. D., RIGAT, B. A., FULLER, M., PANDIT, D., TANG, L., KORNHABER, G. J., HAMURO, Y., CLARKE, J. T. & MAHURAN, D. J. 2009. Identification and characterization of ambroxol as an enzyme enhancement agent for Gaucher disease. *J Biol Chem,* 284**,** 23502-16.

MAGALHAES, J., GEGG, M. E., MIGDALSKA-RICHARDS, A., DOHERTY, M. K., WHITFIELD, P. D. & SCHAPIRA, A. H. 2016. Autophagic lysosome reformation dysfunction in glucocerebrosidase deficient cells: relevance to Parkinson disease. *Hum Mol Genet,* 25**,** 3432-3445.

MAGALHAES, J., GEGG, M. E., MIGDALSKA-RICHARDS, A. & SCHAPIRA, A. H. 2018. Effects of ambroxol on the autophagy-lysosome pathway and mitochondria in primary cortical neurons. *Sci Rep,* 8**,** 1385.

MALHOTRA, J. D. & KAUFMAN, R. J. 2007. The endoplasmic reticulum and the unfolded protein response. *Semin Cell Dev Biol,* 18**,** 716-31.

MANNING-BOG, A. B., SCHULE, B. & LANGSTON, J. W. 2009. Alpha-synuclein-glucocerebrosidase interactions in pharmacological Gaucher models: a biological link between Gaucher disease and parkinsonism. *Neurotoxicology,* 30**,** 1127-32.

MAOR, G., FILOCAMO, M. & HOROWITZ, M. 2013. ITCH regulates degradation of mutant glucocerebrosidase: implications to Gaucher disease. *Hum Mol Genet,* 22**,** 1316-27.

MAREY-SEMPER, I., GELMAN, M. & LEVI-STRAUSS, M. 1995. A selective toxicity toward cultured mesencephalic dopaminergic neurons is induced by the synergistic effects of energetic metabolism impairment and NMDA receptor activation. *J Neurosci,* 15**,** 5912-8.

MARTELLA, G., MADEO, G., MALTESE, M., VANNI, V., PUGLISI, F., FERRARO, E., SCHIRINZI, T., VALENTE, E. M., BONANNI, L., SHEN, J.,

MANDOLESI, G., MERCURI, N. B., BONSI, P. & PISANI, A. 2016. Exposure to low-dose rotenone precipitates synaptic plasticity alterations in PINK1 heterozygous knockout mice. *Neurobiol Dis,* 91**,** 21-36.
MARTINEZ, T. N. & GREENAMYRE, J. T. 2012. Toxin models of mitochondrial dysfunction in Parkinson's disease. *Antioxid Redox Signal,* 16**,** 920-34.
MASSEY, A., KIFFIN, R. & CUERVO, A. M. 2004. Pathophysiology of chaperone-mediated autophagy. *Int J Biochem Cell Biol,* 36**,** 2420-34.
MASUDA-SUZUKAKE, M., NONAKA, T., HOSOKAWA, M., OIKAWA, T., ARAI, T., AKIYAMA, H., MANN, D. M. & HASEGAWA, M. 2013. Prion-like spreading of pathological α-synuclein in brain. *Brain,* 136**,** 1128-38.
MAZZULLI, J. R., XU, Y. H., SUN, Y., KNIGHT, A. L., MCLEAN, P. J., CALDWELL, G. A., SIDRANSKY, E., GRABOWSKI, G. A. & KRAINC, D. 2011. Gaucher disease glucocerebrosidase and alpha-synuclein form a bidirectional pathogenic loop in synucleinopathies. *Cell,* 146**,** 37-52.
MAZZULLI, J. R., ZUNKE, F., ISACSON, O., STUDER, L. & KRAINC, D. 2016. α-Synuclein-induced lysosomal dysfunction occurs through disruptions in protein trafficking in human midbrain synucleinopathy models. *Proc Natl Acad Sci U S A,* 113**,** 1931-6.
MCGLINCHEY, R. P. & LEE, J. C. 2013. Emerging insights into the mechanistic link between α-synuclein and glucocerebrosidase in Parkinson's disease. *Biochemical Society Transactions,* 41**,** 1509-1512.
MCKERAN, R. O., BRADBURY, P., TAYLOR, D. & STERN, G. 1985. Neurological involvement in type 1 (adult) Gaucher's disease. *J Neurol Neurosurg Psychiatry,* 48**,** 172-5.
MCNAUGHT, K. S., BELIZAIRE, R., ISACSON, O., JENNER, P. & OLANOW, C. W. 2003. Altered proteasomal function in sporadic Parkinson's disease. *Exp Neurol,* 179**,** 38-46.
MCNAUGHT, K. S., MYTILINEOU, C., JNOBAPTISTE, R., YABUT, J., SHASHIDHARAN, P., JENNERT, P. & OLANOW, C. W. 2002. Impairment of the ubiquitin-proteasome system causes dopaminergic cell death and inclusion body formation in ventral mesencephalic cultures. *J Neurochem,* 81**,** 301-6.
MCNAUGHT, K. S., PERL, D. P., BROWNELL, A. L. & OLANOW, C. W. 2004. Systemic exposure to proteasome inhibitors causes a progressive model of Parkinson's disease. *Ann Neurol,* 56**,** 149-62.
MCNEILL, A., DURAN, R., HUGHES, D. A., MEHTA, A. & SCHAPIRA, A. H. 2012a. A clinical and family history study of Parkinson's disease in heterozygous glucocerebrosidase mutation carriers. *J Neurol Neurosurg Psychiatry,* 83**,** 853-4.
MCNEILL, A., DURAN, R., PROUKAKIS, C., BRAS, J., HUGHES, D., MEHTA, A., HARDY, J., WOOD, N. W. & SCHAPIRA, A. H. 2012b. Hyposmia and cognitive impairment in Gaucher disease patients and carriers. *Mov Disord,* 27**,** 526-32.
MCNEILL, A., MAGALHAES, J., SHEN, C., CHAU, K. Y., HUGHES, D., MEHTA, A., FOLTYNIE, T., COOPER, J. M., ABRAMOV, A. Y., GEGG, M. & SCHAPIRA, A. H. 2014. Ambroxol improves lysosomal biochemistry in glucocerebrosidase mutation-linked Parkinson disease cells. *Brain,* 137**,** 1481-95.
MENG, L., MOHAN, R., KWOK, B. H., ELOFSSON, M., SIN, N. & CREWS, C. M. 1999. Epoxomicin, a potent and selective proteasome inhibitor, exhibits

in vivo antiinflammatory activity. *Proceedings of the National Academy of Sciences of the United States of America,* 96**,** 10403-10408.
MIGDALSKA-RICHARDS, A., DALY, L., BEZARD, E. & SCHAPIRA, A. H. 2016. Ambroxol effects in glucocerebrosidase and alpha-synuclein transgenic mice. *Ann Neurol,* 80**,** 766-775.
MIGDALSKA-RICHARDS, A. & SCHAPIRA, A. H. 2016. The relationship between glucocerebrosidase mutations and Parkinson disease. *J Neurochem,* 139 Suppl 1**,** 77-90.
MIGDALSKA-RICHARDS, A., WEGRZYNOWICZ, M., RUSCONI, R., DEANGELI, G., DI MONTE, D. A., SPILLANTINI, M. G. & SCHAPIRA, A. H. V. 2017. The L444P Gba1 mutation enhances alpha-synuclein induced loss of nigral dopaminergic neurons in mice. *Brain,* 140**,** 2706-2721.
MIYAZAKI, I., ISOOKA, N., IMAFUKU, F., SUN, J., KIKUOKA, R., FURUKAWA, C. & ASANUMA, M. 2020. Chronic Systemic Exposure to Low-Dose Rotenone Induced Central and Peripheral Neuropathology and Motor Deficits in Mice: Reproducible Animal Model of Parkinson's Disease. *Int J Mol Sci,* 21.
MIZUSHIMA, N., YOSHIMORI, T. & LEVINE, B. 2010. Methods in mammalian autophagy research. *Cell,* 140**,** 313-26.
MOFFITT, K. D., CHAMBERS, J. P., DIVEN, W. F., GLEW, R. H., WENGER, D. A. & FARRELL, D. F. 1978. Characterization of lysosomal hydrolases that are elevated in Gaucher's disease. *Arch Biochem Biophys,* 190**,** 247-60.
MOLLENHAUER, B., BATRLA, R., EL-AGNAF, O., GALASKO, D. R., LASHUEL, H. A., MERCHANT, K. M., SHAW, L. M., SELKOE, D. J., UMEK, R., VANDERSTICHELE, H., ZETTERBERG, H., ZHANG, J., CASPELL-GARCIA, C., COFFEY, C., HUTTEN, S. J., FRASIER, M. & TAYLOR, P. 2017. A user's guide for α-synuclein biomarker studies in biological fluids: Perianalytical considerations. *Mov Disord,* 32**,** 1117-1130.
MOLLENHAUER, B., TRAUTMANN, E., OTTE, B., NG, J., SPREER, A., LANGE, P., SIXEL-DÖRING, F., HAKIMI, M., VONSATTEL, J. P., NUSSBAUM, R., TRENKWALDER, C. & SCHLOSSMACHER, M. G. 2012. α-Synuclein in human cerebrospinal fluid is principally derived from neurons of the central nervous system. *J Neural Transm (Vienna),* 119**,** 739-46.
MONTFORT, M., CHABAS, A., VILAGELIU, L. & GRINBERG, D. 2004. Functional analysis of 13 GBA mutant alleles identified in Gaucher disease patients: Pathogenic changes and "modifier" polymorphisms. *Hum Mutat,* 23**,** 567-75.
MU, T. W., ONG, D. S., WANG, Y. J., BALCH, W. E., YATES, J. R., 3RD, SEGATORI, L. & KELLY, J. W. 2008. Chemical and biological approaches synergize to ameliorate protein-folding diseases. *Cell,* 134**,** 769-81.
MULLIN, S., SMITH, L., LEE, K., D'SOUZA, G., WOODGATE, P., ELFLEIN, J., HÄLLQVIST, J., TOFFOLI, M., STREETER, A., HOSKING, J., HEYWOOD, W. E., KHENGAR, R., CAMPBELL, P., HEHIR, J., CABLE, S., MILLS, K., ZETTERBERG, H., LIMOUSIN, P., LIBRI, V., FOLTYNIE, T. & SCHAPIRA, A. H. V. 2020. Ambroxol for the Treatment of Patients With Parkinson Disease With and Without Glucocerebrosidase Gene Mutations: A Nonrandomized, Noncontrolled Trial. *JAMA Neurology,* 77**,** 427-434.
MURPHY, K. E., GYSBERS, A. M., ABBOTT, S. K., SPIRO, A. S., FURUTA, A., COOPER, A., GARNER, B., KABUTA, T. & HALLIDAY, G. M. 2015.

Lysosomal-associated membrane protein 2 isoforms are differentially affected in early Parkinson's disease. *Mov Disord,* 30**,** 1639-47.
MURPHY, K. E., GYSBERS, A. M., ABBOTT, S. K., TAYEBI, N., KIM, W. S., SIDRANSKY, E., COOPER, A., GARNER, B. & HALLIDAY, G. M. 2014. Reduced glucocerebrosidase is associated with increased alpha-synuclein in sporadic Parkinson's disease. *Brain,* 137**,** 834-48.
NAGATSU, T., LEVITT, M. & UDENFRIEND, S. 1964. TYROSINE HYDROXYLASE. THE INITIAL STEP IN NOREPINEPHRINE BIOSYNTHESIS. *J Biol Chem,* 239**,** 2910-7.
NALLS, M. A., DURAN, R., LOPEZ, G., KURZAWA-AKANBI, M., MCKEITH, I. G., CHINNERY, P. F., MORRIS, C. M., THEUNS, J., CROSIERS, D., CRAS, P., ENGELBORGHS, S., DE DEYN, P. P., VAN BROECKHOVEN, C., MANN, D. M., SNOWDEN, J., PICKERING-BROWN, S., HALLIWELL, N., DAVIDSON, Y., GIBBONS, L., HARRIS, J., SHEERIN, U. M., BRAS, J., HARDY, J., CLARK, L., MARDER, K., HONIG, L. S., BERG, D., MAETZLER, W., BROCKMANN, K., GASSER, T., NOVELLINO, F., QUATTRONE, A., ANNESI, G., DE MARCO, E. V., ROGAEVA, E., MASELLIS, M., BLACK, S. E., BILBAO, J. M., FOROUD, T., GHETTI, B., NICHOLS, W. C., PANKRATZ, N., HALLIDAY, G., LESAGE, S., KLEBE, S., DURR, A., DUYCKAERTS, C., BRICE, A., GIASSON, B. I., TROJANOWSKI, J. Q., HURTIG, H. I., TAYEBI, N., LANDAZABAL, C., KNIGHT, M. A., KELLER, M., SINGLETON, A. B., WOLFSBERG, T. G. & SIDRANSKY, E. 2013. A multicenter study of glucocerebrosidase mutations in dementia with Lewy bodies. *JAMA Neurol,* 70**,** 727-35.
NEDERGAARD, S., FLATMAN, J. A. & ENGBERG, I. 1993. Nifedipine- and omega-conotoxin-sensitive Ca2+ conductances in guinea-pig substantia nigra pars compacta neurones. *J Physiol,* 466**,** 727-47.
NEUMANN, J., BRAS, J., DEAS, E., O'SULLIVAN, S. S., PARKKINEN, L., LACHMANN, R. H., LI, A., HOLTON, J., GUERREIRO, R., PAUDEL, R., SEGARANE, B., SINGLETON, A., LEES, A., HARDY, J., HOULDEN, H., REVESZ, T. & WOOD, N. W. 2009. Glucocerebrosidase mutations in clinical and pathologically proven Parkinson's disease. *Brain,* 132**,** 1783-94.
NEUMANN, M., KAHLE, P. J., GIASSON, B. I., OZMEN, L., BORRONI, E., SPOOREN, W., MÜLLER, V., ODOY, S., FUJIWARA, H., HASEGAWA, M., IWATSUBO, T., TROJANOWSKI, J. Q., KRETZSCHMAR, H. A. & HAASS, C. 2002. Misfolded proteinase K-resistant hyperphosphorylated alpha-synuclein in aged transgenic mice with locomotor deterioration and in human alpha-synucleinopathies. *J Clin Invest,* 110**,** 1429-39.
NISHIMURA, T. & TOOZE, S. A. 2020. Emerging roles of ATG proteins and membrane lipids in autophagosome formation. *Cell Discov,* 6**,** 32.
OLZMANN, J. A., KOPITO, R. R. & CHRISTIANSON, J. C. 2013. The mammalian endoplasmic reticulum-associated degradation system. *Cold Spring Harb Perspect Biol,* 5.
ORVISKY, E., PARK, J. K., LAMARCA, M. E., GINNS, E. I., MARTIN, B. M., TAYEBI, N. & SIDRANSKY, E. 2002. Glucosylsphingosine accumulation in tissues from patients with Gaucher disease: correlation with phenotype and genotype. *Molecular Genetics and Metabolism,* 76**,** 262-270.
OSELLAME, L. D., RAHIM, A. A., HARGREAVES, I. P., GEGG, M. E., RICHARD-LONDT, A., BRANDNER, S., WADDINGTON, S. N.,

SCHAPIRA, A. H. & DUCHEN, M. R. 2013. Mitochondria and quality control defects in a mouse model of Gaucher disease--links to Parkinson's disease. *Cell Metab,* 17**,** 941-53.

OUESLATI, A. 2016. Implication of Alpha-Synuclein Phosphorylation at S129 in Synucleinopathies: What Have We Learned in the Last Decade? *J Parkinsons Dis,* 6**,** 39-51.

OUESLATI, A., FOURNIER, M. & LASHUEL, H. A. 2010. Role of post-translational modifications in modulating the structure, function and toxicity of alpha-synuclein: implications for Parkinson's disease pathogenesis and therapies. *Prog Brain Res,* 183**,** 115-45.

OUESLATI, A., XIMERAKIS, M. & VEKRELLIS, K. 2014. Protein Transmission, Seeding and Degradation: Key Steps for α-Synuclein Prion-Like Propagation. *Exp Neurobiol,* 23**,** 324-36.

PACELLI, C., GIGUÈRE, N., BOURQUE, M. J., LÉVESQUE, M., SLACK, R. S. & TRUDEAU, L. 2015. Elevated Mitochondrial Bioenergetics and Axonal Arborization Size Are Key Contributors to the Vulnerability of Dopamine Neurons. *Curr Biol,* 25**,** 2349-60.

PÅHLMAN, S., HOEHNER, J. C., NÅNBERG, E., HEDBORG, F., FAGERSTRÖM, S., GESTBLOM, C., JOHANSSON, I., LARSSON, U., LAVENIUS, E., ÖRTOFT, E. & SÖDERHOLM, H. 1995. Differentiation and survival influences of growth factors in human neuroblastoma. *European Journal of Cancer,* 31**,** 453-458.

PAHLMAN, S., ODELSTAD, L., LARSSON, E., GROTTE, G. & NILSSON, K. 1981. Phenotypic changes of human neuroblastoma cells in culture induced by 12-O-tetradecanoyl-phorbol-13-acetate. *Int J Cancer,* 28**,** 583-9.

PAHLMAN, S., RUUSALA, A. I., ABRAHAMSSON, L., MATTSSON, M. E. & ESSCHER, T. 1984. Retinoic acid-induced differentiation of cultured human neuroblastoma cells: a comparison with phorbolester-induced differentiation. *Cell Differ,* 14**,** 135-44.

PALASZ, E., WYSOCKA, A., GASIOROWSKA, A., CHALIMONIUK, M., NIEWIADOMSKI, W. & NIEWIADOMSKA, G. 2020. BDNF as a Promising Therapeutic Agent in Parkinson's Disease. *International journal of molecular sciences* [Online], 21. [Accessed 2020/02//].

PANTAZOPOULOU, M., BREMBATI, V., KANELLIDI, A., BOUSSET, L., MELKI, R. & STEFANIS, L. 2020. Distinct alpha-Synuclein species induced by seeding are selectively cleared by the Lysosome or the Proteasome in neuronally differentiated SH-SY5Y cells. *J Neurochem*.

PAREDES-RODRIGUEZ, E., VEGAS-SUAREZ, S., MORERA-HERRERAS, T., DE DEURWAERDERE, P. & MIGUELEZ, C. 2020. The Noradrenergic System in Parkinson's Disease. *Front Pharmacol,* 11**,** 435.

PARK, C. & CUERVO, A. M. 2013. Selective autophagy: talking with the UPS. *Cell Biochem Biophys,* 67**,** 3-13.

PCHELINA, S., EMELYANOV, A., BAYDAKOVA, G., ANDOSKIN, P., SENKEVICH, K., NIKOLAEV, M., MILIUKHINA, I., YAKIMOVSKII, A., TIMOFEEVA, A., FEDOTOVA, E., ABRAMYCHEVA, N., USENKO, T., KULABUKHOVA, D., LAVRINOVA, A., KOPYTOVA, A., GARAEVA, L., NUZHNYI, E., ILLARIOSHKIN, S. & ZAKHAROVA, E. 2017. Oligomeric alpha-synuclein and glucocerebrosidase activity levels in GBA-associated Parkinson's disease. *Neurosci Lett,* 636**,** 70-76.

PELLED, D., TRAJKOVIC-BODENNEC, S., LLOYD-EVANS, E., SIDRANSKY, E., SCHIFFMANN, R. & FUTERMAN, A. H. 2005. Enhanced calcium release in the acute neuronopathic form of Gaucher disease. *Neurobiol Dis,* 18**,** 83-8.

PETRUCELLI, L., O'FARRELL, C., LOCKHART, P. J., BAPTISTA, M., KEHOE, K., VINK, L., CHOI, P., WOLOZIN, B., FARRER, M., HARDY, J. & COOKSON, M. R. 2002. Parkin protects against the toxicity associated with mutant alpha-synuclein: proteasome dysfunction selectively affects catecholaminergic neurons. *Neuron,* 36**,** 1007-19.

PHUYAL, S., HESSVIK, N. P., SKOTLAND, T., SANDVIG, K. & LLORENTE, A. 2014. Regulation of exosome release by glycosphingolipids and flotillins. *Febs j,* 281**,** 2214-27.

PICKRELL, A. M. & YOULE, R. J. 2015. The roles of PINK1, parkin, and mitochondrial fidelity in Parkinson's disease. *Neuron,* 85**,** 257-73.

PILCHOVA, I., KLACANOVA, K., DIBDIAKOVA, K., SAKSONOVA, S., STEFANIKOVA, A., VIDOMANOVA, E., LICHARDUSOVA, L., HATOK, J. & RACAY, P. 2017. Proteasome Stress Triggers Death of SH-SY5Y and T98G Cells via Different Cellular Mechanisms. *Neurochemical Research,* 42**,** 3170-3185.

POHL, C. & DIKIC, I. 2019. Cellular quality control by the ubiquitin-proteasome system and autophagy. *Science,* 366**,** 818-822.

POLYMEROPOULOS, M., LAVEDAN, C., LEROY, E., E. IDE, S., DEHEJIA, A., DUTRA, A., PIKE, B., ROOT, H., RUBENSTEIN, J., BOYER, R., STENROOS, E., CHANDRASEKHARAPPA, S., ATHANASSIADOU, A., PAPAPETROPOULOS, T., G. JOHNSON, W., M. LAZZARINI, A., C. DUVOISIN, R., DI IORIO, G., I. GOLBE, L. & NUSSBAUM, R. 1997. *Mutation in the -Synuclein Gene Identified in Families with Parkinson's Disease*.

PRESGRAVES, S. P., AHMED, T., BORWEGE, S. & JOYCE, J. N. 2004. Terminally differentiated SH-SY5Y cells provide a model system for studying neuroprotective effects of dopamine agonists. *Neurotox Res,* 5**,** 579-98.

PRINGSHEIM, T., JETTE, N., FROLKIS, A. & STEEVES, T. D. 2014. The prevalence of Parkinson's disease: a systematic review and meta-analysis. *Mov Disord,* 29**,** 1583-90.

PU, J., GUARDIA, C. M., KEREN-KAPLAN, T. & BONIFACINO, J. 2016. Mechanisms and functions of lysosome positioning. *Journal of Cell Science,* 129**,** 4329 - 4339.

PUSCHMANN, A., ROSS, O. A., VILARINO-GUELL, C., LINCOLN, S. J., KACHERGUS, J. M., COBB, S. A., LINDQUIST, S. G., NIELSEN, J. E., WSZOLEK, Z. K., FARRER, M., WIDNER, H., VAN WESTEN, D., HAGERSTROM, D., MARKOPOULOU, K., CHASE, B. A., NILSSON, K., REIMER, J. & NILSSON, C. 2009. A Swedish family with de novo alpha-synuclein A53T mutation: evidence for early cortical dysfunction. *Parkinsonism Relat Disord,* 15**,** 627-32.

QUYNH DOAN, N. T. & CHRISTENSEN, S. B. 2015. Thapsigargin, Origin, Chemistry, Structure-Activity Relationships and Prodrug Development. *Curr Pharm Des,* 21**,** 5501-17.

RAVIKUMAR, B., ACEVEDO-AROZENA, A., IMARISIO, S., BERGER, Z., VACHER, C., O'KANE, C. J., BROWN, S. D. & RUBINSZTEIN, D. C.

2005. Dynein mutations impair autophagic clearance of aggregate-prone proteins. *Nat Genet,* 37**,** 771-6.
RECZEK, D., SCHWAKE, M., SCHRODER, J., HUGHES, H., BLANZ, J., JIN, X., BRONDYK, W., VAN PATTEN, S., EDMUNDS, T. & SAFTIG, P. 2007. LIMP-2 is a receptor for lysosomal mannose-6-phosphate-independent targeting of beta-glucocerebrosidase. *Cell,* 131**,** 770-83.
REEVE, A., SIMCOX, E. & TURNBULL, D. 2014. Ageing and Parkinson's disease: Why is advancing age the biggest risk factor? *Ageing Research Reviews,* 14**,** 19-30.
REMONDELLI, P. & RENNA, M. 2017. The Endoplasmic Reticulum Unfolded Protein Response in Neurodegenerative Disorders and Its Potential Therapeutic Significance. *Front Mol Neurosci,* 10**,** 187.
ROBAK, L. A., JANSEN, I. E., VAN ROOIJ, J., UITTERLINDEN, A. G., KRAAIJ, R., JANKOVIC, J., HEUTINK, P. & SHULMAN, J. M. 2017. Excessive burden of lysosomal storage disorder gene variants in Parkinson's disease. *Brain,* 140**,** 3191-3203.
ROCHA, E. M., SMITH, G. A., PARK, E., CAO, H., BROWN, E., HALLETT, P. & ISACSON, O. 2015a. Progressive decline of glucocerebrosidase in aging and Parkinson's disease. *Ann Clin Transl Neurol,* 2**,** 433-8.
ROCHA, E. M., SMITH, G. A., PARK, E., CAO, H., GRAHAM, A. R., BROWN, E., MCLEAN, J. R., HAYES, M. A., BEAGAN, J., IZEN, S. C., PEREZ-TORRES, E., HALLETT, P. J. & ISACSON, O. 2015b. Sustained Systemic Glucocerebrosidase Inhibition Induces Brain α-Synuclein Aggregation, Microglia and Complement C1q Activation in Mice. *Antioxid Redox Signal,* 23**,** 550-64.
RON, I. & HOROWITZ, M. 2005. ER retention and degradation as the molecular basis underlying Gaucher disease heterogeneity. *Hum Mol Genet,* 14**,** 2387-98.
RON, I., RAPAPORT, D. & HOROWITZ, M. 2010. Interaction between parkin and mutant glucocerebrosidase variants: a possible link between Parkinson disease and Gaucher disease. *Human Molecular Genetics,* 19**,** 3771-3781.
ROSHAN LAL, T. & SIDRANSKY, E. 2017. The Spectrum of Neurological Manifestations Associated with Gaucher Disease. *Diseases,* 5.
ROSS, R. A. & BIEDLER, J. L. 1985. Presence and regulation of tyrosinase activity in human neuroblastoma cell variants in vitro. *Cancer Res,* 45**,** 1628-32.
ROSS, R. A., BIEDLER, J. L., SPENGLER, B. A. & REIS, D. J. 1981. Neurotransmitter-synthesizing enzymes in 14 human neuroblastoma cell lines. *Cell Mol Neurobiol,* 1**,** 301-11.
RUBINSZTEIN, D. C. 2006. The roles of intracellular protein-degradation pathways in neurodegeneration. *Nature,* 443**,** 780-6.
RUBINSZTEIN, DAVID C., MARIÑO, G. & KROEMER, G. 2011. Autophagy and Aging. *Cell,* 146**,** 682-695.
SAEKI, Y. 2017. Ubiquitin recognition by the proteasome. *The Journal of Biochemistry,* 161**,** 113-124.
SAFTIG, P. & KLUMPERMAN, J. 2009. Lysosome biogenesis and lysosomal membrane proteins: trafficking meets function. *Nat Rev Mol Cell Biol,* 10**,** 623-35.

SALA, G., MARINIG, D., AROSIO, A. & FERRARESE, C. 2016. Role of Chaperone-Mediated Autophagy Dysfunctions in the Pathogenesis of Parkinson's Disease. *Front Mol Neurosci,* 9**,** 157.

SALVADOR, N., AGUADO, C., HORST, M. & KNECHT, E. 2000. Import of a cytosolic protein into lysosomes by chaperone-mediated autophagy depends on its folding state. *J Biol Chem,* 275**,** 27447-56.

SANCHEZ-DANES, A., RICHAUD-PATIN, Y., CARBALLO-CARBAJAL, I., JIMENEZ-DELGADO, S., CAIG, C., MORA, S., DI GUGLIELMO, C., EZQUERRA, M., PATEL, B., GIRALT, A., CANALS, J. M., MEMO, M., ALBERCH, J., LOPEZ-BARNEO, J., VILA, M., CUERVO, A. M., TOLOSA, E., CONSIGLIO, A. & RAYA, A. 2012. Disease-specific phenotypes in dopamine neurons from human iPS-based models of genetic and sporadic Parkinson's disease. *EMBO Mol Med,* 4**,** 380-95.

SANCHEZ-MARTINEZ, A., BEAVAN, M., GEGG, M. E., CHAU, K. Y., WHITWORTH, A. J. & SCHAPIRA, A. H. 2016. Parkinson disease-linked GBA mutation effects reversed by molecular chaperones in human cell and fly models. *Sci Rep,* 6**,** 31380.

SANDERS, L. H. & TIMOTHY GREENAMYRE, J. 2013. Oxidative damage to macromolecules in human Parkinson disease and the rotenone model. *Free Radic Biol Med,* 62**,** 111-120.

SANO, R. & REED, J. C. 2013. ER stress-induced cell death mechanisms. *Biochimica et Biophysica Acta (BBA) - Molecular Cell Research,* 1833**,** 3460-3470.

SARDI, S. P., CHENG, S. H. & SHIHABUDDIN, L. S. 2015. Gaucher-related synucleinopathies: the examination of sporadic neurodegeneration from a rare (disease) angle. *Prog Neurobiol,* 125**,** 47-62.

SARDI, S. P., CLARKE, J., KINNECOM, C., TAMSETT, T. J., LI, L., STANEK, L. M., PASSINI, M. A., GRABOWSKI, G. A., SCHLOSSMACHER, M. G., SIDMAN, R. L., CHENG, S. H. & SHIHABUDDIN, L. S. 2011. CNS expression of glucocerebrosidase corrects alpha-synuclein pathology and memory in a mouse model of Gaucher-related synucleinopathy. *Proc Natl Acad Sci U S A,* 108**,** 12101-6.

SARDI, S. P., CLARKE, J., VIEL, C., CHAN, M., TAMSETT, T. J., TRELEAVEN, C. M., BU, J., SWEET, L., PASSINI, M. A., DODGE, J. C., YU, W. H., SIDMAN, R. L., CHENG, S. H. & SHIHABUDDIN, L. S. 2013. Augmenting CNS glucocerebrosidase activity as a therapeutic strategy for parkinsonism and other Gaucher-related synucleinopathies. *Proc Natl Acad Sci U S A,* 110**,** 3537-42.

SARDI, S. P., VIEL, C., CLARKE, J., TRELEAVEN, C. M., RICHARDS, A. M., PARK, H., OLSZEWSKI, M. A., DODGE, J. C., MARSHALL, J., MAKINO, E., WANG, B., SIDMAN, R. L., CHENG, S. H. & SHIHABUDDIN, L. S. 2017. Glucosylceramide synthase inhibition alleviates aberrations in synucleinopathy models. *Proc Natl Acad Sci U S A,* 114**,** 2699-2704.

SASAKI, A., ARAWAKA, S., SATO, H. & KATO, T. 2015. Sensitive western blotting for detection of endogenous Ser129-phosphorylated α-synuclein in intracellular and extracellular spaces. *Scientific Reports,* 5**,** 14211.

SAVICA, R., ROCCA, W. A. & AHLSKOG, J. E. 2010. When does Parkinson disease start? *Arch Neurol,* 67**,** 798-801.

SCHAPIRA, A. H. 2008. Mitochondria in the aetiology and pathogenesis of Parkinson's disease. *Lancet Neurol,* 7**,** 97-109.

SCHAPIRA, A. H. 2015. Glucocerebrosidase and Parkinson disease: Recent advances. *Mol Cell Neurosci,* 66**,** 37-42.

SCHAPIRA, A. H., CLEETER, M. W., MUDDLE, J. R., WORKMAN, J. M., COOPER, J. M. & KING, R. H. 2006. Proteasomal inhibition causes loss of nigral tyrosine hydroxylase neurons. *Ann Neurol,* 60**,** 253-5.

SCHAPIRA, A. H., COOPER, J. M., DEXTER, D., CLARK, J. B., JENNER, P. & MARSDEN, C. D. 1990. Mitochondrial complex I deficiency in Parkinson's disease. *J Neurochem,* 54**,** 823-7.

SCHAPIRA, A. H., COOPER, J. M., DEXTER, D., JENNER, P., CLARK, J. B. & MARSDEN, C. D. 1989. Mitochondrial complex I deficiency in Parkinson's disease. *Lancet,* 1**,** 1269.

SCHAPIRA, A. H. & TOLOSA, E. 2010. Molecular and clinical prodrome of Parkinson disease: implications for treatment. *Nat Rev Neurol,* 6**,** 309-17.

SCHAPIRA, A. H. V., CHAUDHURI, K. R. & JENNER, P. 2017. Non-motor features of Parkinson disease. *Nat Rev Neurosci,* 18**,** 435-450.

SCHONDORF, D. C., AURELI, M., MCALLISTER, F. E., HINDLEY, C. J., MAYER, F., SCHMID, B., SARDI, S. P., VALSECCHI, M., HOFFMANN, S., SCHWARZ, L. K., HEDRICH, U., BERG, D., SHIHABUDDIN, L. S., HU, J., PRUSZAK, J., GYGI, S. P., SONNINO, S., GASSER, T. & DELEIDI, M. 2014. iPSC-derived neurons from GBA1-associated Parkinson's disease patients show autophagic defects and impaired calcium homeostasis. *Nat Commun,* 5**,** 4028.

SCHONDORF, D. C., IVANYUK, D., BADEN, P., SANCHEZ-MARTINEZ, A., DE CICCO, S., YU, C., GIUNTA, I., SCHWARZ, L. K., DI NAPOLI, G., PANAGIOTAKOPOULOU, V., NESTEL, S., KEATINGE, M., PRUSZAK, J., BANDMANN, O., HEIMRICH, B., GASSER, T., WHITWORTH, A. J. & DELEIDI, M. 2018. The NAD+ Precursor Nicotinamide Riboside Rescues Mitochondrial Defects and Neuronal Loss in iPSC and Fly Models of Parkinson's Disease. *Cell Rep,* 23**,** 2976-2988.

SEHGAL, P., SZALAI, P., OLESEN, C., PRAETORIUS, H. A., NISSEN, P., CHRISTENSEN, S. B., ENGEDAL, N. & MOLLER, J. V. 2017a. Inhibition of the sarco/endoplasmic reticulum (ER) Ca(2+)-ATPase by thapsigargin analogs induces cell death via ER Ca(2+) depletion and the unfolded protein response. *J Biol Chem,* 292**,** 19656-19673.

SEHGAL, P., SZALAI, P., OLESEN, C., PRAETORIUS, H. A., NISSEN, P., CHRISTENSEN, S. B., ENGEDAL, N. & MØLLER, J. V. 2017b. Inhibition of the sarco/endoplasmic reticulum (ER) Ca(2+)-ATPase by thapsigargin analogs induces cell death via ER Ca(2+) depletion and the unfolded protein response. *J Biol Chem,* 292**,** 19656-19673.

SELVARAJ, S. & PIRAMANAYAGAM, S. 2019. Impact of gene mutation in the development of Parkinson's disease. *Genes & Diseases,* 6**,** 120-128.

SESTITO, S., FILOCAMO, M., CERAVOLO, F., FALVO, F., GRISOLIA, M., MORICCA, M. T., CANTAFFA, R., GROSSI, S., STRISCIUGLIO, P. & CONCOLINO, D. 2017. Norrbottnian clinical variant of Gaucher disease in Southern Italy. *J Hum Genet,* 62**,** 507-511.

SHIMURA, H., HATTORI, N., KUBO, S., MIZUNO, Y., ASAKAWA, S., MINOSHIMA, S., SHIMIZU, N., IWAI, K., CHIBA, T., TANAKA, K. & SUZUKI, T. 2000. Familial Parkinson disease gene product, parkin, is a ubiquitin-protein ligase. *Nat Genet,* 25**,** 302-5.

SIDELL, N. 1982. Retinoic Acid-Induced Growth Inhibition and Morphologic Differentiation of Human Neuroblastoma Cells In Vitro2. *JNCI: Journal of the National Cancer Institute,* 68**,** 589-596.

SIDRANSKY, E. & HART, P. S. 2012. Penetrance of PD in Glucocerebrosidase Gene Mutation Carriers. *Neurology,* 79**,** 106-107.

SIDRANSKY, E. & LOPEZ, G. 2012. The link between the GBA gene and parkinsonism. *Lancet Neurol,* 11**,** 986-98.

SIDRANSKY, E., NALLS, M. A., AASLY, J. O., AHARON-PERETZ, J., ANNESI, G., BARBOSA, E. R., BAR-SHIRA, A., BERG, D., BRAS, J., BRICE, A., CHEN, C. M., CLARK, L. N., CONDROYER, C., DE MARCO, E. V., DURR, A., EBLAN, M. J., FAHN, S., FARRER, M. J., FUNG, H. C., GAN-OR, Z., GASSER, T., GERSHONI-BARUCH, R., GILADI, N., GRIFFITH, A., GUREVICH, T., JANUARIO, C., KROPP, P., LANG, A. E., LEE-CHEN, G. J., LESAGE, S., MARDER, K., MATA, I. F., MIRELMAN, A., MITSUI, J., MIZUTA, I., NICOLETTI, G., OLIVEIRA, C., OTTMAN, R., ORR-URTREGER, A., PEREIRA, L. V., QUATTRONE, A., ROGAEVA, E., ROLFS, A., ROSENBAUM, H., ROZENBERG, R., SAMII, A., SAMADDAR, T., SCHULTE, C., SHARMA, M., SINGLETON, A., SPITZ, M., TAN, E. K., TAYEBI, N., TODA, T., TROIANO, A. R., TSUJI, S., WITTSTOCK, M., WOLFSBERG, T. G., WU, Y. R., ZABETIAN, C. P., ZHAO, Y. & ZIEGLER, S. G. 2009. Multicenter analysis of glucocerebrosidase mutations in Parkinson's disease. *N Engl J Med,* 361**,** 1651-61.

SILVA, R. M., RIES, V., OO, T. F., YARYGINA, O., JACKSON-LEWIS, V., RYU, E. J., LU, P. D., MARCINIAK, S. M., RON, D., PRZEDBORSKI, S., KHOLODILOV, N., GREENE, L. A. & BURKE, R. E. 2005. CHOP/GADD153 is a mediator of apoptotic death in substantia nigra dopamine neurons in an in vivo neurotoxin model of parkinsonism. *Journal of Neurochemistry,* 95**,** 974-986.

SNYDER, H., MENSAH, K., THEISLER, C., LEE, J., MATOUSCHEK, A. & WOLOZIN, B. 2003. Aggregated and monomeric alpha-synuclein bind to the S6' proteasomal protein and inhibit proteasomal function. *J Biol Chem,* 278**,** 11753-9.

SPILLANTINI, M. G. & GOEDERT, M. 2000. The alpha-synucleinopathies: Parkinson's disease, dementia with Lewy bodies, and multiple system atrophy. *Ann N Y Acad Sci,* 920**,** 16-27.

SPIRA, P. J., SHARPE, D. M., HALLIDAY, G., CAVANAGH, J. & NICHOLSON, G. A. 2001. Clinical and pathological features of a Parkinsonian syndrome in a family with an Ala53Thr alpha-synuclein mutation. *Ann Neurol,* 49**,** 313-9.

STEFANIS, L. 2012. α-Synuclein in Parkinson's disease. *Cold Spring Harb Perspect Med,* 2**,** a009399.

STEFANIS, L., LARSEN, K. E., RIDEOUT, H. J., SULZER, D. & GREENE, L. A. 2001. Expression of A53T mutant but not wild-type alpha-synuclein in PC12 cells induces alterations of the ubiquitin-dependent degradation system, loss of dopamine release, and autophagic cell death. *J Neurosci,* 21**,** 9549-60.

STOLZ, A. & WOLF, D. H. 2010. Endoplasmic reticulum associated protein degradation: A chaperone assisted journey to hell. *Biochimica et Biophysica Acta (BBA) - Molecular Cell Research,* 1803**,** 694-705.

SUGENO, N., TAKEDA, A., HASEGAWA, T., KOBAYASHI, M., KIKUCHI, A., MORI, F., WAKABAYASHI, K. & ITOYAMA, Y. 2008. Serine 129 phosphorylation of alpha-synuclein induces unfolded protein response-mediated cell death. *J Biol Chem,* 283**,** 23179-88.

SULZER, D. & SURMEIER, D. J. 2013. Neuronal vulnerability, pathogenesis, and Parkinson's disease. *Mov Disord,* 28**,** 715-24.

SUNG, J. Y., KIM, J., PAIK, S. R., PARK, J. H., AHN, Y. S. & CHUNG, K. C. 2001. Induction of neuronal cell death by Rab5A-dependent endocytosis of alpha-synuclein. *J Biol Chem,* 276**,** 27441-8.

SURMEIER, D. J. 2018. Determinants of dopaminergic neuron loss in Parkinson's disease. *The FEBS Journal,* 285**,** 3657-3668.

SURMEIER, D. J., GUZMAN, J. N., SANCHEZ, J. & SCHUMACKER, P. T. 2012. Physiological phenotype and vulnerability in Parkinson's disease. *Cold Spring Harb Perspect Med,* 2**,** a009290.

SURMEIER, D. J., OBESO, J. A. & HALLIDAY, G. M. 2017. Selective neuronal vulnerability in Parkinson disease. *Nat Rev Neurosci,* 18**,** 101-113.

SUZUKI, K. & OHSUMI, Y. 2007. Molecular machinery of autophagosome formation in yeast, Saccharomyces cerevisiae. *FEBS Letters,* 581**,** 2156-2161.

SWAN, M. & SAUNDERS-PULLMAN, R. 2013. The association between ss-glucocerebrosidase mutations and parkinsonism. *Curr Neurol Neurosci Rep,* 13**,** 368.

TAMARGO, R. J., VELAYATI, A., GOLDIN, E. & SIDRANSKY, E. 2012. The role of saposin C in Gaucher disease. *Mol Genet Metab,* 106**,** 257-63.

TAN, E. K., TONG, J., FOOK-CHONG, S., YIH, Y., WONG, M. C., PAVANNI, R. & ZHAO, Y. 2007. Glucocerebrosidase mutations and risk of Parkinson disease in Chinese patients. *Arch Neurol,* 64**,** 1056-8.

TAPIAS, V., HU, X., LUK, K. C., SANDERS, L. H., LEE, V. M. & GREENAMYRE, J. T. 2017. Synthetic alpha-synuclein fibrils cause mitochondrial impairment and selective dopamine neurodegeneration in part via iNOS-mediated nitric oxide production. *Cell Mol Life Sci,* 74**,** 2851-2874.

TATTI, M., MOTTA, M., DI BARTOLOMEO, S., SCARPA, S., CIANFANELLI, V., CECCONI, F. & SALVIOLI, R. 2012. Reduced cathepsins B and D cause impaired autophagic degradation that can be almost completely restored by overexpression of these two proteases in Sap C-deficient fibroblasts. *Hum Mol Genet,* 21**,** 5159-73.

TAYEBI, N., CALLAHAN, M., MADIKE, V., STUBBLEFIELD, B. K., ORVISKY, E., KRASNEWICH, D., FILLANO, J. J. & SIDRANSKY, E. 2001. Gaucher disease and parkinsonism: a phenotypic and genotypic characterization. *Mol Genet Metab,* 73**,** 313-21.

TAYEBI, N., WALKER, J., STUBBLEFIELD, B., ORVISKY, E., LAMARCA, M. E., WONG, K., ROSENBAUM, H., SCHIFFMANN, R., BEMBI, B. & SIDRANSKY, E. 2003. Gaucher disease with parkinsonian manifestations: does glucocerebrosidase deficiency contribute to a vulnerability to parkinsonism? *Mol Genet Metab,* 79**,** 104-9.

TEKRIWAL, A., KERN, D. S., TSAI, J., INCE, N. F., WU, J., THOMPSON, J. A. & ABOSCH, A. 2017. REM sleep behaviour disorder: prodromal and mechanistic insights for Parkinson's disease. *Journal of Neurology, Neurosurgery & Psychiatry,* 88**,** 445.

TEPPOLA, H., SARKANEN, J.-R., JALONEN, T. O. & LINNE, M.-L. Impacts of laminin and polyethyleneimine surface coatings on morphology of differentiating human SH-SY5Y cells and networks. 2018 Singapore. Springer Singapore, 298-301.

TEPPOLA, H., SARKANEN, J. R., JALONEN, T. O. & LINNE, M. L. 2016. Morphological Differentiation Towards Neuronal Phenotype of SH-SY5Y Neuroblastoma Cells by Estradiol, Retinoic Acid and Cholesterol. *Neurochem Res,* 41**,** 731-47.

TESTA, C. M., SHERER, T. B. & GREENAMYRE, J. T. 2005. Rotenone induces oxidative stress and dopaminergic neuron damage in organotypic substantia nigra cultures. *Brain Res Mol Brain Res,* 134**,** 109-18.

THIBAUDEAU, T. A., ANDERSON, R. T. & SMITH, D. M. 2018. A common mechanism of proteasome impairment by neurodegenerative disease-associated oligomers. *Nature Communications,* 9**,** 1097.

TSUJI, S., CHOUDARY, P. V., MARTIN, B. M., STUBBLEFIELD, B. K., MAYOR, J. A., BARRANGER, J. A. & GINNS, E. I. 1987. A mutation in the human glucocerebrosidase gene in neuronopathic Gaucher's disease. *N Engl J Med,* 316**,** 570-5.

TSUJI, S., MARTIN, B. M., BARRANGER, J. A., STUBBLEFIELD, B. K., LAMARCA, M. E. & GINNS, E. I. 1988. Genetic heterogeneity in type 1 Gaucher disease: multiple genotypes in Ashkenazic and non-Ashkenazic individuals. *Proc Natl Acad Sci U S A,* 85**,** 2349-52.

TURPIN, J. C., DUBOIS, G., BRICE, A., MASSON, M., NADAUD, M. C., BOUTRY, J. M., SCHRAM, A. W., TAGER, J. M. & BAUMANN, N. Parkinsonian Symptomatology in a Patient with Type I (Adult) Gaucher's Disease. 1988 Boston, MA. Springer US, 103-105.

TYLKI-SZYMAŃSKA, A., CZARTORYSKA, B., VANIER, M.-T., POORTHUIS, B., GROENER, J., ŁUGOWSKA, A., MILLAT, G., VACCARO, A. & JURKIEWICZ, E. 2007. Non-neuronopathic Gaucher disease due to saposin C deficiency. *Clinical Genetics,* 72**,** 538-542.

UGALDE, C. L., FINKELSTEIN, D. I., LAWSON, V. A. & HILL, A. F. 2016. Pathogenic mechanisms of prion protein, amyloid-β and α-synuclein misfolding: the prion concept and neurotoxicity of protein oligomers. *Journal of Neurochemistry,* 139**,** 162-180.

VAN HEESBEEN, H. J. & SMIDT, M. P. 2019. Entanglement of Genetics and Epigenetics in Parkinson's Disease. *Front Neurosci,* 13**,** 277.

VEKRELLIS, K., XILOURI, M., EMMANOUILIDOU, E. & STEFANIS, L. 2009. Inducible over-expression of wild type alpha-synuclein in human neuronal cells leads to caspase-dependent non-apoptotic death. *J Neurochem,* 109**,** 1348-62.

VELAYATI, A., YU, W. H. & SIDRANSKY, E. 2010. The role of glucocerebrosidase mutations in Parkinson disease and Lewy body disorders. *Curr Neurol Neurosci Rep,* 10**,** 190-8.

VILA, M., BOVÉ, J., DEHAY, B., RODRÍGUEZ-MUELA, N. & BOYA, P. 2011. Lysosomal membrane permeabilization in Parkinson disease. *Autophagy,* 7**,** 98-100.

VITNER, E. B., DEKEL, H., ZIGDON, H., SHACHAR, T., FARFEL-BECKER, T., EILAM, R., KARLSSON, S. & FUTERMAN, A. H. 2010. Altered expression and distribution of cathepsins in neuronopathic forms of Gaucher disease and in other sphingolipidoses. *Hum Mol Genet,* 19**,** 3583-90.

VOGES, D., ZWICKL, P. & BAUMEISTER, W. 1999. The 26S proteasome: a molecular machine designed for controlled proteolysis. *Annu Rev Biochem,* 68**,** 1015-68.

VOGIATZI, T., XILOURI, M., VEKRELLIS, K. & STEFANIS, L. 2008. Wild type alpha-synuclein is degraded by chaperone-mediated autophagy and macroautophagy in neuronal cells. *J Biol Chem,* 283**,** 23542-56.

VOLPICELLI-DALEY, L. A., LUK, K. C., PATEL, T. P., TANIK, S. A., RIDDLE, D. M., STIEBER, A., MEANEY, D. F., TROJANOWSKI, J. Q. & LEE, V. M. 2011. Exogenous α-synuclein fibrils induce Lewy body pathology leading to synaptic dysfunction and neuron death. *Neuron,* 72**,** 57-71.

VOTYAKOVA, T. V. & REYNOLDS, I. J. 2001. ΔΨm-Dependent and -independent production of reactive oxygen species by rat brain mitochondria. *Journal of Neurochemistry,* 79**,** 266-277.

WAKABAYASHI, K., TANJI, K., ODAGIRI, S., MIKI, Y., MORI, F. & TAKAHASHI, H. 2013. The Lewy body in Parkinson's disease and related neurodegenerative disorders. *Mol Neurobiol,* 47**,** 495-508.

WALKER, D. G., LUE, L. F., ADLER, C. H., SHILL, H. A., CAVINESS, J. N., SABBAGH, M. N., AKIYAMA, H., SERRANO, G. E., SUE, L. I. & BEACH, T. G. 2013. Changes in properties of serine 129 phosphorylated α-synuclein with progression of Lewy-type histopathology in human brains. *Exp Neurol,* 240**,** 190-204.

WALKER, L., STEFANIS, L. & ATTEMS, J. 2019. Clinical and neuropathological differences between Parkinson's disease, Parkinson's disease dementia and dementia with Lewy bodies – current issues and future directions. *Journal of Neurochemistry,* 150**,** 467-474.

WANG, T., LI, C., HAN, B., WANG, Z., MENG, X., ZHANG, L., HE, J. & FU, F. 2020. Neuroprotective effects of Danshensu on rotenone-induced Parkinson's disease models in vitro and in vivo. *BMC Complement Med Ther,* 20**,** 20.

WATABE-UCHIDA, M., ZHU, L., OGAWA, S. K., VAMANRAO, A. & UCHIDA, N. 2012. Whole-brain mapping of direct inputs to midbrain dopamine neurons. *Neuron,* 74**,** 858-73.

WEBB, J. L., RAVIKUMAR, B., ATKINS, J., SKEPPER, J. N. & RUBINSZTEIN, D. C. 2003. Alpha-Synuclein is degraded by both autophagy and the proteasome. *J Biol Chem,* 278**,** 25009-13.

WEN, Y., LI, W., POTEET, E. C., XIE, L., TAN, C., YAN, L. J., JU, X., LIU, R., QIAN, H., MARVIN, M. A., GOLDBERG, M. S., SHE, H., MAO, Z., SIMPKINS, J. W. & YANG, S. H. 2011. Alternative mitochondrial electron transfer as a novel strategy for neuroprotection. *J Biol Chem,* 286**,** 16504-15.

WENGER, D. A., CLARK, C., SATTLER, M. & WHARTON, C. 1978. Synthetic substrate ß-glucosidase activity in leukocytes: A reproducible method for the identification of patients and carriers of Gaucher's disease. *Clinical Genetics,* 13**,** 145-153.

WESSELBORG, S. & STORK, B. 2015. Autophagy signal transduction by ATG proteins: from hierarchies to networks. *Cell Mol Life Sci,* 72**,** 4721-57.

WESTBROEK, W., GUSTAFSON, A. M. & SIDRANSKY, E. 2011. Exploring the link between glucocerebrosidase mutations and parkinsonism. *Trends Mol Med,* 17**,** 485-93.

WESTBROEK, W., NGUYEN, M., SIEBERT, M., LINDSTROM, T., BURNETT, R. A., AFLAKI, E., JUNG, O., TAMARGO, R., RODRIGUEZ-GIL, J. L., ACOSTA, W., HENDRIX, A., BEHRE, B., TAYEBI, N., FUJIWARA, H., SIDHU, R., RENVOISE, B., GINNS, E. I., DUTRA, A., PAK, E., CRAMER, C., ORY, D. S., PAVAN, W. J. & SIDRANSKY, E. 2016. A new glucocerebrosidase-deficient neuronal cell model provides a tool to probe pathophysiology and therapeutics for Gaucher disease. *Dis Model Mech,* 9**,** 769-78.

WINDER-RHODES, S. E., EVANS, J. R., BAN, M., MASON, S. L., WILLIAMS-GRAY, C. H., FOLTYNIE, T., DURAN, R., MENCACCI, N. E., SAWCER, S. J. & BARKER, R. A. 2013. Glucocerebrosidase mutations influence the natural history of Parkinson's disease in a community-based incident cohort. *Brain,* 136**,** 392-9.

WONG, E. & CUERVO, A. M. 2010. Integration of clearance mechanisms: the proteasome and autophagy. *Cold Spring Harb Perspect Biol,* 2**,** a006734.

WONG, K., SIDRANSKY, E., VERMA, A., MIXON, T., SANDBERG, G. D., WAKEFIELD, L. K., MORRISON, A., LWIN, A., COLEGIAL, C., ALLMAN, J. M. & SCHIFFMANN, R. 2004. Neuropathology provides clues to the pathophysiology of Gaucher disease. *Molecular Genetics and Metabolism,* 82**,** 192-207.

WOODARD, C. M., CAMPOS, B. A., KUO, S. H., NIRENBERG, M. J., NESTOR, M. W., ZIMMER, M., MOSHAROV, E. V., SULZER, D., ZHOU, H., PAULL, D., CLARK, L., SCHADT, E. E., SARDI, S. P., RUBIN, L., EGGAN, K., BROCK, M., LIPNICK, S., RAO, M., CHANG, S., LI, A. & NOGGLE, S. A. 2014. iPSC-derived dopamine neurons reveal differences between monozygotic twins discordant for Parkinson's disease. *Cell Rep,* 9**,** 1173-82.

XICOY, H., WIERINGA, B. & MARTENS, G. J. M. 2017. The SH-SY5Y cell line in Parkinson’s disease research: a systematic review. *Molecular Neurodegeneration,* 12**,** 10.

XILOURI, M., BREKK, O. R. & STEFANIS, L. 2013. Alpha-synuclein and Protein Degradation Systems: a Reciprocal Relationship. *Molecular Neurobiology,* 47**,** 537-551.

XILOURI, M. & STEFANIS, L. 2016. Chaperone mediated autophagy in aging: Starve to prosper. *Ageing Research Reviews,* 32**,** 13-21.

XILOURI, M., VOGIATZI, T., VEKRELLIS, K., PARK, D. & STEFANIS, L. 2009. Abberant alpha-synuclein confers toxicity to neurons in part through inhibition of chaperone-mediated autophagy. *PLoS One,* 4**,** e5515.

XU, Y. H., SUN, Y., RAN, H., QUINN, B., WITTE, D. & GRABOWSKI, G. A. 2011. Accumulation and distribution of α-synuclein and ubiquitin in the CNS of Gaucher disease mouse models. *Molecular genetics and metabolism,* 102**,** 436-447.

YAN, J. Q., YUAN, Y. H., CHU, S. F., LI, G. H. & CHEN, N. H. 2018. E46K Mutant α-Synuclein Is Degraded by Both Proteasome and Macroautophagy Pathway. *Molecules,* 23.

YANG, S. Y., GEGG, M., CHAU, D. & SCHAPIRA, A. 2020. Glucocerebrosidase activity, cathepsin D and monomeric alpha-synuclein interactions in a stem cell derived neuronal model of a PD associated GBA1 mutation. *Neurobiol Dis,* 134**,** 104620.

YAP, T. L., GRUSCHUS, J. M., VELAYATI, A., WESTBROEK, W., GOLDIN, E., MOAVEN, N., SIDRANSKY, E. & LEE, J. C. 2011. Alpha-synuclein interacts with Glucocerebrosidase providing a molecular link between Parkinson and Gaucher diseases. *J Biol Chem,* 286**,** 28080-8.

YAP, T. L., VELAYATI, A., SIDRANSKY, E. & LEE, J. C. 2013. Membrane-bound alpha-synuclein interacts with glucocerebrosidase and inhibits enzyme activity. *Mol Genet Metab,* 108**,** 56-64.

YIĞIT, E. N., SÖNMEZ, E., SÖĞÜT, M. S., ÇAKIR, T. & KURNAZ, I. A. 2018. Validation of an In-Vitro Parkinson's Disease Model for the Study of Neuroprotection. *Proceedings,* 2**,** 1559.

YIM, W. W. & MIZUSHIMA, N. 2020. Lysosome biology in autophagy. *Cell Discov,* 6**,** 6.

YOSHII, SAORI R., KUMA, A., AKASHI, T., HARA, T., YAMAMOTO, A., KURIKAWA, Y., ITAKURA, E., TSUKAMOTO, S., SHITARA, H., EISHI, Y. & MIZUSHIMA, N. 2016. Systemic Analysis of Atg5-Null Mice Rescued from Neonatal Lethality by Transgenic ATG5 Expression in Neurons. *Developmental Cell,* 39**,** 116-130.

YUN, S. P., KIM, D., KIM, S., KIM, S., KARUPPAGOUNDER, S. S., KWON, S.-H., LEE, S., KAM, T.-I., LEE, S., HAM, S., PARK, J. H., DAWSON, V. L., DAWSON, T. M., LEE, Y. & KO, H. S. 2018. α-Synuclein accumulation and GBA deficiency due to L444P GBA mutation contributes to MPTP-induced parkinsonism. *Molecular Neurodegeneration,* 13**,** 1.

ZHANG, B., KEHM, V., GATHAGAN, R., LEIGHT, S. N., TROJANOWSKI, J. Q., LEE, V. M. & LUK, K. C. 2019. Stereotaxic Targeting of Alpha-Synuclein Pathology in Mouse Brain Using Preformed Fibrils. *Methods Mol Biol,* 1948**,** 45-57.

ZHANG, G., XIA, Y., WAN, F., MA, K., GUO, X., KOU, L., YIN, S., HAN, C., LIU, L., HUANG, J., XIONG, N. & WANG, T. 2018. New Perspectives on Roles of Alpha-Synuclein in Parkinson's Disease. *Frontiers in Aging Neuroscience,* 10.

ZHOU, J., BROE, M., HUANG, Y., ANDERSON, J. P., GAI, W. P., MILWARD, E. A., PORRITT, M., HOWELLS, D., HUGHES, A. J., WANG, X. & HALLIDAY, G. M. 2011. Changes in the solubility and phosphorylation of α-synuclein over the course of Parkinson's disease. *Acta Neuropathol,* 121**,** 695-704.

ZUCCA, F. A., SEGURA-AGUILAR, J., FERRARI, E., MUÑOZ, P., PARIS, I., SULZER, D., SARNA, T., CASELLA, L. & ZECCA, L. 2017. Interactions of iron, dopamine and neuromelanin pathways in brain aging and Parkinson's disease. *Progress in Neurobiology,* 155**,** 96-119.